NASA CONTRACTOR REPORT

NASA CR-2499

NASA CR-2499

HIGH REYNOLDS NUMBER TEST OF A NACA 65_1-213, a = 0.5 AIRFOIL AT TRANSONIC SPEEDS

Kenneth P. Burdges, James A. Blackwell, Jr., and Gerald A. Pounds

Prepared by
LOCKHEED-GEORGIA COMPANY
Marietta, Ga. 30060
for Langley Research Center

NATIONAL AERONAUTICS AND SPACE ADMINISTRATION • WASHINGTON, D. C. • MARCH 1975

1. Report No.	2. Government Accession No.	3. Recipient's Catalog No.
NASA CR-2499		

4. Title and Subtitle	5. Report Date
HIGH REYNOLDS NUMBER TEST OF A NACA 65_1-213, a = 0.5 AIRFOIL AT TRANSONIC SPEEDS	March 1975
	6. Performing Organization Code
7. Author(s)	8. Performing Organization Report No.
Kenneth P. Burdges, James A. Blackwell, Jr., and Gerald A. Pounds	
9. Performing Organization Name and Address	10. Work Unit No.
Lockheed Aircraft Corporation Lockheed-Georgia Company 86 South Cobb Drive Marietta, GA 30060	505-06-31-02
	11. Contract or Grant No.
	NAS1-12325
12. Sponsoring Agency Name and Address	13. Type of Report and Period Covered
National Aeronautics & Space Administration Washington, DC 20546	Contractor Report
	14. Sponsoring Agency Code

15. Supplementary Notes

Topical report.

16. Abstract

Wind-Tunnel tests have been conducted in the Lockheed-Georgia Company's Compressible Flow Facility to determine the transonic two-dimensional aerodynamic characteristics of a NACA 65_1-213 a = 0.50 airfoil. The results are correlated with data on this same airfoil section obtained in the NASA-Langley 8-Foot Transonic Pressure Tunnel and the NAE high Reynolds number 15x60-inch two-dimensional test facility. The tests were conducted over a Mach number range from 0.60 to 0.80 and an angle of attack range from -1° to 8°. Reynolds numbers, based on the airfoil chord, were varied from about 3.0×10^6 to 32.0×10^6.

17. Key Words (Suggested by Author(s))	18. Distribution Statement
NACA 65_1-213 airfoil High Reynolds number test Transonic aerodynamics Data correlation	Unclassified - Unlimited STAR Category 02

19. Security Classif. (of this report)	20. Security Classif. (of this page)	21. No. of Pages	22. Price*
Unclassified	Unclassified	162	$6.25

*For sale by the National Technical Information Service, Springfield, Virginia 22151

HIGH REYNOLDS NUMBER TEST OF A NACA 65_1-213, a = 0.5 AIRFOIL AT TRANSONIC SPEEDS

By Kenneth P. Burdges, James A. Blackwell, Jr.,
and Gerald A. Pounds
Lockheed-Georgia Company

SUMMARY

An investigation was conducted in the Lockheed-Georgia Company Compressible Flow Facility to determine the transonic two-dimensional aerodynamic characteristics of a NACA 65_1-213, a = 0.5 airfoil over a wide Reynolds number range indicative of both conventional wind tunnel and full scale flight values. The results are correlated with unpublished data on this airfoil section obtained in the NASA 8-foot transonic pressure tunnel and the NAE high Reynolds number 15 x 60 inch two-dimensional test facility. The tests were conducted over a Mach number range from 0.60 to 0.80 and an angle of attack range from -1° to 8°. Reynolds numbers based on the airfoil chord, were varied from about 3.0×10^6 to 32.0×10^6.

The results of the investigation indicated that variations in wind tunnel wall porosity had a significant effect on the airfoil performance for conditions where shock-induced separation was present. Correlation of the data obtained in this investigation with test data on the same airfoil section from the NASA 8-foot transonic pressure tunnel and the NAE 15 x 60 inch two-dimensional high Reynolds number test facility indicated that generally good agreement was obtained. The effects of varying Reynolds number on the normal-force and pitching moment characteristics were generally small. For attached flow conditions, the effect on drag coefficient for large changes in Reynolds number was generally consistent with conventional flat plate drag variations. Also, for attached flow large Reynolds number variations had practically no effect on airfoil shock location. For shock induced separated flow conditions, Reynolds number had a substantial effect on trailing edge pressure coefficients and the shock location moved aft about 5 percent of the airfoil chord.

INTRODUCTION

Over the past decade, there have been several correlations of wind tunnel and flight data to determine the effects of large changes in Reynolds number on the aerodynamic performance of transport aircraft. These correlations have covered a wide range of aircraft size and technology, such as the NASA F-8 supercritical wing airplane, the Lockheed C-5A, the Lockheed C-141, and the Lockheed T-33. The results of these studies have indicated that the magnitude of Reynolds number scale effects on aerodynamic performance varies considerably depending upon both airplane configuration geometry and airfoil technology.

As new full-scale transport aircraft are designed which incorporate the latest advances in aerodynamic technology, it is imperative that the effect of large Reynolds number variations on the aerodynamic performance of these aircraft be known and understood. In particular, the relationship of configuration geometry and airfoil technology to Reynolds number scale effects needs to be established.

Recognizing the need for an experimental facility to evaluate Reynolds number scale effects, the Lockheed-Georgia Company has constructed a new transonic wind tunnel capable of simulating Reynolds numbers of conventional transonic wind tunnel facilities as well as those near full-scale aircraft flight values. This tunnel, referred to as the Compressible Flow Facility (CFF), is described in reference 1 and has the capability of performing both two- and three-dimensional testing at transonic speeds and at large Reynolds numbers.

As a result of the need to establish experimentally the effects of large variations of Reynolds number on airfoils of varying technology, NASA has contracted with the Lockheed-Georgia Company to test in the Lockheed CFF a series of airfoils. These airfoils will be representative of various types of aircraft such as those mentioned above and will be investigated over a large Reynolds number range indicative of both wind tunnel and flight values.

It is the purpose of this report to present the experimental results and establish the Reynolds number scale effects on the first airfoil of this test series — the NACA 65_1-213, a = 0.5 airfoil. This airfoil was selected as representative of conventional airfoil technology and has been used on aircraft such as the Lockheed T-33.

A second airfoil typical of that used on the NASA F-8 supercritical wing airplane was also tested in this series. These results are reported in reference 2.

In this report, a description of the model and test facility will be presented followed by the test procedures and test conditions. The discussion of the results will be divided primarily into two sections. The first section presents the basic force data and representative pressure data on the NACA 65_1-213, a = 0.5 airfoil to establish the transonic characteristics of the airfoil at various angles of attack, Mach numbers, and Reynolds numbers. A complete set of the pressure distribution data measured during this test is given in the Appendix. Correlation of data from the present tests with unpublished measurements of Arvo Luoma of NASA-Langley on the same airfoil section in the NASA 8-foot transonic pressure tunnel and the NAE high Reynolds number 15 x 60 in. 2-D test facility are included where test conditions match. In the second section, the Reynolds number scale effects on the NACA 65_1-213, a = 0.5 airfoil based on the CFF data will be established and discussed.

SYMBOLS

Values are given both in SI and the U. S. Customary Units. The measurements and calculations were made in the U. S. Customary Units.

a	mean-line designation
b	model span, cm (in.)
C_p	pressure coefficient
$C_{p,sonic}$	pressure coefficient for local Mach number of 1.0
c	chord of airfoil, cm (in.)
c_d	section profile drag coefficient
c'_d	point drag coefficient
c'_{d_m}	maximum value of c'_d in wake
c_m	section pitching-moment coefficient about quarter chord
c_n	section normal force coefficient
d	external diameter of wake rake total head tubes, cm (in.)
h	vertical distance in wake profile, cm (in.)
H	total pressure, N/m^2 (lb/ft^2)
k	roughness height, cm (in.)
M	freestream Mach number
p	static pressure, N/m^2 (lb/ft^2)
q	dynamic pressure, N/m^2 (lb/ft^2)
R_N	Reynolds number based on freestream conditions and airfoil chord
R_k	roughness Reynolds number based on roughness height and velocity and kinematic viscosity at top of roughness
x	ordinate along airfoil chord line measured from airfoil leading edge, cm (in.)

y	ordinate along airfoil span measured from tunnel centerline, cm (in.)
z	ordinate vertical to airfoil chord line, cm (in.)
α	geometric angle of airfoil chord line, degrees
δ	flat plate laminar boundary-layer height, cm (in.)
γ	ratio of specific heats

Subscripts:

t.e.	trailing edge
T	transition strip location
o	zero normal force
1	tunnel station one chord length downstream of model
∞	denotes freestream conditions

Abbreviations:

CFF	Lockheed Compressible Flow Facility
l.s.	lower surface
NASA	NASA 8-foot transonic pressure tunnel
u.s.	upper surface
NAE	NAE 15 x 60 inch two-dimensional test facility

APPARATUS AND TEST PROCEDURES

Model

The two-dimensional model of the NACA 65_1-213, a = 0.5 airfoil used in this investigation is shown installed in the Lockheed CFF in figure 1. A sketch of the airfoil section is given in figure 2 and the design ordinates are listed in table I. The model has a chord of 17.78 cm (7.00 in.) and a span of 50.80 cm (20.00 in.) so that the model completely spans the CFF two-dimensional test section. The model was fabricated from 17-4PH stainless steel.

Surface pressure orifices were installed near the mid-span region of the model on the upper and lower surfaces so as to provide a chordwise distribution of pressures. Additional pressure orifices were placed strategically along the span to measure the two-dimensionality of the flow. Orifice locations for the pressure tubes are shown in table II.

The model contour accuracy was checked at three spanwise stations by template and feeler gage. The deviations from the mean contour are generally within ±.025 (.001 in.), except for small areas on the lower surface where the deviation reached ±.050 mm (.002 in.). The variation in angle of attack across the span of the model was found to be 3 minutes. The airfoil surface was fair and smooth with conventional transonic model surface finish.

Test Facility

The general arrangement of the Lockheed Compressible Flow Facility (CFF) is shown in figure 3. The tunnel is of the blow-down type, exhausting directly to the atmosphere. The air storage capability is 368 m^3 (13,000 ft^3) at 413 dynes/cm^2 (600 psia). A sleeve-type control valve accurately maintains the settling chamber stagnation pressure at selected pressure less than or equal to the 172 dynes/cm^2 (250 psia) maximum and at mass flow rates less than 1089 kg/sec (2400 lb/sec). The test section is 50.8 cm (20.0 in.) wide by 71.2 cm (28.0 in.) high by 183 cm (72.0 in.) long and is enclosed in a 3.7 m (12.0 ft.)

diameter plenum chamber. The top and bottom walls of the two-dimensional test section have variable porosity capability (from 0 to 10 percent), obtained by sliding two parallel plates with .635 cm (.250 in.) diameter holes slanted 60 degrees from the vertical. The 2-D test section side walls are not porous. A more detailed description of the facility may be found in reference 1.

Wake Survey Rake

The fixed wake survey rake used for section drag measurements is described in figure 4 and shown installed in the tunnel in figure 1. The wake rake was mounted at the tunnel centerline one chord length behind the airfoil model. The rake has a total of 90 total head measurement tubes and 4 static pressure tubes. The wake rake tubes are .15 cm (.06 in.) in diameter. Two static tubes are located on a horizontal plane at the tunnel centerline and the other two static tubes are located .64c above and below the tunnel centerline. The wake rake has been calibrated in the tunnel without a model present.

Data has been obtained in previous CFF airfoil tests similar to that conducted herein with the wake rake installed and removed to determine its influence on the flow over the airfoil. These unpublished data indicated the wake rake had negligible effects on the normal-force coefficient, the pitching-moment coefficient, and the airfoil pressure distribution. Although no such investigation was done for the present tests, it is felt, based on this previously obtained data, that the wake rake did not have any effect on the flow over the NACA 65_1-213, a = 0.5 airfoil.

Instrumentation

Measurements of the static pressures on the airfoil surfaces and the wake rake pressures were made using electronically actuated pressure scanning valves. The full-scale range of the quarter percent accuracy statham transducers in the valves were selected to provide maximum accuracy for the wind tunnel conditions tested (wake rake ±12.5 psi and airfoil pressures ±50 psi). CEC force balance

pressure transducers were used in conjunction with CEC servo amplifiers to provide a precise measurement of the atmospheric pressure, stagnation pressure, and test section static pressure to 0.05% of the 250 psi capacity. These transducers allow determination of the test section Mach number to an accuracy of ±.002 at the highest stagnation pressure.

Angle of attack was measured with a calibrated potentiometer operated by the angle of attack drive mechanism.

Raw pressure data was recorded on magnetic tape utilizing the CFF high speed data acquisition system. The data acquisition system consists of a Lockheed Electronics Company MAC-16 computer and associated peripheral equipment. The raw data was reduced to coefficient form with a CDC 1700 computer.

TESTS AND METHODS

Test Conditions

The aerodynamic characteristics of the NACA 65_1-213, a = 0.5 airfoil were investigated over a wide range of test conditions. The angle of attack of the airfoil was varied from -1 to 8 degrees and the Mach number range investigated was from 0.60 to 0.80. The Reynolds number based on airfoil chord was varied from 3.0×10^6 to 32×10^6 by varying tunnel stagnation pressure. A tabulation of the nominal test conditions is presented in table III.

Data Reduction

The static pressure measurements at the airfoil surface were reduced to standard pressure coefficients and then machine integrated by a double parabolic integration routine to obtain section normal force and section pitching moment coefficients about the quarter chord using the following equations:

$$c_n = \int_{l.s.} C_p \, d\left(\frac{x}{c}\right) - \int_{u.s.} C_p \, d\left(\frac{x}{c}\right) \tag{1}$$

and

$$c_m = \int_{l.s.} C_p\left(0.25 - \frac{x}{c}\right) d\left(\frac{x}{c}\right) - \int_{u.s.} C_p\left(0.25 - \frac{x}{c}\right) d\left(\frac{x}{c}\right) \tag{2}$$

Section profile drag measurements were computed from the wake survey rake measurements by the method of reference 3 utilizing the following equations:

$$c_d = \int_{wake} c'_d \, d\left(\frac{h}{c}\right) + \Delta c_d \tag{3}$$

$$c'_d = 2\left(\frac{H_1}{H_\infty}\right)^{\frac{\gamma-1}{\gamma}} \left(\frac{p_1}{p_\infty}\right)^{\frac{1}{\gamma}} \left\{ \frac{1 - \left(\frac{p_1}{H_1}\right)^{\frac{\gamma-1}{\gamma}}}{1 - \left(\frac{p_\infty}{H_\infty}\right)^{\frac{\gamma-1}{\gamma}}} \right\}^{\frac{1}{2}} \left[1 - \left\{ \frac{1 - \left(\frac{p_\infty}{H_1}\right)^{\frac{\gamma-1}{\gamma}}}{1 - \left(\frac{p_\infty}{H_\infty}\right)^{\frac{\gamma-1}{\gamma}}} \right\}^{\frac{1}{2}} \right] \tag{4}$$

The Δc_d is a correction for the wake rake total head tube displacement effect when in a transverse velocity gradient. This correction is discussed in reference 3 and is given by equation 5.

$$\Delta c_d = 0.36 \frac{d}{c} c'_{d_m} \tag{5}$$

Transition

The airfoil was tested with roughness particles located on both surfaces at 0.05c for Reynolds numbers from 3 to 12 million. The roughness size was chosen for each Reynolds number according to reference 4. At Reynolds numbers greater than 12 million, the airfoil was tested with free transition (natural boundary layer transition).

The roughness particle height used for each test Reynolds number is shown in figure 5. The roughness strips were 0.13 cm (0.05 in.) wide and consisted of Ballotini glass beads set in a plastic adhesive. Oil flows were conducted to verify that transition occurred at the strip for the selected particle heights. A typical oil flow photograph demonstrating boundary layer transition at the strip is presented in figure 6.

Additional tests to investigate the effects of particle height and density were accomplished. Tests were made over the entire Reynolds number range with the roughness strip removed to establish the movement of the natural transition point on the airfoil as a function of Reynolds number. These additional tests will be analyzed in the DISCUSSION section.

Tunnel Porosity

The wind tunnel wall porosity of the Lockheed CFF is variable between 0 and 10%. Since one of the objectives of this test was to obtain a good correlation with data obtained in other facilities, it was desirable to simulate as closely as possible the wind tunnel wall interference present in these tests. Therefore, the criteria for selecting the porosity for the CFF tests was that the pressure distribution level and shape and the force data be the same, at a given angle of attack, for the data obtained in the NASA 8-foot transonic pressure tunnel and the present tests. The NASA 8-foot transonic pressure tunnel has slotted upper and lower walls and the slot opening in the region of the airfoil was about 6 percent of the upper and lower walls.

To determine the required porosity a range of porosity values were run in the CFF. These data will be presented and discussed in detail in the DISCUSSION section. It was concluded from this study that a wall porosity of 4% achieved the best data correlation and was used for the entire test program unless otherwise noted.

Tunnel Wall Effects

An estimate of the standard subsonic wind tunnel boundary corrections (lift interference and blockage) has been calculated for this test using the method of reference 5. The corrections to pressure coefficient, normal force coefficient, pitching moment coefficient, and drag coefficient for a porosity of 4% were generally less than 1 percent of the measured values. The correction to angle of attack was, however, quite large. This is illustrated in figure 7. These corrections have not been applied to the data presented herein.

As shown in table II, orifices were located at various spanwise stations on the airfoil to determine the effect of the tunnel side walls on the two-dimensionality of the flow. Analysis of the pressure data for various flow conditions indicated very little variation in the pressure coefficient across the airfoil span. A typical variation at both subcritical and supercritical

flow conditions is presented in figure 8. This conclusion was further substantiated by observations of oil flow patterns at the airfoil-wall intersection. Disturbances in this juncture were confined to a very small region.

Test Repeatability

A measure of the data accuracy is its repeatability. A repeatability check for two runs at $M = 0.6$, $\alpha = 3°$, and $R_N = 26 \times 10^6$ are shown in figure 9. As can be seen, the difference in pressure distribution and force data are negligible indicating the data to be of good quality.

RESULTS AND DISCUSSION

The results obtained in the transition study and the tunnel-wall porosity effects study will be presented and analyzed first to provide the framework for the presentation of the basic airfoil results. This will be followed by a discussion of the basic data for the various test conditions obtained in the CFF. Completing the discussion will be the analysis of the Reynolds number effects on the aerodynamic performance of the airfoil. As appropriate, the data from the present investigation will be compared in various sections to data obtained on the same airfoil in the NASA 8-foot transonic pressure tunnel and the NAE high Reynolds number 15 x 60 inch two-dimensional test facility to establish the degree of correlation present between the various facilities.

Transition Study

The objective of this study was to verify that the transition fixing techniques (following ref. 4) used in this test resulted in turbulent boundary layer flow behind the transition strip without excessive particle drag. This was accomplished by testing the airfoil (1) transition free, (2) transition fixed with particle height varying, and (3) transition fixed with varying particle density within the transition strip.

This variation of airfoil drag with normal force coefficient for transition free and for four particle heights at a Mach number of 0.6 is shown in figure 10. The effect on airfoil drag of increasing particle height at low normal force coefficients is generally to shift the curve to a higher level by a constant increment. At the higher normal force coefficients, where separation is beginning to occur on the airfoil, increases in particle height tend to aggravate the separation and result in significantly higher drag.

The drag data from figure 10 at normal force coefficients of 0.2 and 0.5 are plotted versus particle height in figure 11. From this figure, it can be seen that no excess particle drag should be expected for particle heights slightly lower than the laminar boundary layer height. The effect of various particle sizes on airfoil pressure distribution is small as shown in figure 12.

The effect of transition strip particle density on drag is shown in figure 13. As can be seen, the data is very sensitive to the manner in which the particles are applied. Generally, the very dense particle application resulted in an excessive particle drag of six drag counts. The transition fixed data with varying particle height of figure 11 was obtained with the very dense particle applications. These data were run at the beginning of the test program before the effect of strip density was known. To be consistent with the remainder of the data in this report which was obtained with sparce particle applications, the effects of varying transition particle height on section drag, shown in figures 10 and 11, have been corrected downward by six drag counts.

Tunnel Wall Porosity Effects Study

This study had two primary objectives. The first was to determine the general effects of varying wall porosity on the NACA 65_1-213, a = .5 airfoil. The second objective of this study was to select the value of wall porosity for which the test would be conducted.

The general effect of varying wall porosity on the airfoil pressure distributions at subcritical and supercritical conditions are shown in figures 14 and 15. The effect of increasing porosity, subcritically, is to lower the negative pressure coefficient level on both the upper and lower surfaces. At supercritical speeds (fig. 15), the same variation in pressure level with increasing porosity is evident. For the 2% porosity case, the flow behind the shock over the aft part of the airfoil upper surface is separated. As porosity is increased, this flow approaches an unseparated flow condition and the shock moves aft slightly.

The variation of normal-force and drag coefficients with porosity for the above subcritical and supercritical cases are shown in figures 16 and 17. Subcritically, most of the force data variation takes place between porosities of 0 and 4%. At supercritical conditions (fig. 17), larger variations are noted in the data with increasing porosity. This is due to the effects of porosity on the airfoil upper-surface separation characteristics as noted in figure 15 earlier.

To obtain a good correlation of the present data with data obtained in other facilities on this same airfoil section, it was desirable to select a value of wall porosity in the CFF that yielded similar wall interference effects to those inherent in other investigations. As set forth in the TEST AND METHODS section, the criteria for determining the CFF wall-porosity value was that the force data and the pressure distribution level and shape for the NASA 8-foot transonic pressure tunnel tests and the present investigation to be same at a given angle of attack.

Pressure coefficient data and force data for the present tests with varying wall porosity are shown in figures 16 and 17 compared to the NASA 8-foot transonic pressure tunnel data for both subcritical and supercritical conditions, respectively. The pressure data correlation is for both upper and lower surfaces, and the pressure data points are representative of variations over the entire chord. It is evident that a wall porosity value of 4% yields the best overall correlation with the NASA data. Therefore, this value was used for the remainder of the test program reported herein.

Basic Results

Complete basic force data for the various test conditions are presented in this section. The most comprehensive tests on this airfoil were made for a Reynolds number of six million and are described first. Only selected pressure distributions are shown in this section with a complete set included in the appendix.

Reynolds number of six million. - The basic force data at a Reynolds number of six million are presented in figures 18 to 23. At Mach numbers of 0.60, 0.70 and 0.75, the force data from the NASA 8-foot transonic pressure tunnel are also shown. Good agreement of the slopes of the normal-force coefficient versus angle of attack curves for the present tests and the NASA data, through the Mach number range, demonstrate that the wind tunnel wall interference effects between the two tunnels are closely matched.

At all Mach numbers, the correlation of the pitching-moment coefficient versus normal-force coefficient curves generally indicate a slight difference in zero-lift pitching moment, but otherwise the agreement is good.

The correlation of drag coefficient with normal-force coefficient between the CFF and NASA data is excellent at Mach numbers of 0.60 and 0.70. The drag correlation at a Mach number of 0.75 is still good considering the large amount of drag present on the airfoil at this Mach number. Also, slight deviations in Mach number can cause large changes in drag when the airfoil is well into the drag rise. Since some slight deviations from the nominal Mach number occur in the data, constant Mach number fairings are included on the basic drag data plots (solid line). The constant Mach number fairings were obtained from the drag-rise plots presented in figure 23.

An airfoil pressure distribution for a subcritical test condition ($M = 0.60$, $\alpha = 0°$) is presented in figure 24. Correlation between the CFF pressure data and the NASA 8-foot transonic pressure tunnel results is very good over the entire airfoil. A minor difference occurs on the upper surface in the mid-chord region. The NASA data has a subtle difference in shape from the CFF data which is smoother. This difference becomes more apparent as Mach number is increased (fig. 25).

At supercritical conditions with a strong shock where the flow is not separated ($M = 0.75$, $\alpha = 0°$, fig. 26) agreement between the NASA data and the CFF data remains very good. Correlation is shown in figure 27 ($M = 0.75$, $\alpha = 3°$) for a case with supercritical flow followed by extensive shock-induced separation. There is a small difference in shock location which may be due to the slight differences in mid-chord airfoil geometry or by small differences in wind tunnel wall effects. Otherwise, the correlation of the pressure distributions is good.

Reynolds number of three million. - Test data and correlations are presented for three million Reynolds number in figures 28 through 36. Agreement between the CFF data and the NASA data generally follow the same patterns as were described for the six million Reynolds number data.

Reynolds number of nine million. - No NASA data were available at nine million Reynolds number. Therefore, the data for this Reynolds number are presented without any correlation in figures 37 through 42. These data, however, appear to be consistent with the other results.

Reynolds number of twelve million. - Data for R_N = 12 million are given in figures 43 through 54. Correlation of the subcritical force characteristics for M = 0.6 between the NASA and CFF data is presented in figure 43. Agreement is good, except that the drag of the CFF data is higher than the NASA data. This difference is believed to be associated with movement of the boundary layer transition location to the airfoil leading edge in the CFF tests. This will be discussed further in the Reynolds Number Effects section.

Correlation of force data from the CFF, NASA and NAE tunnels is presented for a Mach number of 0.70 in figure 45. Agreement between the three sets of normal-force and pitching-moment data is generally good. The main differences are in that the NAE data has a more positive α_o than the NASA and CFF data which agree closely. All three sets of data have difference values of C_{m_o} but show similar variation of pitching-moment with increasing normal-force. The drag data at M = 0.70 from the NASA and NAE tunnels agree fairly well and the CFF drag data is influenced by an apparent difference in transition location.

Correlation of force data for a Mach number of 0.75 from the three tunnels is shown in figure 47. Normal-force and pitching-moment characteristics follow the same patterns as described for a Mach number of 0.70. The drag data show a spread that is exaggerated by the differences in Mach number at which the data were taken. At M = .75, the airfoil is well into the drag rise, as can be seen in figure 48, and small differences in Mach number cause large variations in drag.

Correlation of airfoil pressure distributions between the NASA data and the CFF data at a Reynolds number of 12 million are shown for Mach numbers of 0.60, 0.70, and 0.75 in figures 49 through 52. Agreement follows the same pattern as was discussed for the six million Reynolds number data.

Correlation of the NAE pressure distribution data with the CFF data is shown in figures 53 and 54. Inspection of the subcritical comparison ($M = 0.70$, $\alpha = 0°$), shows slight differences over most of the airfoil surface. These differences are most likely due to the difference in wall effects between the CFF data (porosity = 4%, slanted) and the NAE data (porosity = 20%, normal).

The apparent influence of the wind tunnel walls can be more dramatically seen in figure 54 which shows the airfoil pressure distributions at supercritical conditions ($M = .75$, $\alpha = 3°$). The more aft shock location and reduced trailing-edge separation of the NAE data follows the trend shown in figure 15 for increasing porosity. It should be noted that the Mach number differences for the two sets of data may account for part of the difference in shock location and separation pattern.

Reynolds number of seventeen million. - An additional set of correlation data for the three tunnels is presented in figures 55 through 67 for a Reynolds number of 17 million. Generally, the correlations indicate similar trends to that previously discussed for 12 million Reynolds number. The one exception is the variation in angle of attack for zero normal-force. The NASA data show a positive shift in α_o that does not occur at other Reynolds numbers. In addition, the NAE data show a slightly different α_o as previously mentioned. For a given angle of attack, this results in small differences in normal-force coefficient. Part of the disagreement in correlation of the pressure distributions in figures 61 to 67 is due to the differences in normal-force coefficient for a constant angle of attack.

Reynolds number at facility maximum. - The facility maximum Reynolds number data are shown in figures 68 through 77. The comparison of CFF and NAE data at this Reynolds number indicates the same trends as the lower Reynolds number data.

Trailing Edge Pressure Coefficient Variation

The variation of airfoil trailing edge pressure coefficient with Mach number is presented in figures 78, 79 and 80 for all the Reynolds numbers tested. As can be seen the Mach number for trailing edge pressure divergence decreases rather rapidly with increasing angle of attack. Also, as Reynolds number is increased the Mach number for trailing edge pressure divergence increases. The largest improvement occurs between 3 and 9 million Reynolds number.

Shock Location

The shock locations for various flow conditions are summarized in figure 81. The shock location is defined as the chordwise point on the airfoil where the shock discontinuity in the pressure distribution is initiated. For conditions where the flow behind the shock remains attached, the data in figure 81 indicates the shock location moves progressively rearward as Mach number is increased and there is very little change in shock location as angle of attack is varied (at a constant Mach number). As shock-induced separation occurs, the shock location begins to move forward with increasing angle of attack.

For conditions where a strong shock exists but no shock-induced separation is present (e.g. $M = 0.75$, $\alpha = 0°$), the effect of Reynolds number on shock location, as shown in figure 81, is minimal. However, for cases where shock-induced separation is present (e.g. $M = 0.75$, $\alpha = 3°$) a small change in shock location does occur (approximately 5% chord).

Reynolds Number Effects

In this section the effects of Reynolds number on airfoil characteristics will be summarized. Some correlation of Reynolds number effects obtained from the NASA 8-foot transonic pressure tunnel and the NAE 15 x 60 two-dimensional test facility will be included.

A summary of airfoil force parameters at a Mach number of 0.6 is shown in figure 82. The corresponding parameters obtained from the NASA 8-foot transonic

pressure tunnel data are included. The angle for zero normal force for the CFF data was found to be unaffected by Reynolds number. The normal-force curve slope was found to show a modest scale effect up to $R_N = 10 \times 10^6$. The pitching moment at zero normal force was found to be unaffected by Reynolds number, but the parameter, dc_m/dc_n, shows a modest scale effect up to $R_N = 10 \times 10^6$. The NASA data agree well with the Reynolds number effects observed in the CFF data.

Similar Reynolds number data for M = 0.7 is shown in figure 83 for the data from the CFF, NASA, and NAE tunnels. The Reynolds number effects shown by the CFF data follow the same pattern as the M = .6 data and are generally supported by the NASA and NAE data.

The Reynolds number effects upon subcritical airfoil drag are shown in figure 84 for M = 0.6. The NASA data show a conventional scale effect that would match theoretical drag calculations for transition at 5% chord. The CFF free transition drag data indicate that transition moves to the airfoil leading edge at $R_N = 9 \times 10^6$. The fixed transition data for a grit strip at 5% chord matches the NASA data at $R_N = 3$ and 6×10^6, but at 9 and 12 million Reynolds number, the fixed transition drag data matches the free transition data at a level 6 to 8 counts higher than the NASA data for transition at 5% chord. This same trend is evident in the Reynolds number effects on drag at M = 0.7 shown in figure 85. It is significant to note that the NAE data serves to bridge between the NASA data and CFF data at Reynolds numbers between 12 and 17 million Reynolds number. It is suspected that this transition movement 5% chord to the leading edge in the CFF tests relative to the NASA data is caused by differences in either the freestream turbulence levels or model relative surface finish.

The effect of Reynolds number on trailing edge pressure for attached and separated flow are presented in figure 86. The attached flow condition of M = 0.75 and $\alpha = 0°$ shows a modest effect of Reynolds number. The separated flow condition chosen is M = 0.75 and $\alpha = 3°$ which exhibits a substantial Reynolds number effect. Similar effects are shown for the movement of upper surface shock location in figure 86. At attached flow condition of M = 0.75 and $\alpha = 0°$ the shock does not move at all over the entire Reynolds number

range investigated. However, for the separated flow conditions of $M = 0.75$ and $\alpha = 3^\circ$ the shock does move aft about 5% of the airfoil chord over the Reynolds number range from 3 to 32 million.

CONCLUSIONS

A test program has been conducted on a NACA 65_1-213, a = 0.5 airfoil over the Mach number range from 0.6 to 0.8 at various angles of attack and at Reynolds numbers from 3 to 32 million based on chord. These data have been presented in both basic data form and summary form with correlation data from two other test facilities included.

Analysis of these data has produced the following conclusions:

1. Variations in wind tunnel wall porosity resulted in small changes in the aerodynamic performance of the airfoil for conditions where the flow was attached. However, for cases where shock-induced separation was present, wall porosity was found to have a significant effect on the airfoil characteristics.

2. Correlation of the test data from the present tests with the NASA 8-foot transonic pressure tunnel data and the NAE 15 x 60 inch two-dimensional test facility data indicated that generally good agreement was obtained.

3. The effects of varying the Reynolds number on the normal-force and pitching-moment characteristics were found to be generally small. For attached flow conditions, the effect of varying Reynolds number on drag coefficient was generally consistent with conventional flat plate drag variations. Also, for attached flow large Reynolds number variations had practically no effect on shock location. For shock induced separated flow conditions, Reynolds number had a substantial effect on trailing-edge pressure coefficients and the shock location moved aft about 5 percent of the airfoil chord.

REFERENCES

1. Pounds, G. A.; and Stanewsky, E.: The Research Compressible Flow Facility. Lockheed-Georgia Company ER-9219, 1967.

2. Burdges, Kenneth P.; Blackwell, James A., Jr.; and Pounds, Gerald A.: High Reynolds Number Test of a NASA 10-Percent-Thick Supercritical Airfoil Section at Transonic Speeds. NASA CR132468, 1974. (Title unclassified, paper classified).

3. Pankhurst, R. C.; and Holder, D. W.: Wind-Tunnel Technique. Sir Isaac Pitman & Sons Ltd., London, p 276, 1965.

4. Braslow, Albert L.; and Knox, Eugene C.: Simplified Method for Determining of Critical Height of Distributed Roughness Particles for Boundary Layer Transition at Mach Numbers from 0 to 5. NACA TN 4363, 1958.

5. Garner, H. C.; Rogers, E. W. E.; Acum, W. E. A.; and Maskell, E. C.: Subsonic Wind Tunnel Wall Corrections, AGARDograph 109, 1966.

TABLE I. - DESIGN ORDINATES FOR NACA 65_1-213, a = 0.5 AIRFOIL

UPPER SURFACE	
X/C	Z/C
0.000	0.000
.384	1.062
.621	1.291
1.105	1.643
2.335	2.283
4.814	3.258
7.305	4.024
9.804	4.672
14.812	5.713
19.831	6.511
24.857	7.116
29.889	7.559
34.924	7.848
39.964	7.983
45.008	7.943
50.066	7.707
55.115	7.255
60.134	6.634
65.138	5.889
70.130	5.044
75.112	4.138
80.089	3.191
85.061	2.244
90.035	1.332
95.013	0.530
100.0	0.0

LOWER SURFACE	
X/C	Z/C
0.000	0.000
0.616	0.924
.879	-1.097
1.395	-1.349
2.665	-1.765
5.186	-2.376
7.695	-2.836
10.196	-3.220
15.188	-3.817
20.169	-4.263
25.143	-4.592
30.111	-4.823
35.076	-4.962
40.036	-5.011
44.992	-4.947
49.934	-4.767
54.885	-4.469
59.866	-4.072
64.862	-3.599
69.870	-3.062
74.888	-2.486
79.911	-1.885
84.939	-1.286
89.965	- .718
94.988	- .242
100.0	0.0

Leading Edge Radius = 1.174 Percent Chord

Slope of radius through L.E. = 0.084

TABLE II. - ORIFICE LOCATIONS FOR NACA 65_1-213, a = 0.5 AIRFOIL MODEL

Orifice No.	Model Surface	Location X/C	Location Distance off ℄ % Span	Orifice No.	Model Surface	Location X/C	Location Distance off ℄ % Span
1	Upper	0.	.05	34	Lower	.01	.05
2	↓	.01	↓	35	↓	.02	↓
3		.02		36		.05	
4		.05		37		.075	
5		.075		38		.10	
6		.10		39		.15	
7		.15		40		.17	
8		.20		41		.30	
9		.25		42		.35	
10		.30		43		.40	
11		.35		44		.45	
12		.375		45		.50	
13		.40		46		.55	
14		.425		47		.60	
15		.45		48		.65	
16		.475		49		.70	
17		.50		50		.80	
18		.525		51		.90	
19		.5375		52		.95	
20		.55		53	Upper	.35	.25
21		.5625		54	↓	.40	↓
22		.575		55		.45	
23		.5875		56		.48	
24		.60		57		.55	
25		.625		58		.60	
26		.65		59		.65	
27		.71		60		.70	
28		.75		61		.50	0.00
29		.80		62		↓	.1
30		.85		63			.15
31		.90		64	↓	↓	.35
32		.95	↓	65			.45
33	↓	.97					

TABLE III. - NOMINAL TEST CONDITION MATRIX FOR 65_1-213, a = 0.5 AIRFOIL

LOW REYNOLDS NUMBER STUDY
R_N = 3, 6, 9, 12 x 10^6

α	M = .60	.68	.70	.72	.75	.78	.80
-1	X	X	X	X	X	X	X
0	X	X	X	X	X	X	X
1	X	X	X	X	X	X	X
2	X	X	X	X	X		
3	X	X	X	X	X		
4	X	X	X	X			
5	X	X	X				
6	X	X	X				
8	X						

HIGH REYNOLDS NUMBER STUDY
R_N = 17 x 10^6 AND FACILITY MAXIMUM*

α	M = .60	.68	.70	.72	.75	.78
-1	X	X	X	X	X	X
0	X	X	X	X	X	X
1	X	X	X	X	X	X
2	X	X	X	X	X	
3	X	X	X	X	X	
4	X	X	X	X		
6						
8						

*Facility Maximum R_N = 25 x 10^6 for M = 0.60
Facility Maximum R_N = 32 x 10^6 for M = 0.68 to .80.

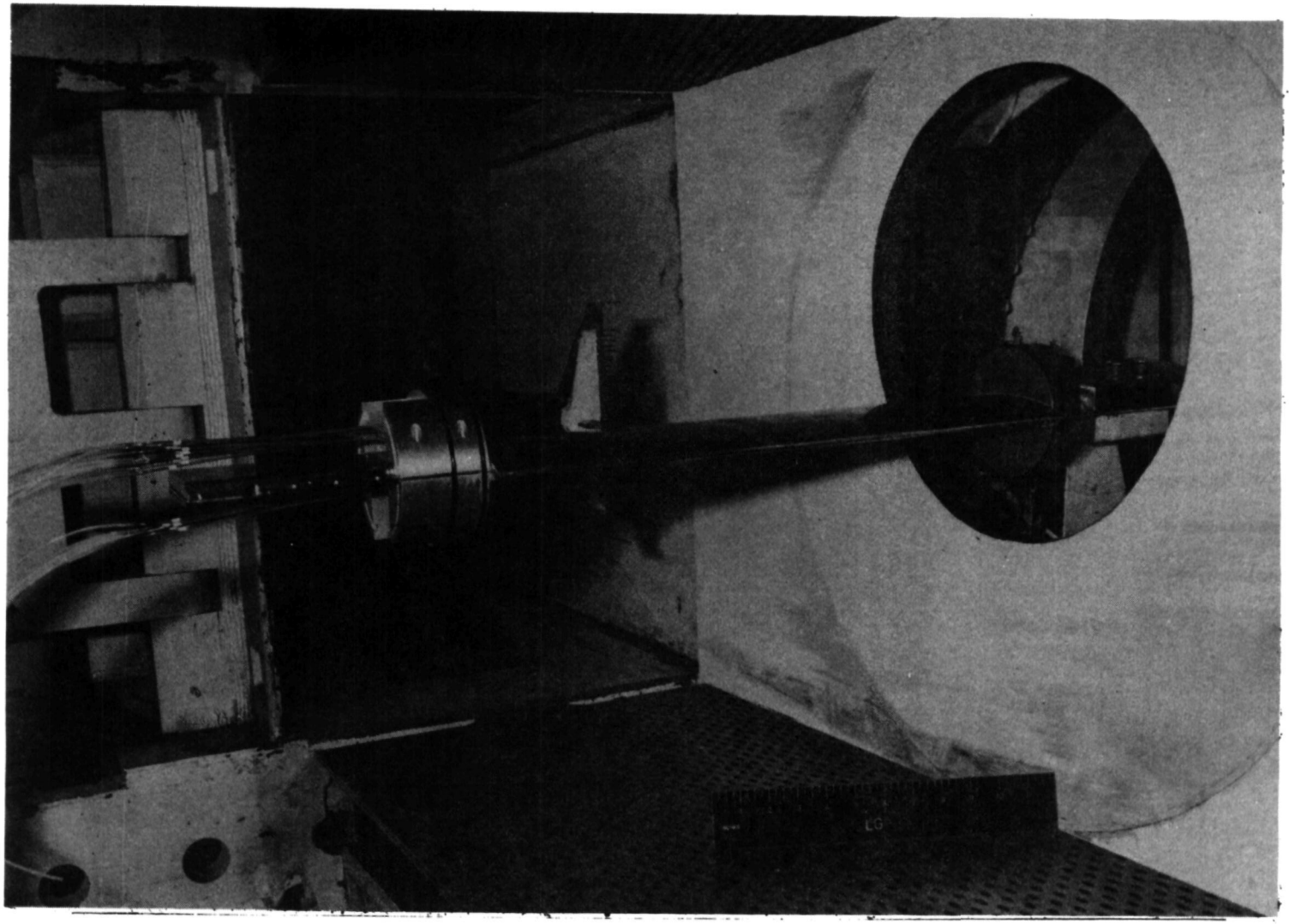

Figure 1 . - Model of NACA 65_1-213, a = 0.5 airfoil installed in CFF (left wall removed).

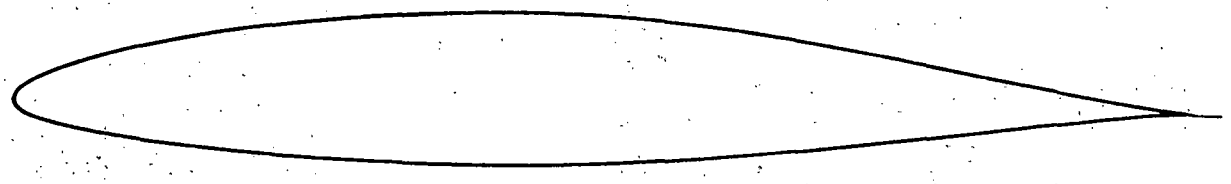

Figure 2 . - Sketch of NACA 65_1-213, a = 0.5 airfoil.

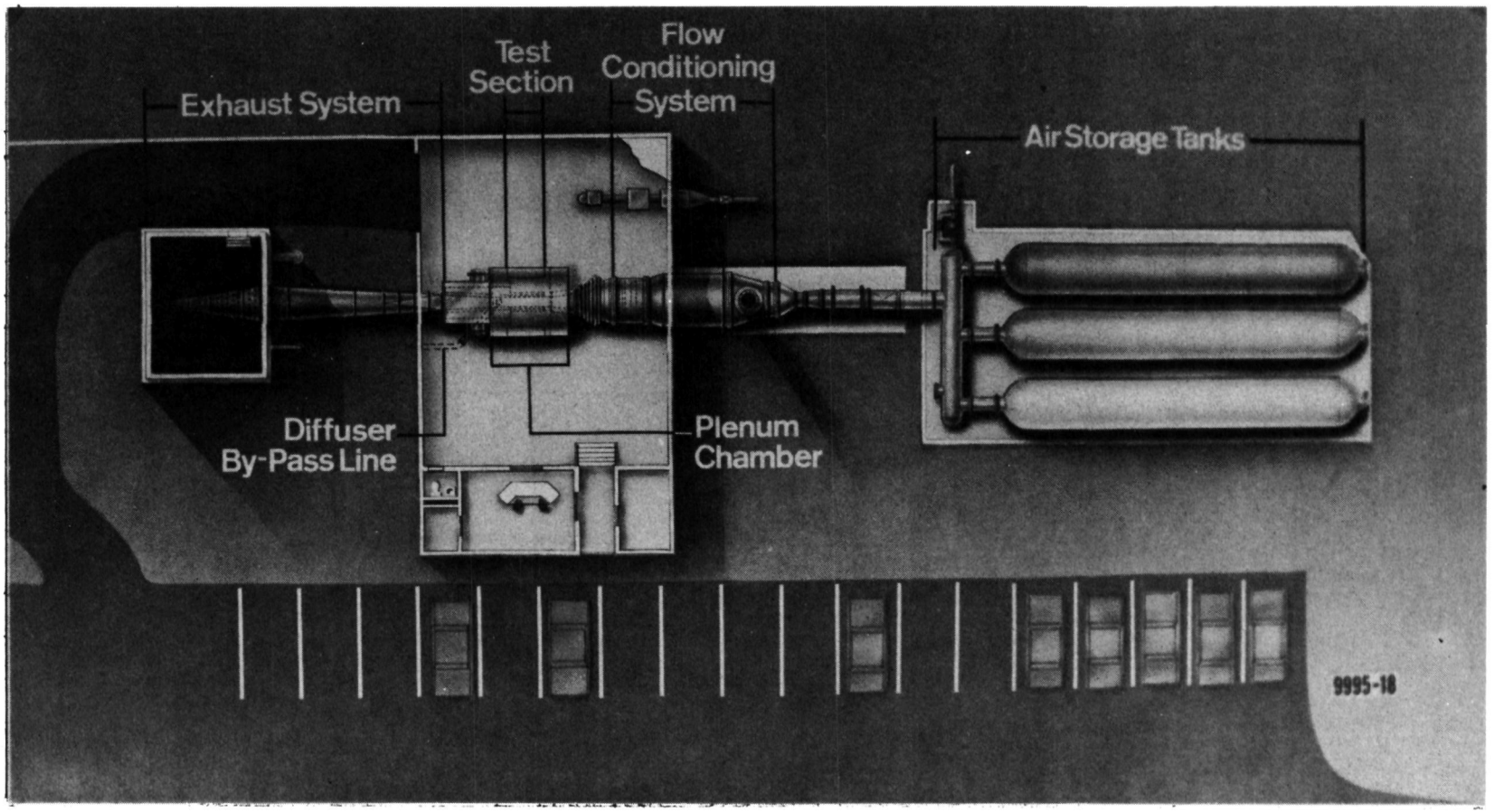

Figure 3 . - Lockheed-Georgia compressible flow facility.

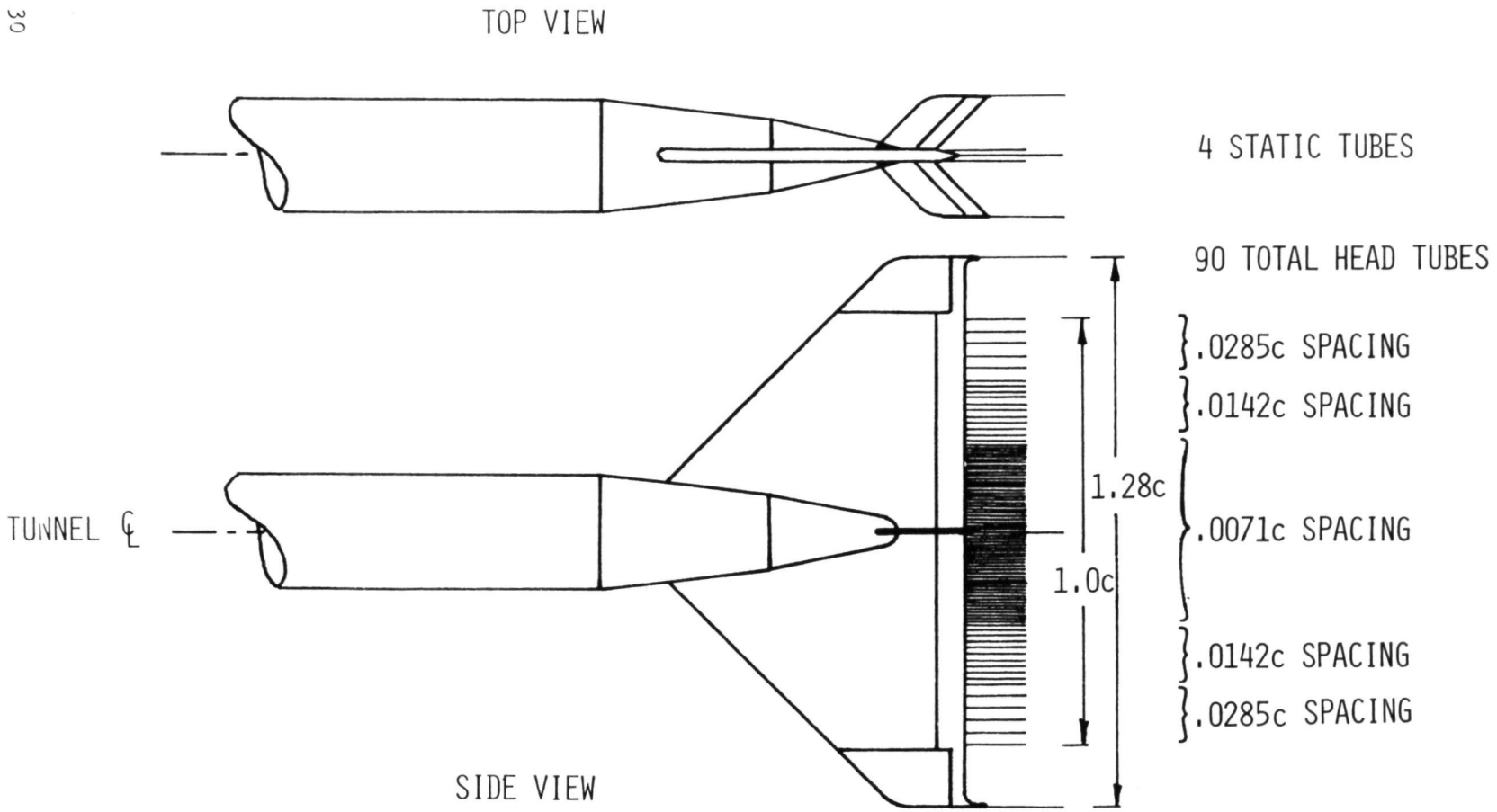

Figure 4. - Compressible flow facility wake rake.

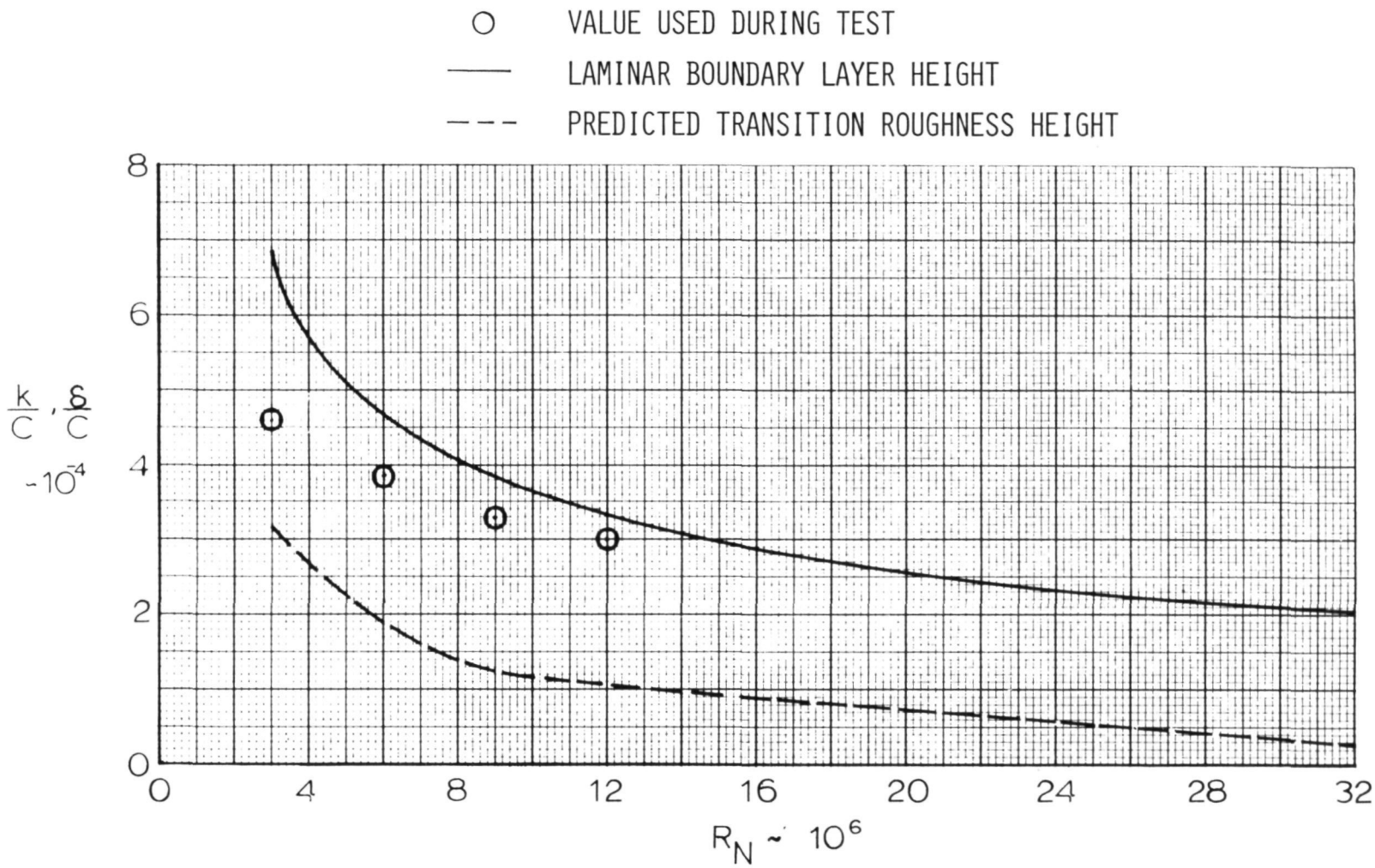

Figure 5. - Variation of laminar boundary layer height and transition particle size with Reynolds number. M = 0.6.

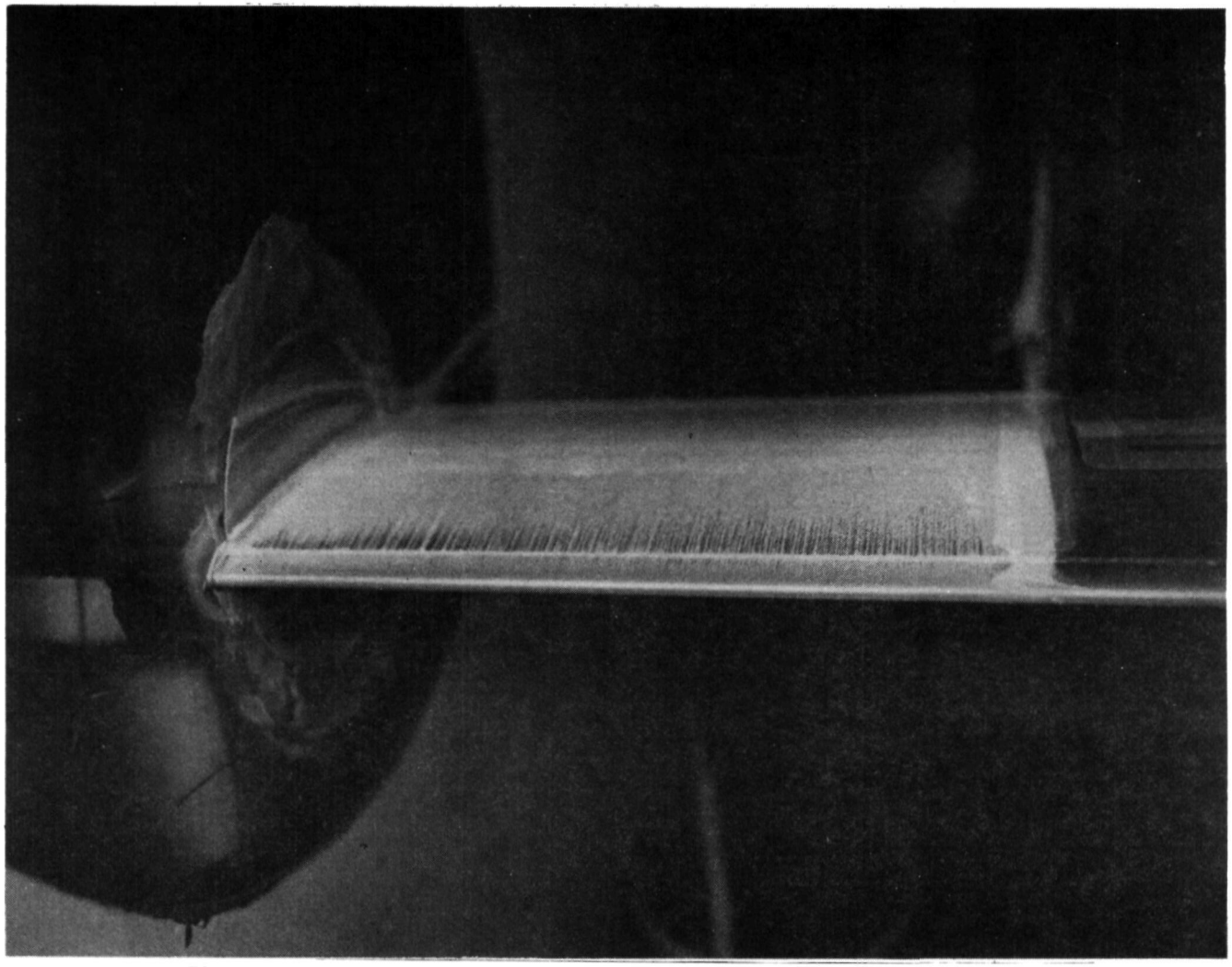

Figure 6. - Oil-flow photograph of airfoil upper surface, M = 0.60, $R_N = 6 \times 10^6$, $\alpha = 0°$, $X/C_T = .05$, k = .00039c.

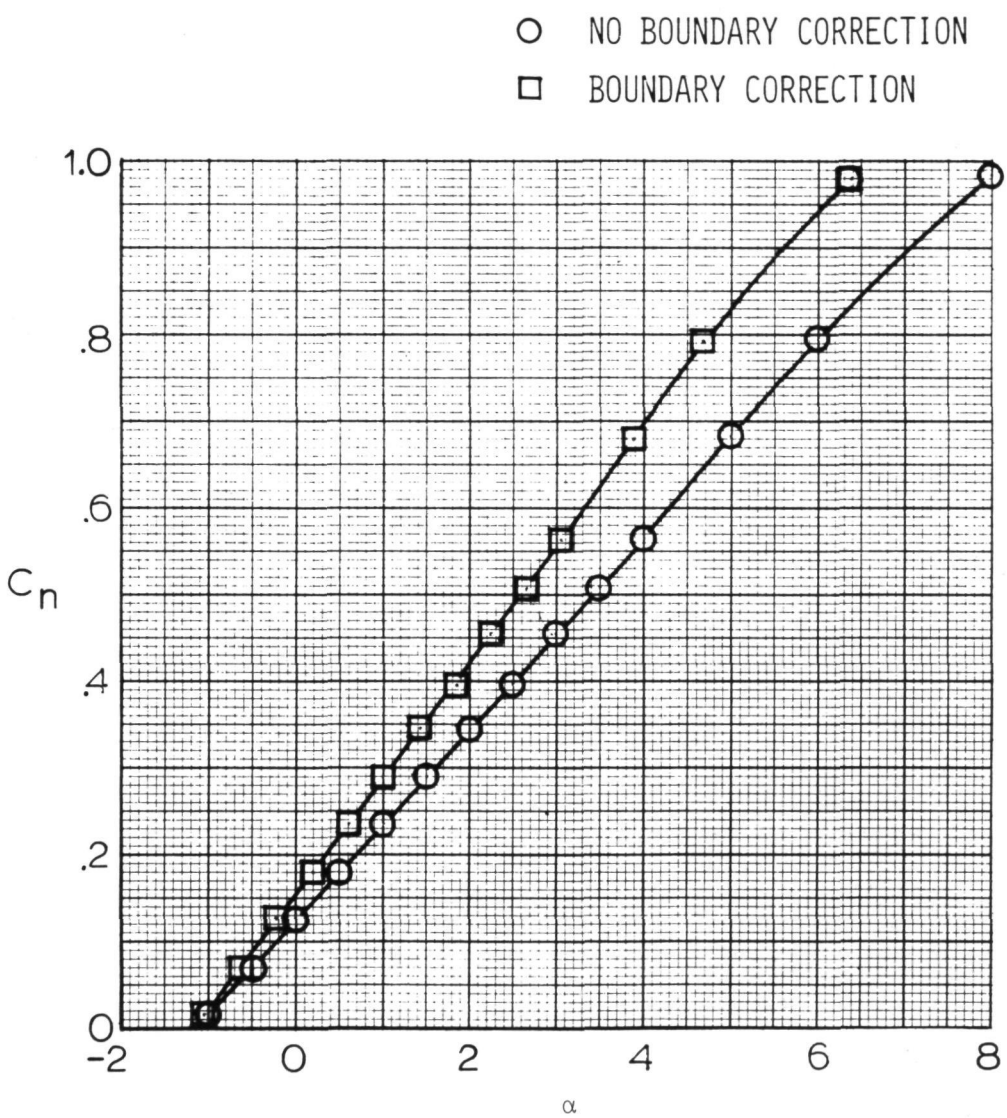

Figure 7 . - Effect of standard subsonic wind tunnel wall boundary corrections on the variation of section normal force with angle of attack. $M = 0.60$, $R_N = 6 \times 10^6$, porosity = 4%.

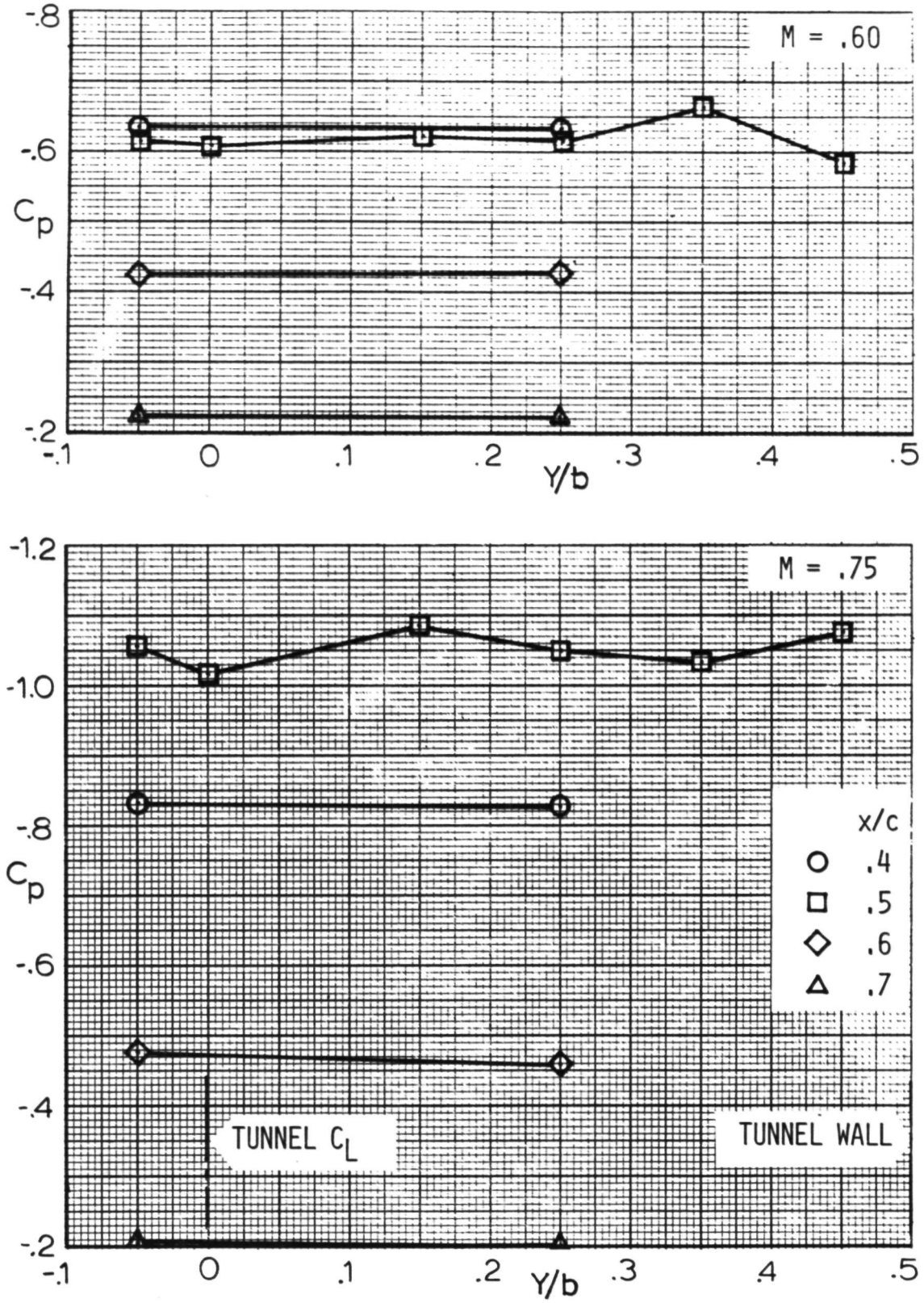

Figure 8 . - Variation of airfoil pressures across tunnel, $R_N = 6 \times 10^6$, $\alpha = 0°$.

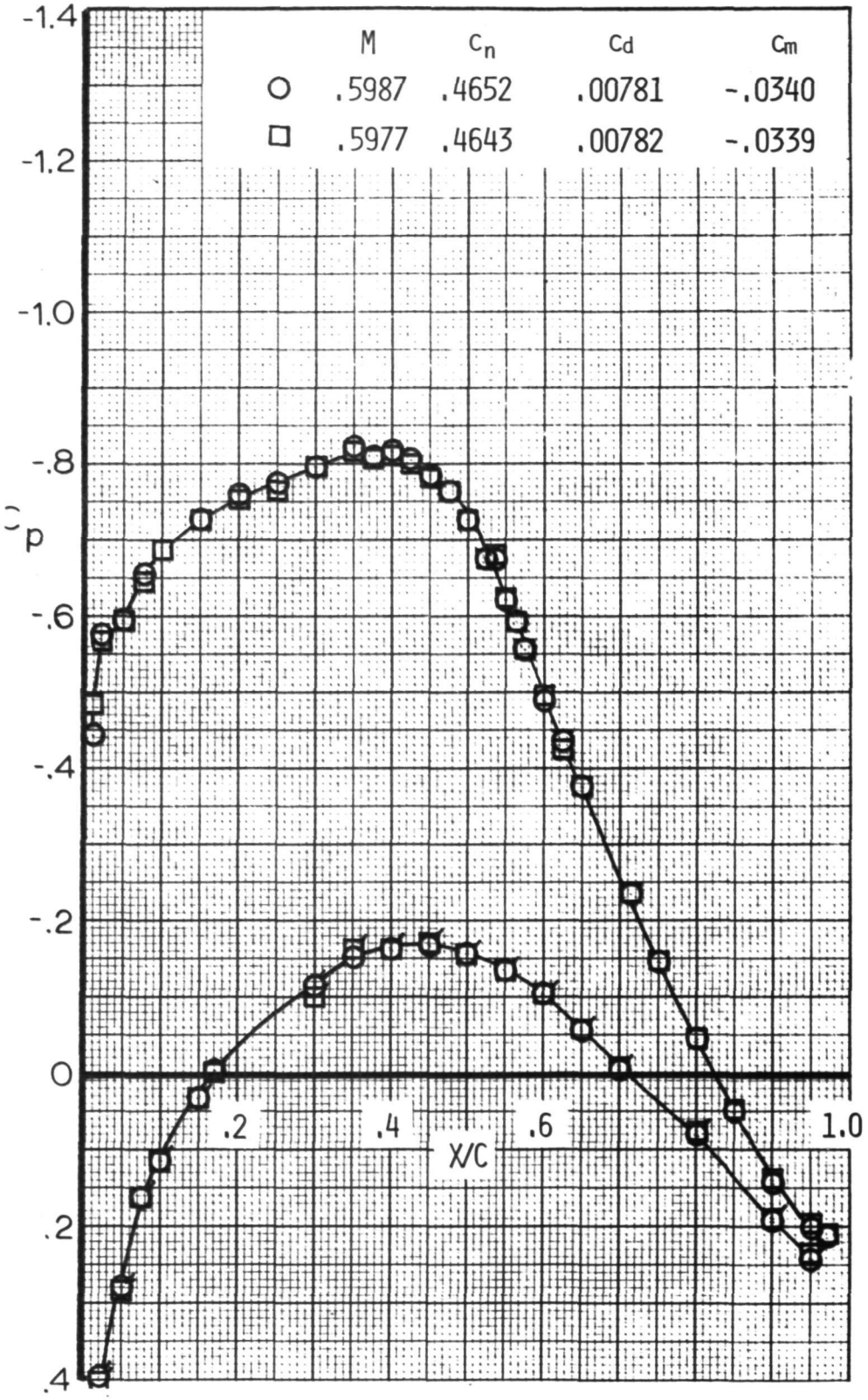

Figure 9. - Repeatability check at M = 0.6, $R_N = 26 \times 10^6$, $\alpha = 3°$ (Flags denote l.s.).

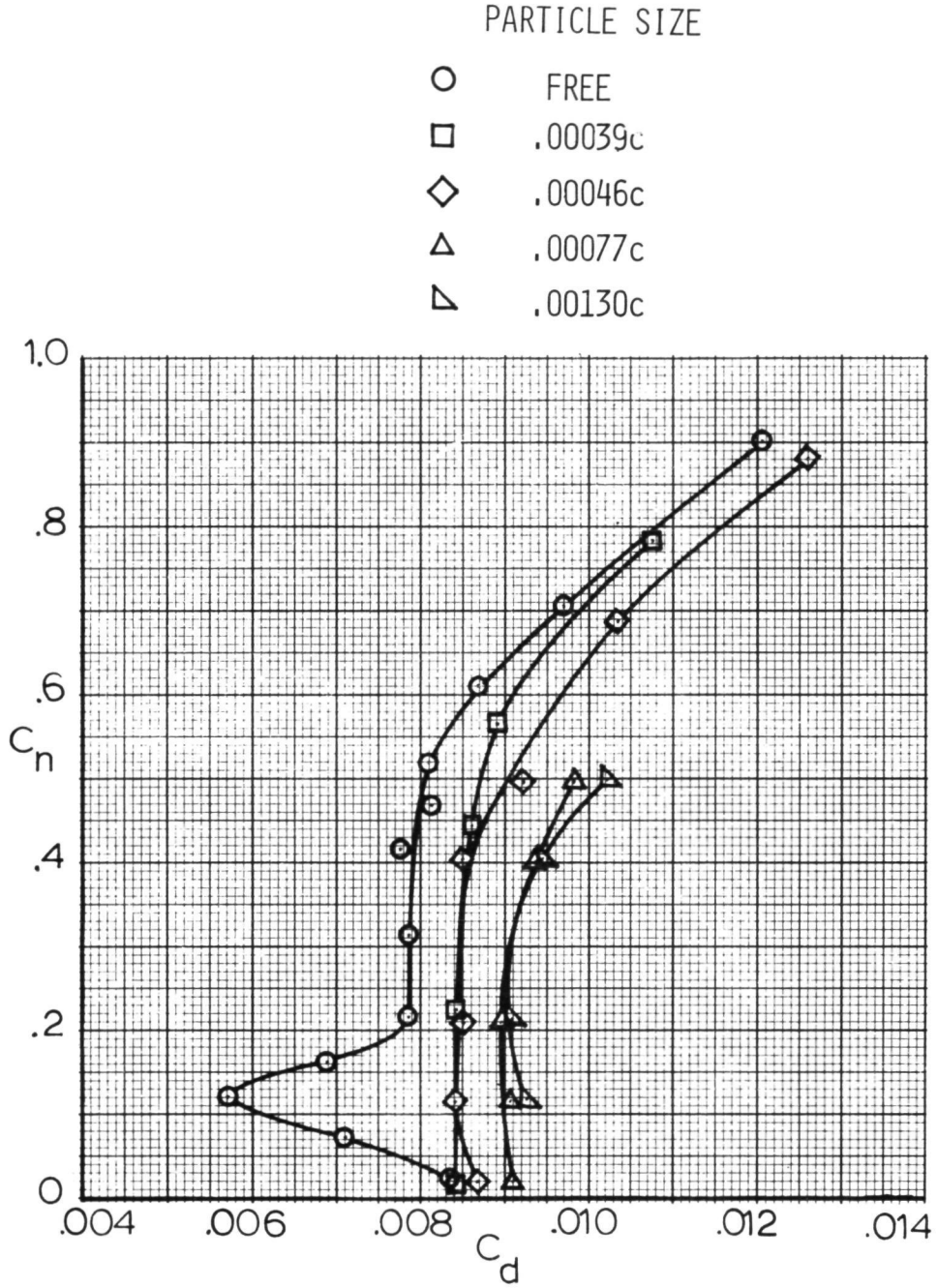

Figure 10. - Effect of transition particle size on drag, M = 0.6, $R_N = 6 \times 10^6$, $X/C_T = .05$, porosity = 6%.

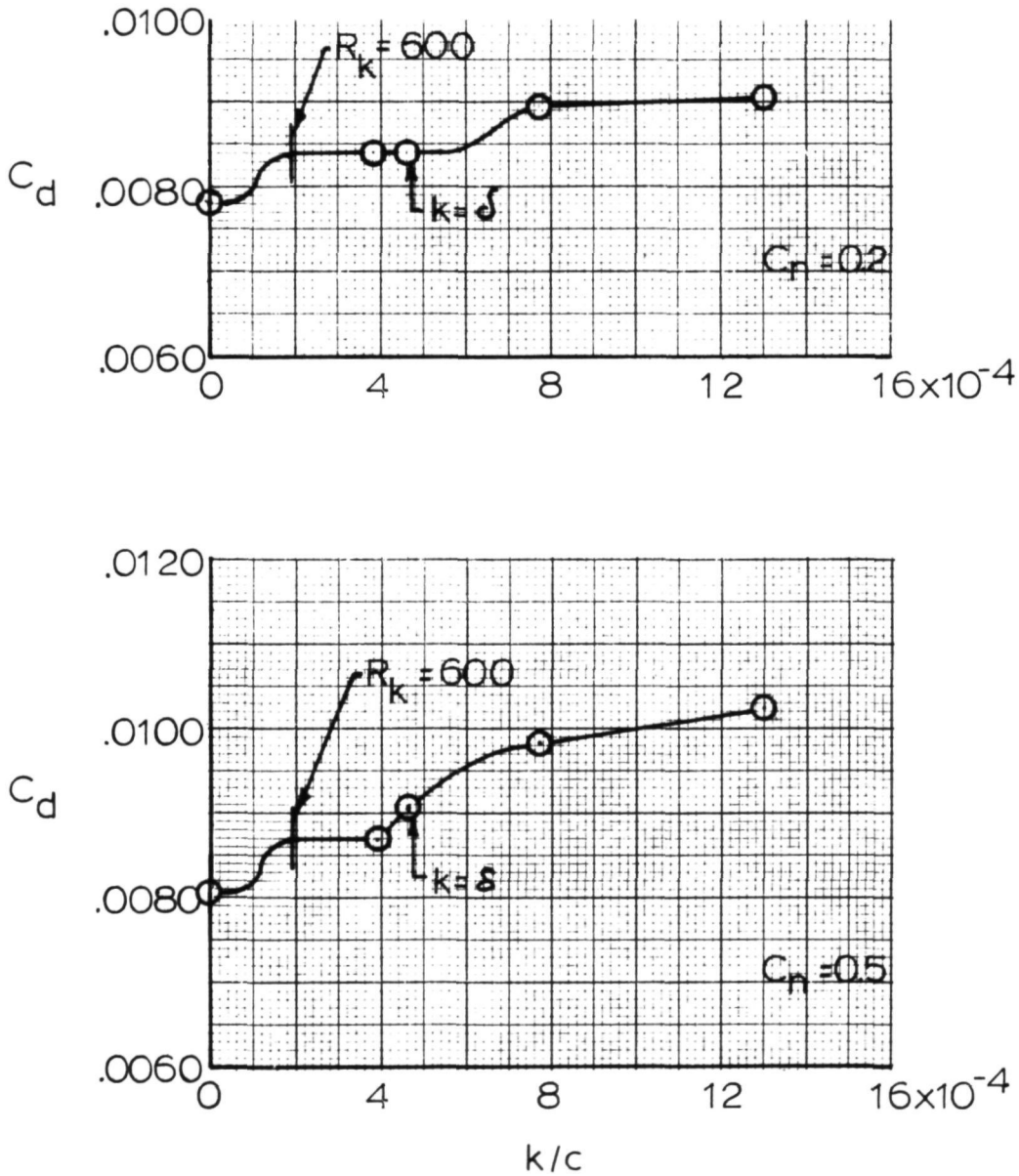

Figure 11. - Effect of transition particle size on drag, M = .6, $R_N = 6 \times 10^6$, $X/C_T = .05$.

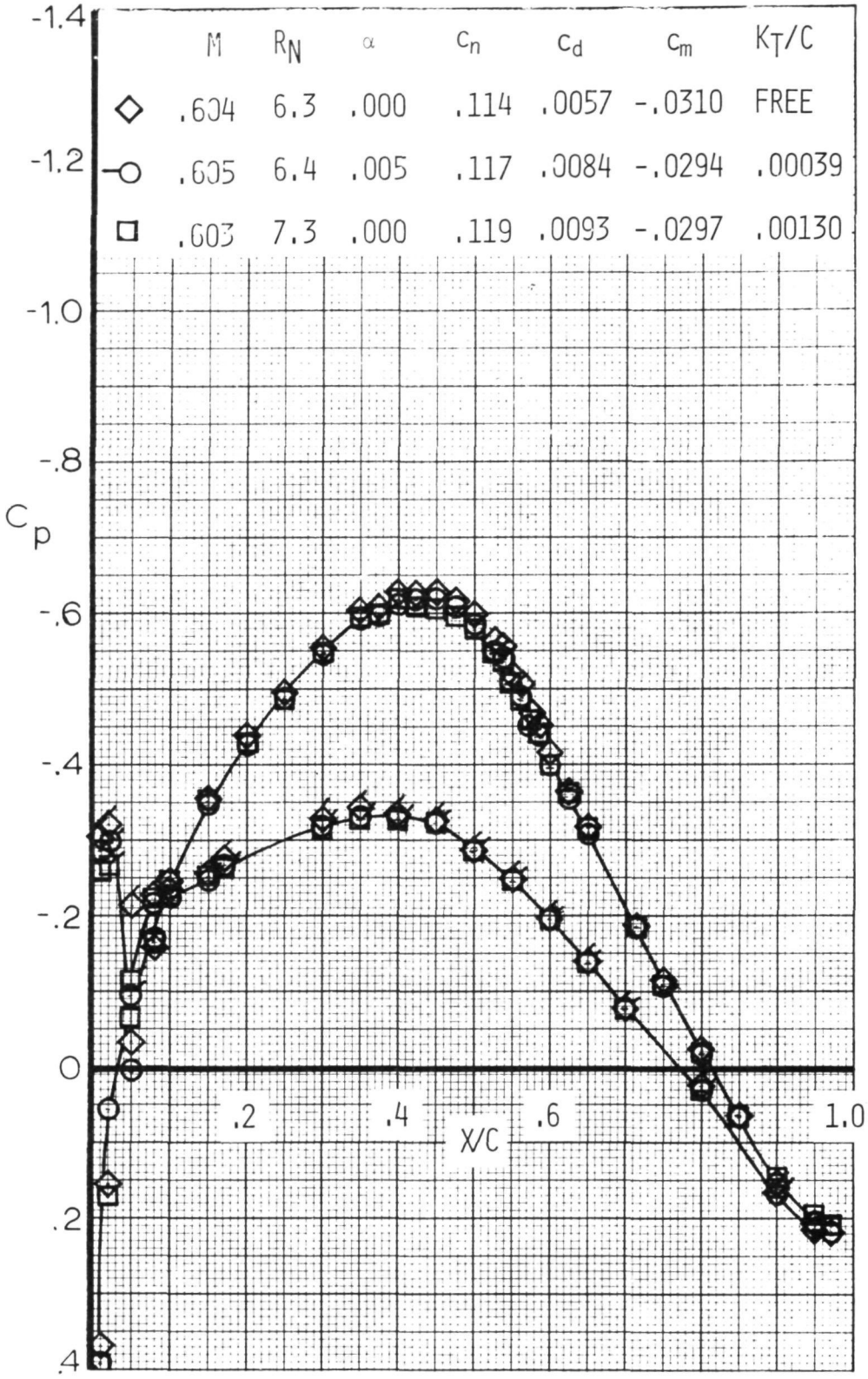

Figure 12. - Effect of transition particle size on airfoil pressure distribution, M = .6, R_N = 6 x 10 , X/C_T = .05, porosity = 6% (Flags denote l.s.)

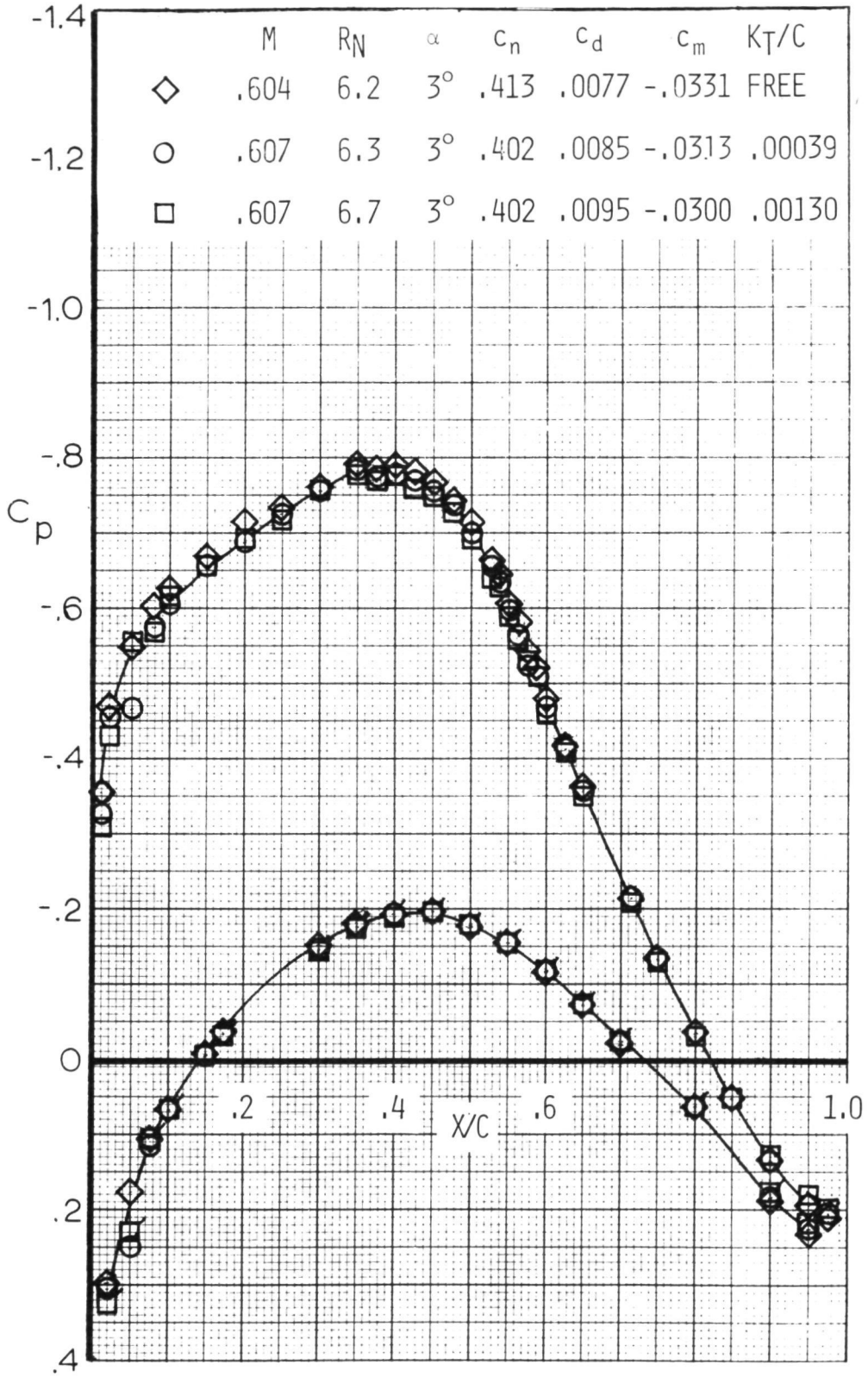

Figure 12.- Concluded.

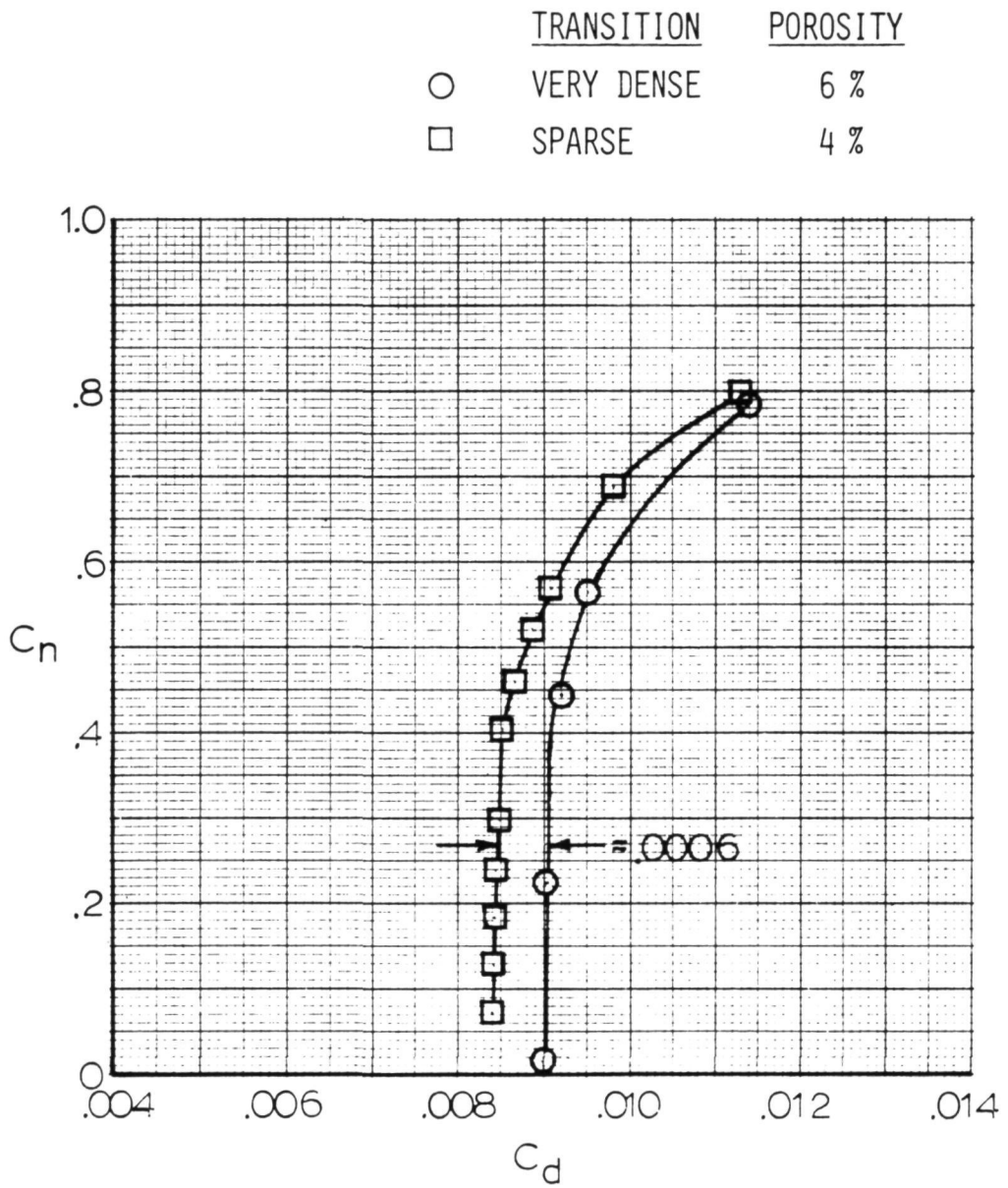

Figure 13. - Effect of transition particle density on drag, M = 0.6, $R_N = 6 \times 10^6$, $X/C_T = .05$, k = .00039c.

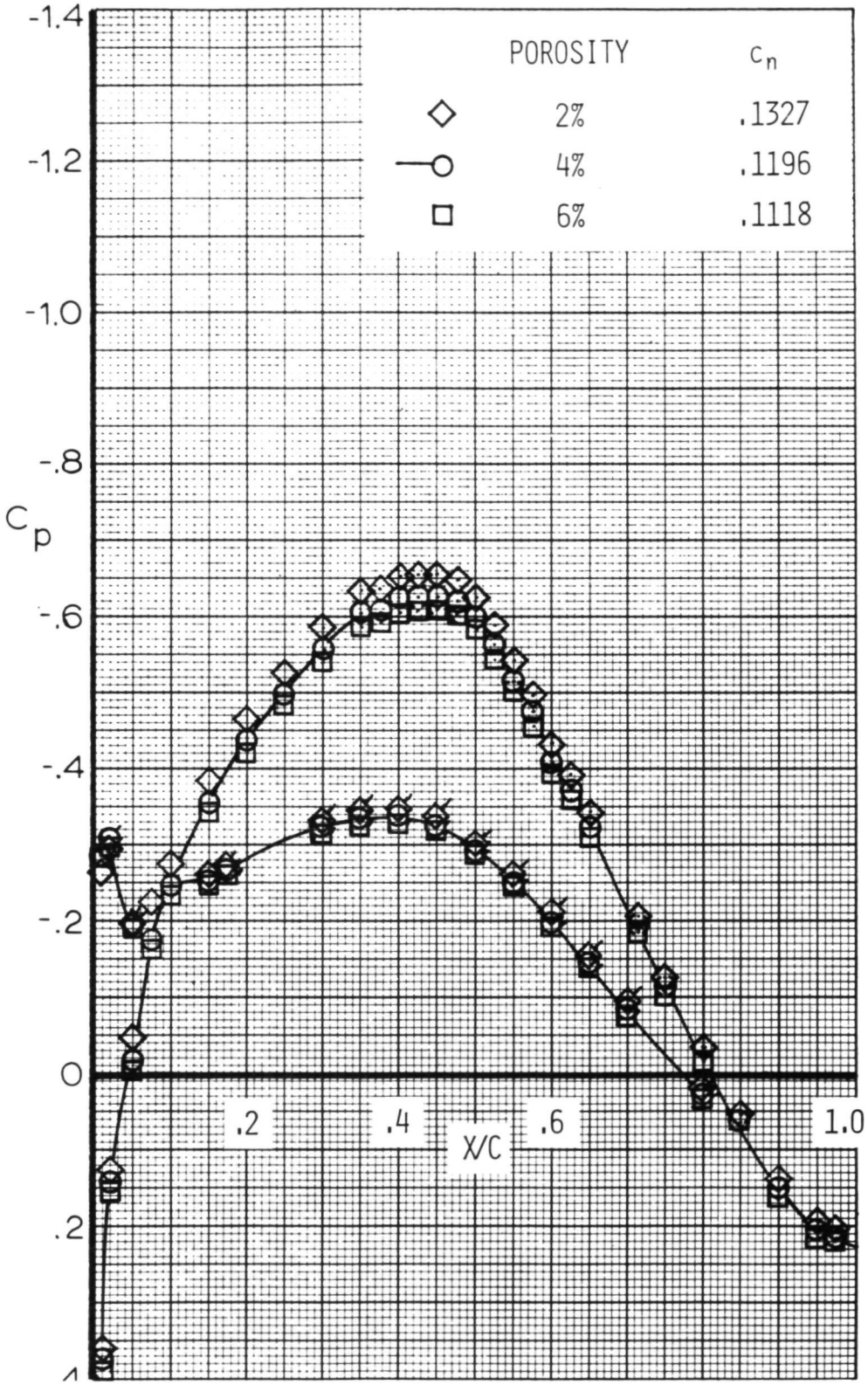

Figure 14. - Effect of wall porosity on airfoil pressure distribution at subcritical conditions for M = 0.6 and α = 0.0° (Flags denote l.s.).

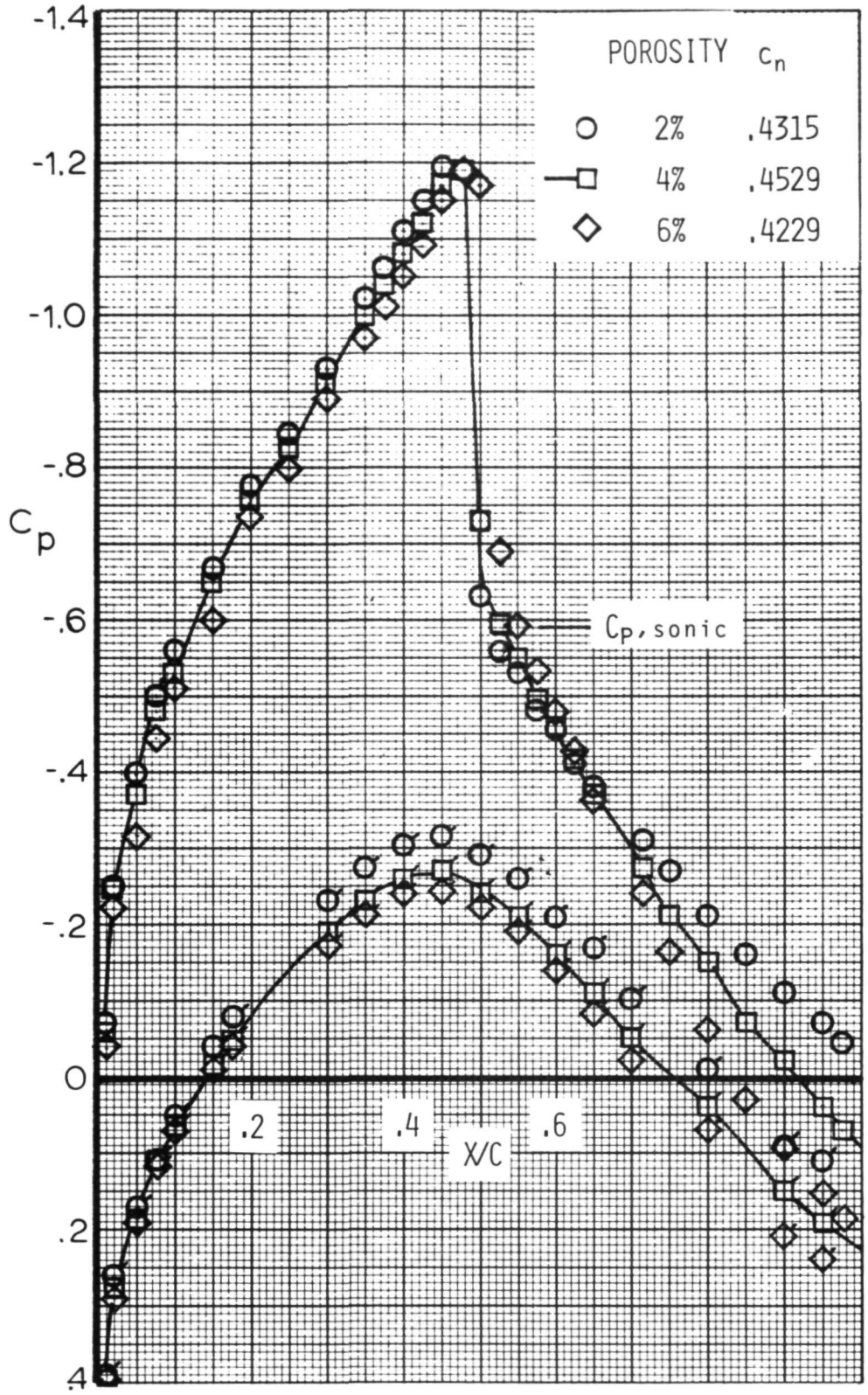

Figure 15. - Effect of wall porosity on airfoil pressure distribution at supercritical conditions for M = 0.75 and α = 3.0° (Flags denote l.s.).

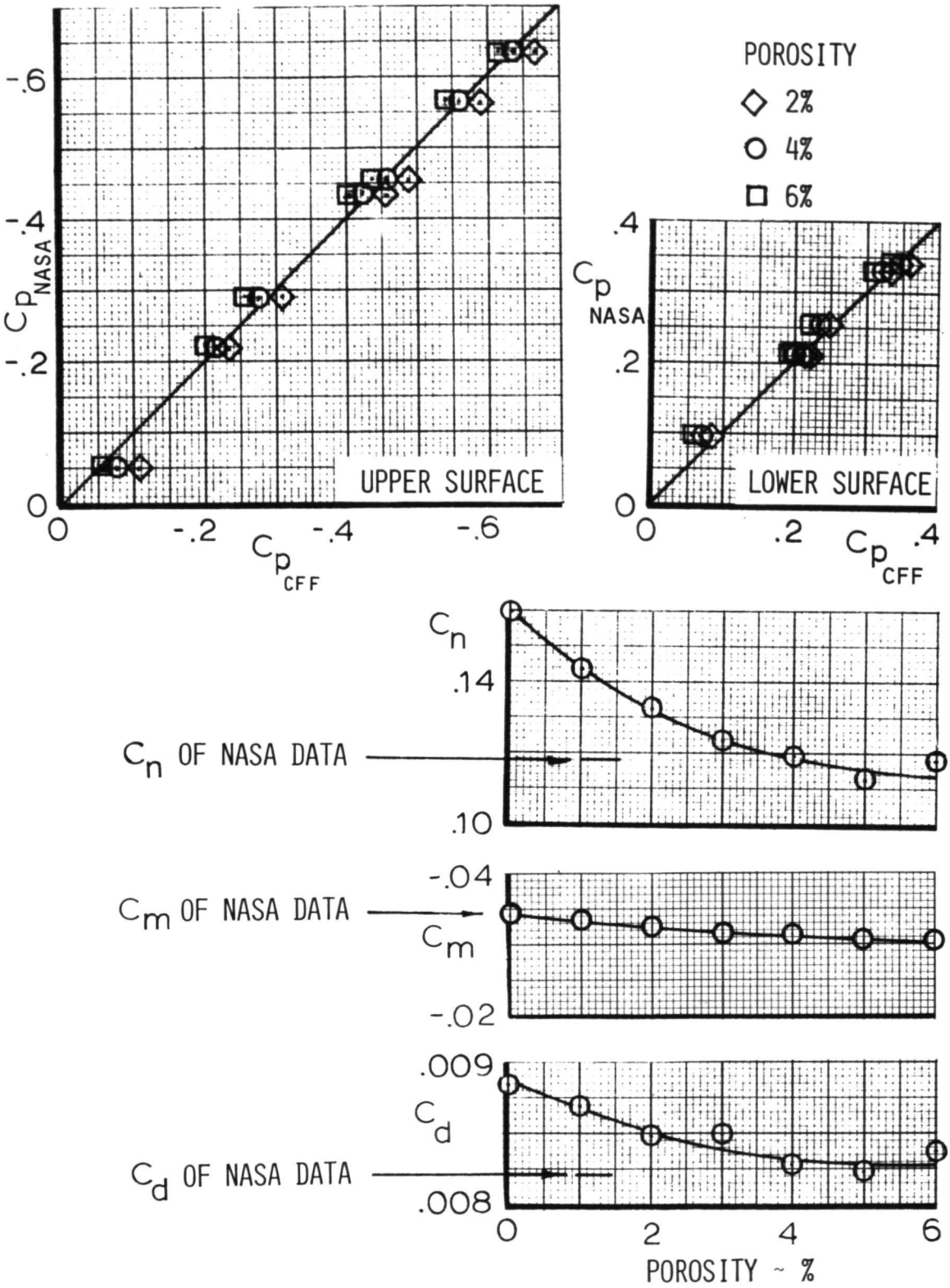

Figure 16. - Summary of porosity effects at subcritical conditions, $M = 0.6$, $R_N = 6 \times 10^6$, $X/C_T = .05$, $\alpha = 0°$.

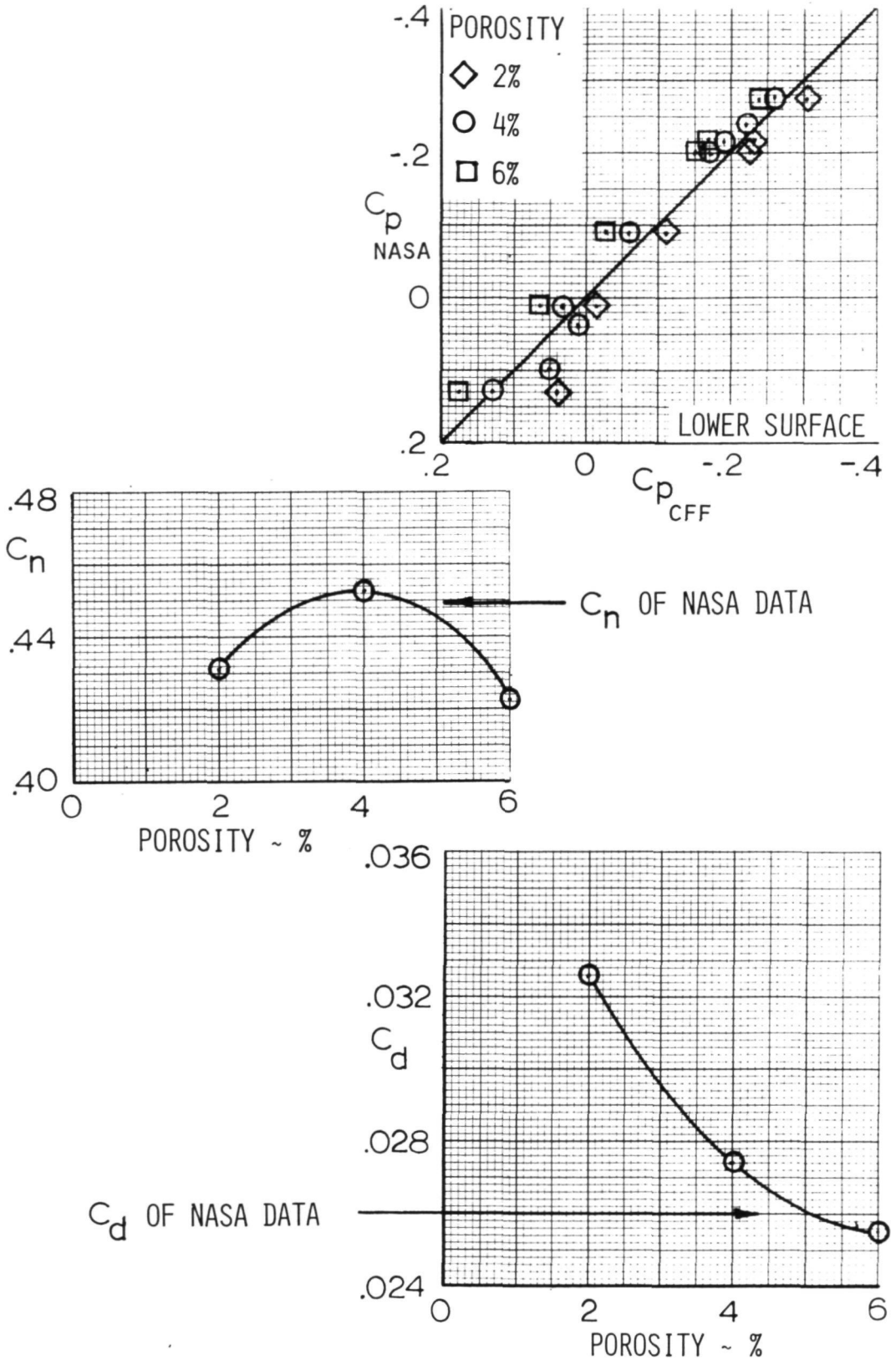

Figure 17. - Summary of porosity effects at supercritical conditions, $M = .75$ $R_N = 6 \times 10^6$, $X/C_T = .05$, $\alpha = 3°$.

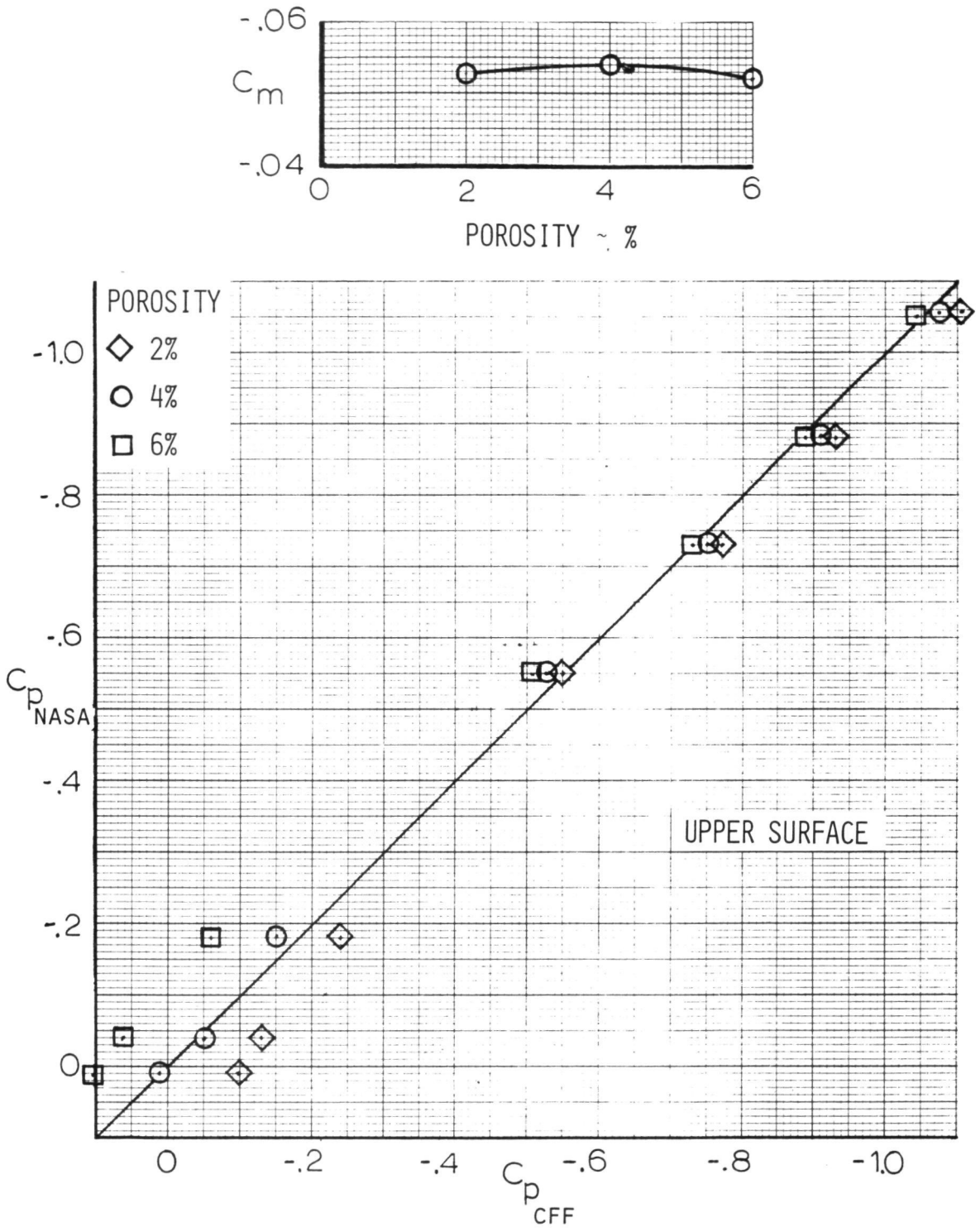

Figure 17 . - Concluded.

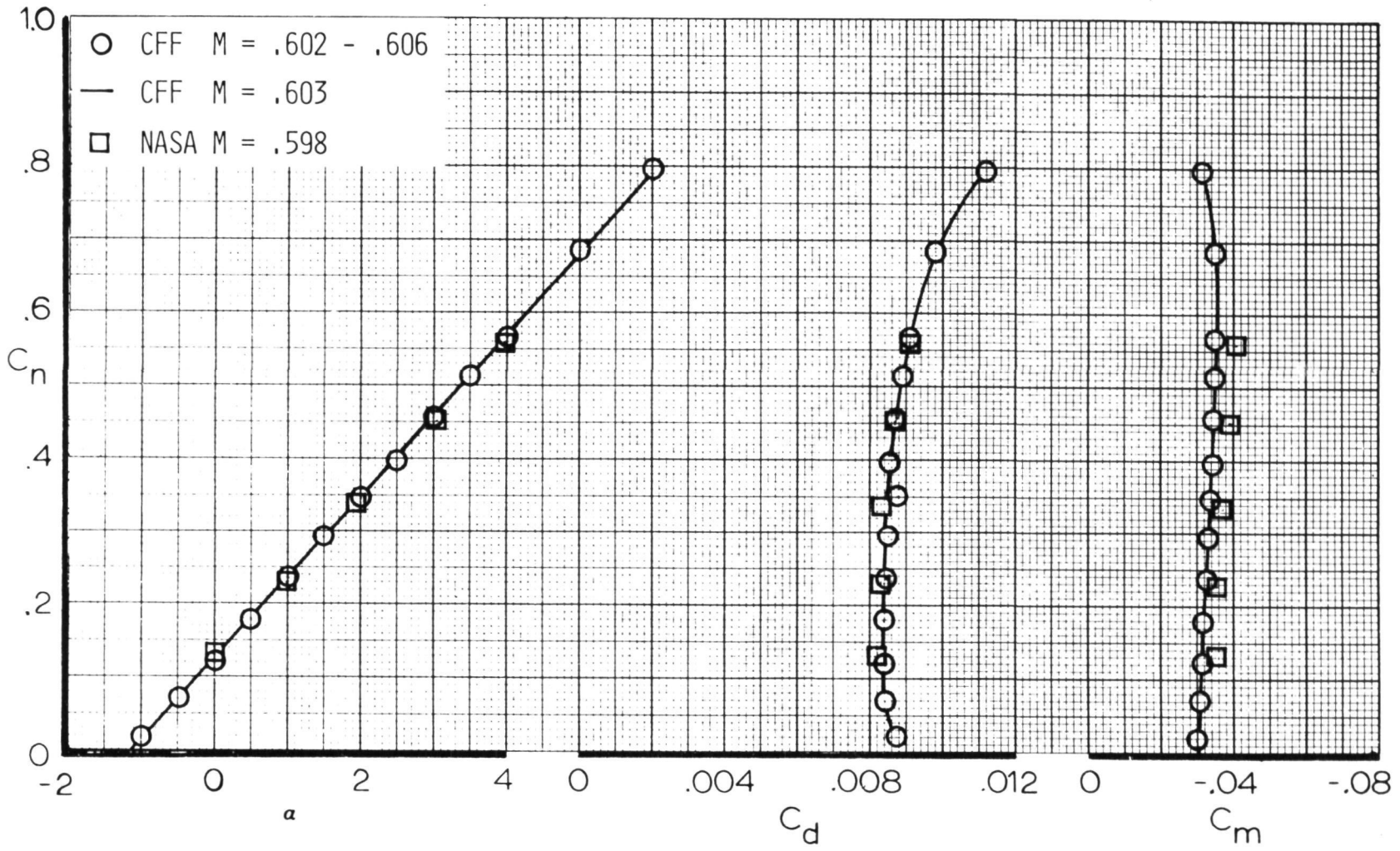

Figure 18. - Airfoil force data for M = 0.60 , R_N = 6 x 10^6, X/C_T = 0.05.

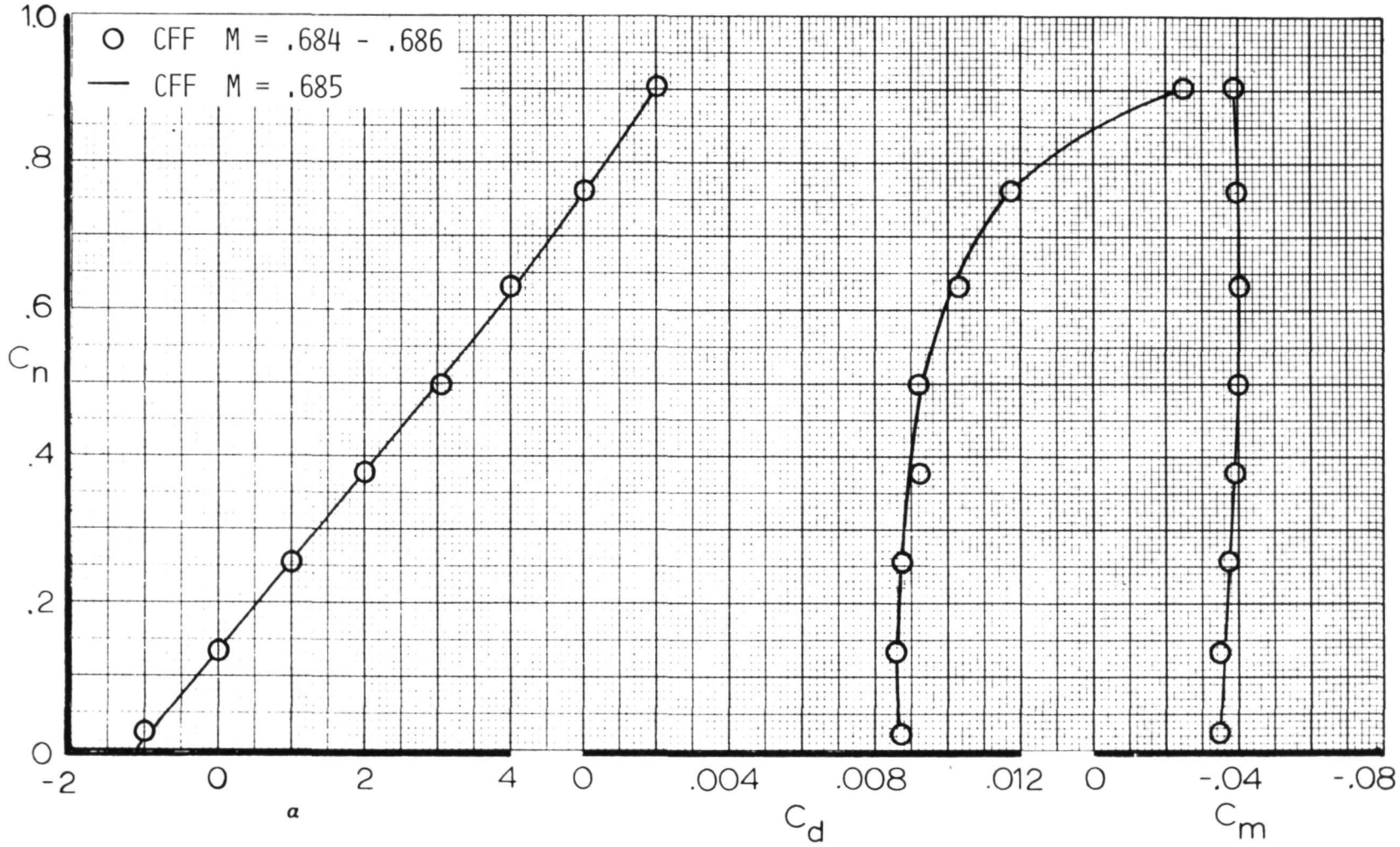

Figure 19. - Airfoil force data for M = 0.68 , R_N = 6 x 10^6, X/C_T = 0.05.

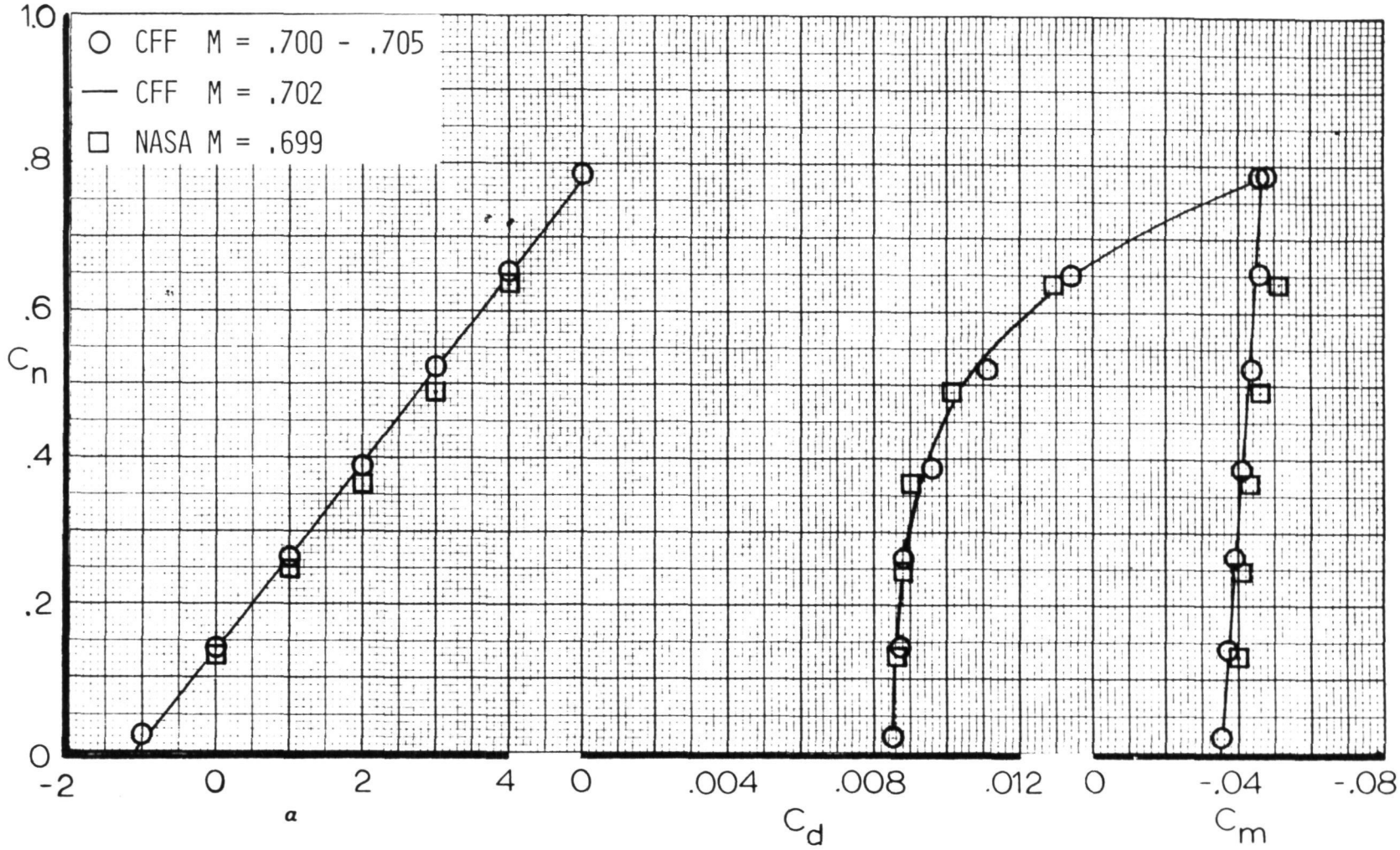

Figure 20. - Airfoil force data for M = 0.70 , R_N = 6 x 10^6, X/C_T = 0.05.

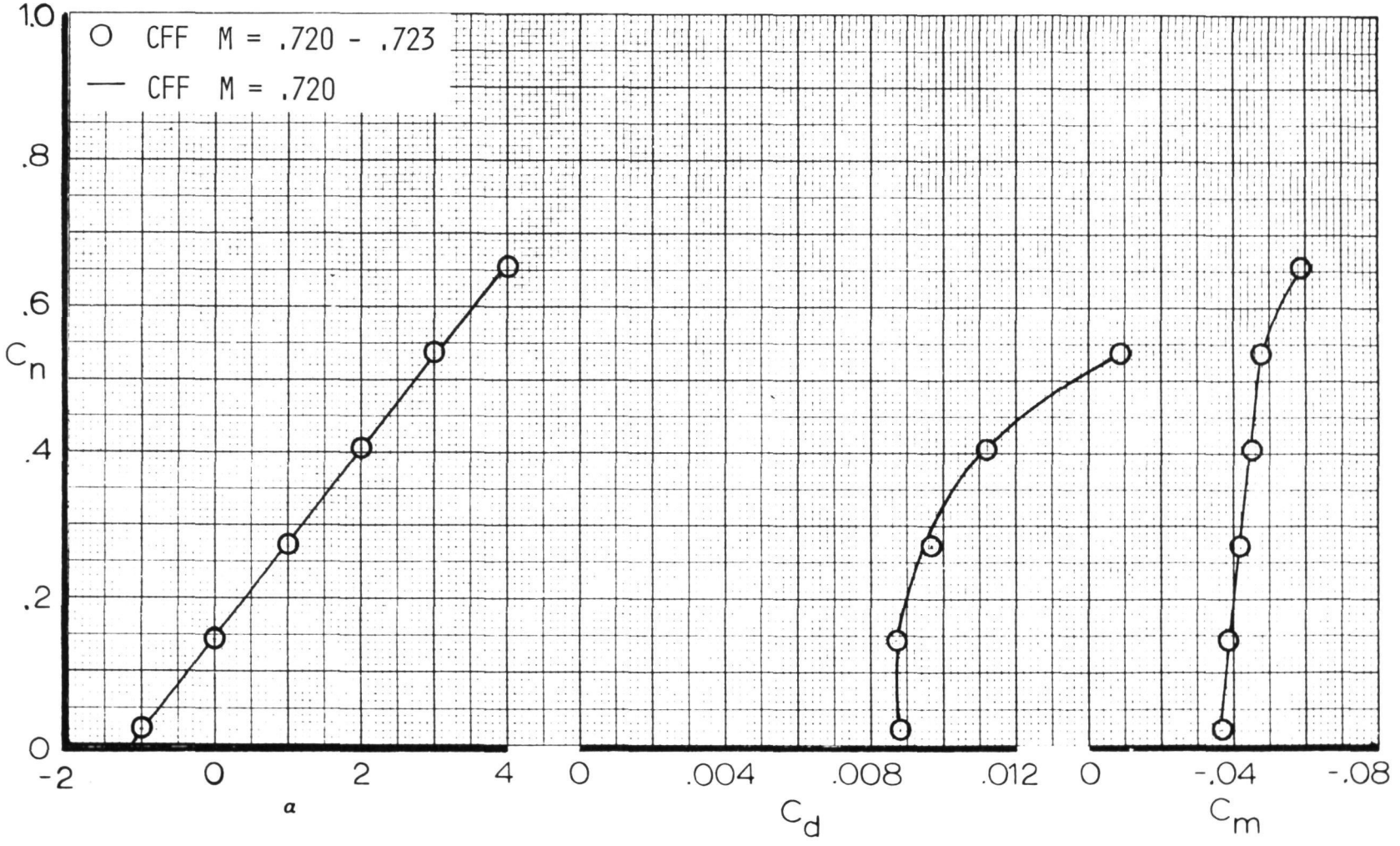

Figure 21. - Airfoil force data for M = 0.72 , R_N = 6 x 10^6, X/C_T = 0.05.

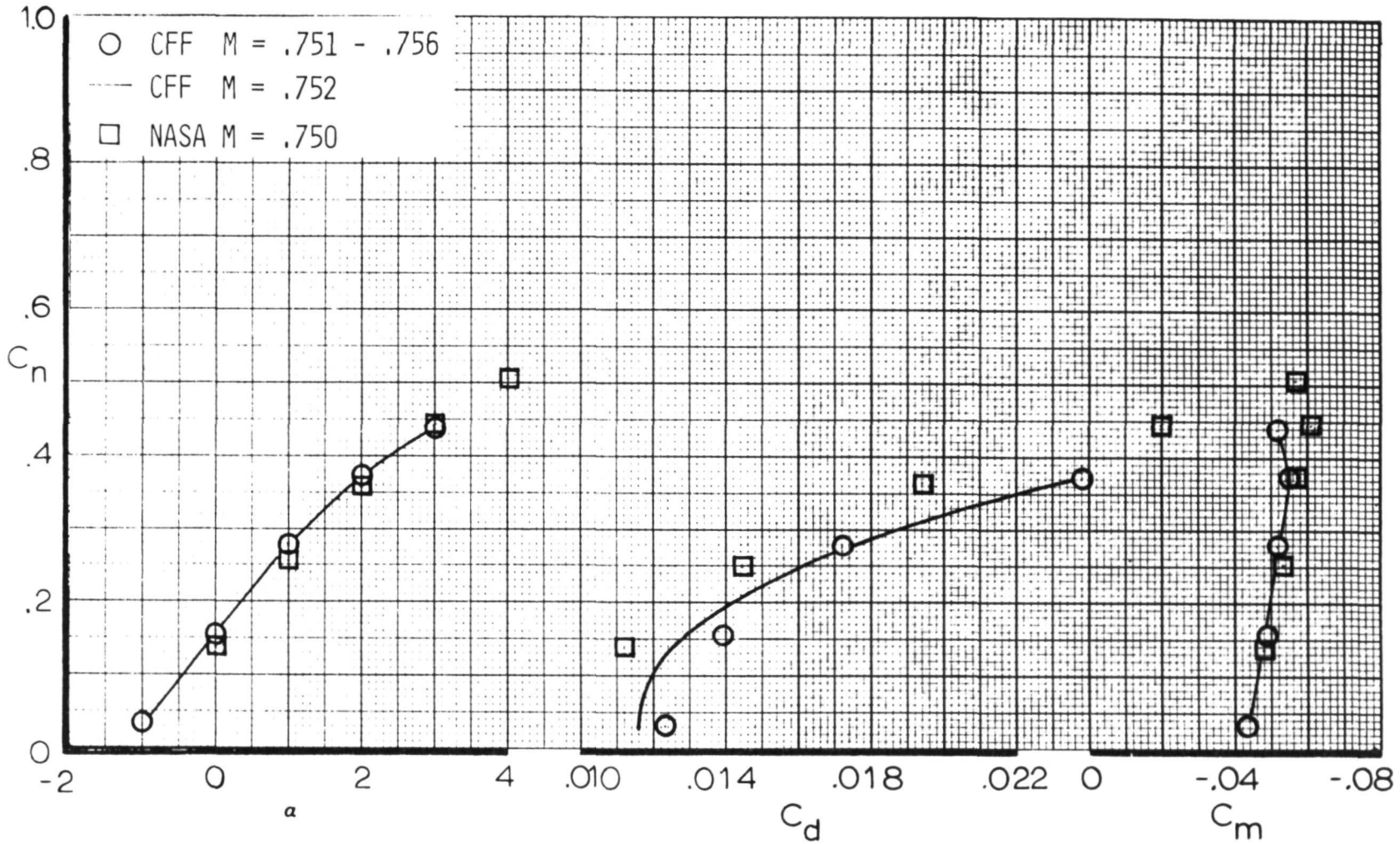

Figure 22 . - Airfoil force data for M = 0.75 , R_N = 6 x 10^6, X/C_T = 0.05.

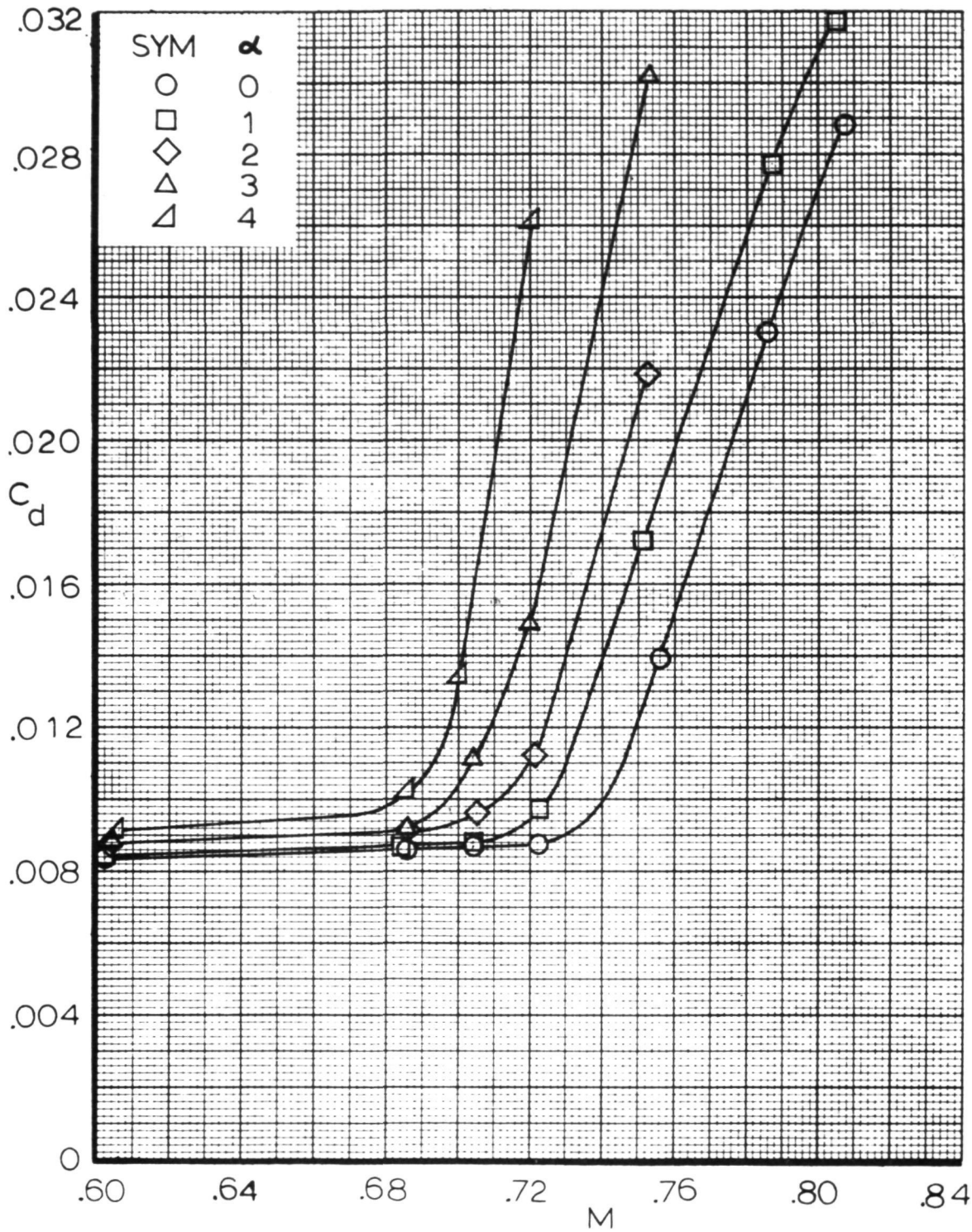

Figure 23. - Airfoil drag rise characteristics, $R_N = 6 \times 10^6$ $X/C_T = .05$.

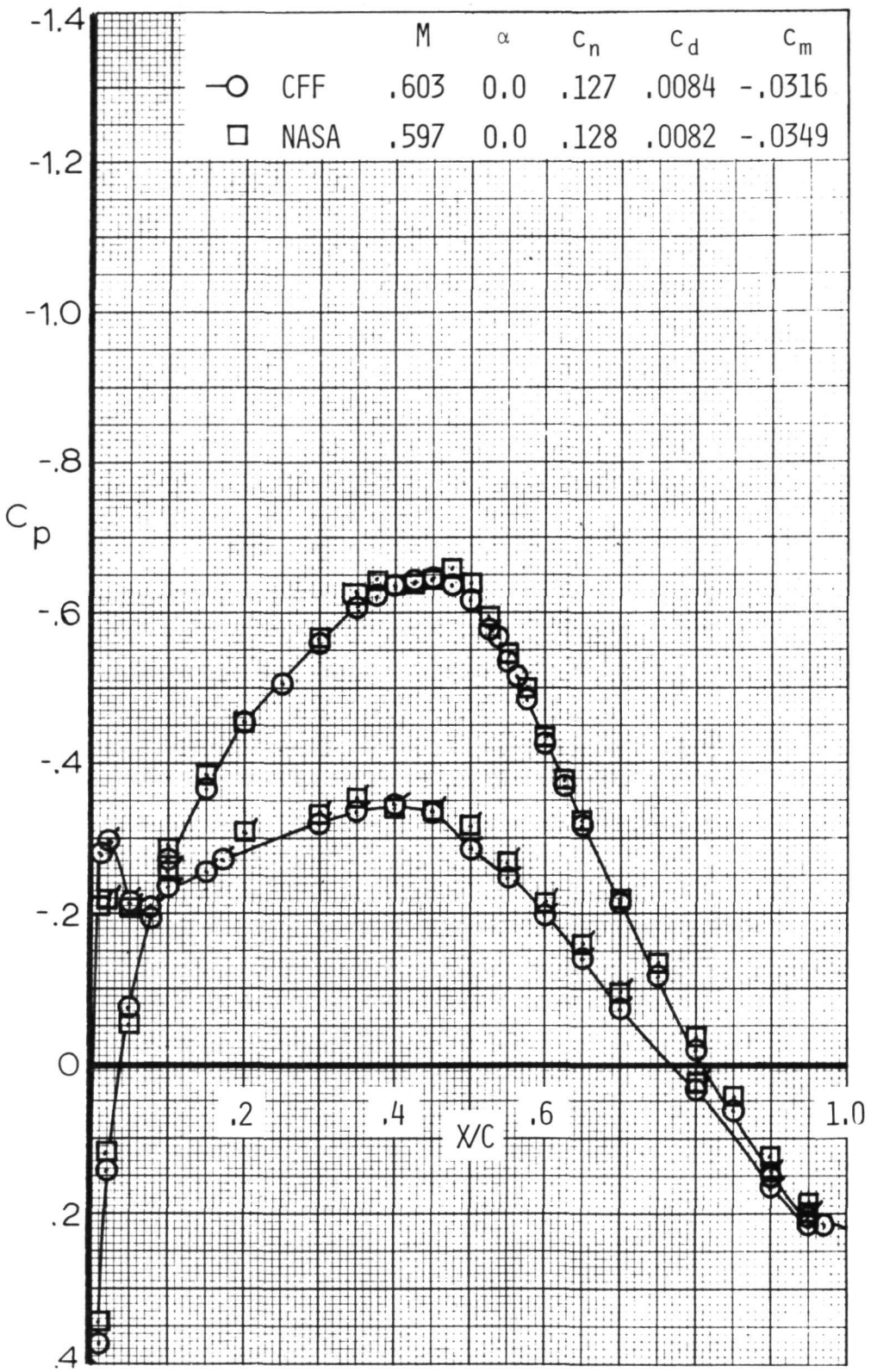

Figure 24. - Airfoil pressure distribution correlation at M = 0.6, $R_N = 6 \times 10^6$, $\alpha = 0^\circ$ (Flags denote l.s.).

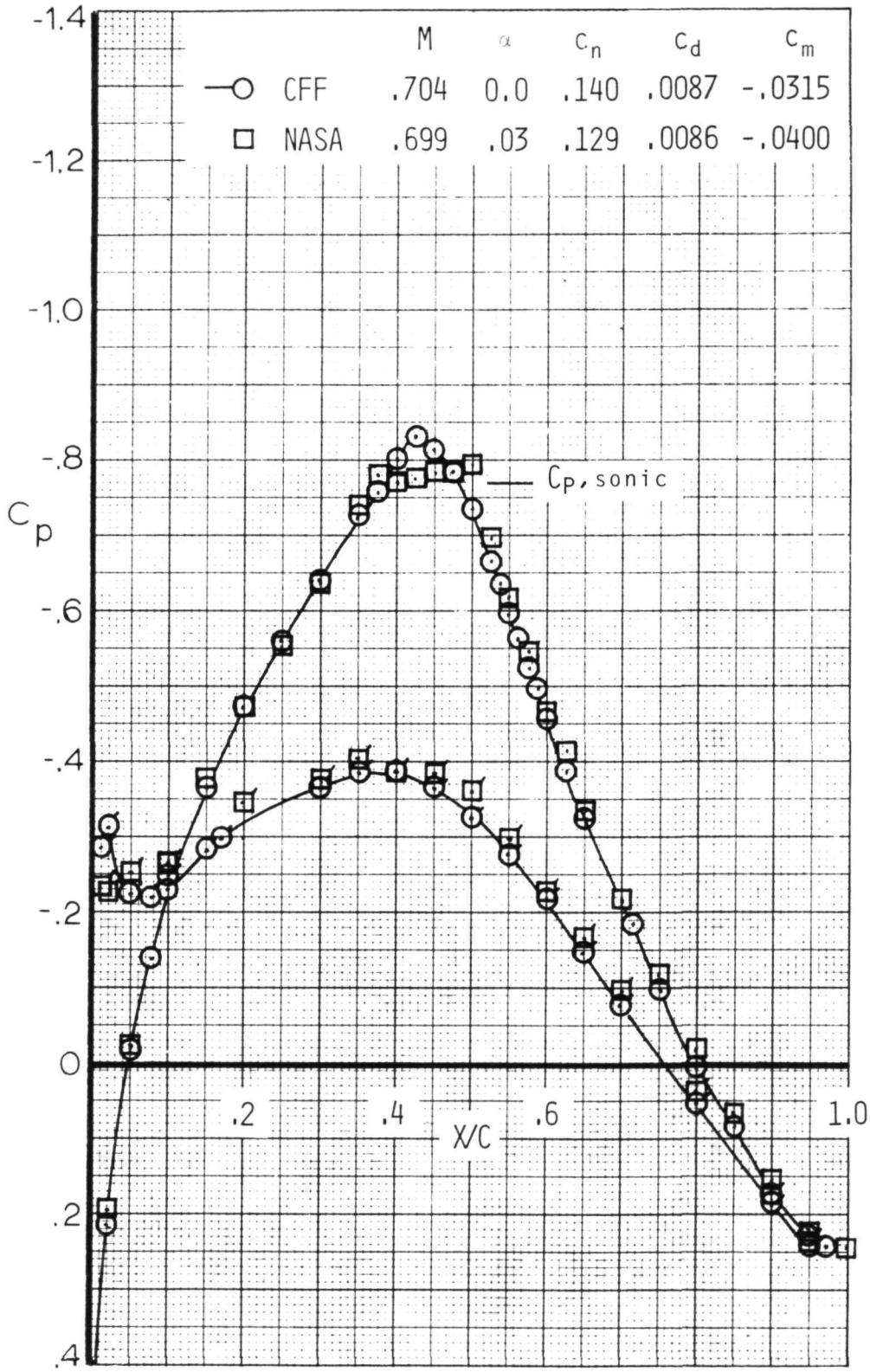

Figure 25. - Airfoil pressure distribution correlation at M = 0.7, $R_N = 6 \times 10^6$, $\alpha = 0$ (Flags denote l.s.)

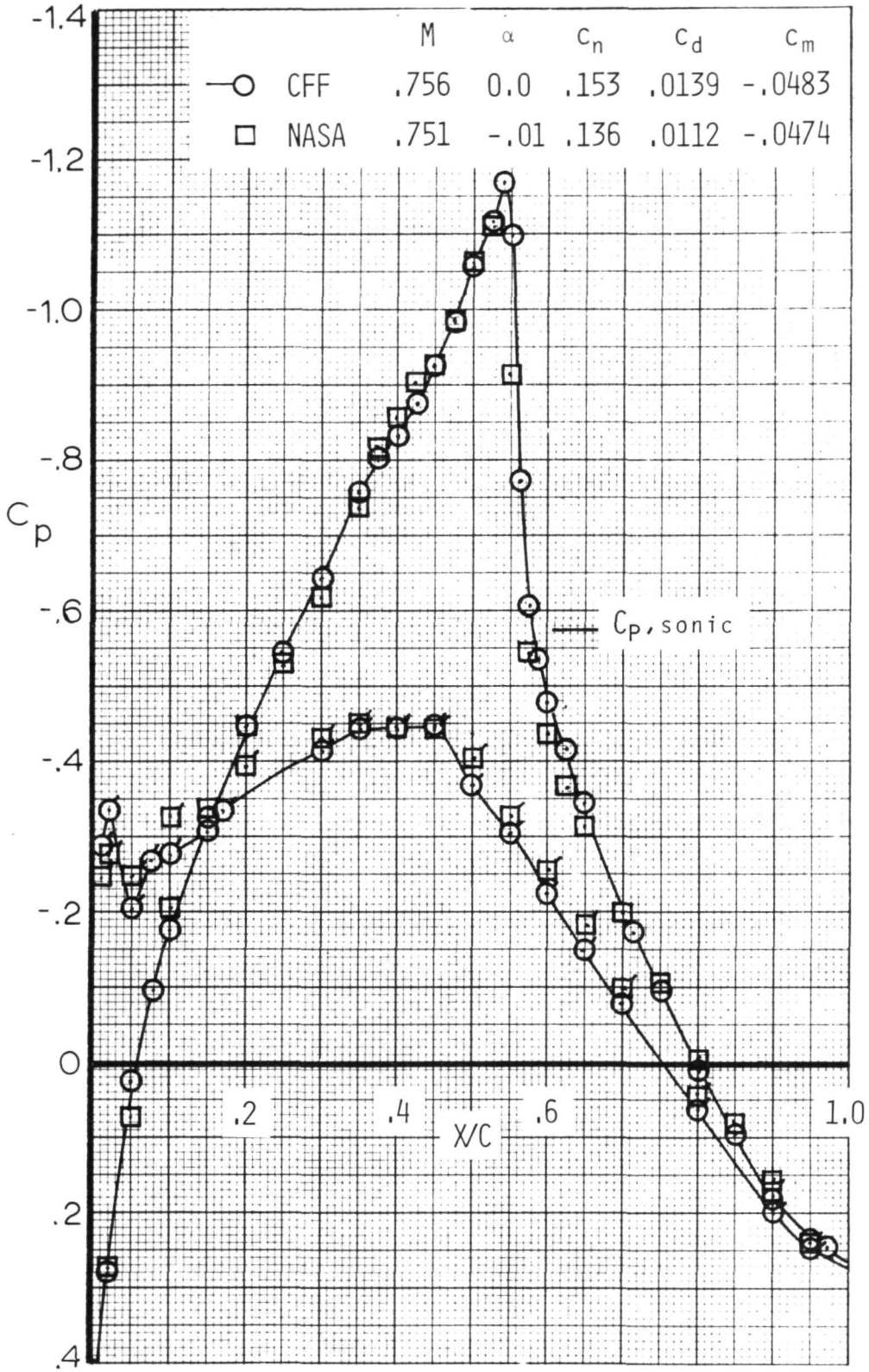

Figure 26. - Airfoil pressure distribution correlation at M = .75, R_N = 6 x 10^6, α = 0° (Flags denote l.s.).

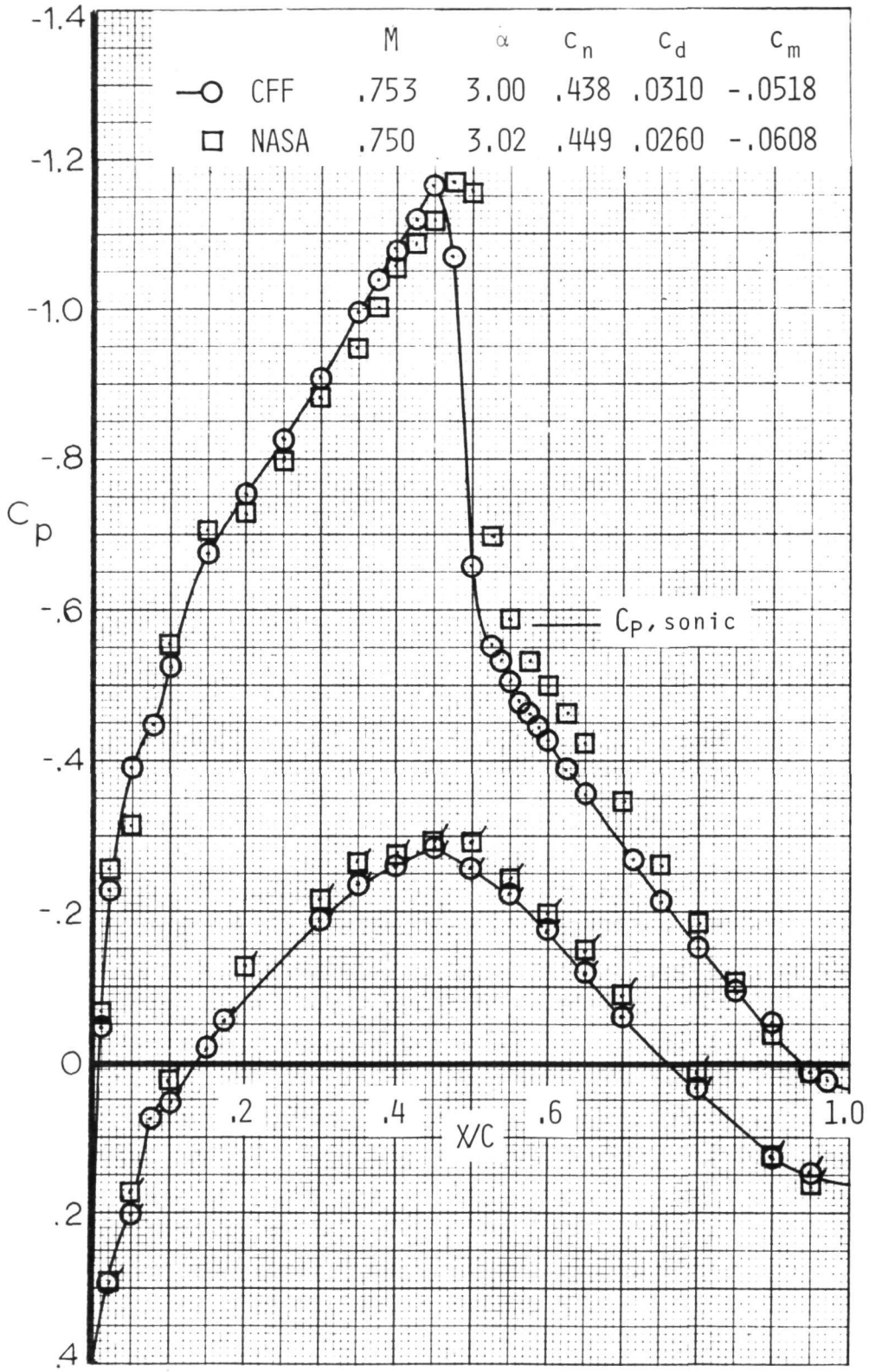

Figure 27. - Airfoil pressure distribution correlation at M = .75, $R_N = 6 \times 10^6$, $\alpha = 3^\circ$ (Flags denote l.s.).

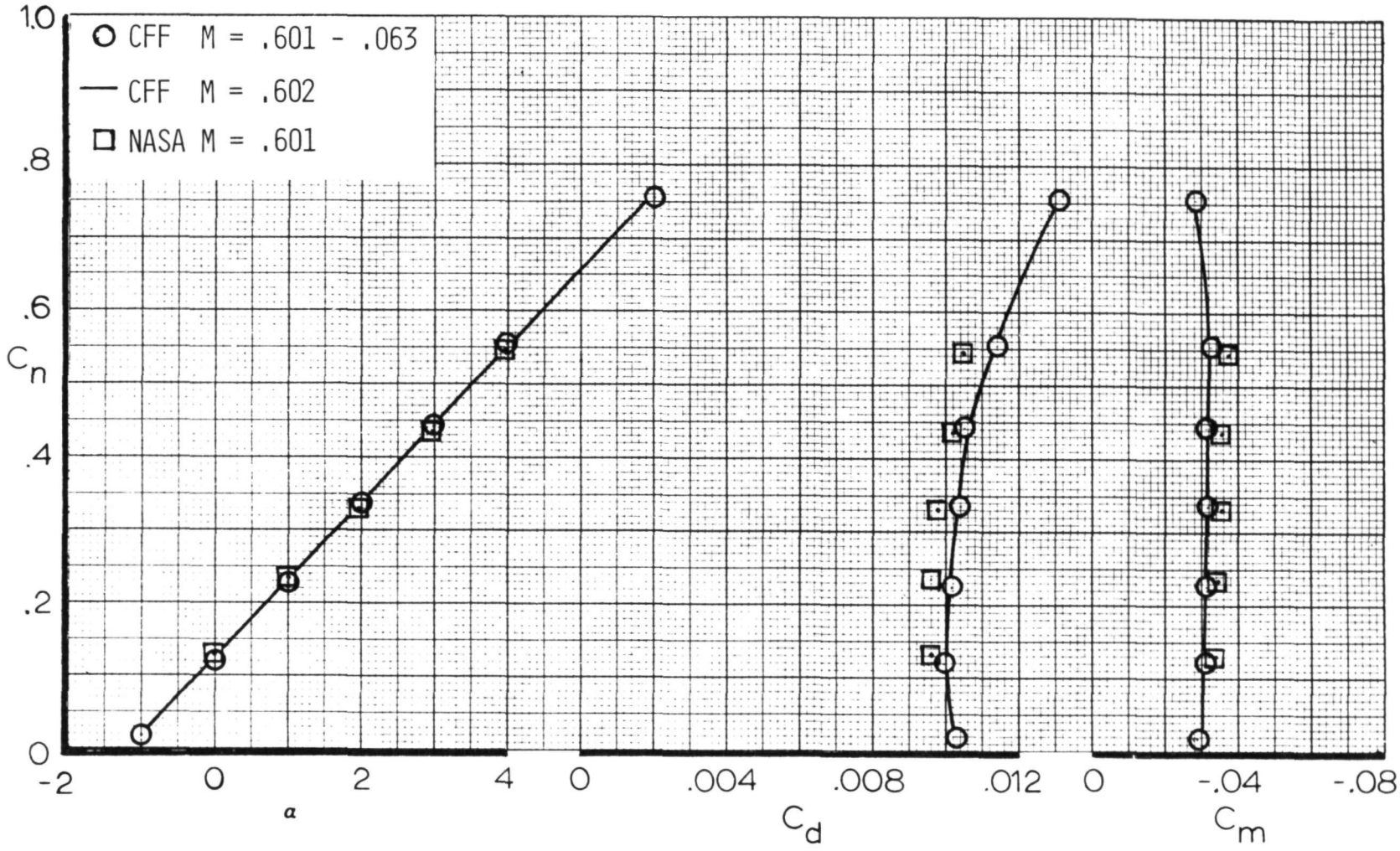

Figure 28. - Airfoil force data for M = 0.60 , $R_N = 3 \times 10^6$, $X/C_T = 0.05$.

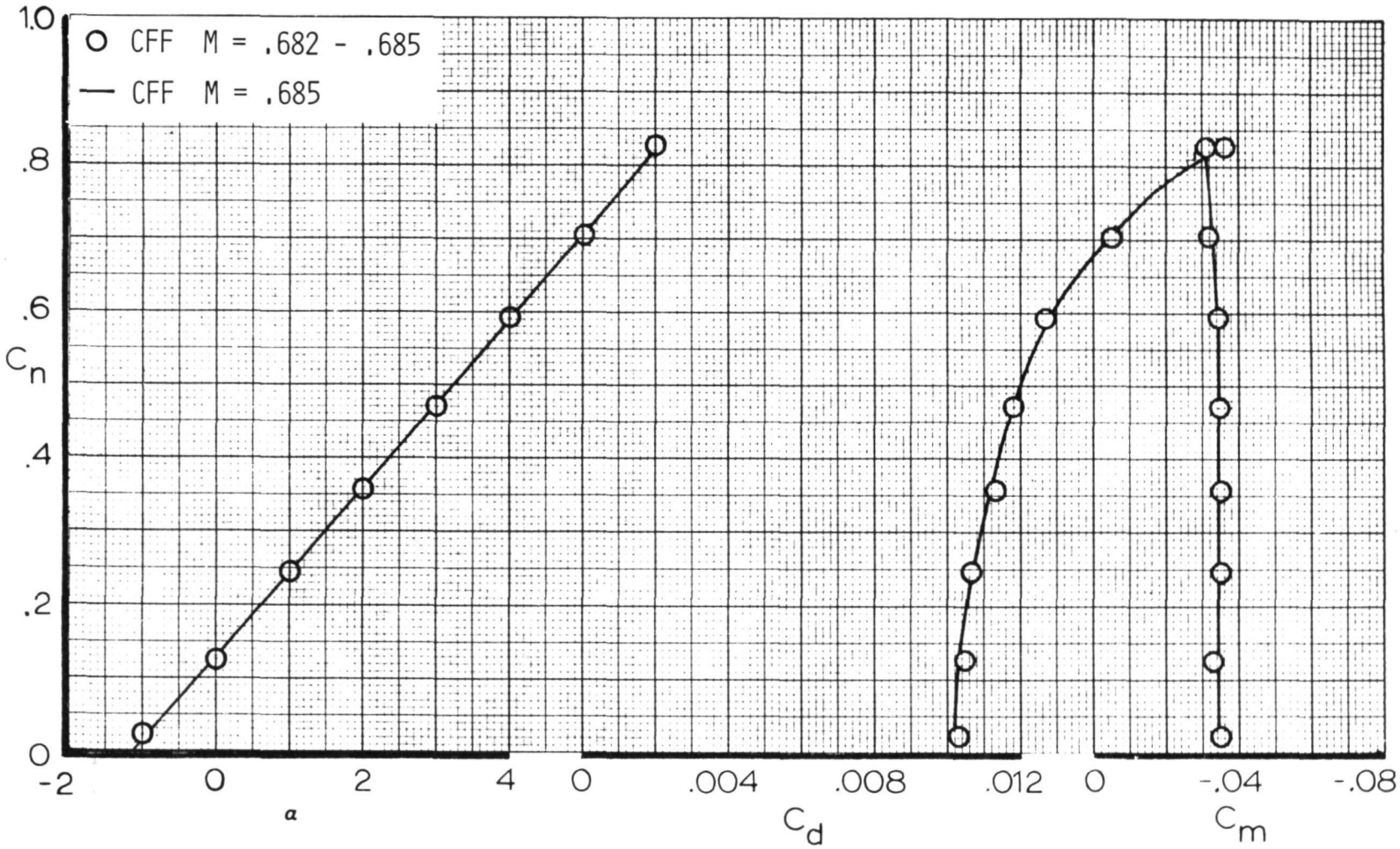

Figure 29. - Airfoil force data for M = 0.68 , R_N = 3 x 10^6, X/C_T = 0.05.

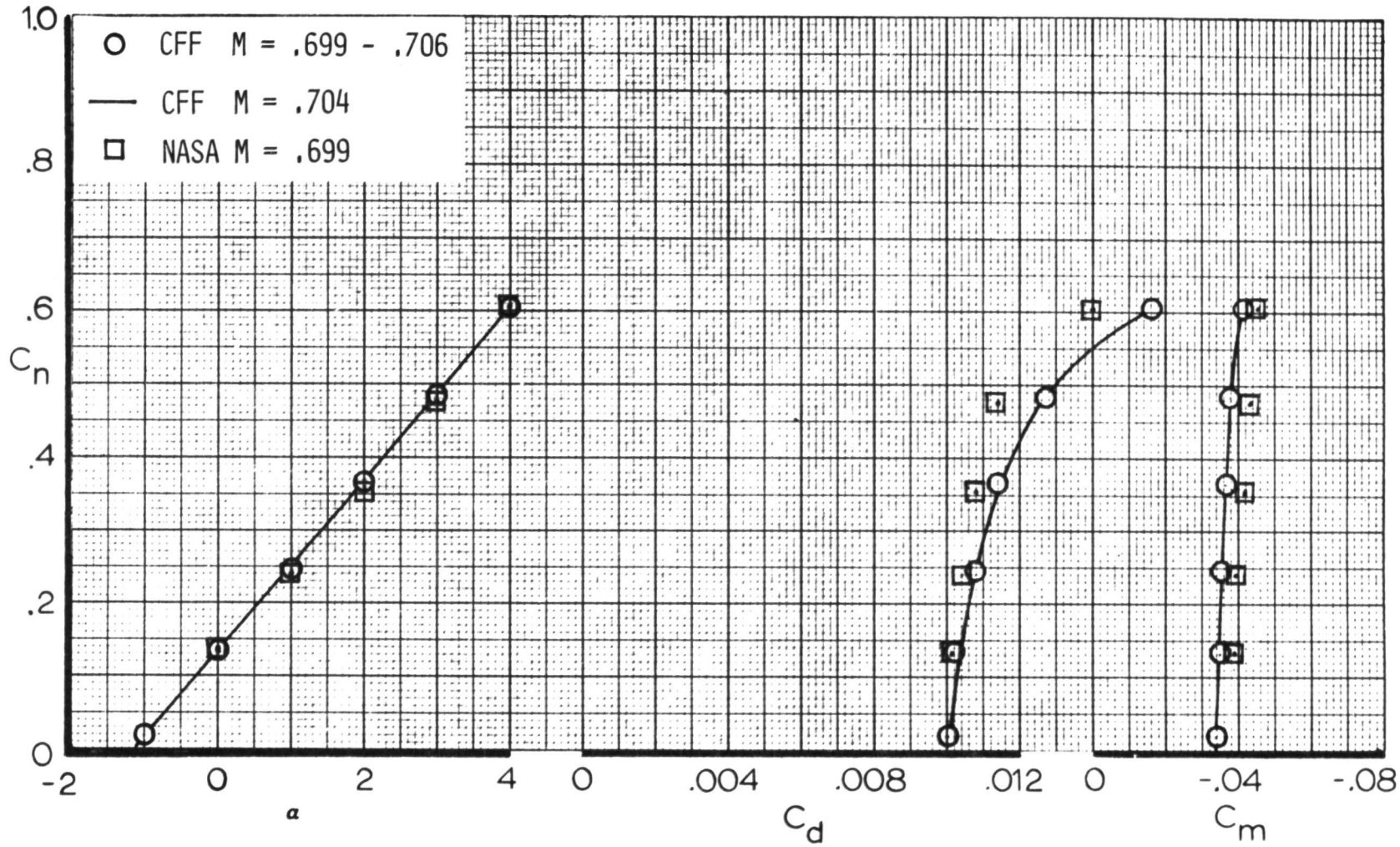

Figure 30. - Airfoil force data for M = 0.70 , R_N = 3 x 10^6, X/C_T = 0.05.

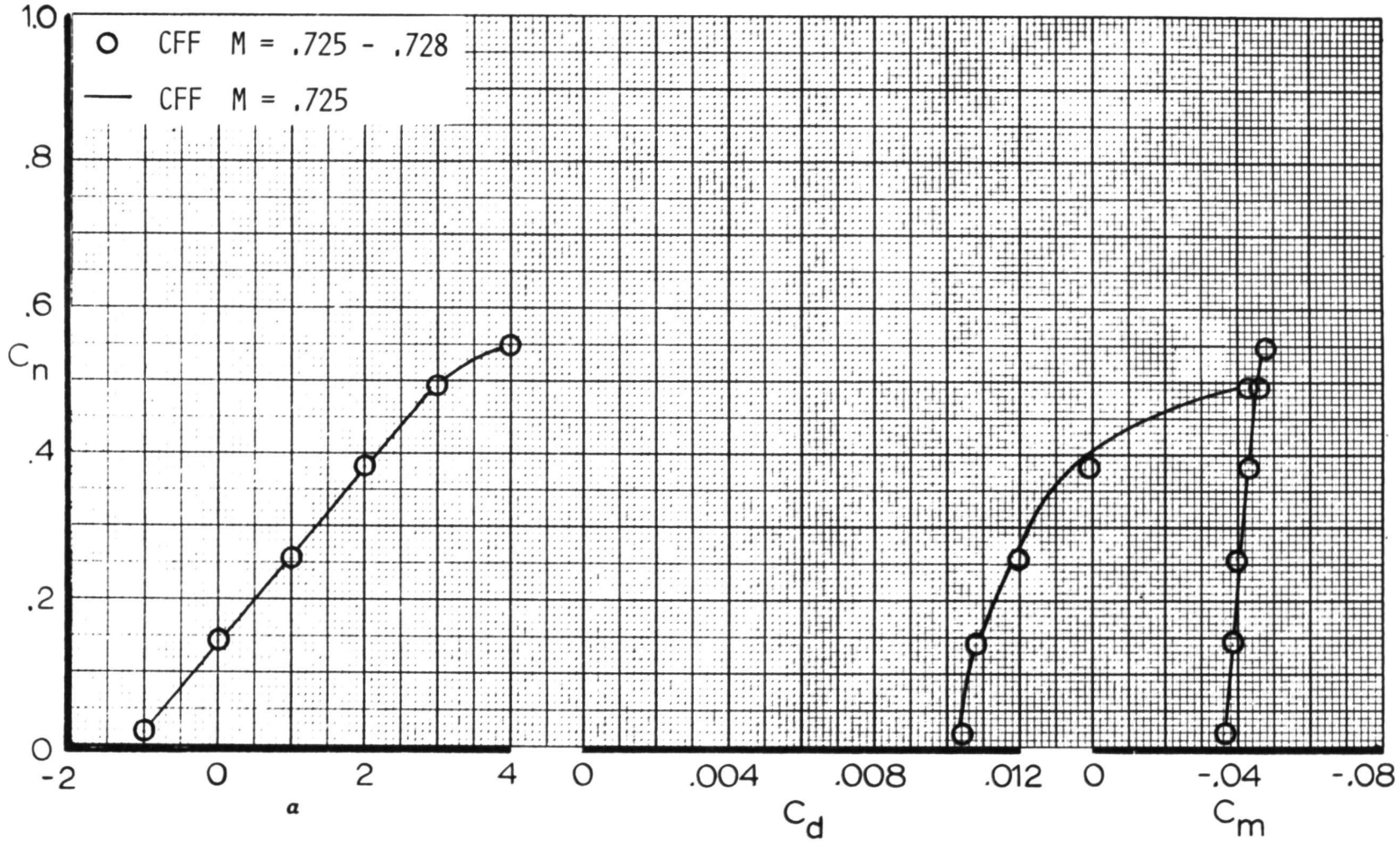

Figure 31. - Airfoil force data for M = 0.72 , R_N = 3 x 10^6, X/C_T = 0.05.

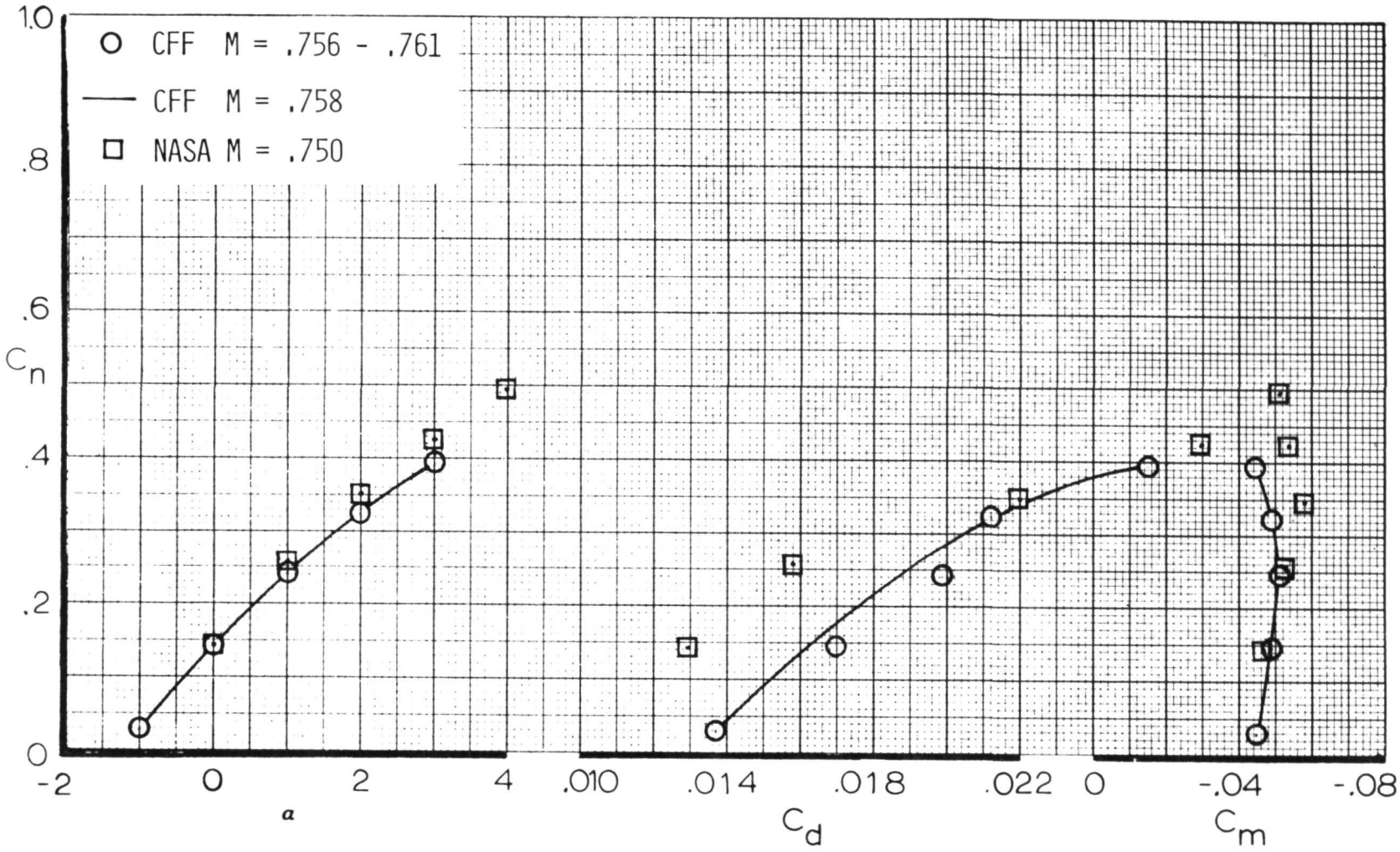

Figure 32. - Airfoil force data for M = 0.76 , $R_N = 3 \times 10^6$, $X/C_T = 0.05$.

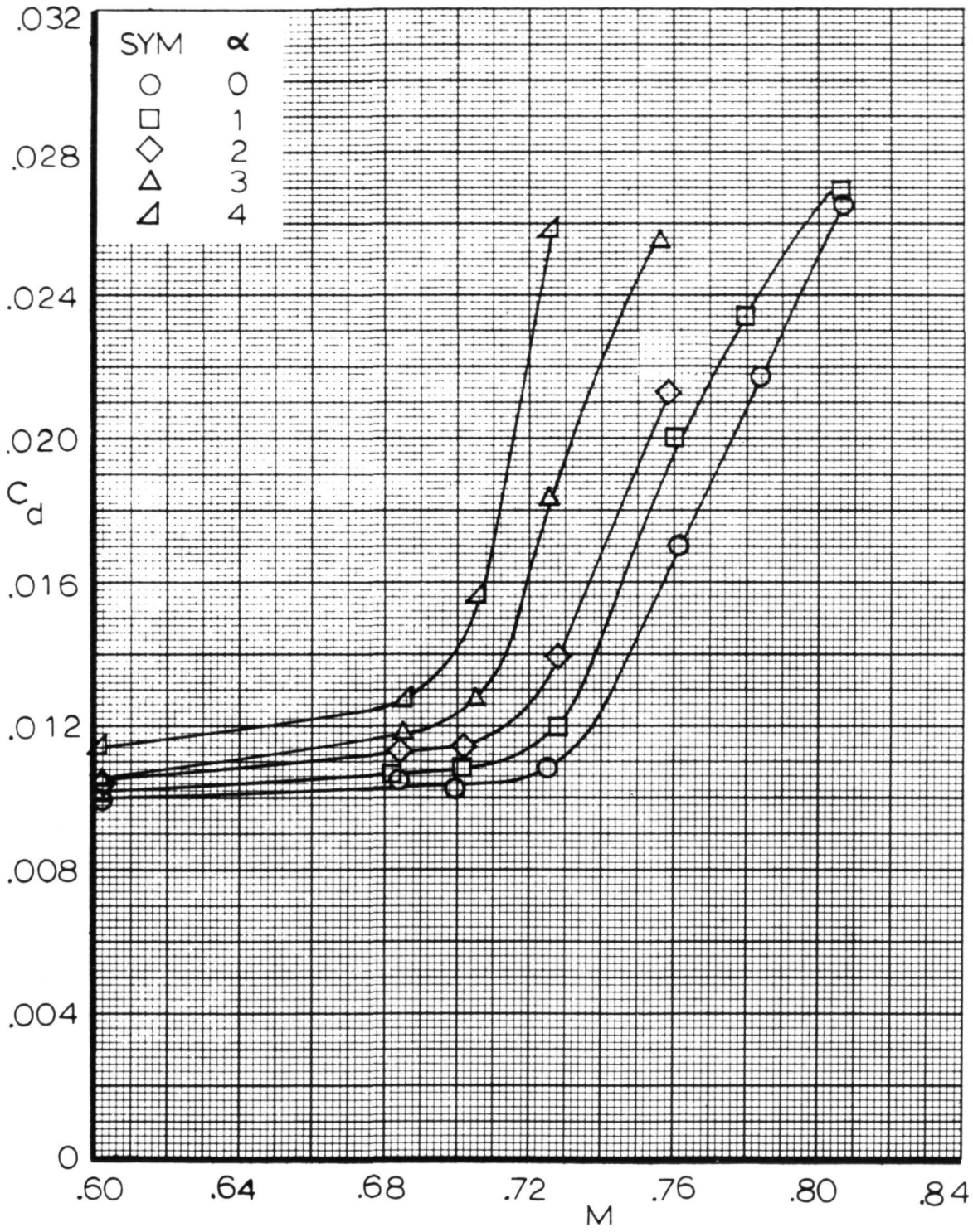

Figure 33. - Airfoil drag rise characteristics, $R_N = 3 \times 10^6$, $X/C_T = .05$.

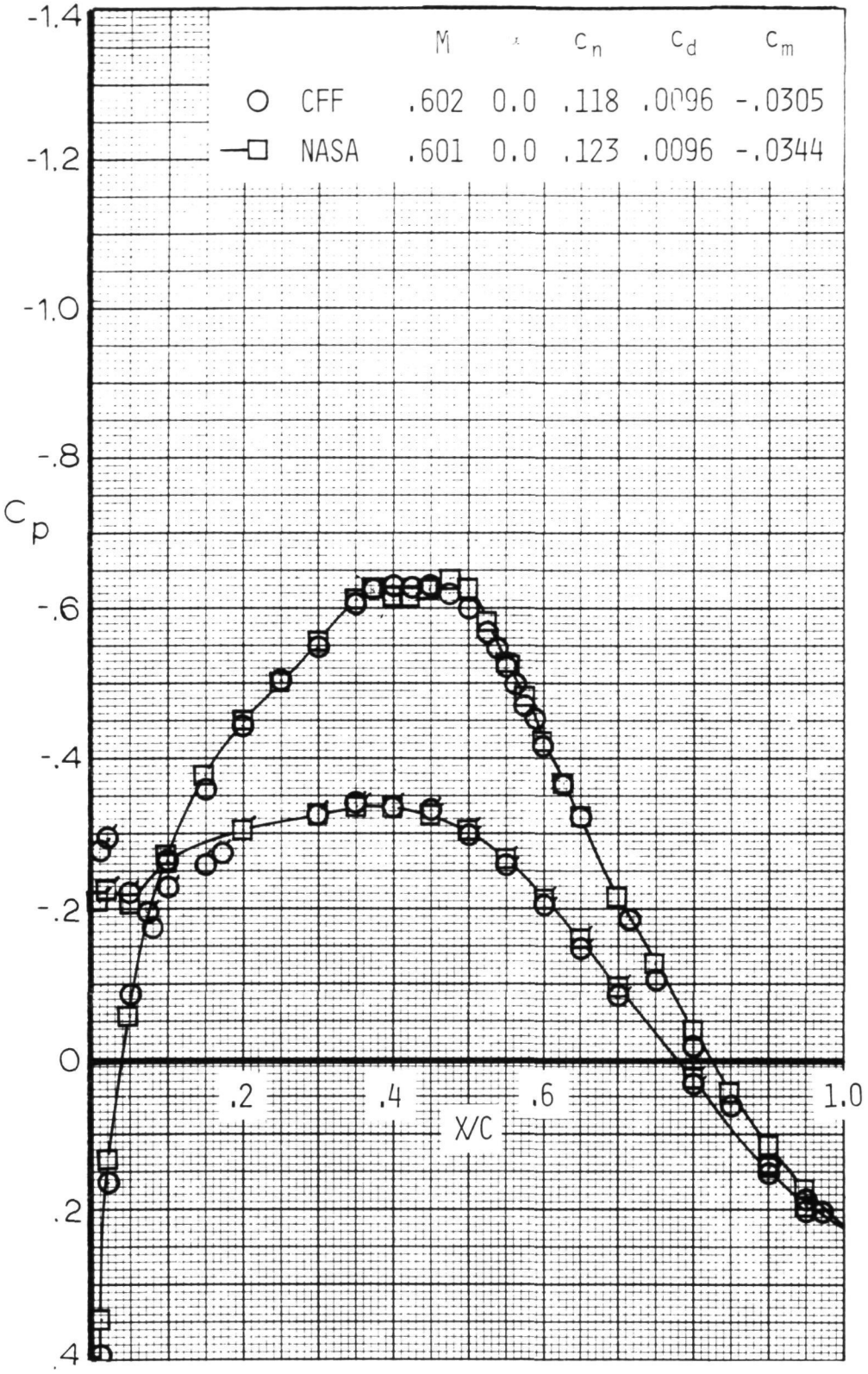

Figure 34. - Airfoil pressure distribution correlation at M = 0.6, $R_N = 3 \times 10^6$, $\alpha = 0°$ (Flags denote l.s.).

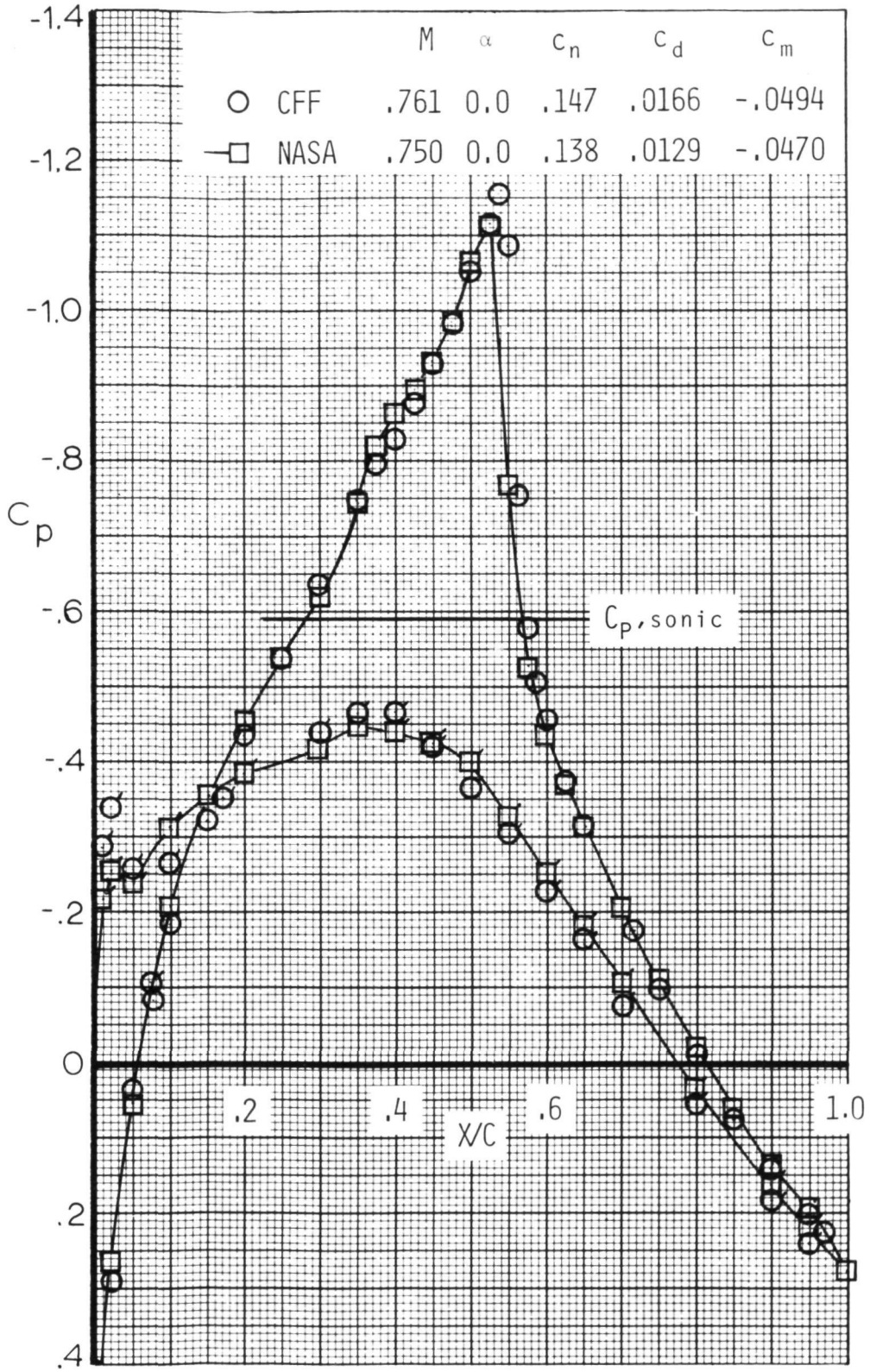

Figure 35. - Airfoil pressure distribution correlation at M = 0.75, $R_N = 3 \times 10^6$, $\alpha = 0°$ (Flags denote l.s.).

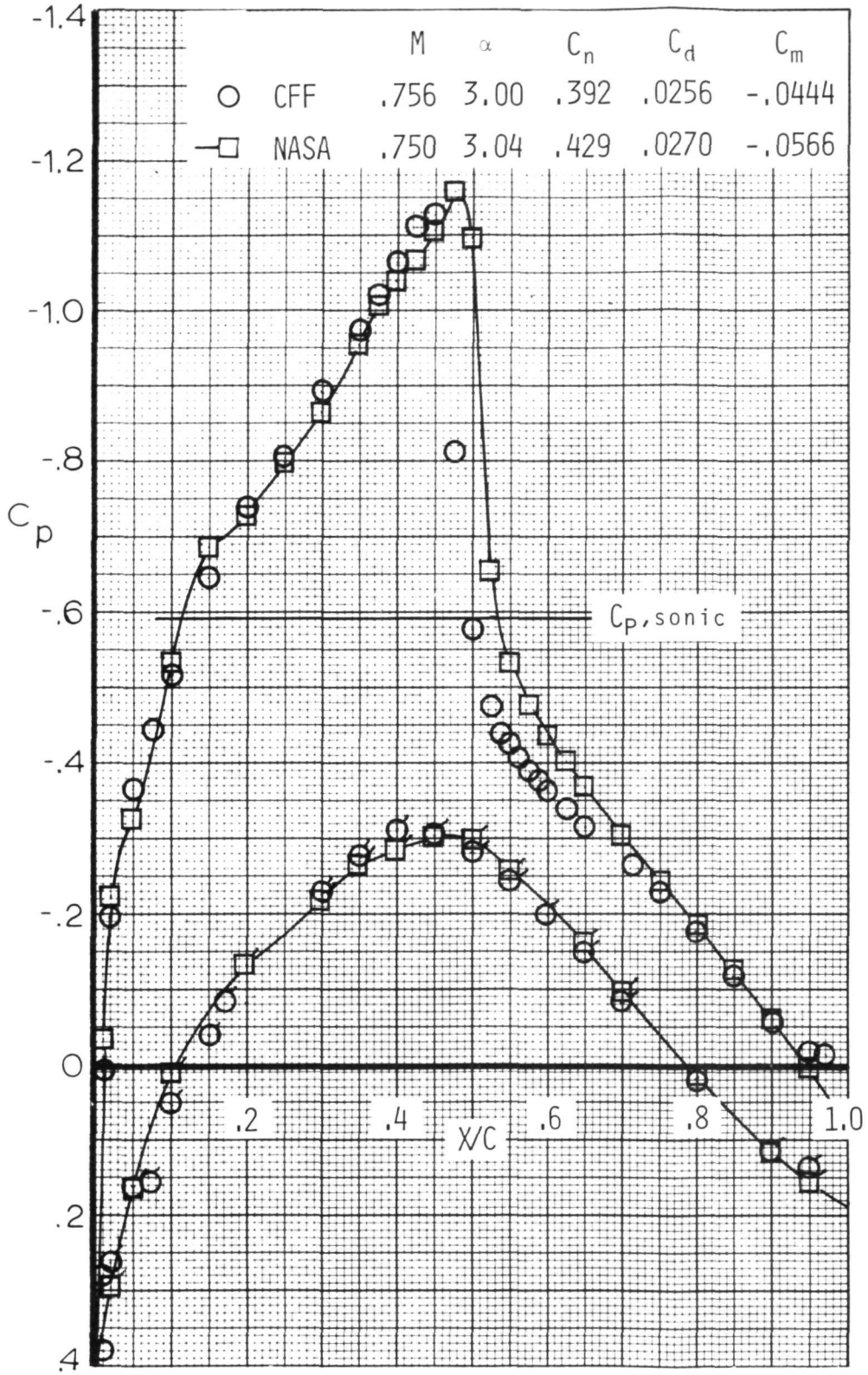

Figure 36. - Airfoil pressure distribution correlation at M = 0.75, $R_N = 3 \times 10^6$, $\alpha = 3^\circ$ (Flags denote l.s.).

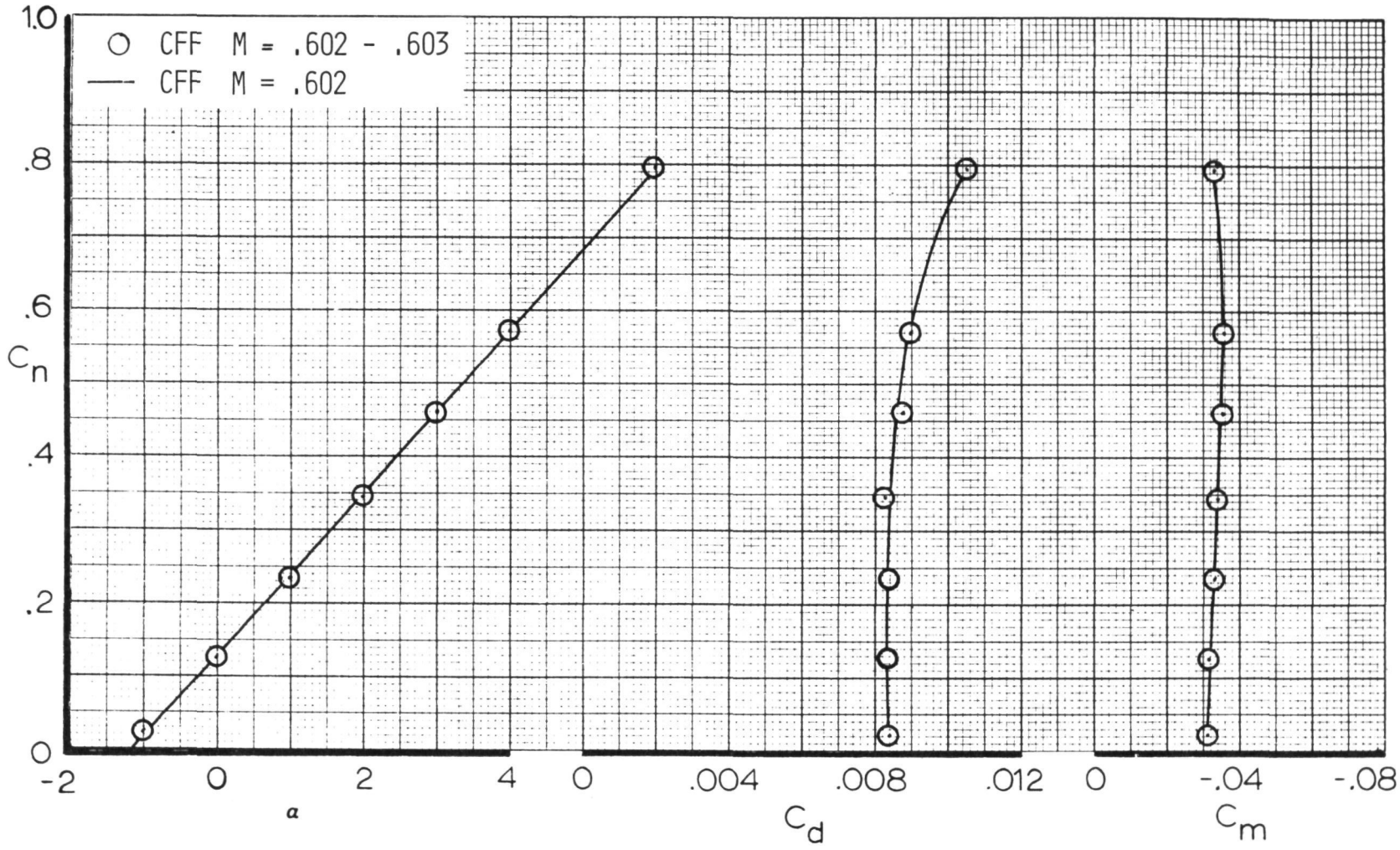

Figure 37. - Airfoil force data for M = 0.60 , R_N = 9 x 10^6, X/C_T = 0.05.

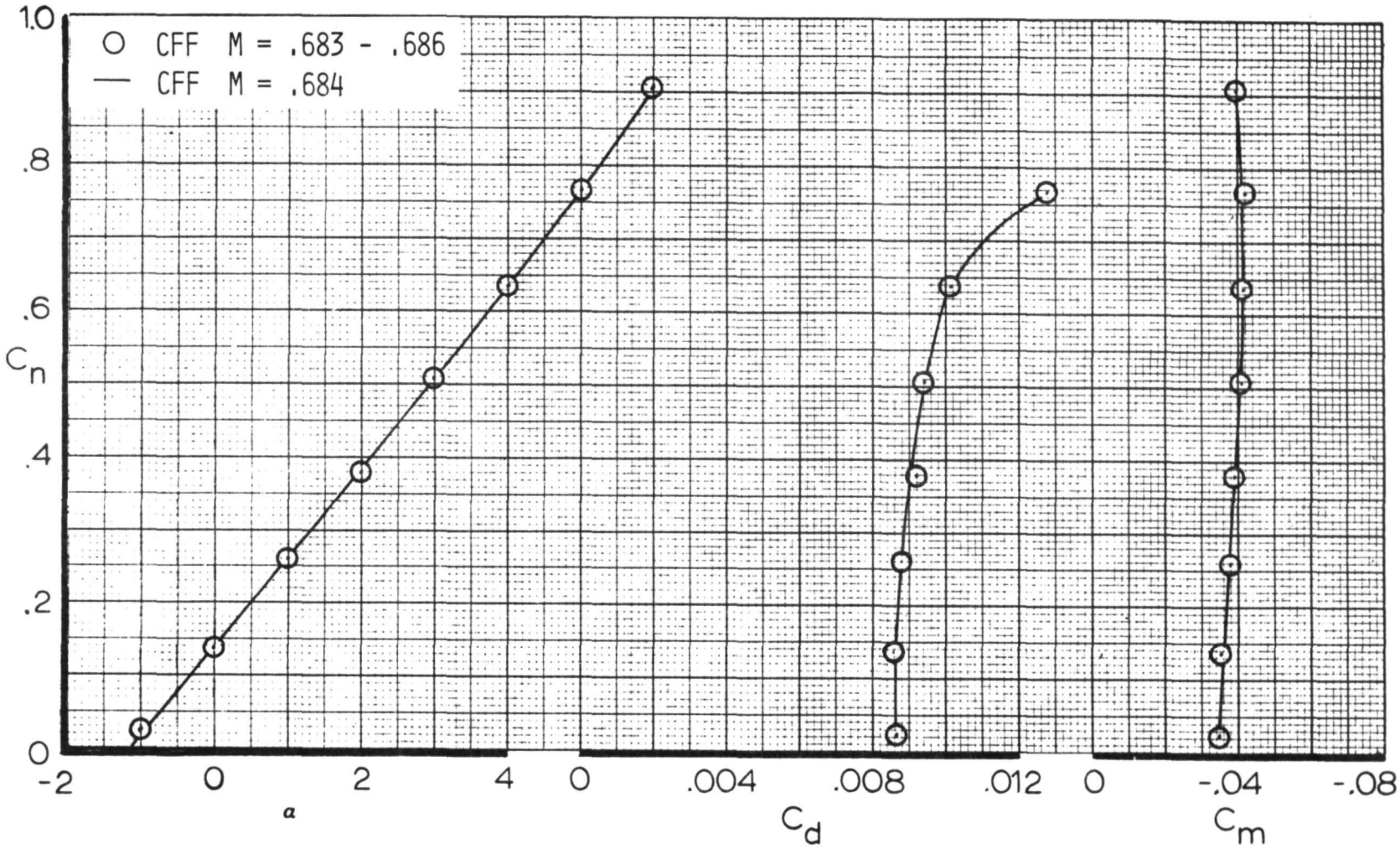

Figure 38. - Airfoil force data for M = 0.68 , R_N = 9 x 10^6, X/C_T = 0.05.

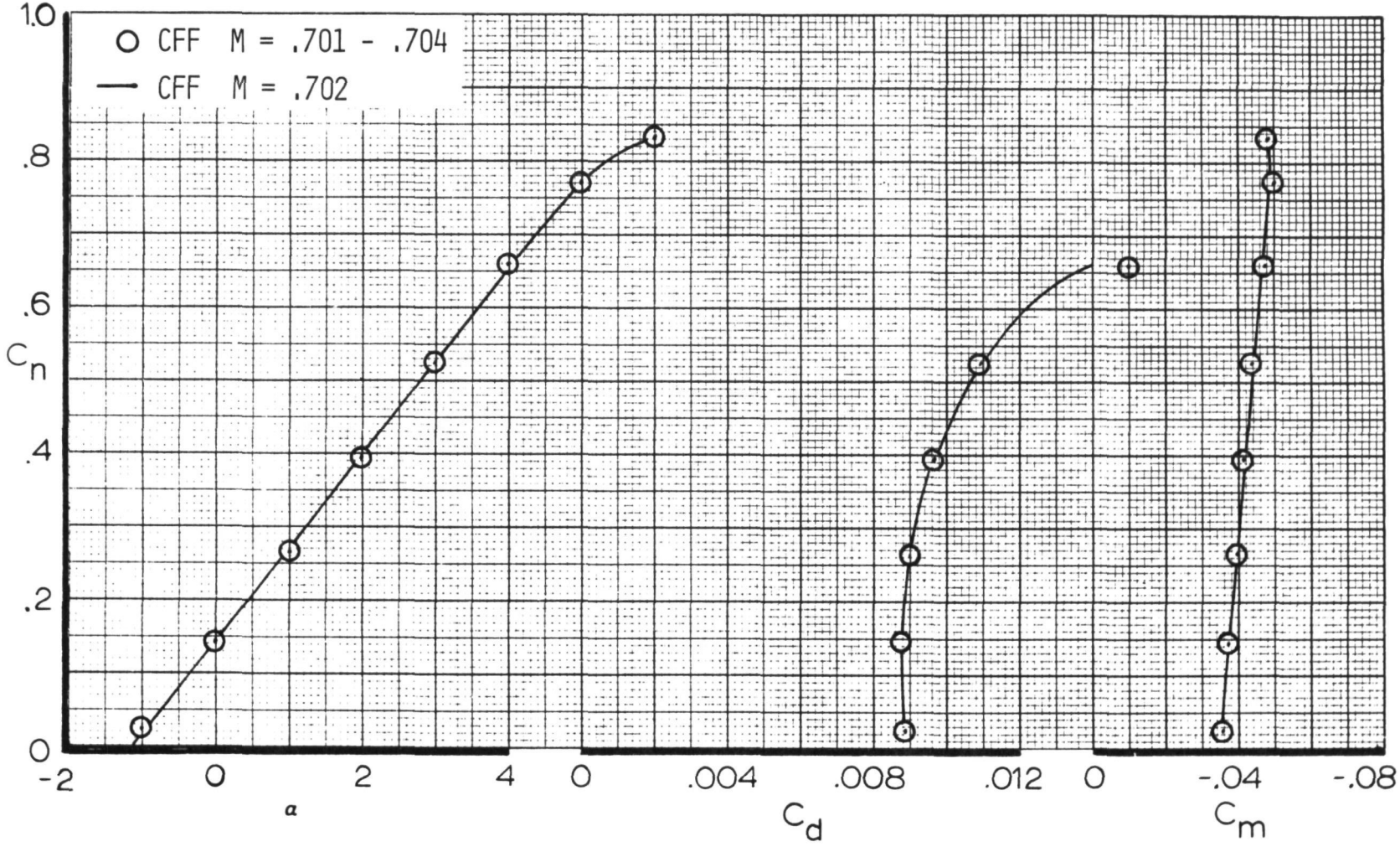

Figure 39. · Airfoil force data for M = 0.70 , R_N = 9 x 10^6, X/C_T = 0.05.

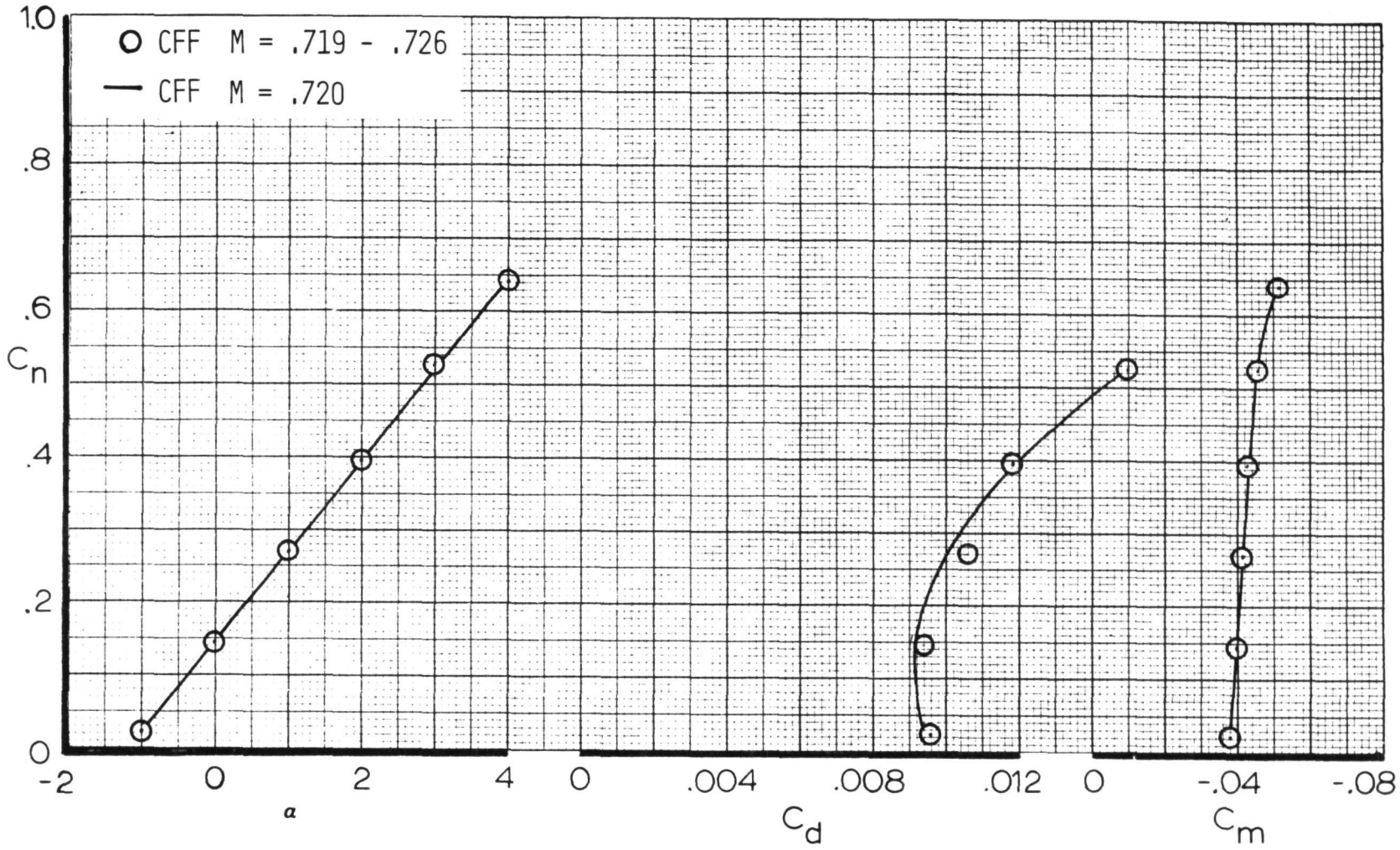

Figure 40. - Airfoil force data for M = 0.72 , R_N = 9 x 10^6, X/C_T = 0.05.

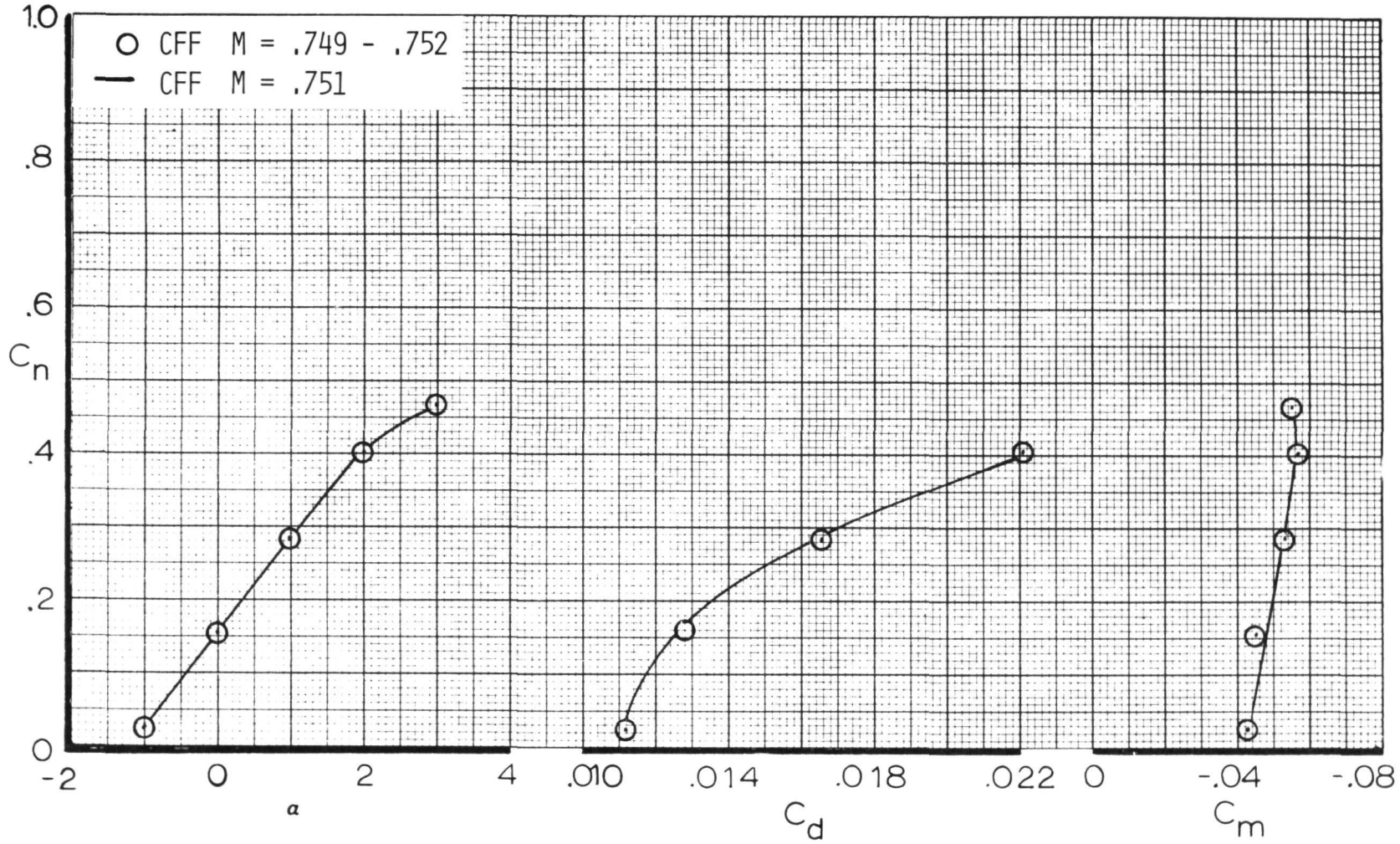

Figure 41. - Airfoil force data for M = 0.75 , R_N = 9 x 10^6, X/C_T = 0.05.

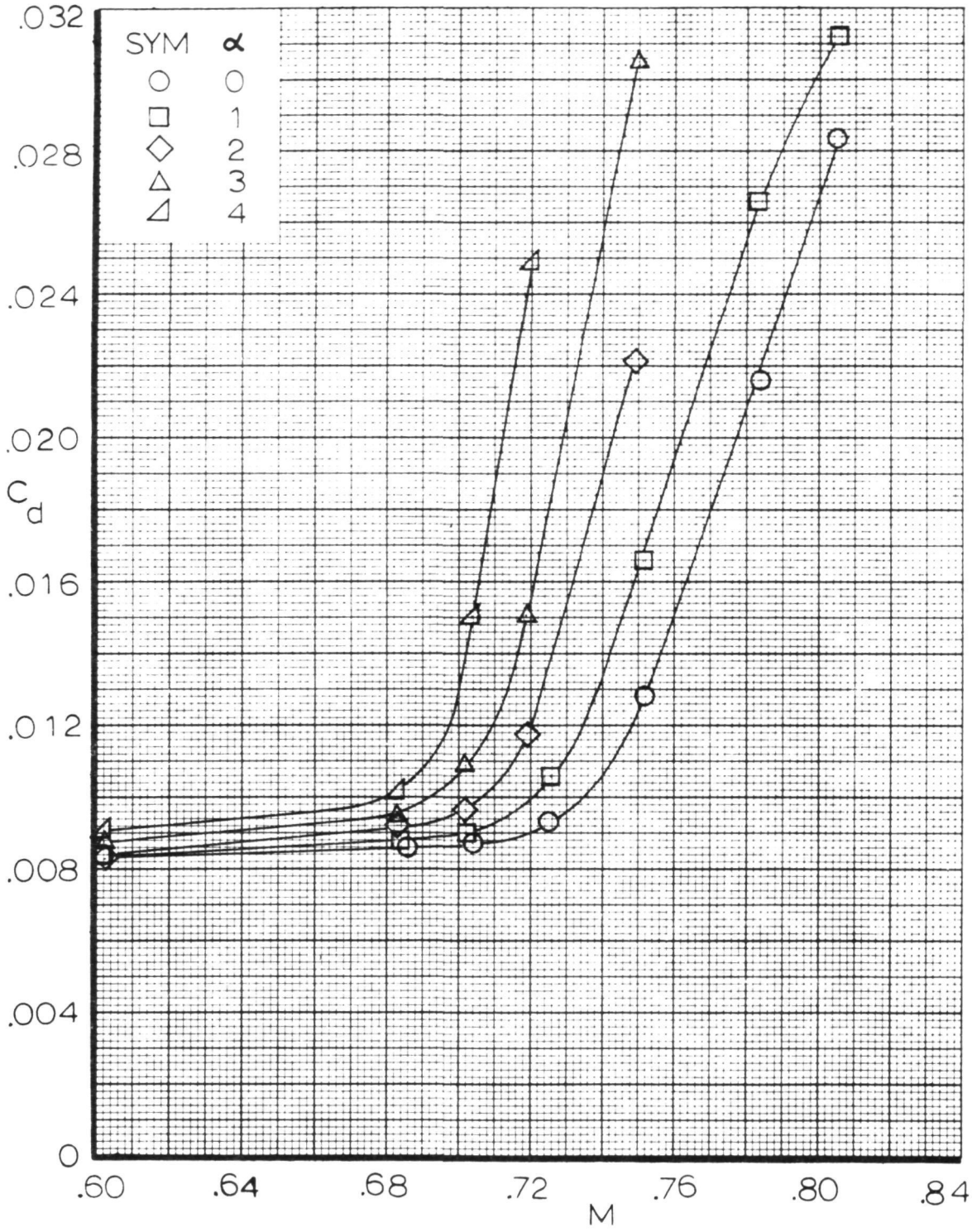

Figure 42. - Airfoil drag rise characteristics, $R_N = 9 \times 10^6$, $X/C_T = .05$.

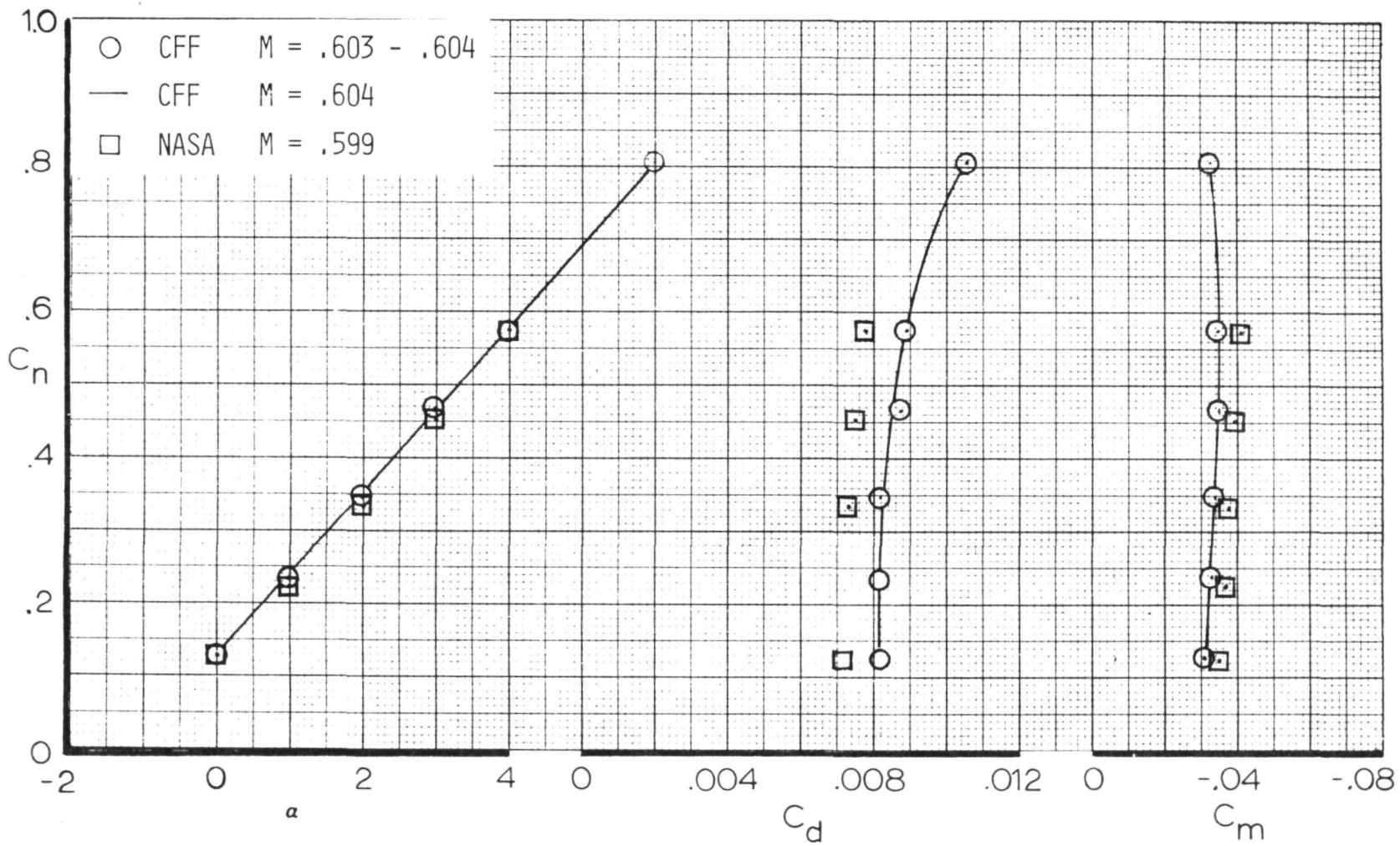

Figure 43. - Airfoil force data for M = 0.60 , R_N = 12 x 10^6, X/C_T = 0.05.

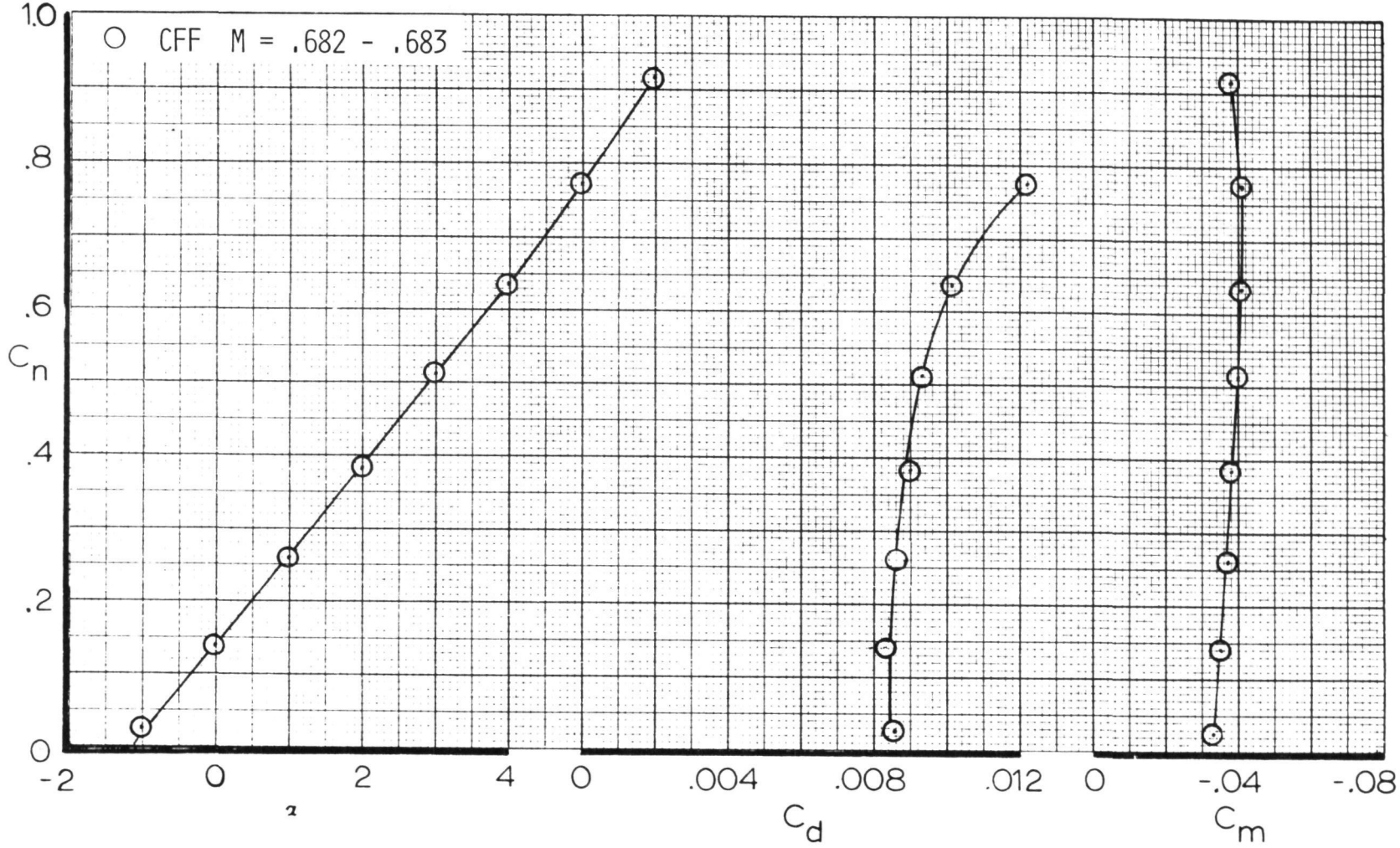

Figure 44. - Airfoil force data for M = 0.68 , R_N = 12 x 10^6, X/C_T = 0.05

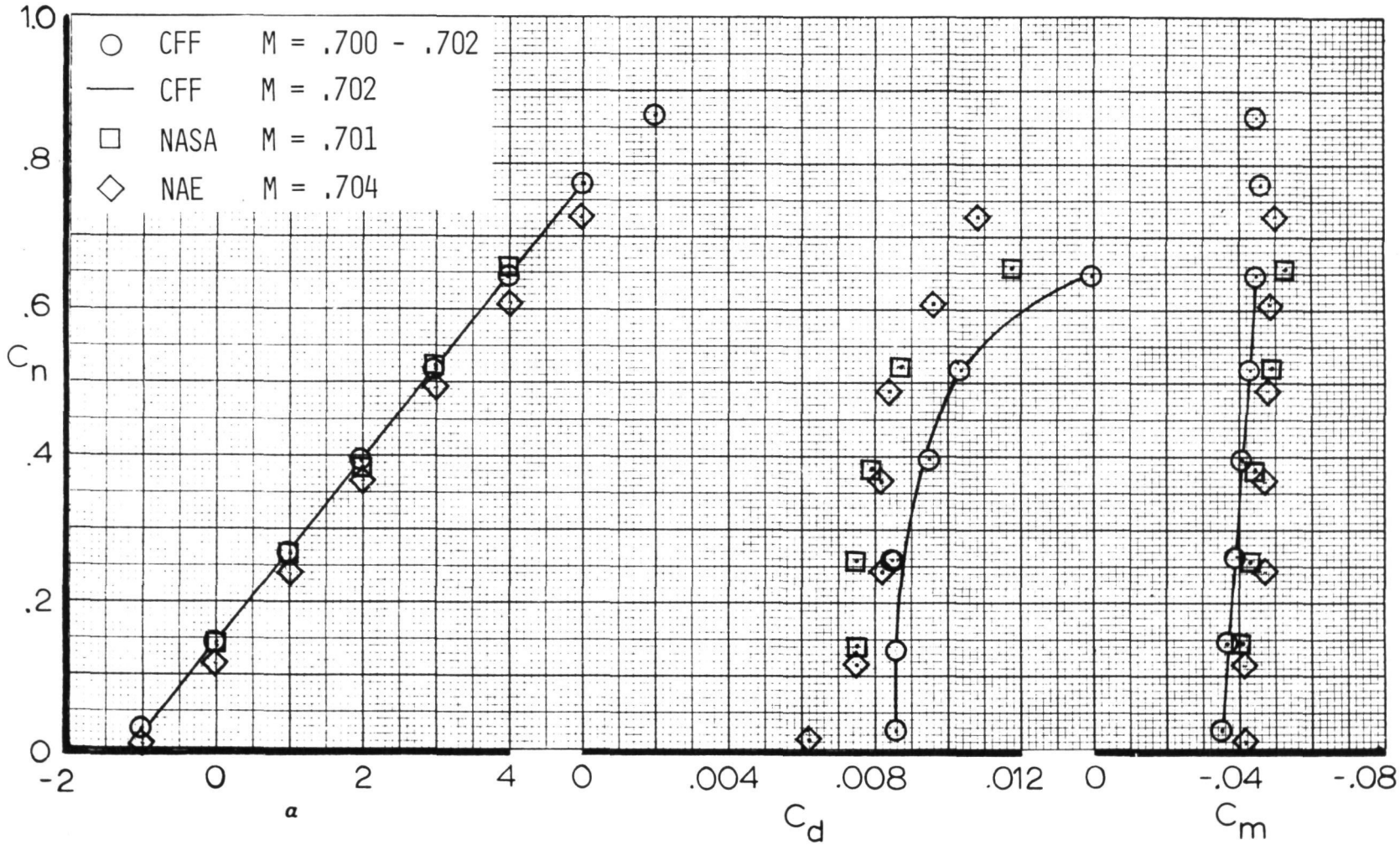

Figure 45. - Airfoil force data for M = 0.70 , R_N = 12 x 10^6, X/C_T = 0.05.

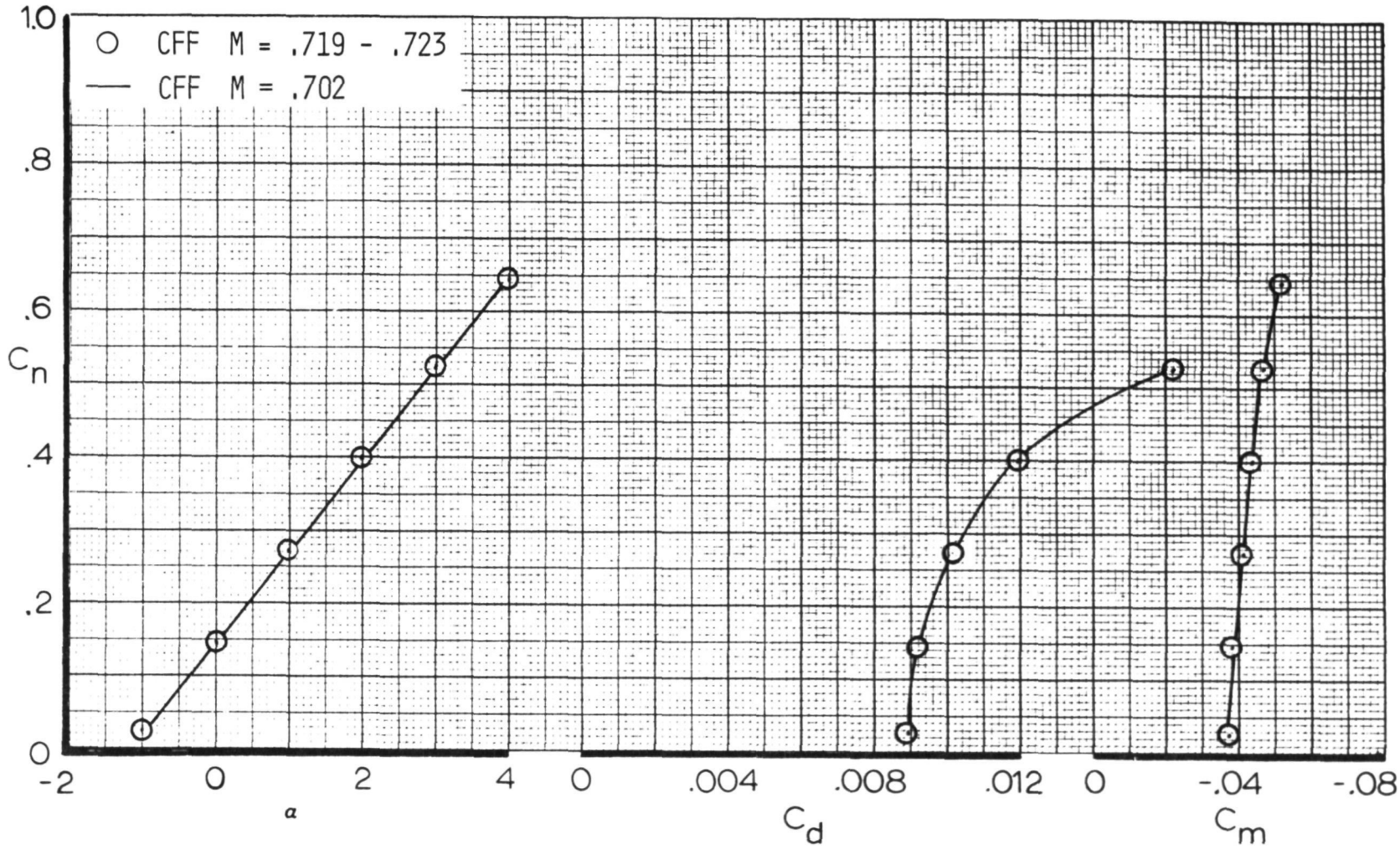

Figure 46. - Airfoil force data for M = 0.72 , R_N = 12 x 10^6, X/C_T = 0.05.

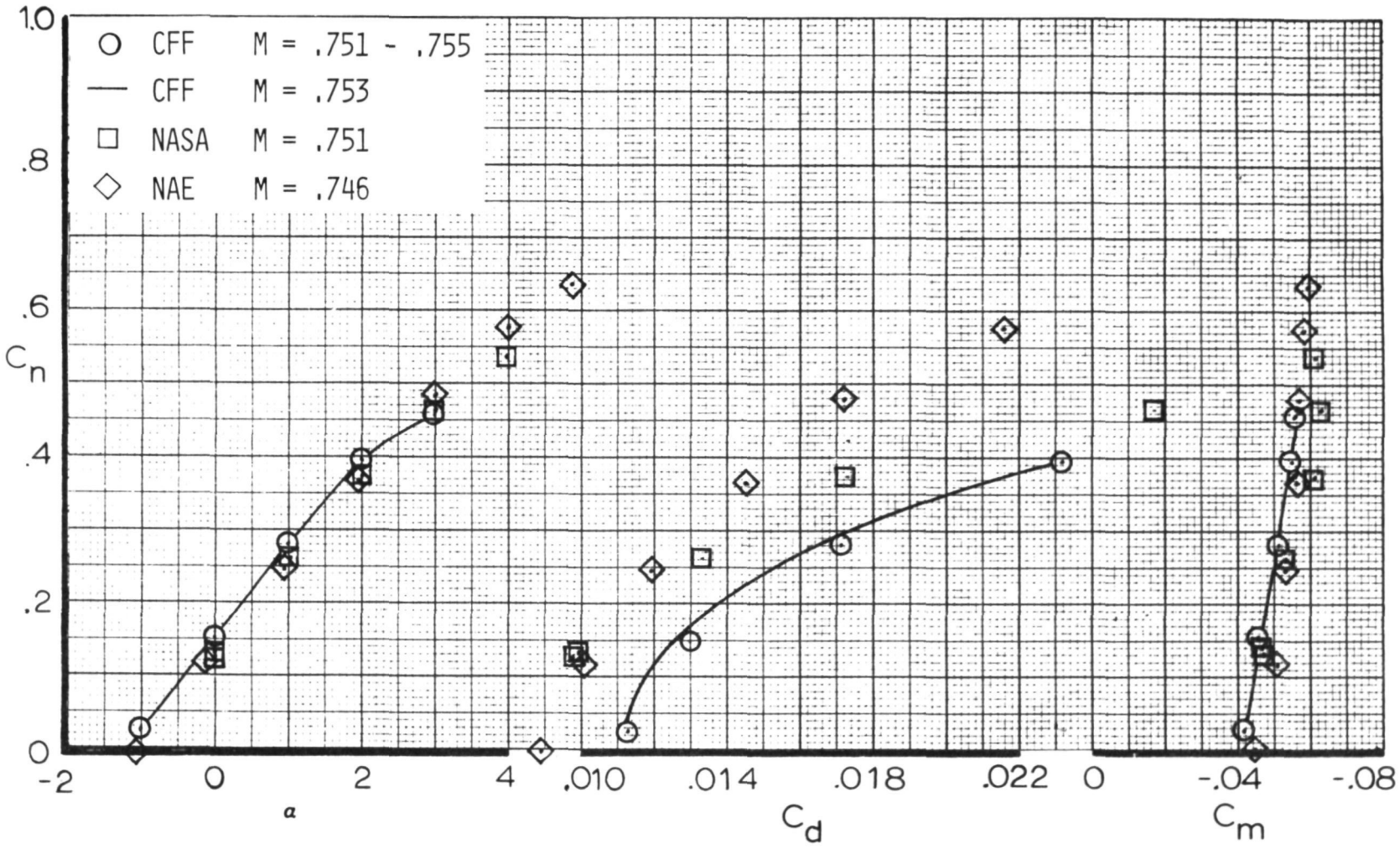

Figure 47. - Airfoil force data for M = 0.75 , R_N = 12 x 10^6, X/C_T = 0.05.

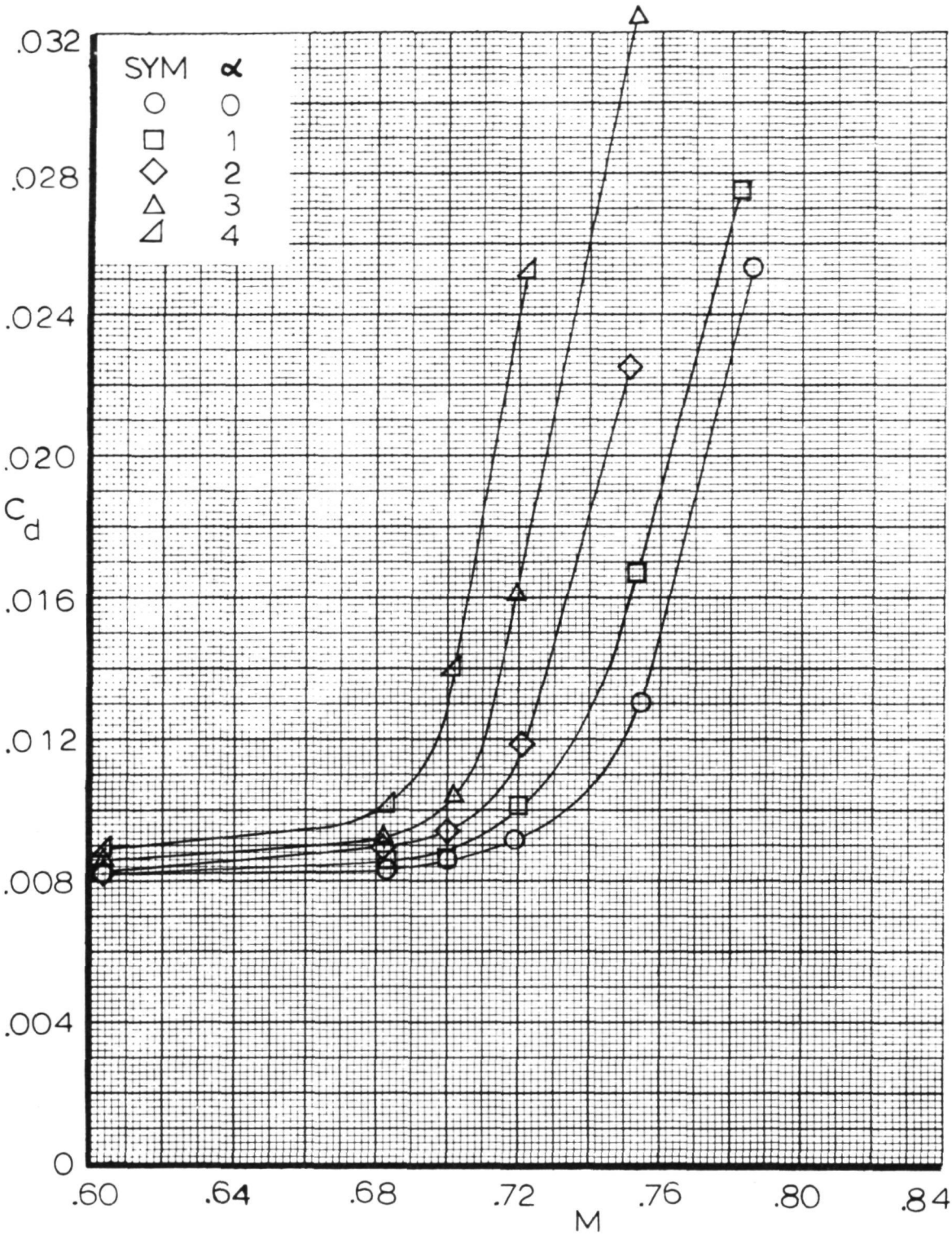

Figure 48. - Airfoil drag rise characteristics, $R_N = 12 \times 10^6$, $X/C_T = .05$.

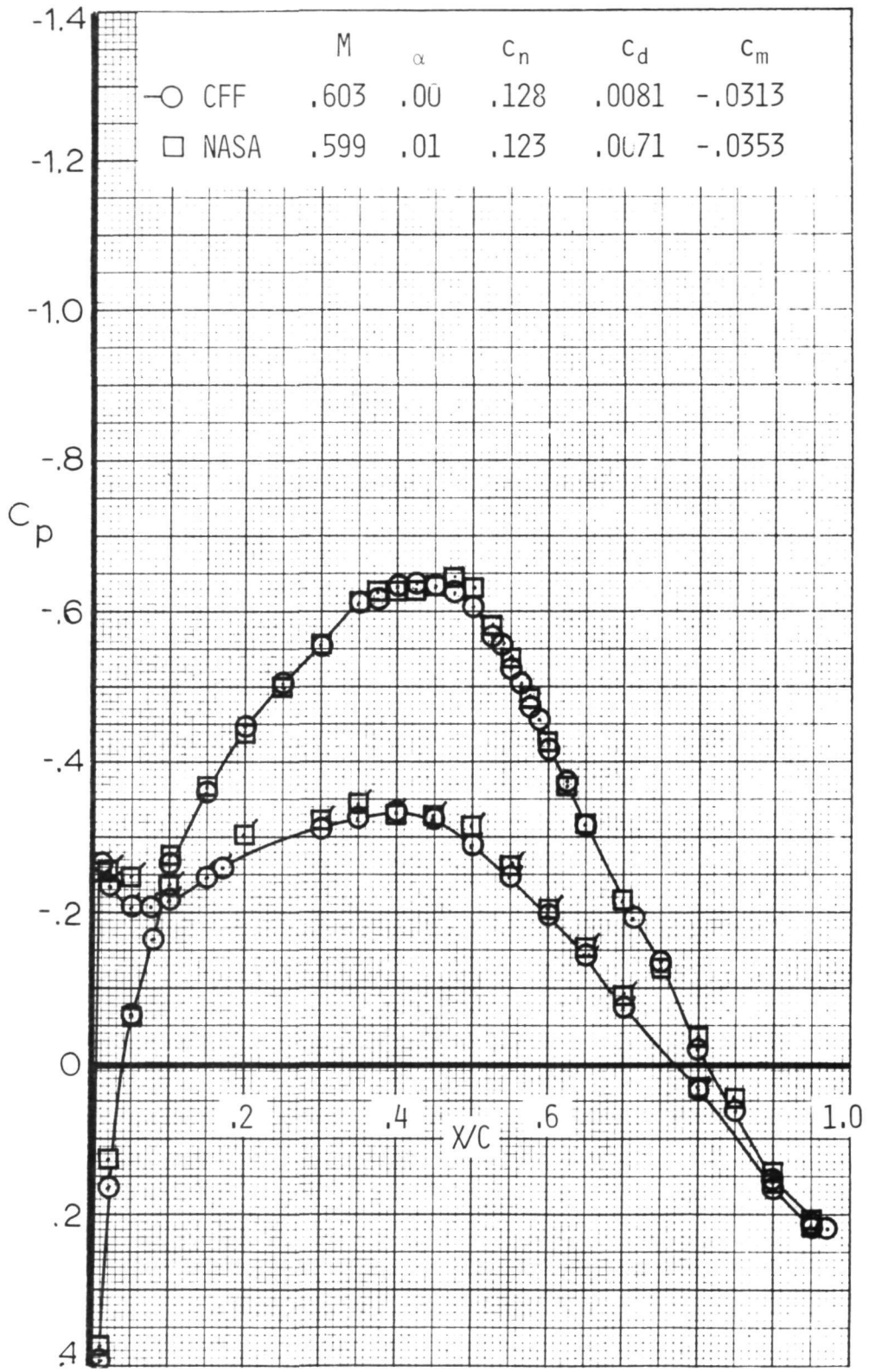

Figure 49. - Airfoil pressure distribution correlation at M = .6, $R_N = 12 \times 10^6$, $\alpha = 0°$.

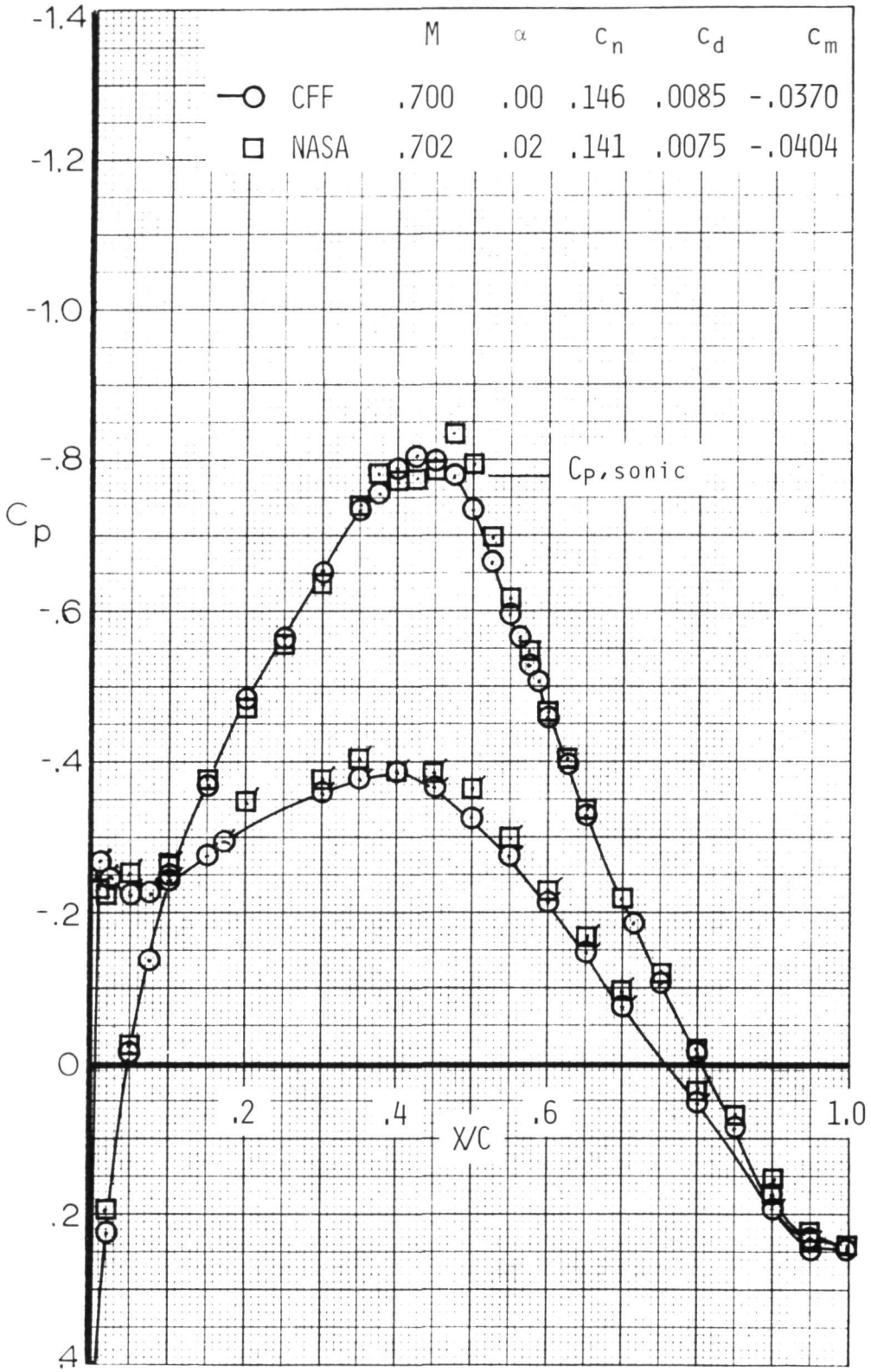

Figure 50. - Airfoil pressure distribution correlation at M = .7, R_N = 12 x 10^6, α = 0° (Flags denote l.s.).

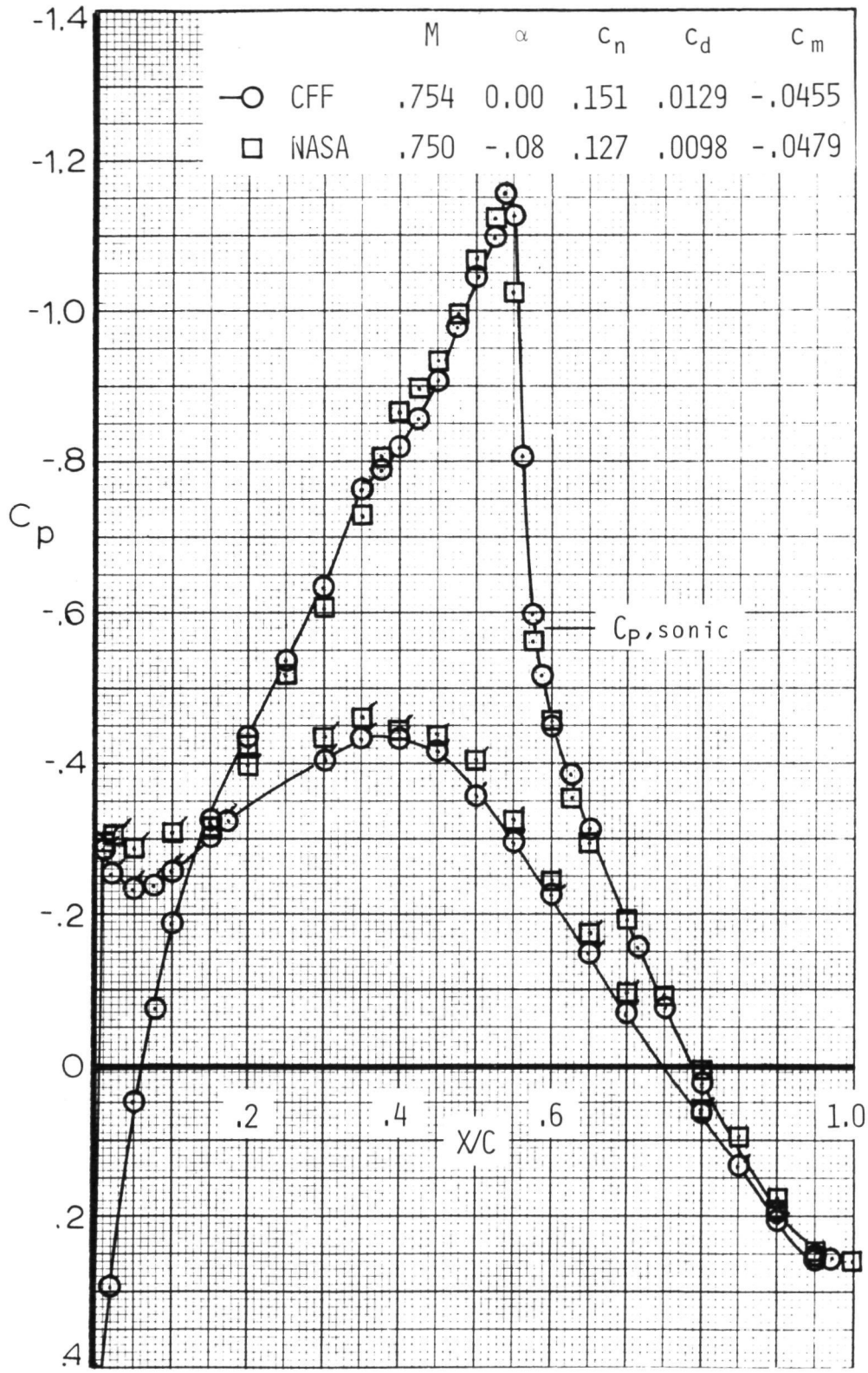

Figure 51. - Airfoil pressure distribution correlation at M = .75, R_N = 12 x 10^6, α = 0° (Flags denote l.s.)

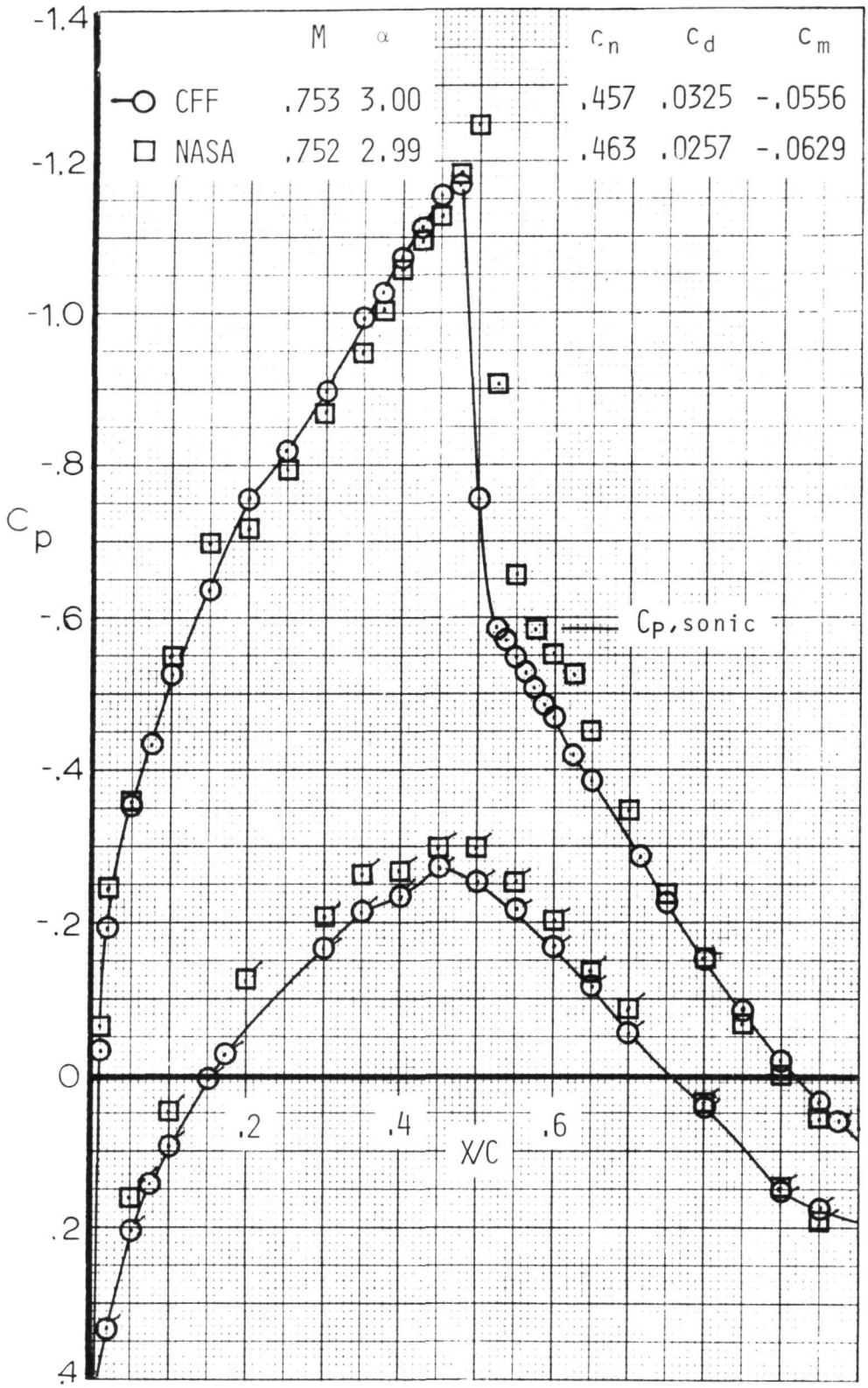

Figure 52. - Airfoil pressure distribution correlation at M = .75, R_N = 12 x 10^6, α = 3° (Flags denote l.s.)

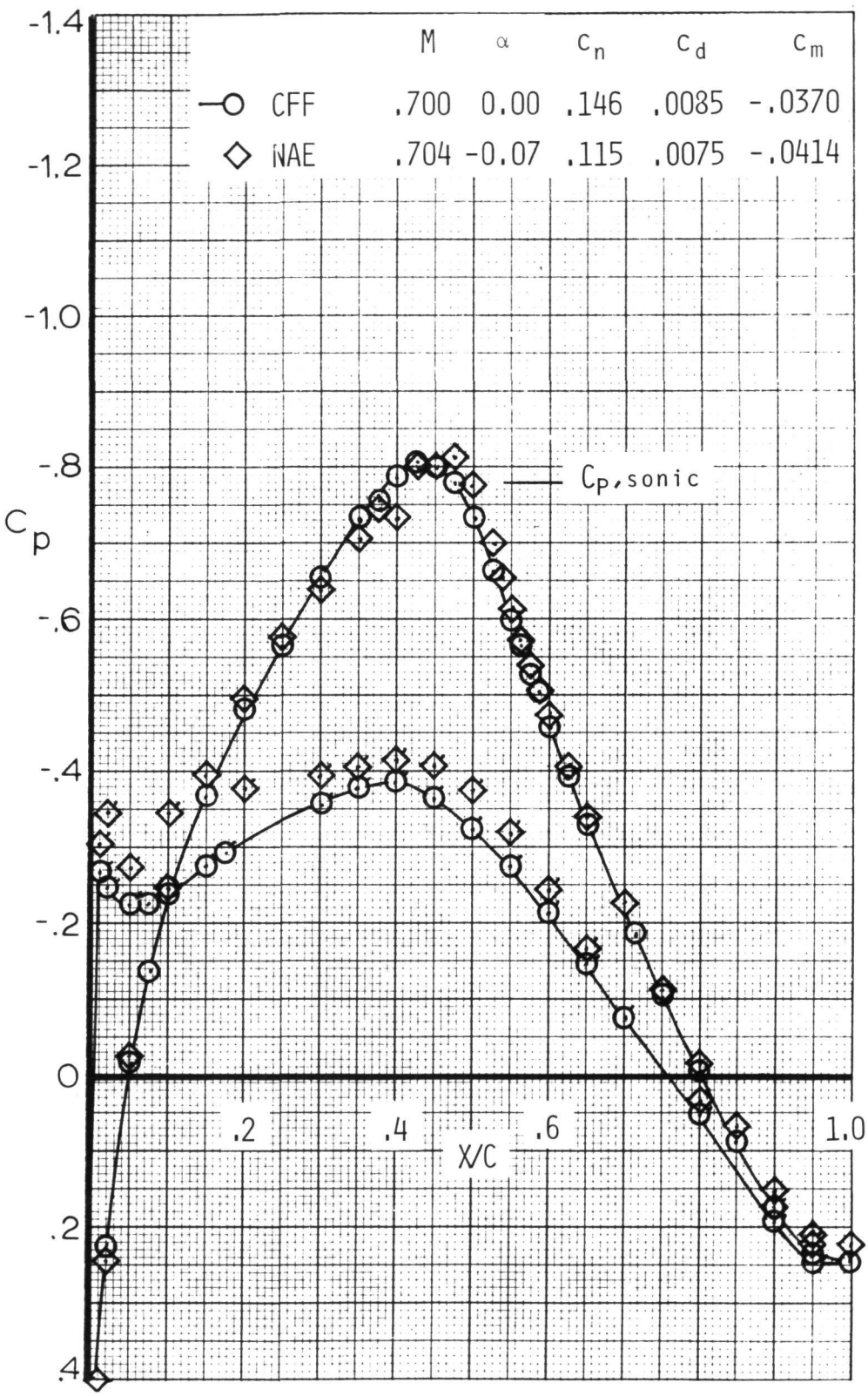

Figure 53. - Airfoil pressure distribution correlation at M = .7, R_N = 12 x 10^6, α = 0° (Flags denote l.s.).

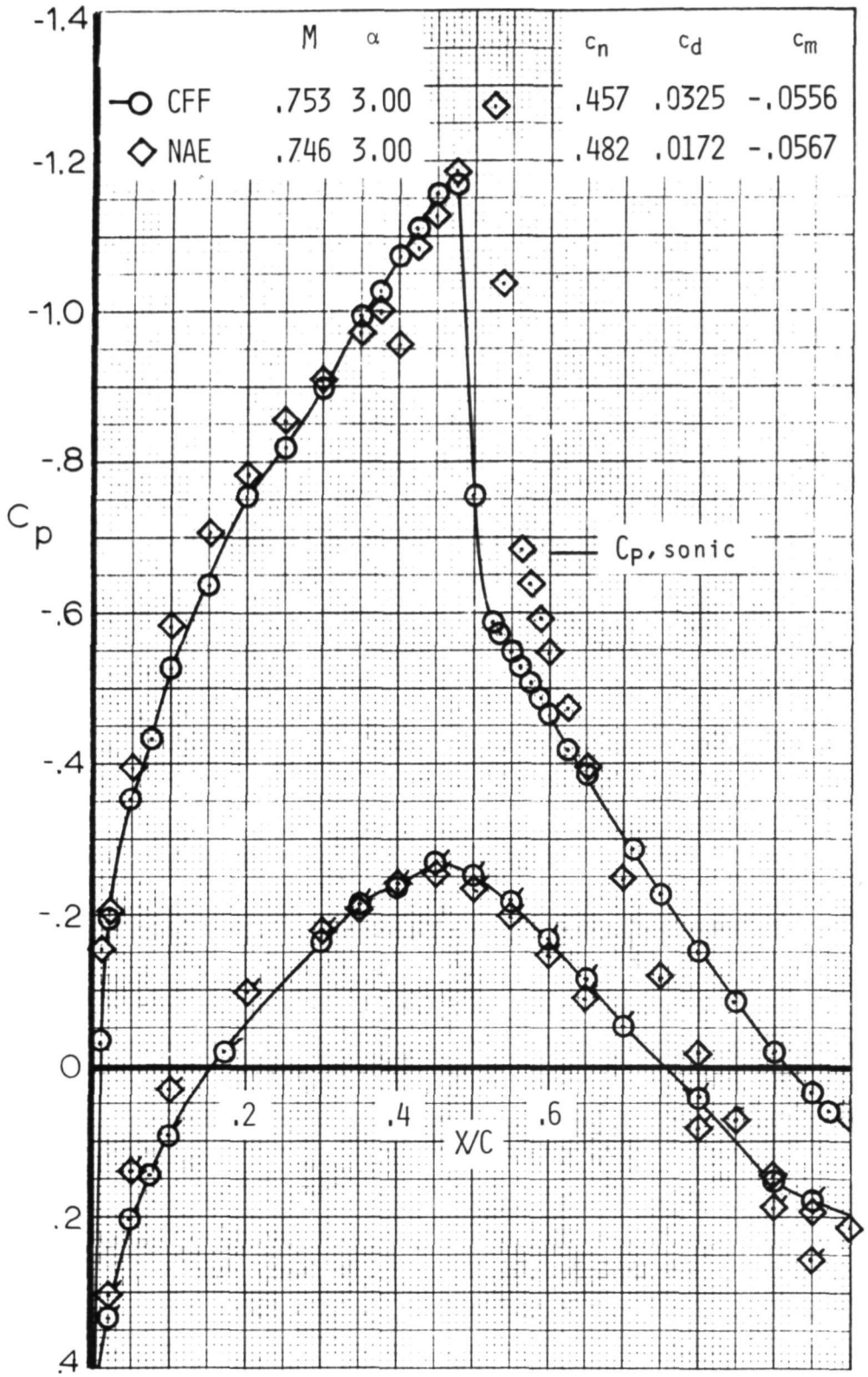

Figure 54. - Airfoil pressure distribution correlation at M = .75, R_N = 12 x 10^6, α = 3° (Flags denote l.s.).

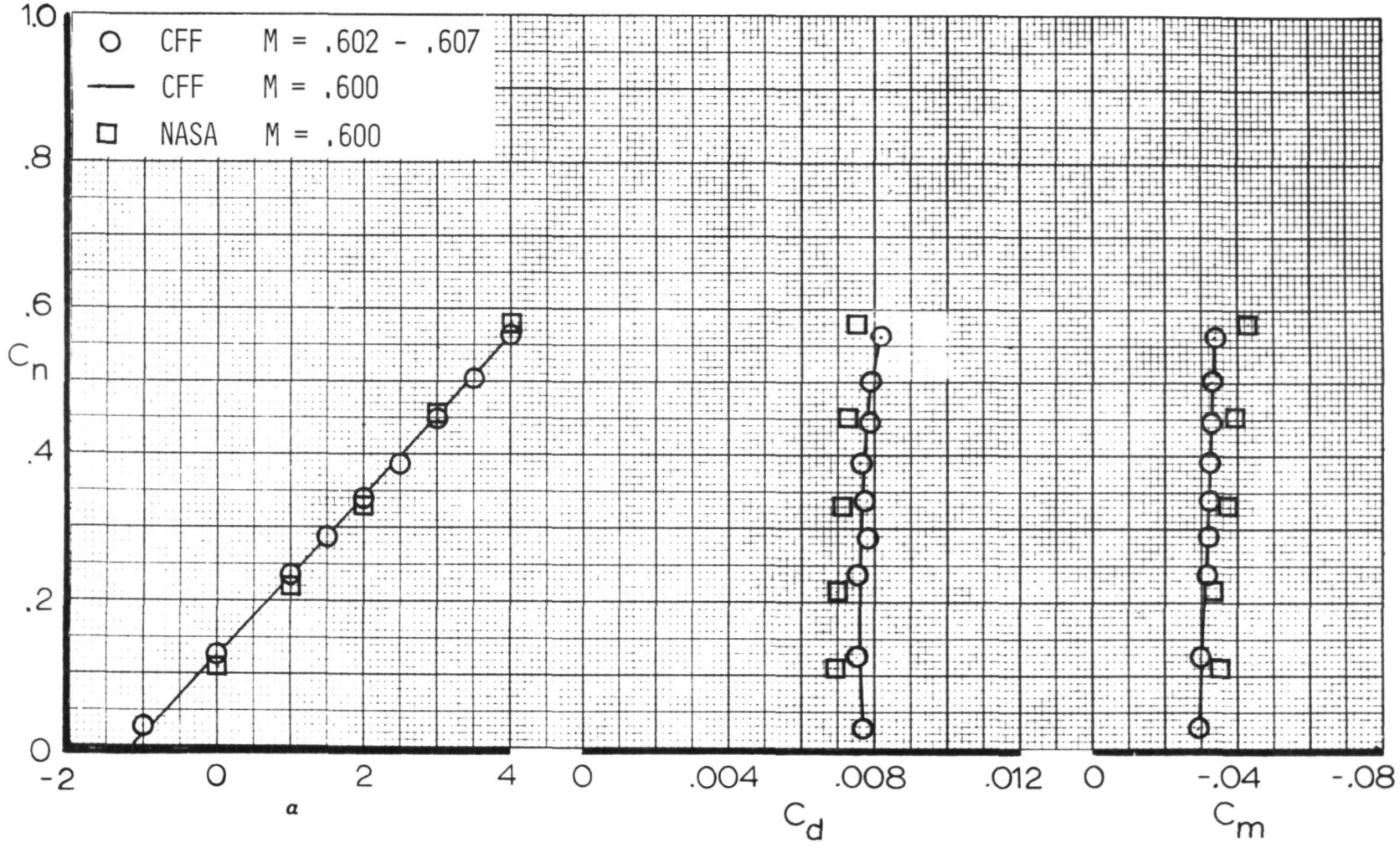

Figure 55. - Airfoil force data for M = 0.60 , R_N = 17 x 10^6, X/C_T = Free.

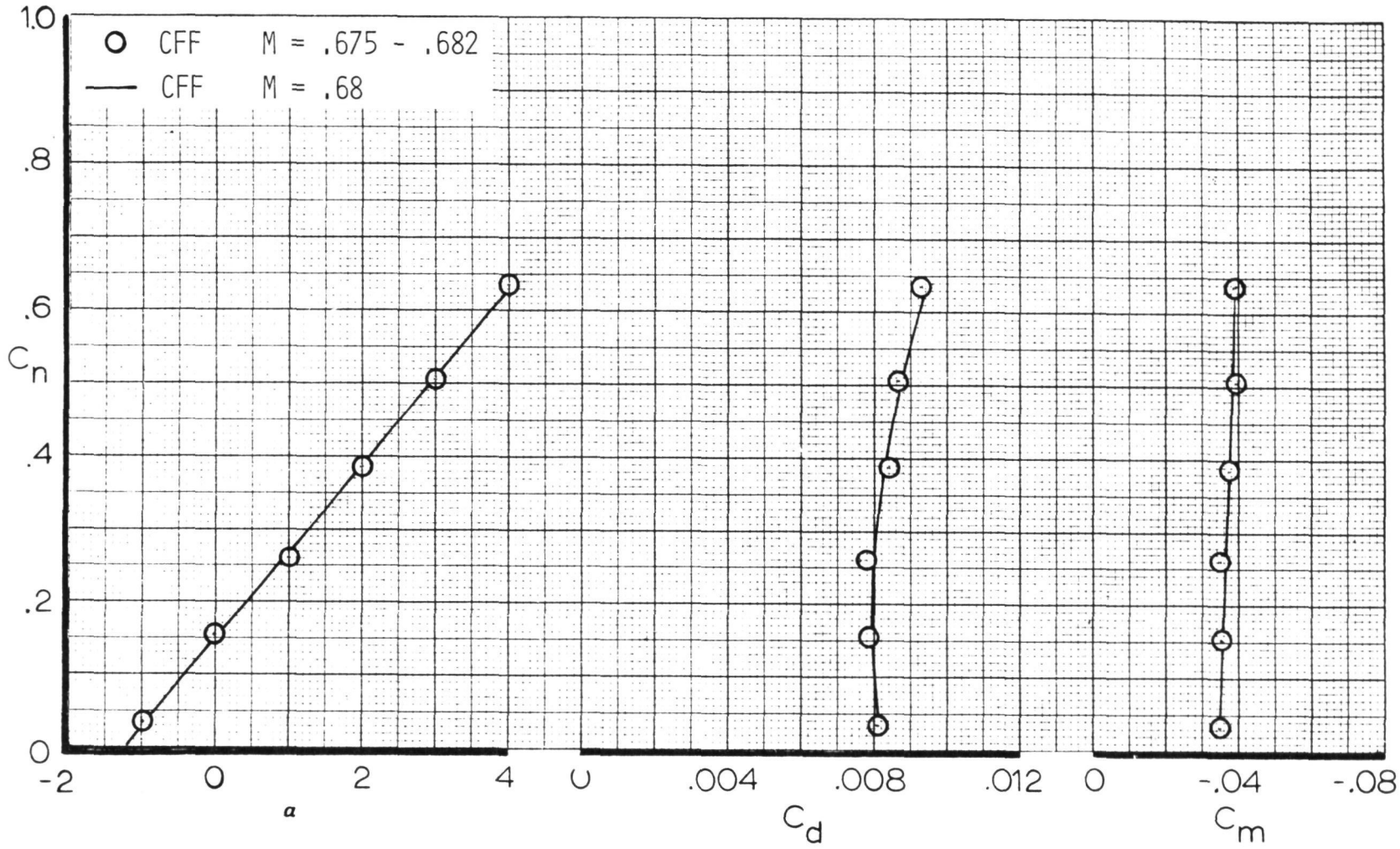

Figure 56. - Airfoil force data for M = 0.68 , R_N = 17 x 10^6, X/C_T = Free.

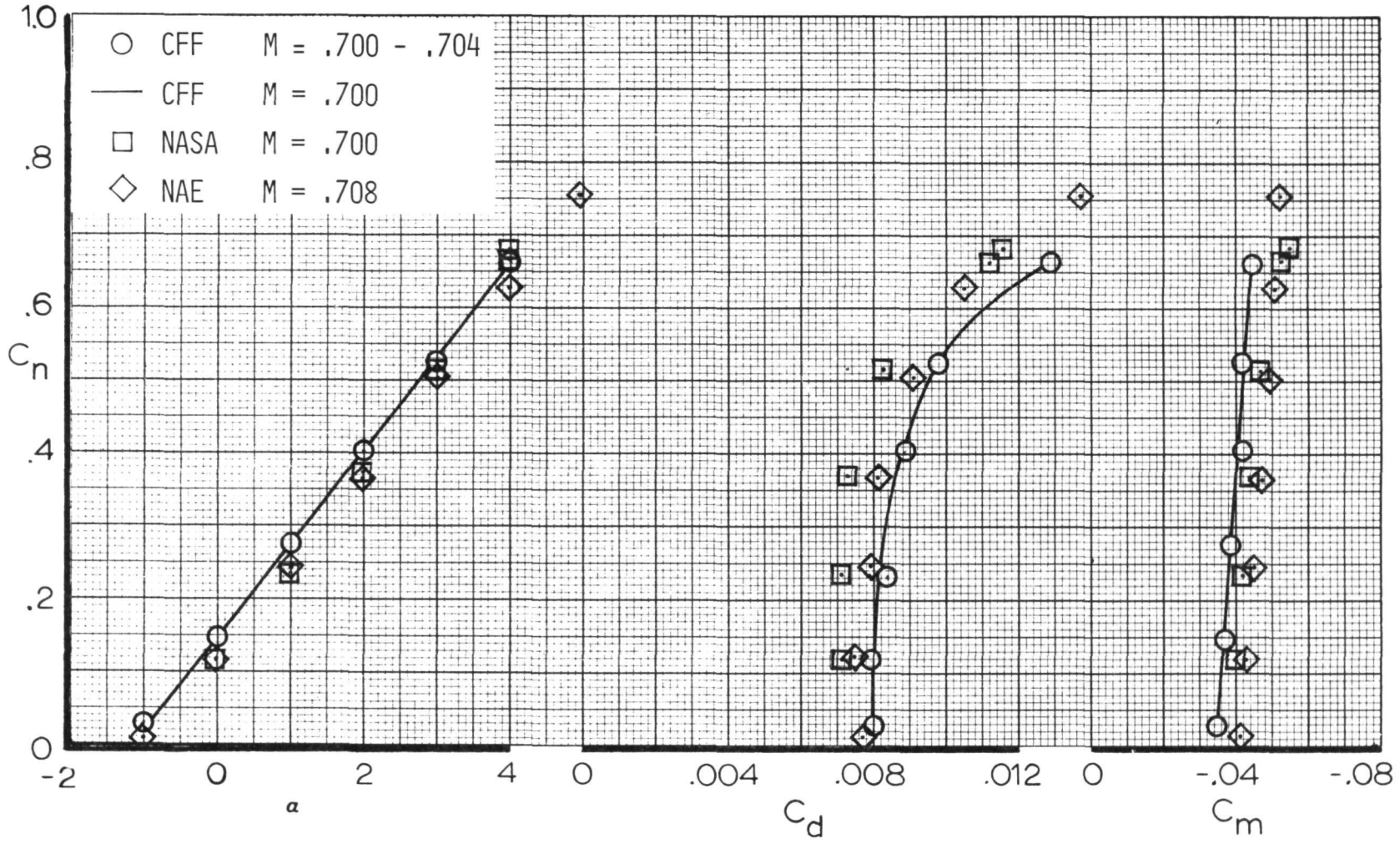

Figure 57. - Airfoil force data for M = 0.70 , R_N = 17 X 10^6, X/C_T = Free.

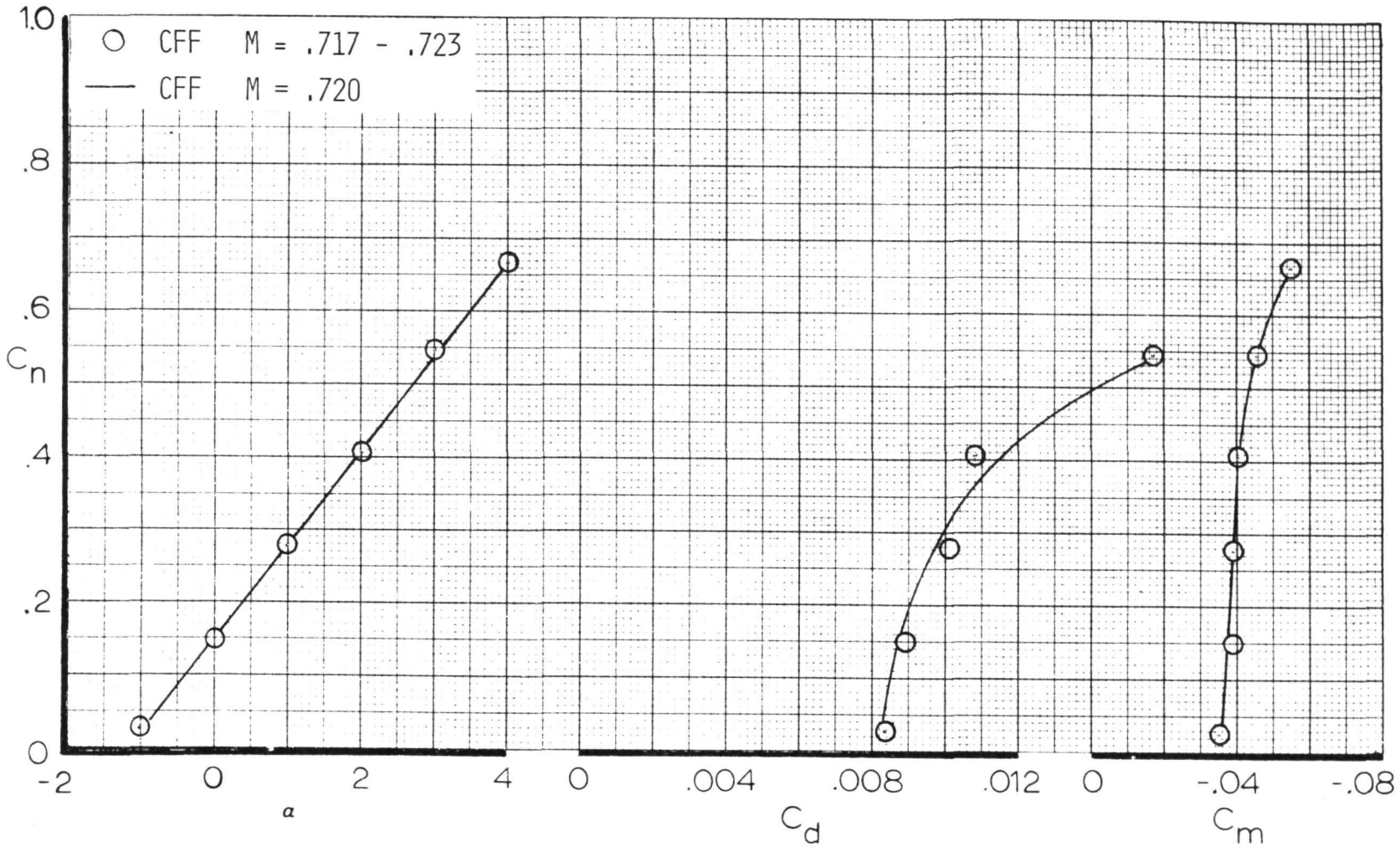

Figure 58. - Airfoil force data for M = 0.72 , R_N = 17 x 10^6, X/C_T = Free.

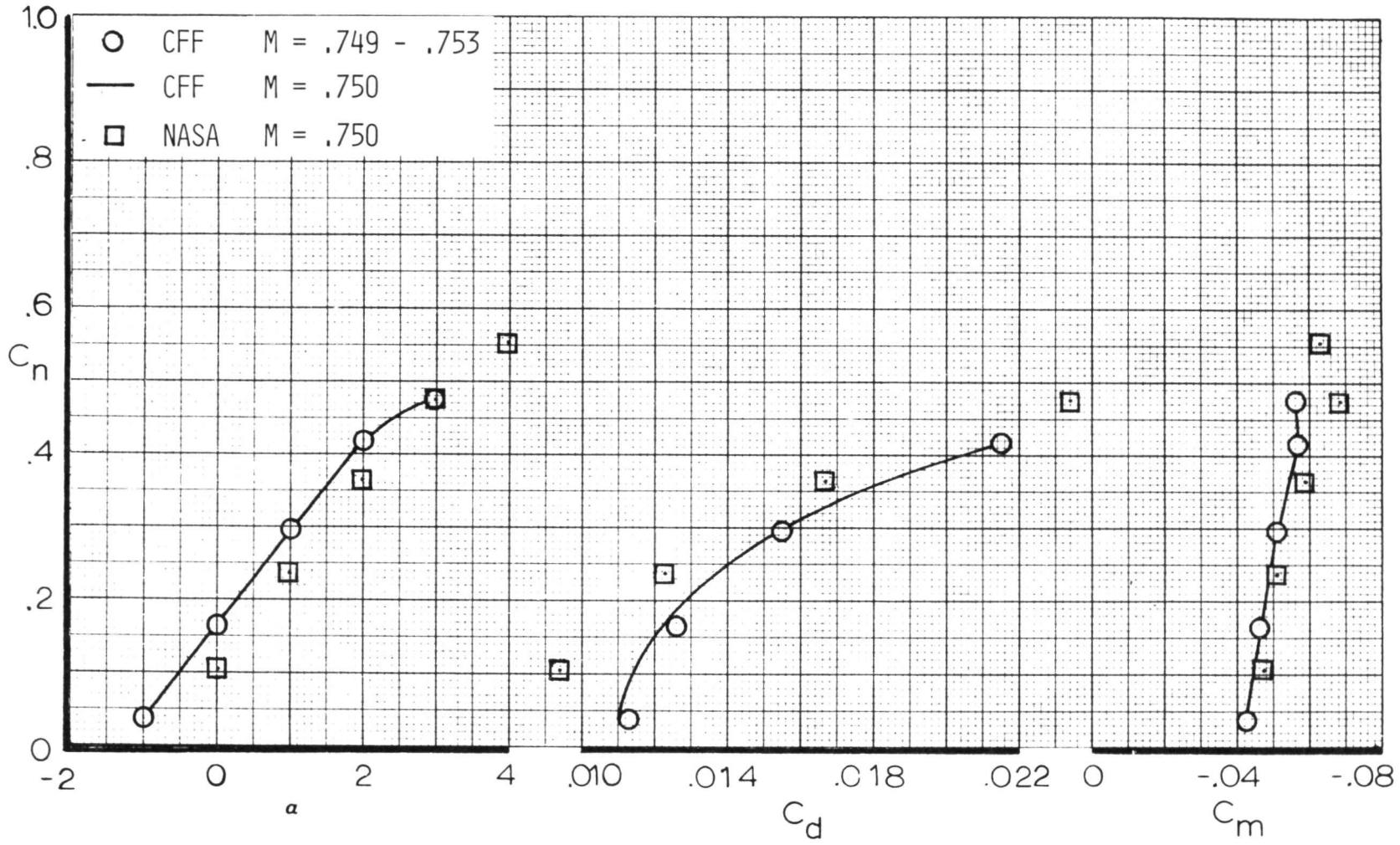

Figure 59. - Airfoil force data for M = 0.75 , R_N = 17 x 10^6, X/C_T = Free.

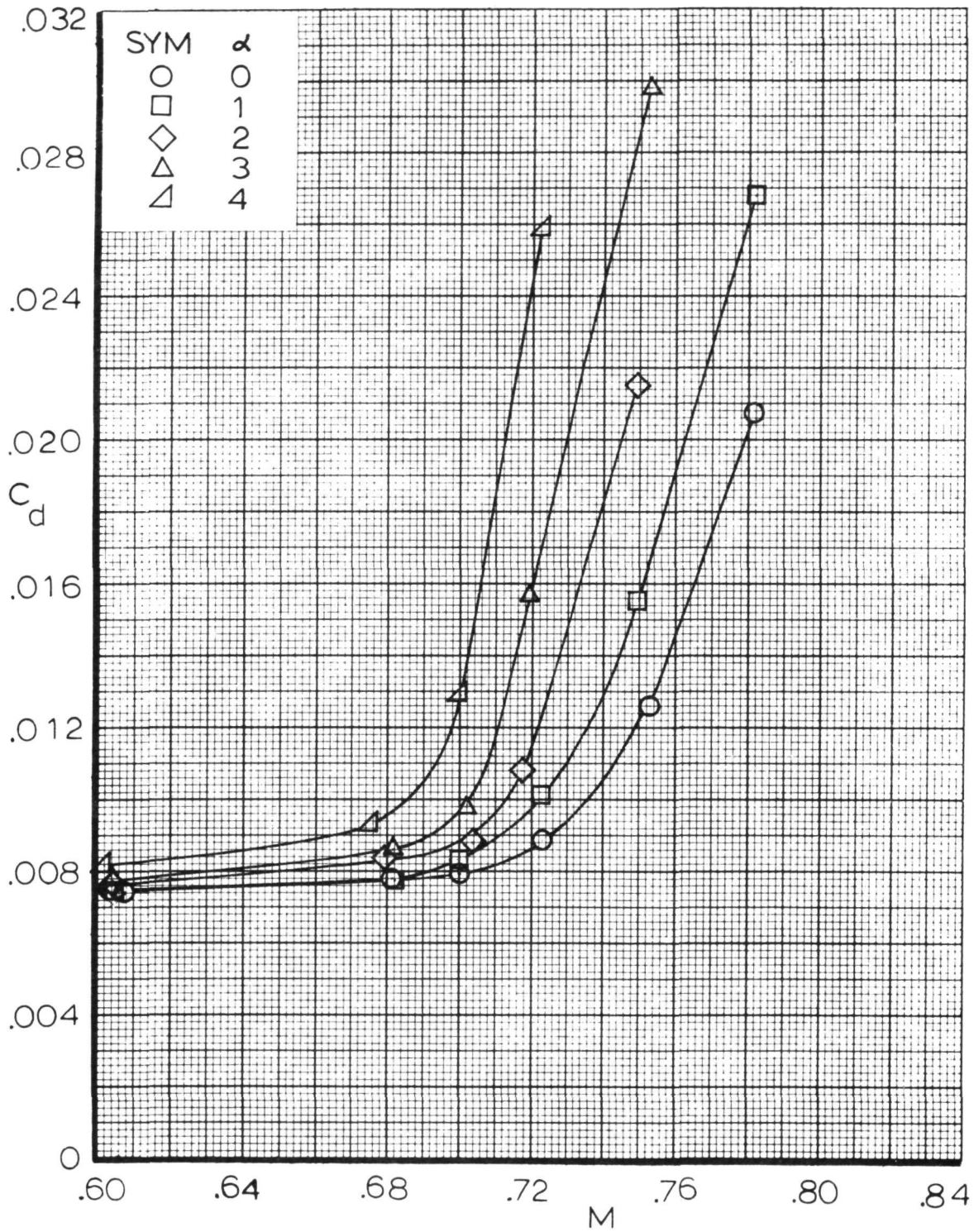

Figure 60. - Airfoil drag rise characteristics, $R_N = 17 \times 10^6$.

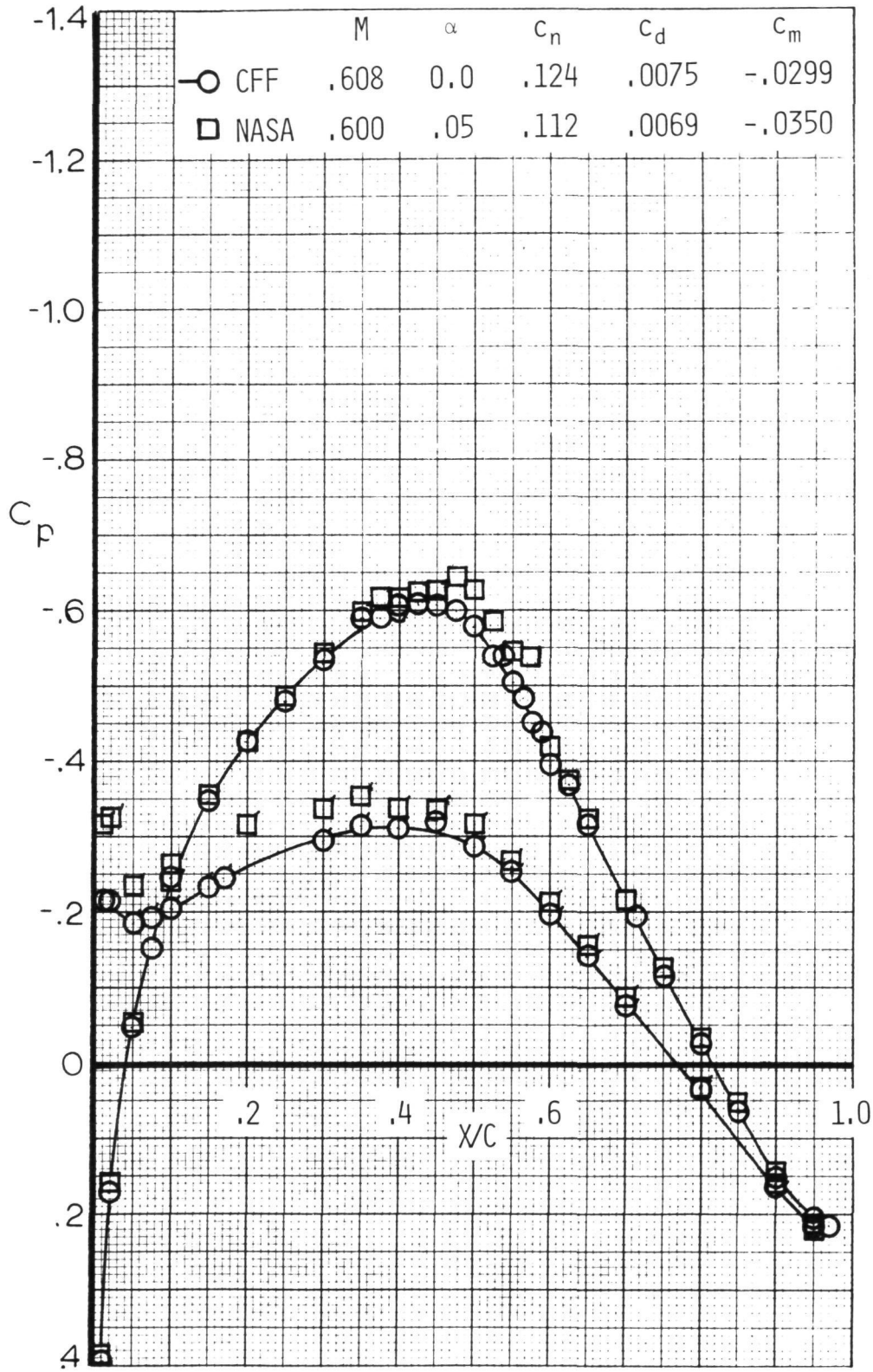

Figure 61. - Airfoil pressure distribution correlation at M = .6, R_N = 17 x 10^6, α = 0° (Flags denote l.s.).

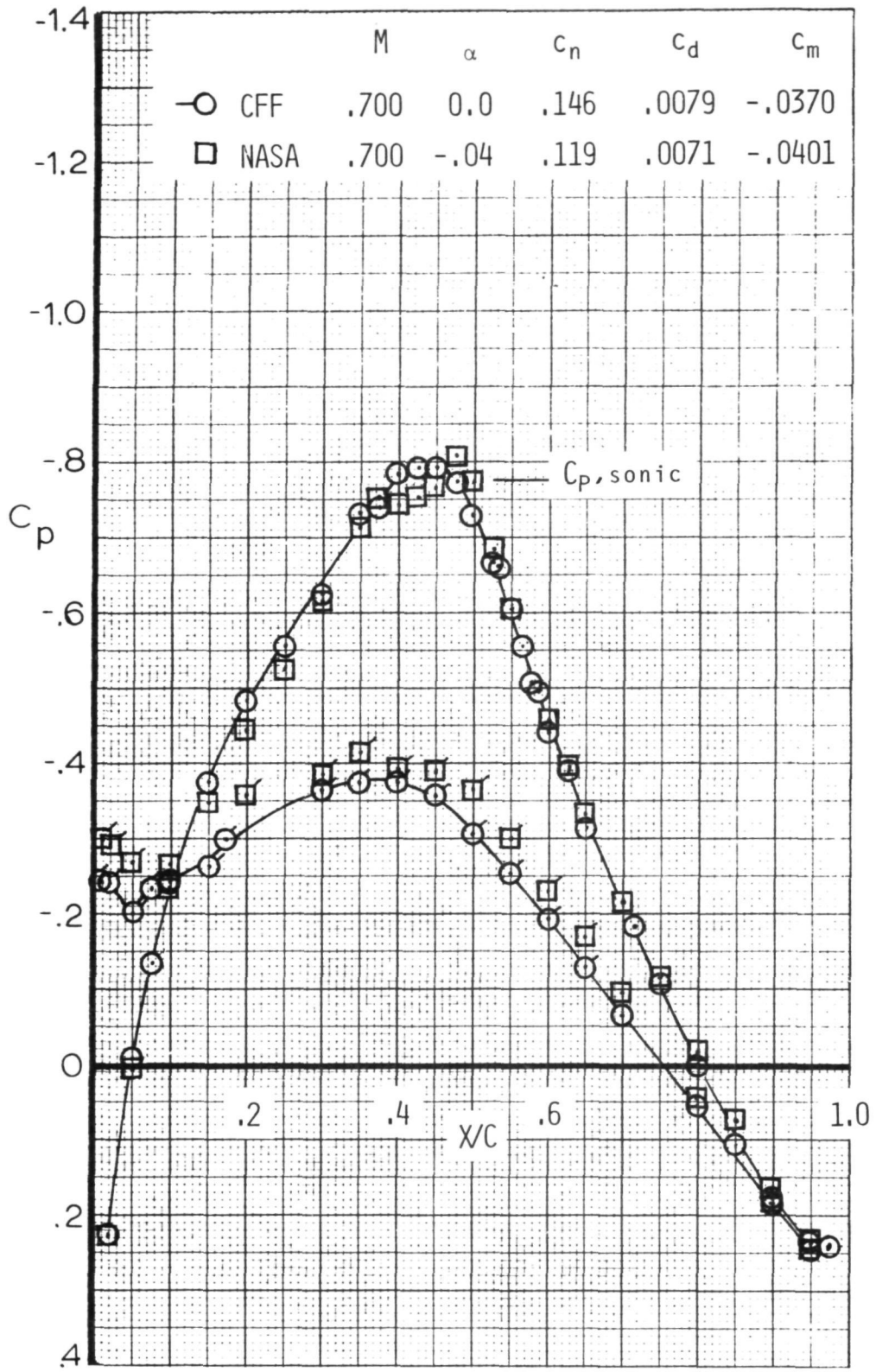

Figure 62. - Airfoil pressure distribution correlation at M = .7, R_N = 17 x 10^6, α = 0° (Flags denote l.s.).

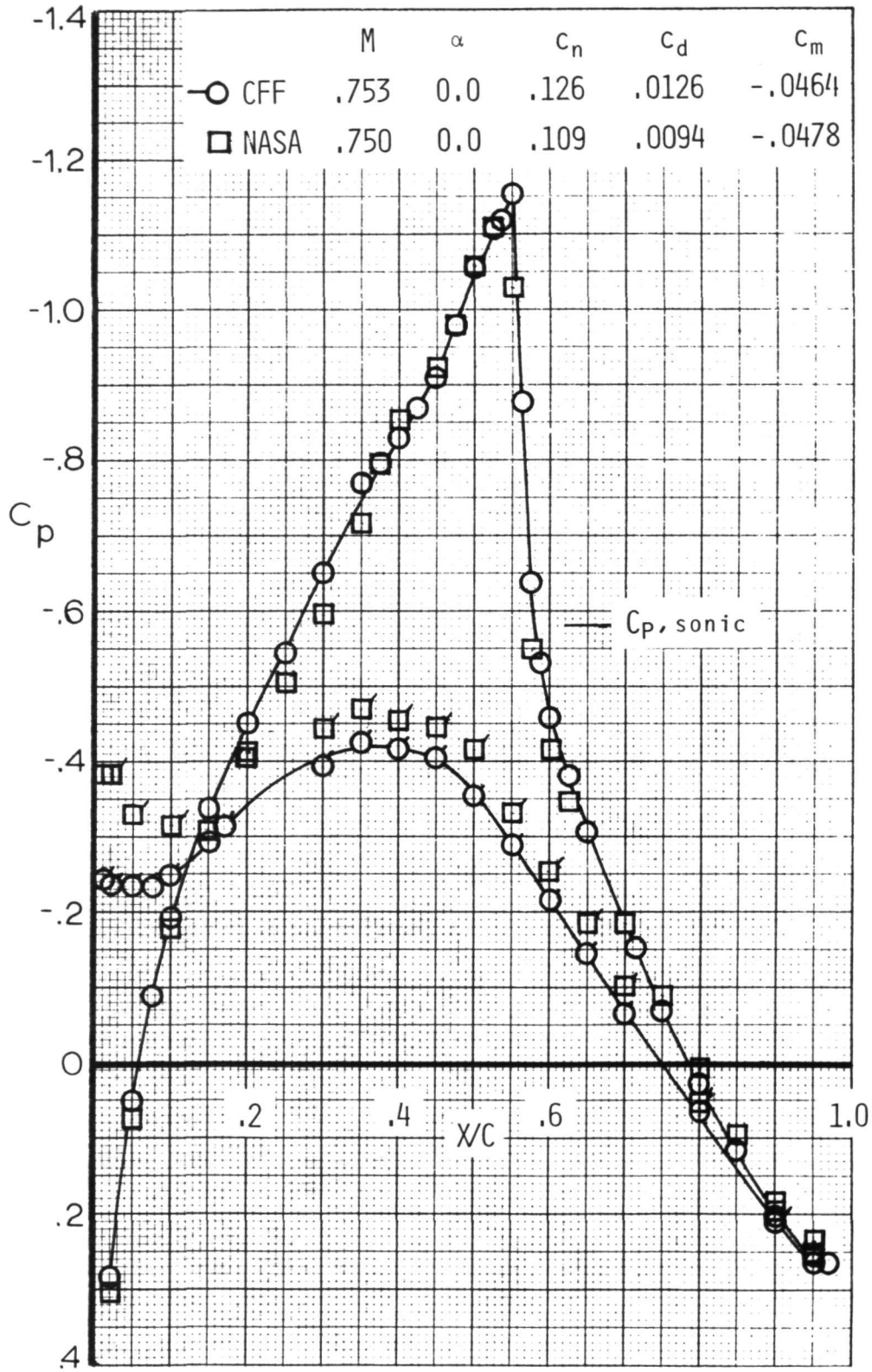

Figure 63. - Airfoil pressure distribution correlation at M = .75, R_N = 17 x 10^6, α = 0° (Flags denote l.s.).

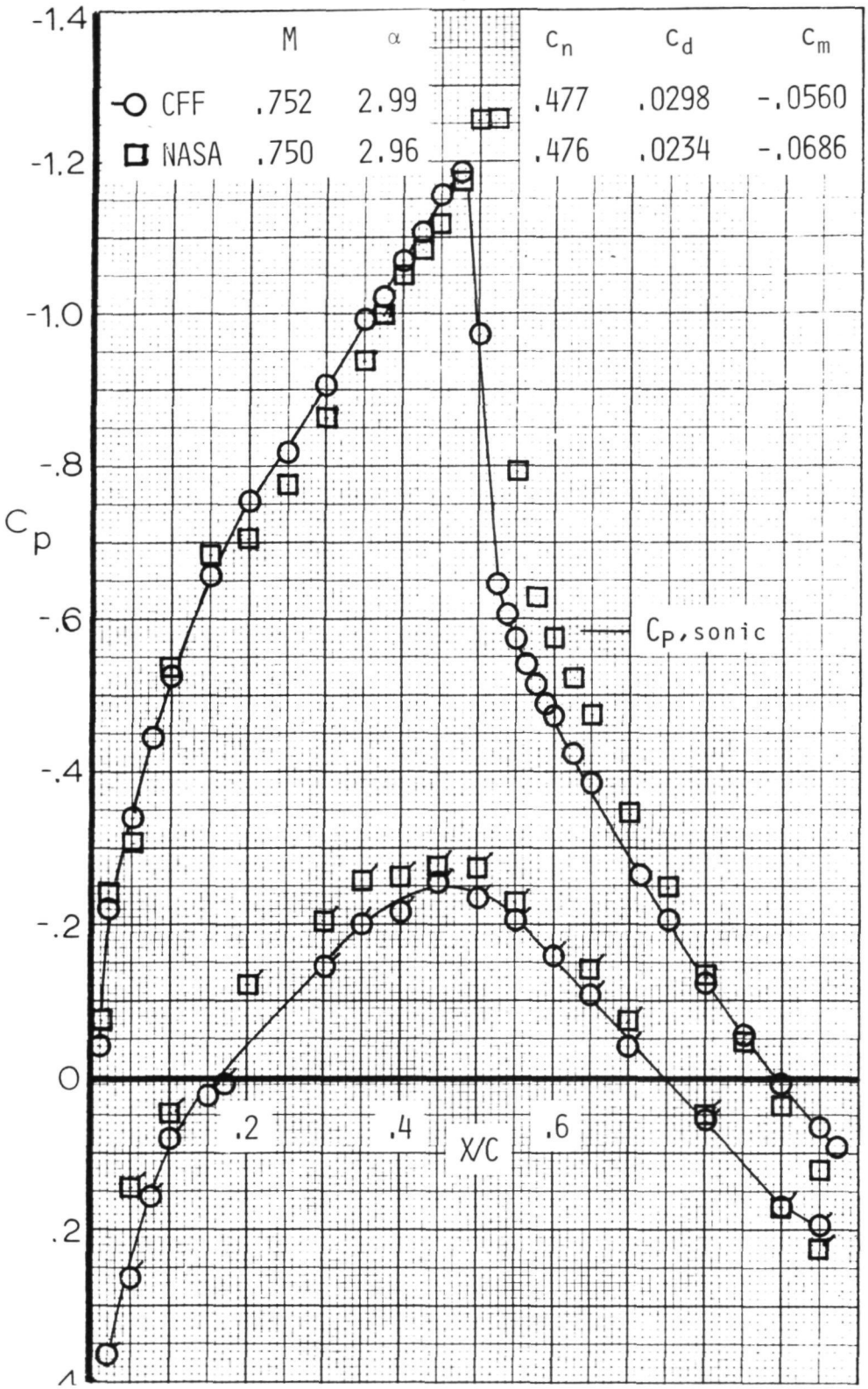

Figure 64. - Airfoil pressure distribution correlation at M = .75, R_N = 17 x 10^6, α = 3° (Flags denote l.s.).

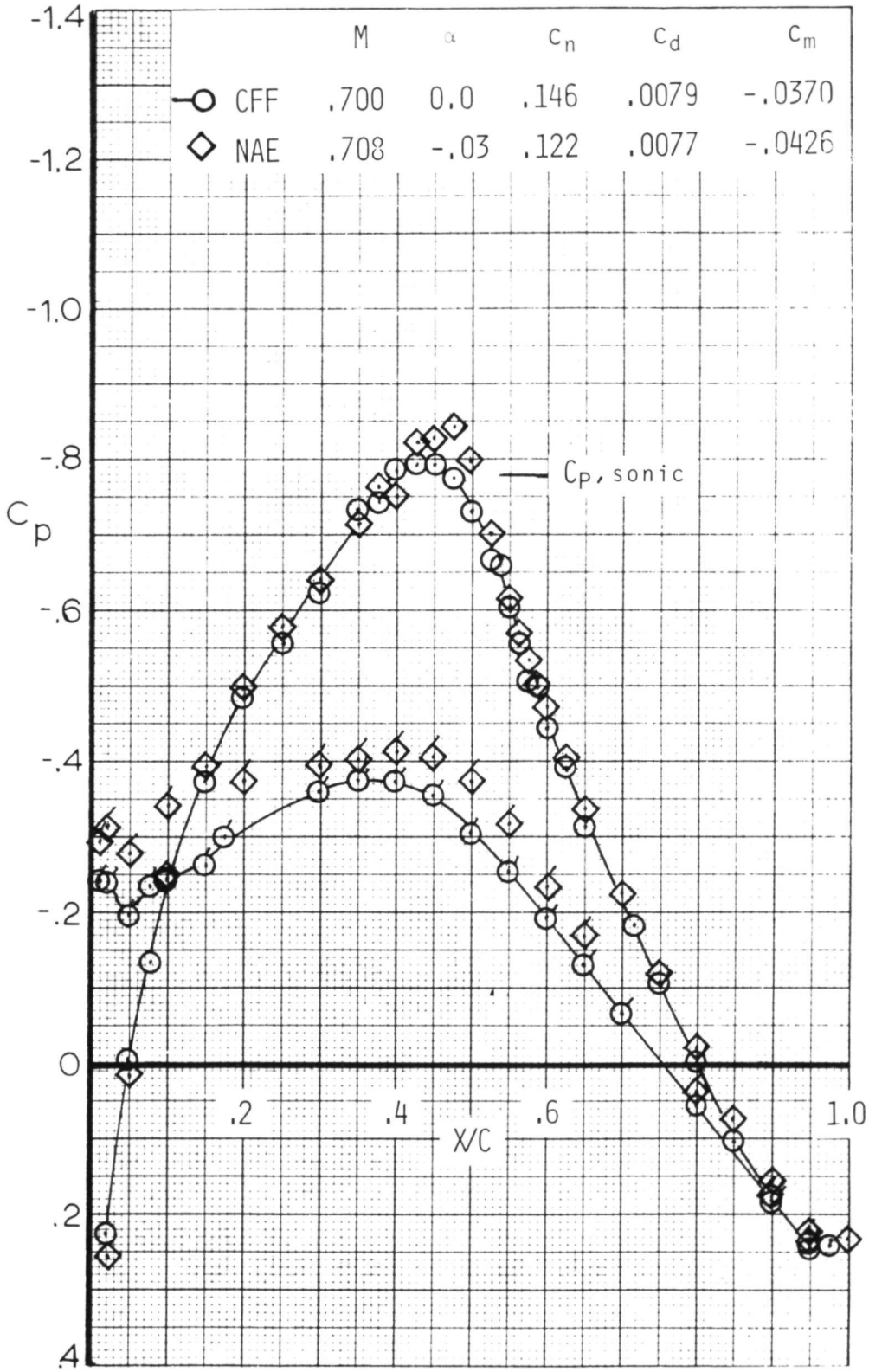

Figure 65. - Airfoil pressure distribution correlation at M = .7, R_N = 17 x 10^6, α = 0° (Flags denote l.s.).

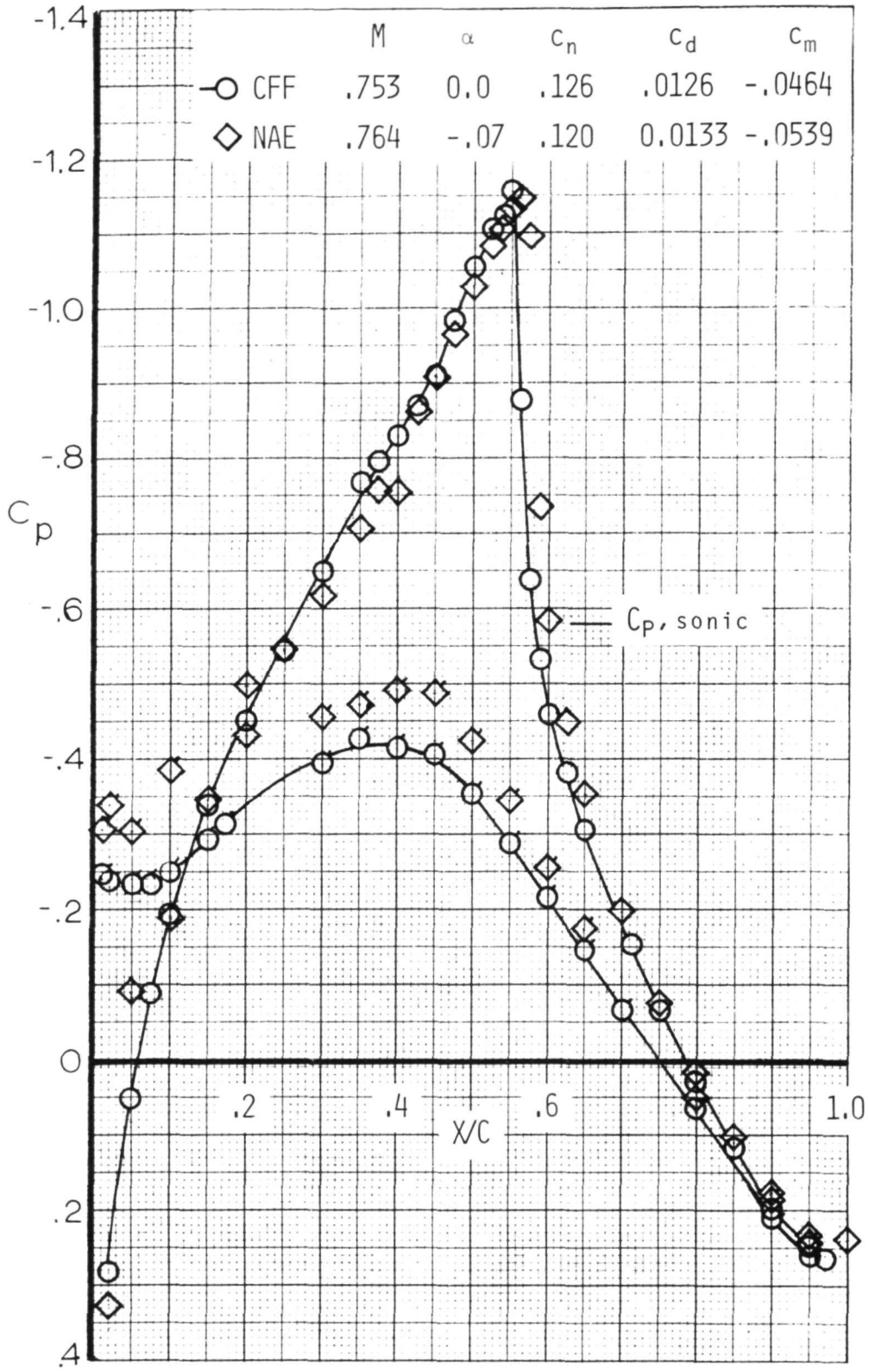

Figure 66. - Airfoil pressure distribution correlation at M = .75, R_N = 17 x 10^6, α = 0° (Flags denote l.s.).

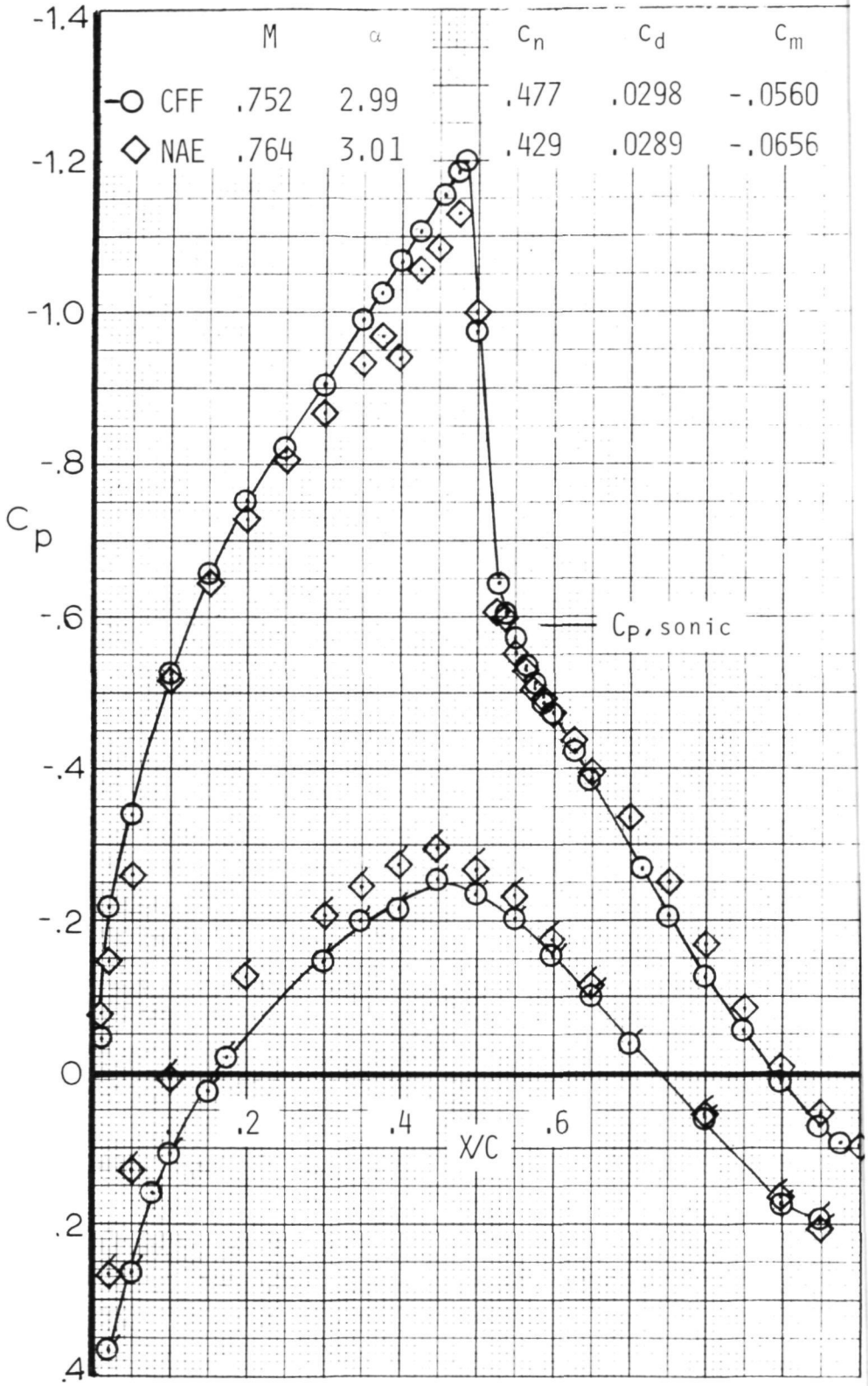

Figure 67. - Airfoil pressure distribution correlation at M = .75, R_N = 17 x 10^6, α = 3° (Flags denote l.s.).

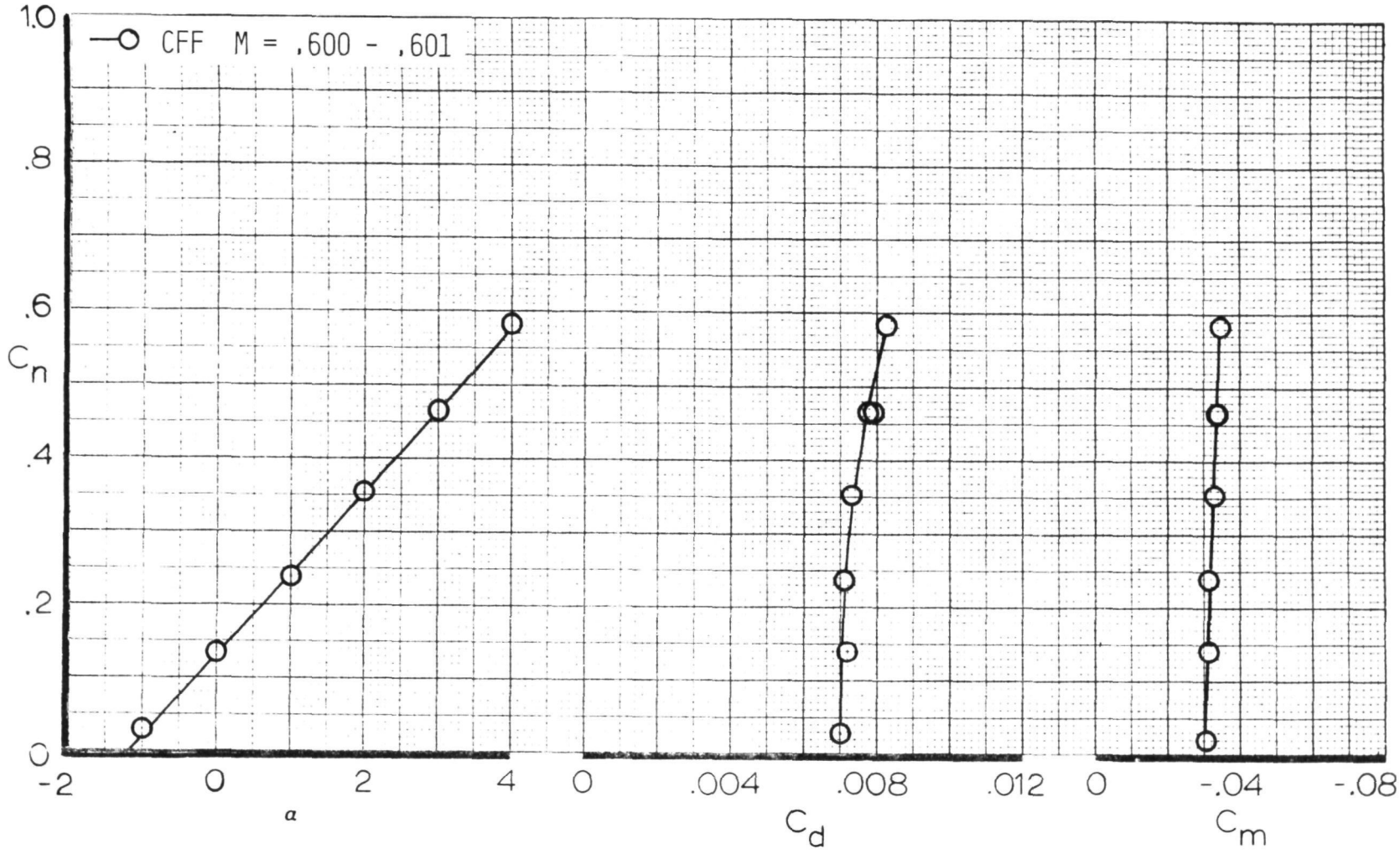

Figure 68. - Airfoil force data for M = 0.60 , R_N = 25 x 10^6, X/C_T = Free.

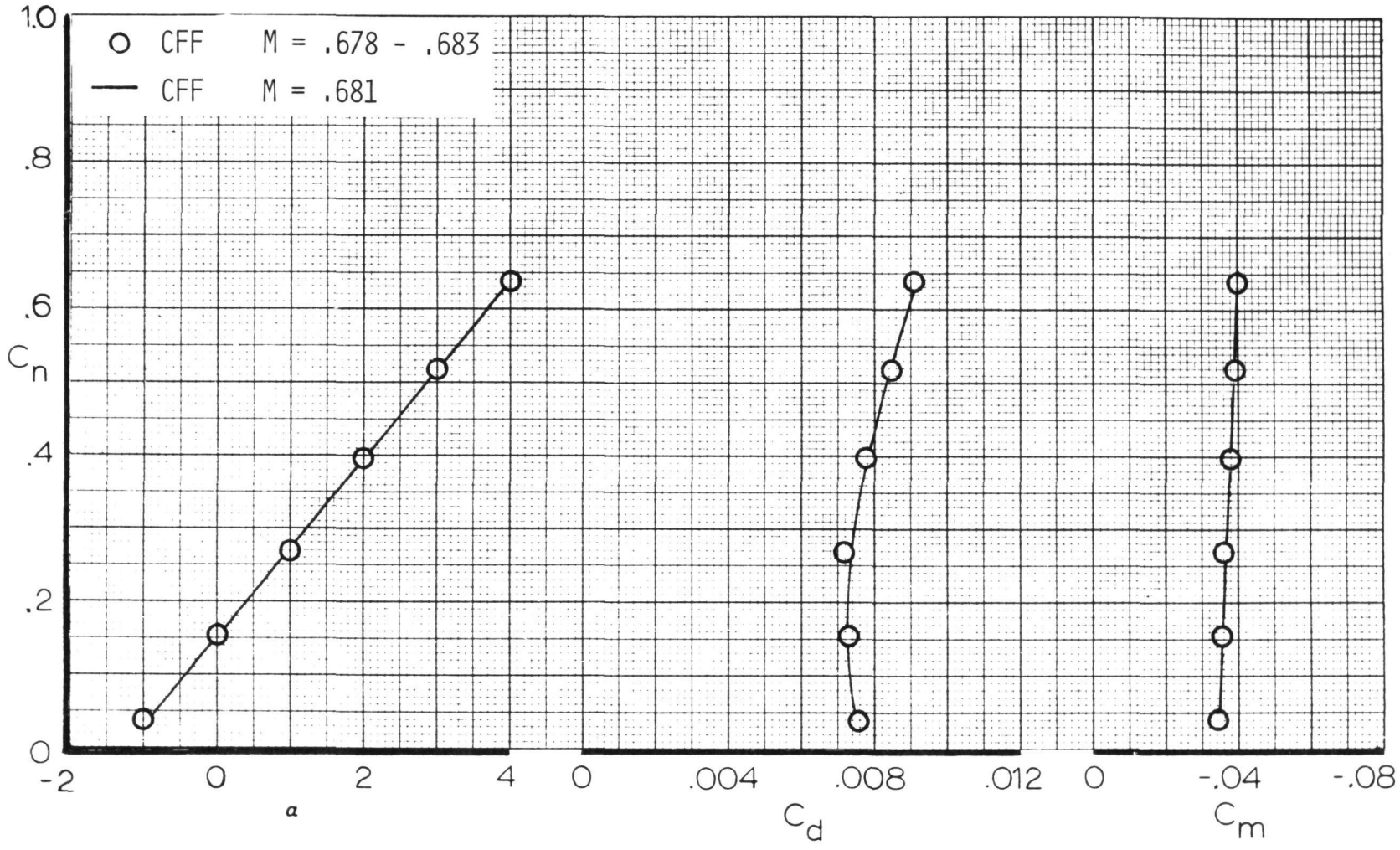

Figure 69. - Airfoil force data for M = 0.68 , R_N = 32 x 10^6, X/C_T = Free.

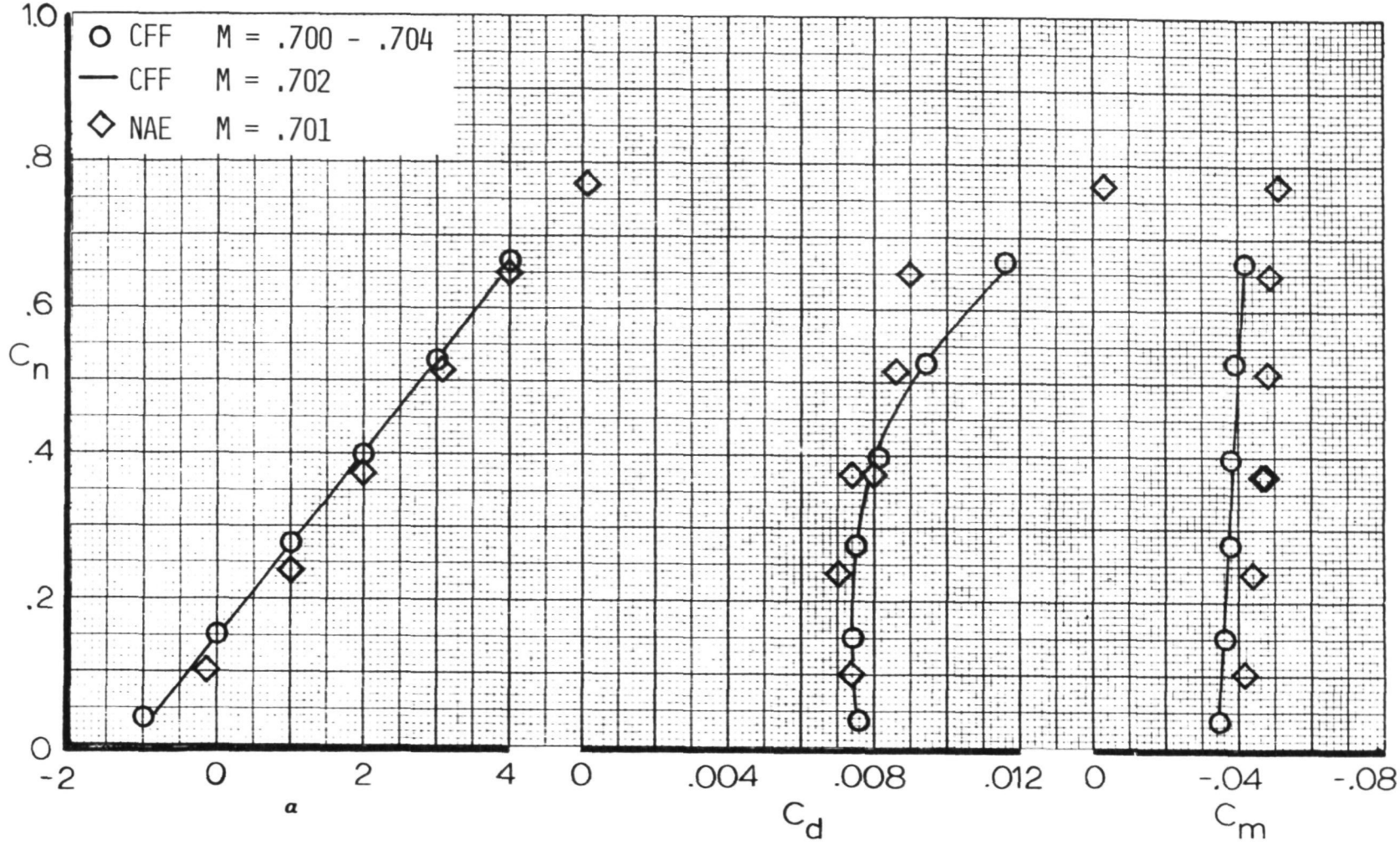

Figure 70. - Airfoil force data for M = 0.70 , R_N = 32 x 10^6, X/C_T = Free.

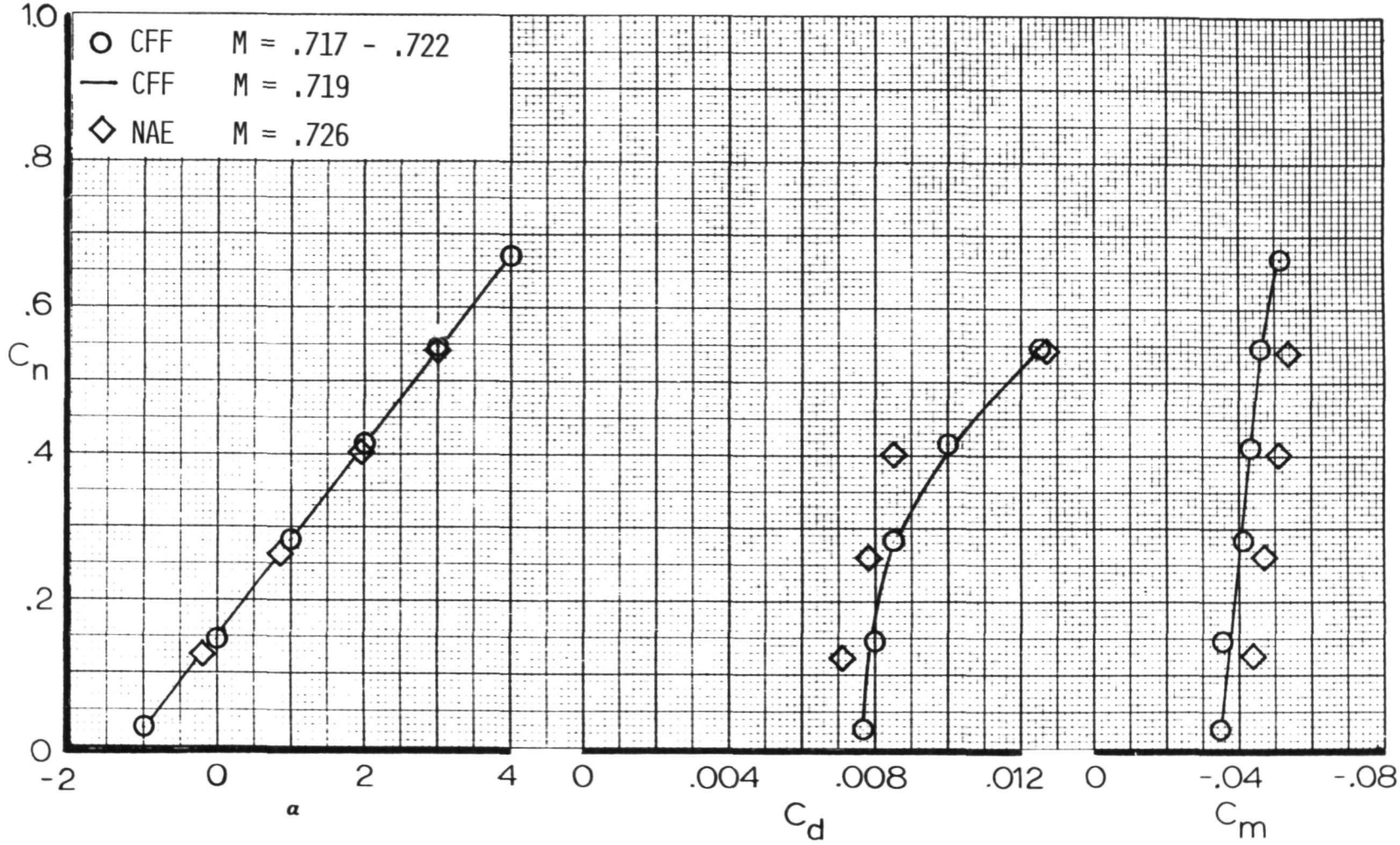

Figure 71. - Airfoil force data for M = 0.72 , R_N = 32 x 10^6, X/C_T = Free.

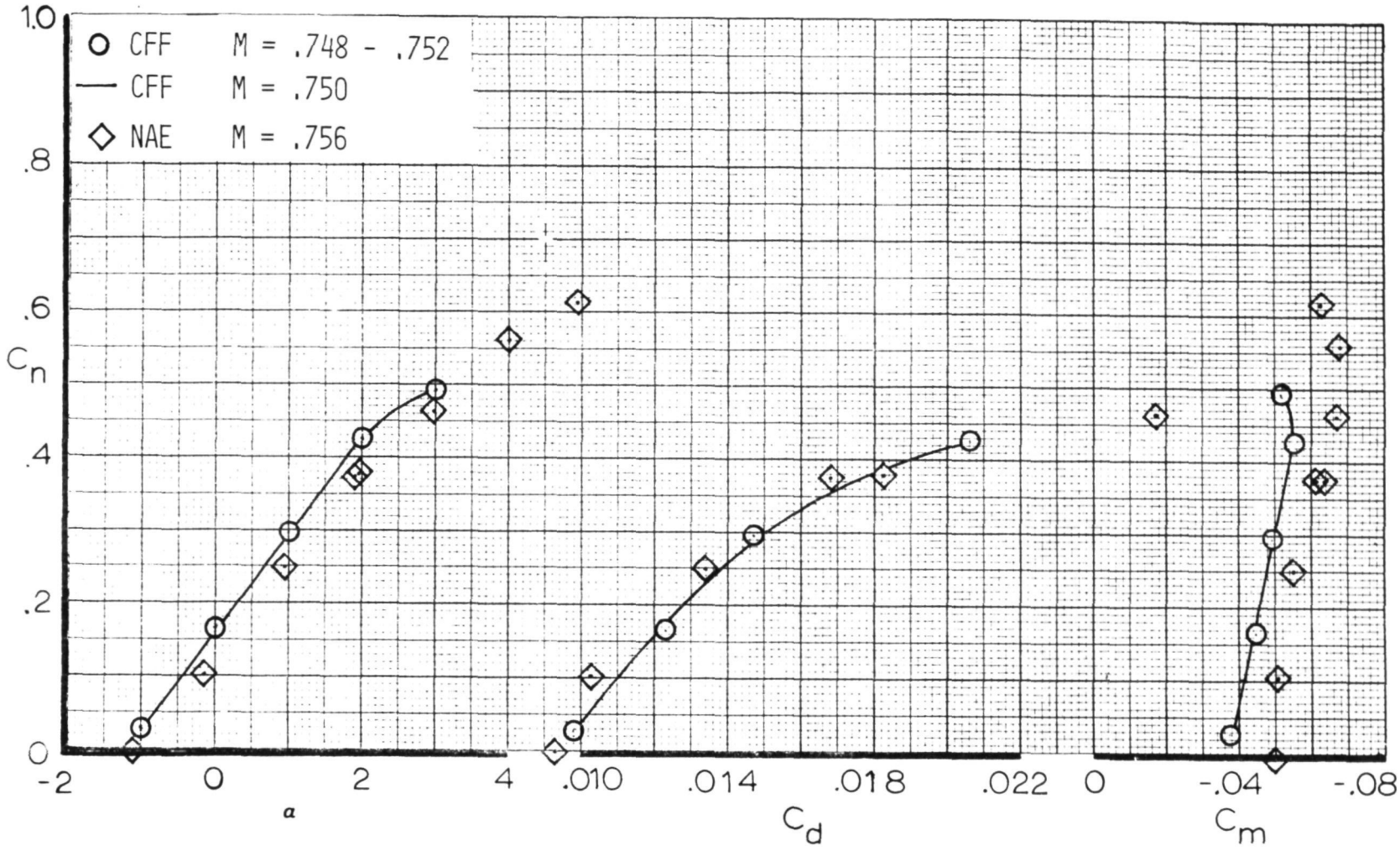

Figure 72. - Airfoil force data for M = 0.75 , R_N = 32 x 10^6, X/C_T = Free.

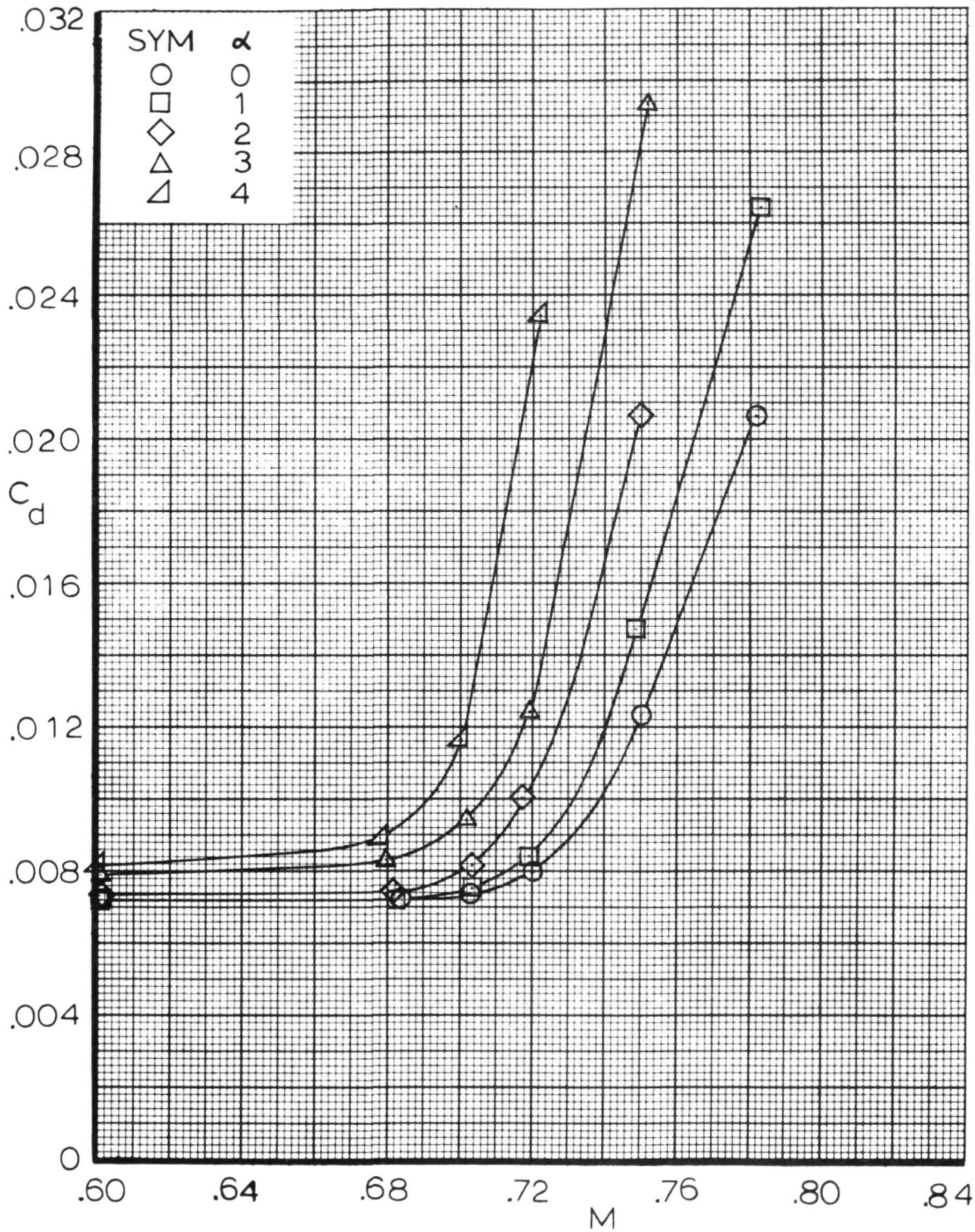

Figure 73. - Airfoil drag rise characteristics, $R_N = 25 \times 10^6$ for M = 0.60 and $R_N = 32 \times 10^6$ for M = .68 to 0.80.

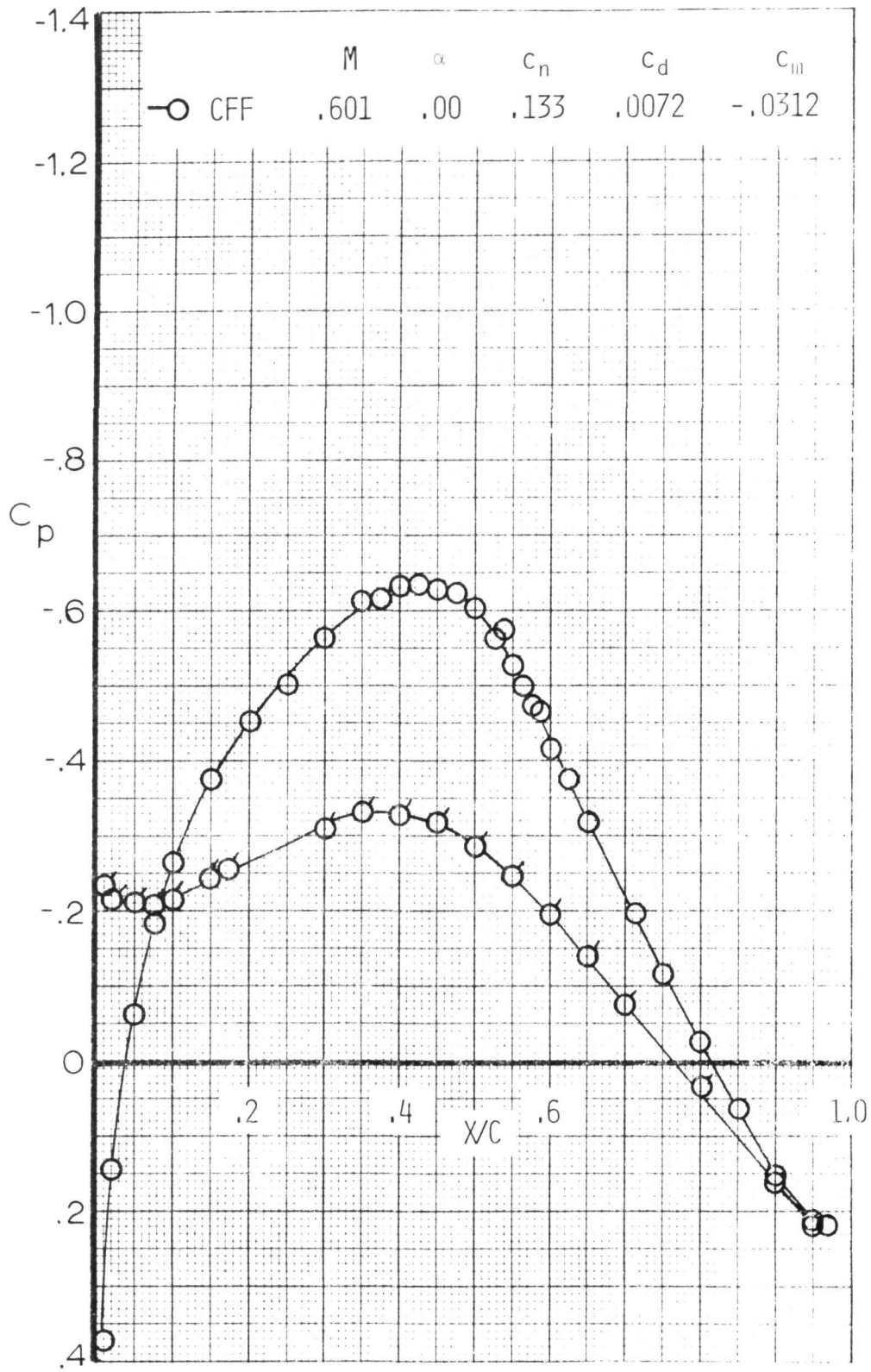

Figure 74. - Airfoil pressure distribution at M = 0.6, $R_N = 25 \times 10^6$, $\alpha = 0^\circ$ (Flags denote l.s.).

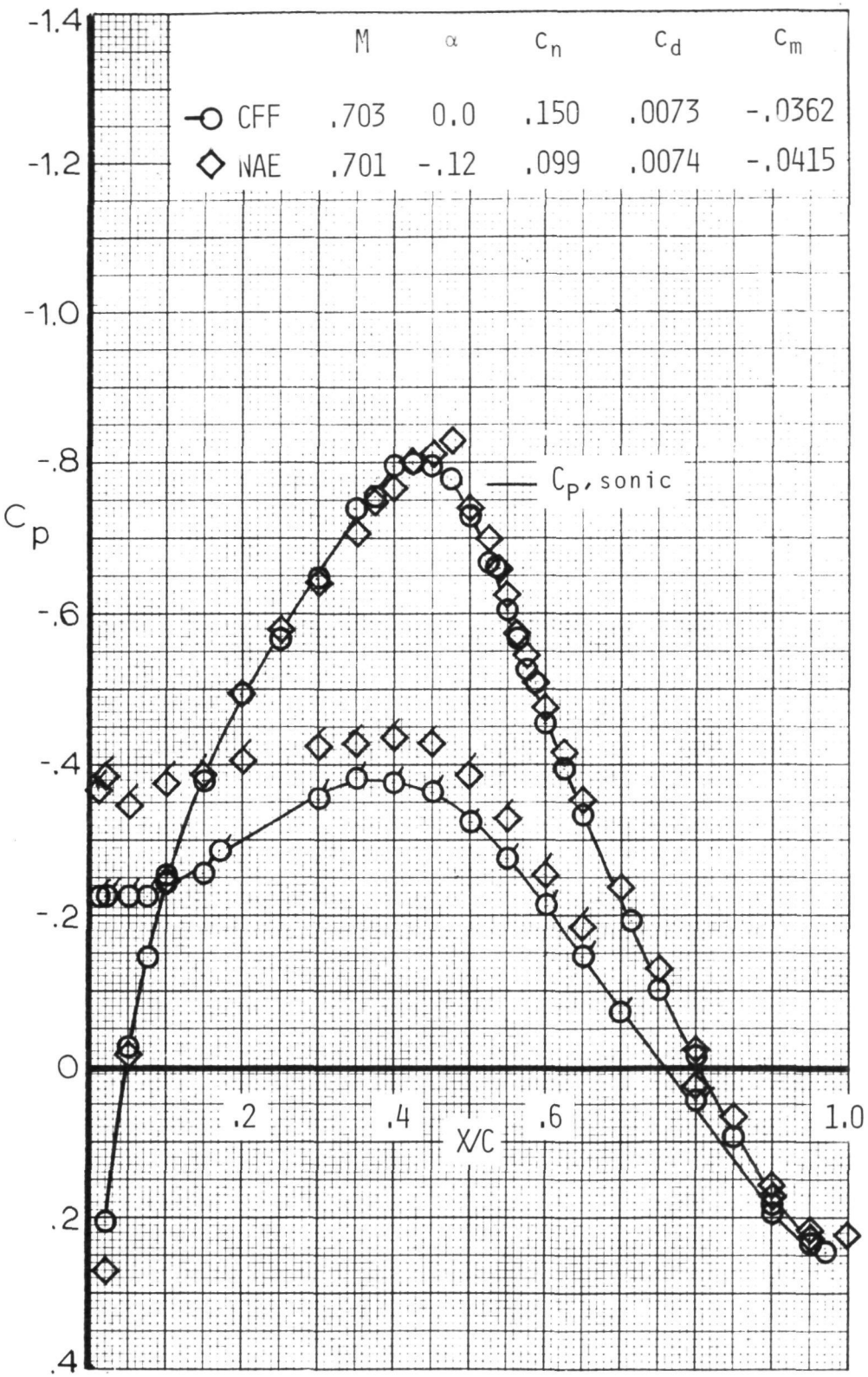

Figure 75. - Airfoil pressure distribution correlation at M = .7, R_N = 32 x 10^6, α = 0° (Flags denote l.s.).

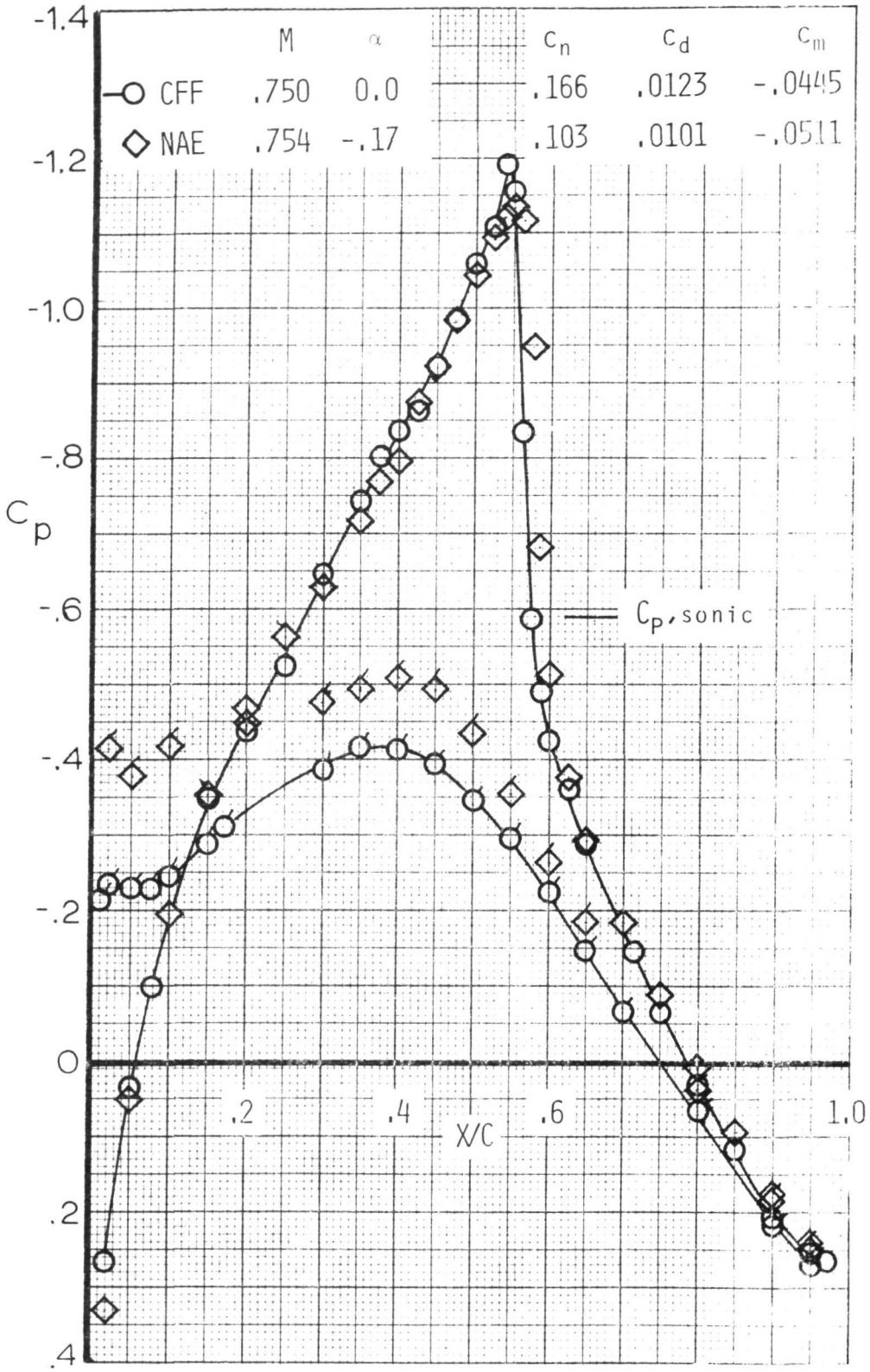

Figure 76. - Airfoil pressure distribution correlation at M = .75, R_N = 32 x 10^6, α = 0° (Flags denote l.s.).

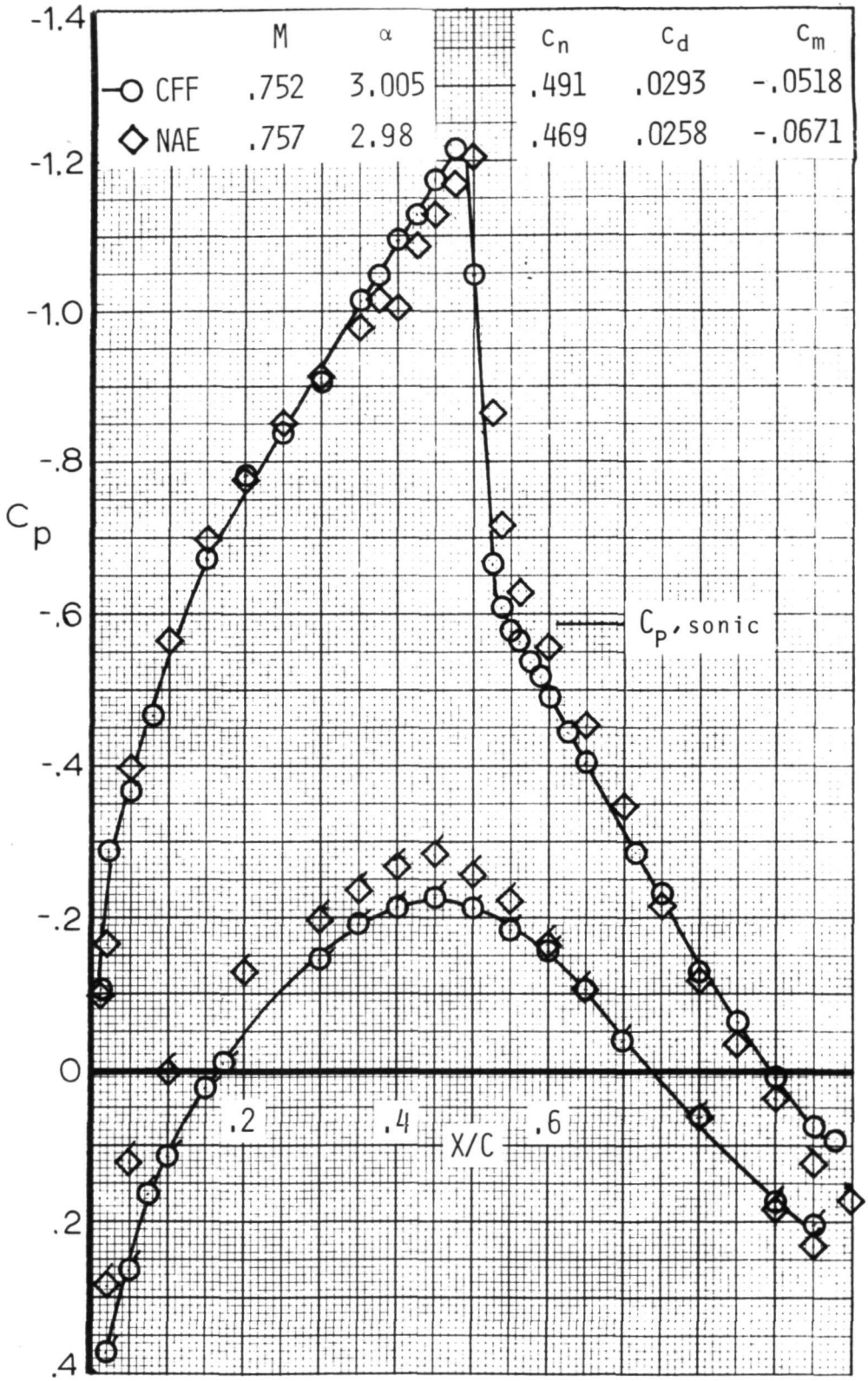

Figure 77. - Airfoil pressure distribution correlation at M = .75, R_N = 32 x 10^6, α = 3° (Flags denote l.s.).

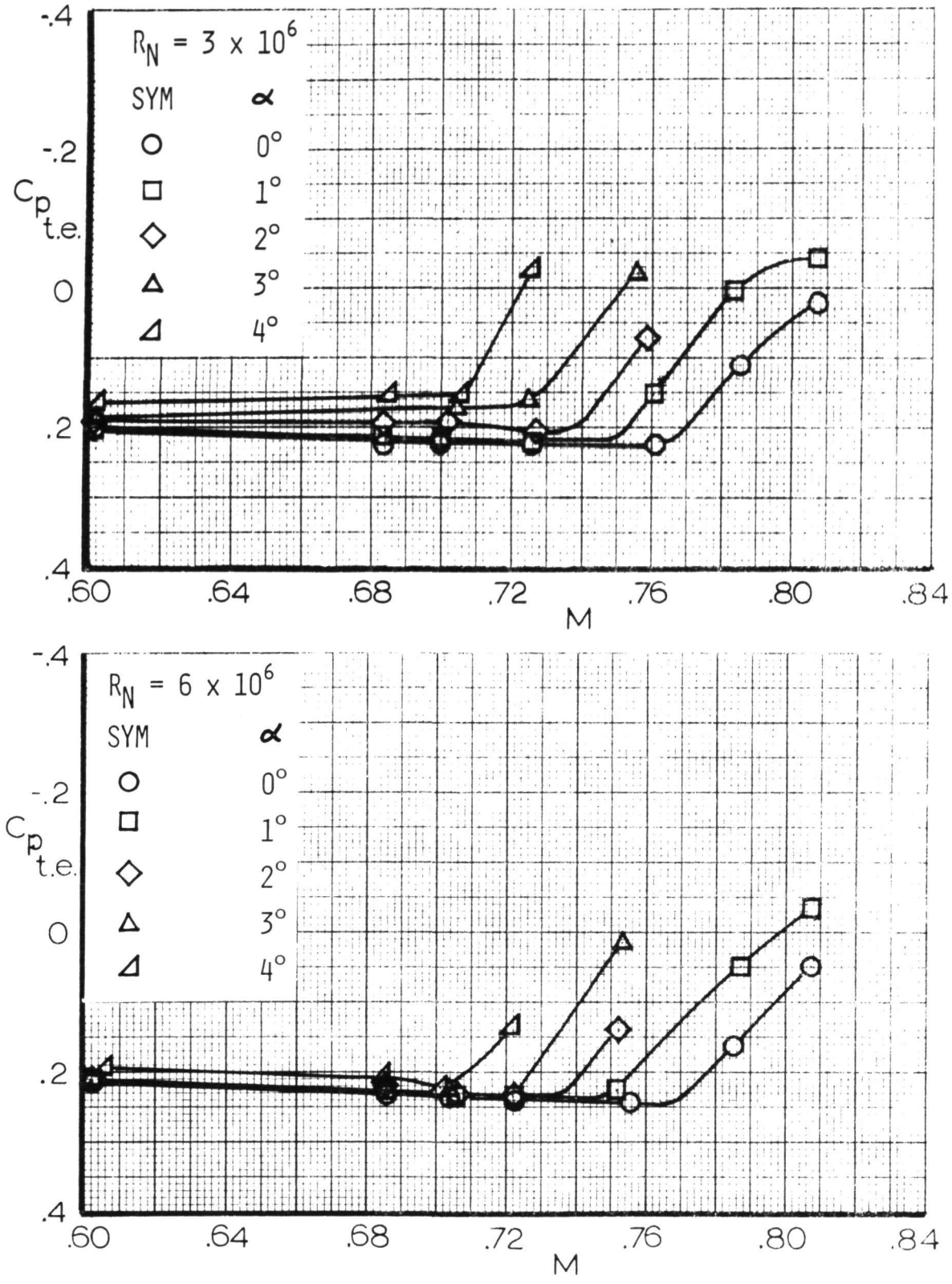

Figure 78. - Airfoil trailing edge pressure vs. Mach number.

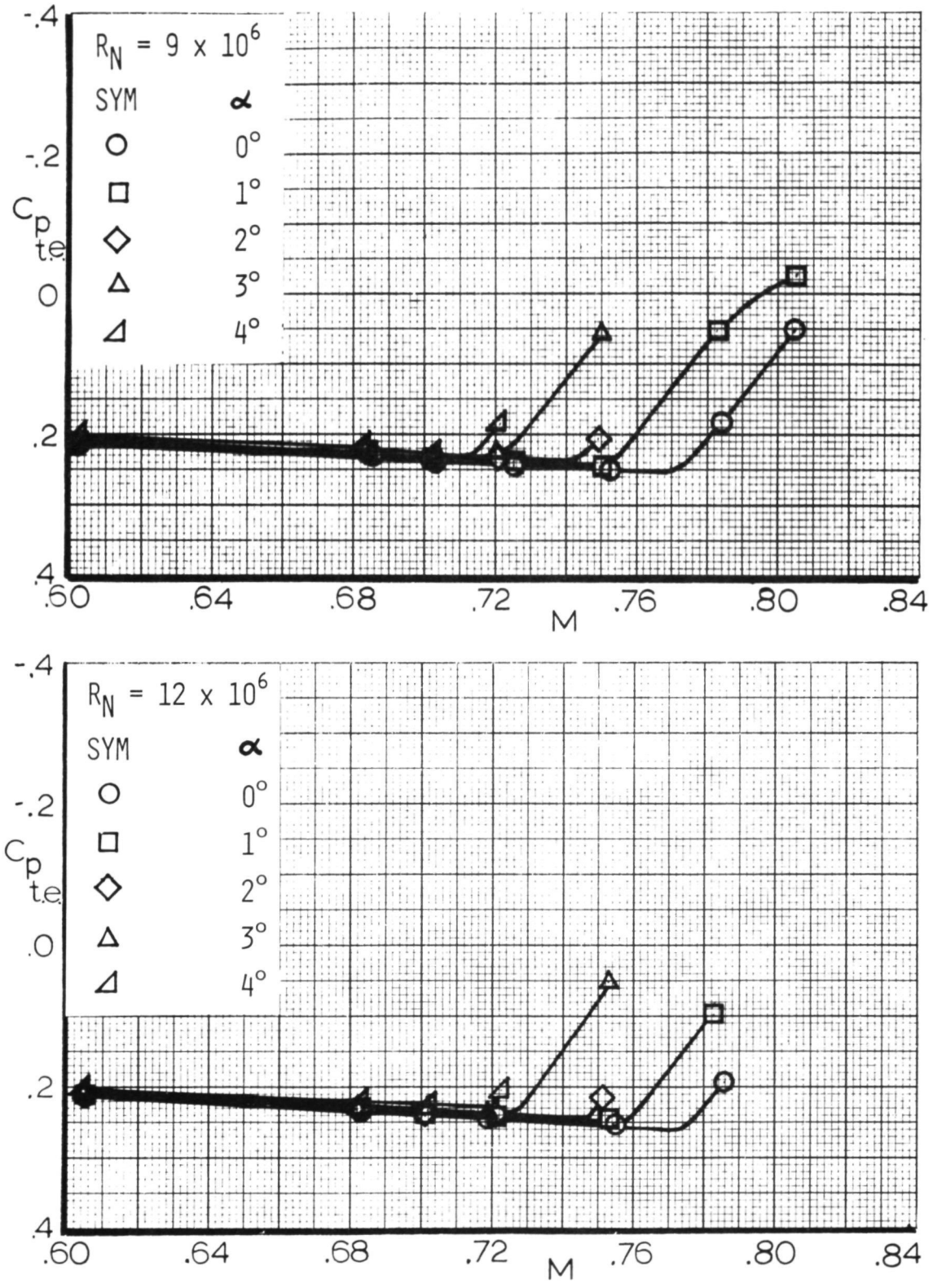

Figure 79. - Airfoil trailing edge pressure vs. Mach number.

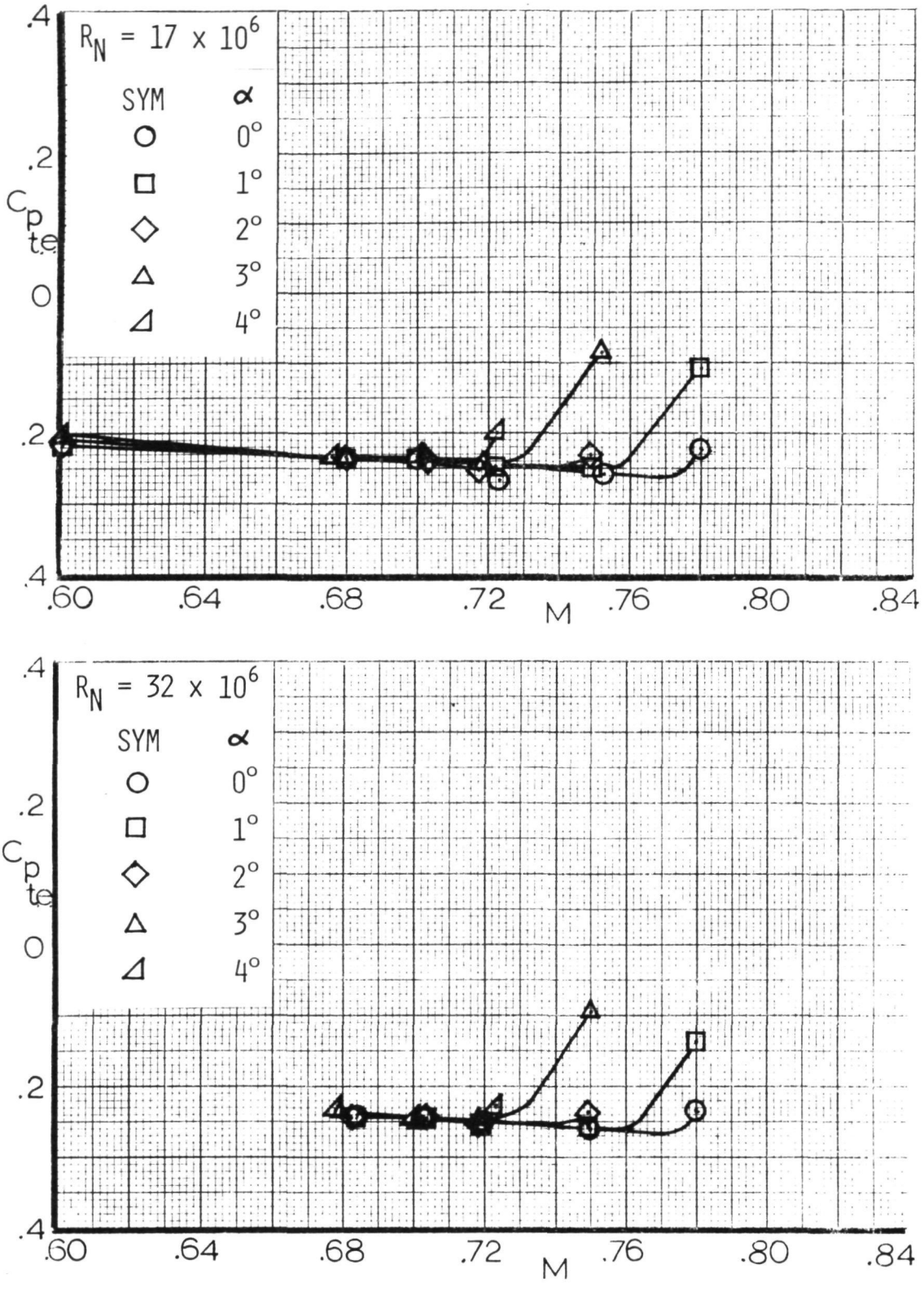

Figure 80. - Airfoil trailing edge pressure vs. Mach number.

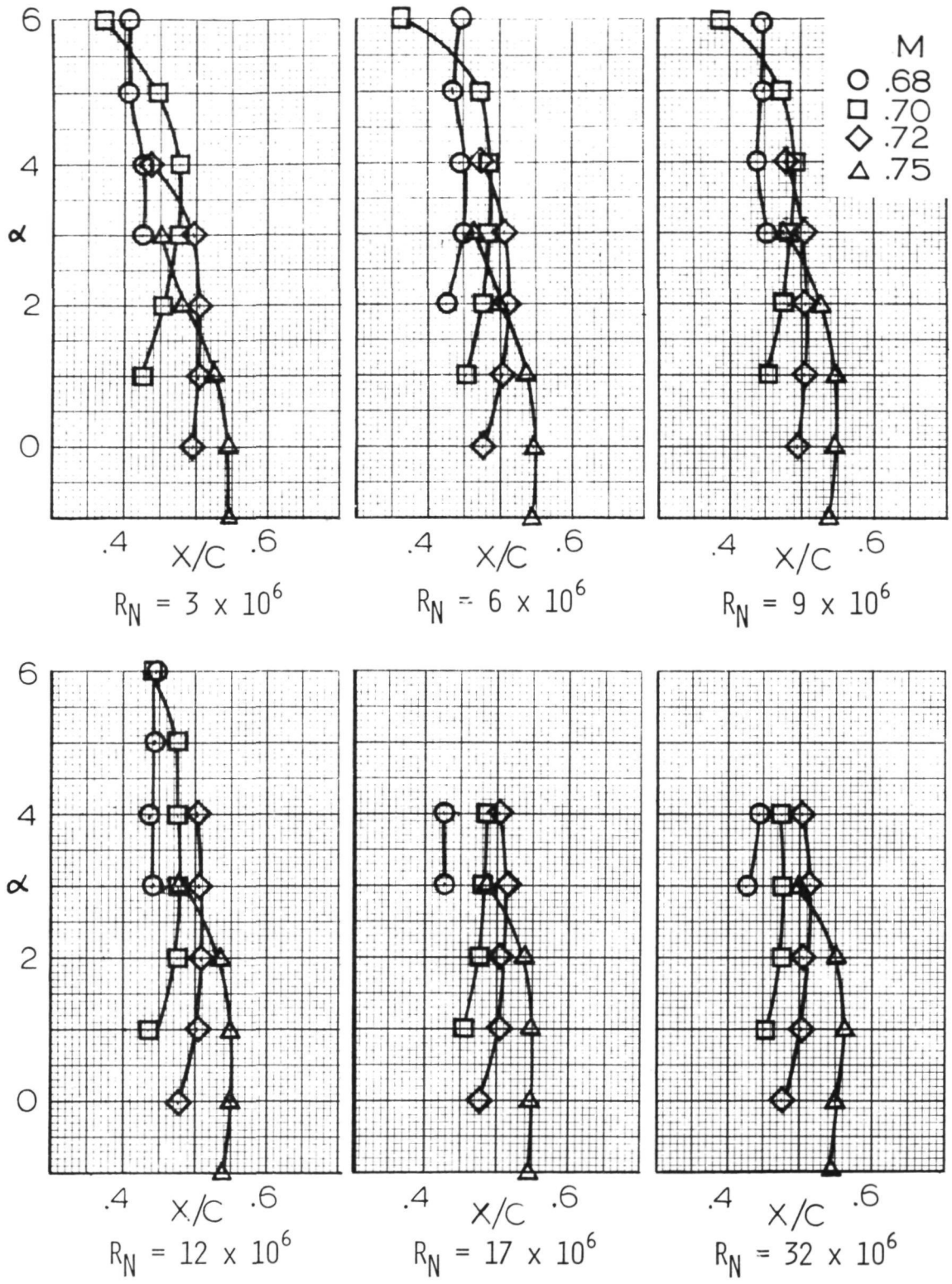

Figure 81. - Airfoil shock location for various Reynolds numbers.

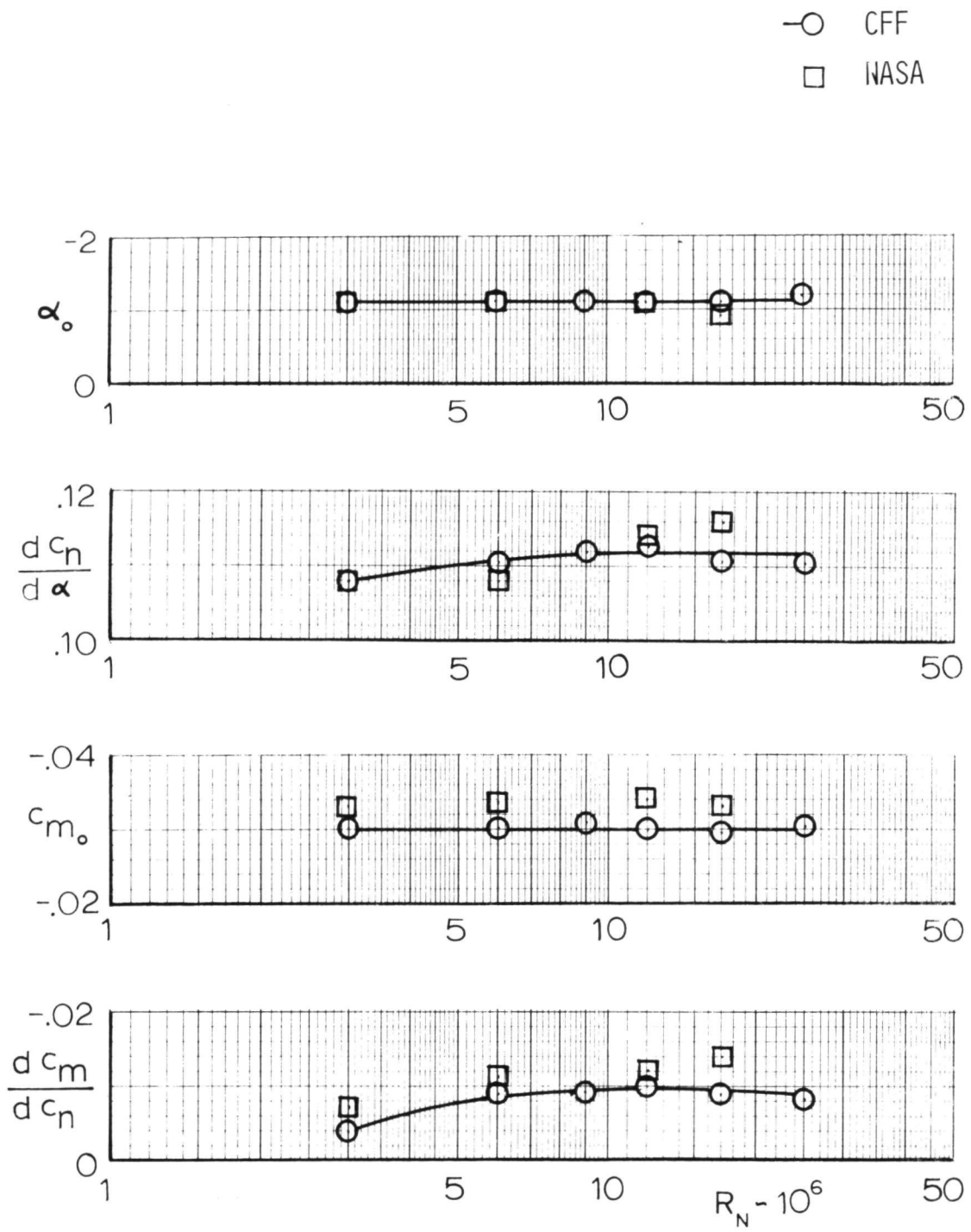

Figure 82 . - Effect of Reynolds number on airfoil force data, M = .6, X/C_T = .05.

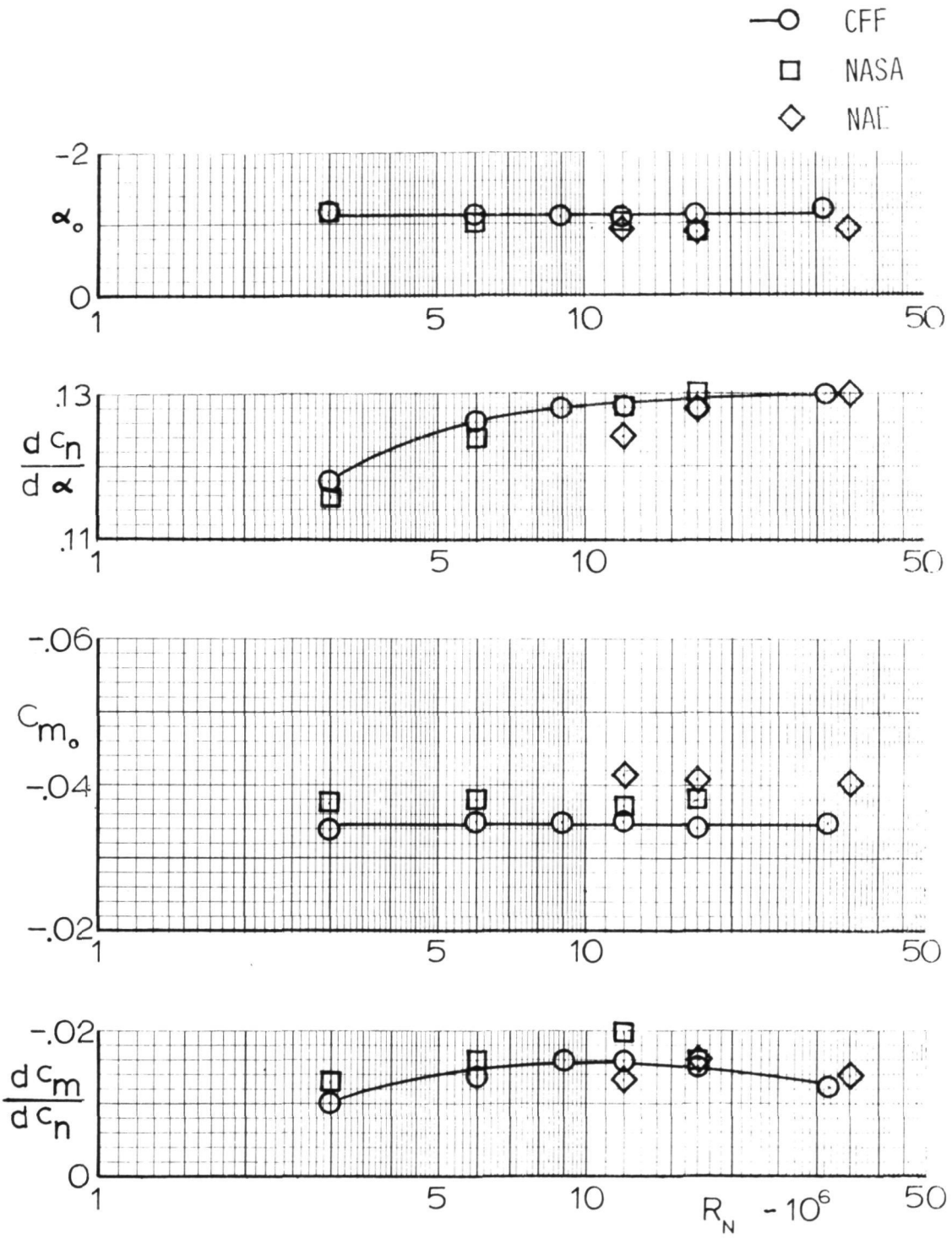

Figure 83. - Effect of Reynolds number on force data, M = .7, X/C_T = .05.

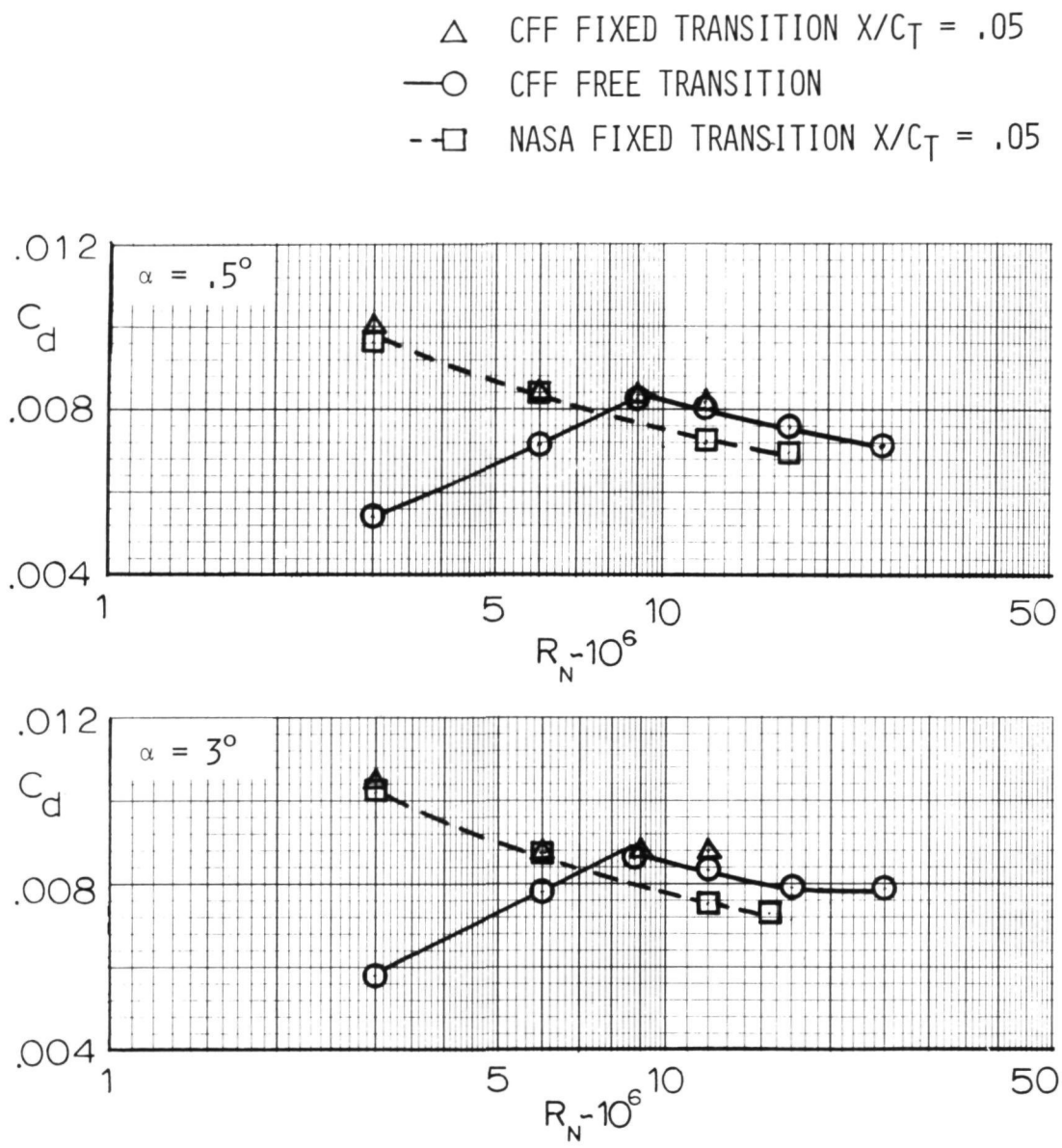

Figure 84. - Effect of Reynolds number on airfoil drag, M = 0.6.

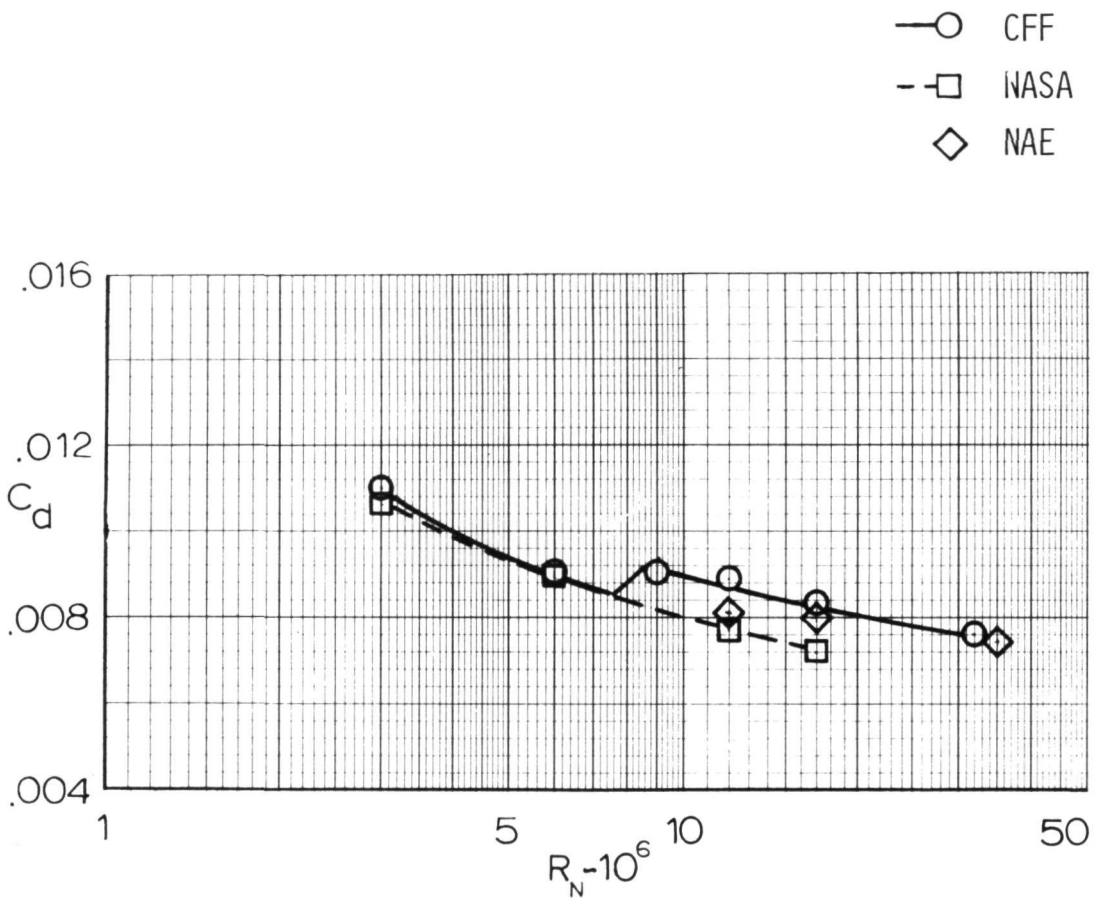

Figure 85. - Effect of Reynolds number on airfoil drag, M = .7, C_n = .3, X/C_T = .05.

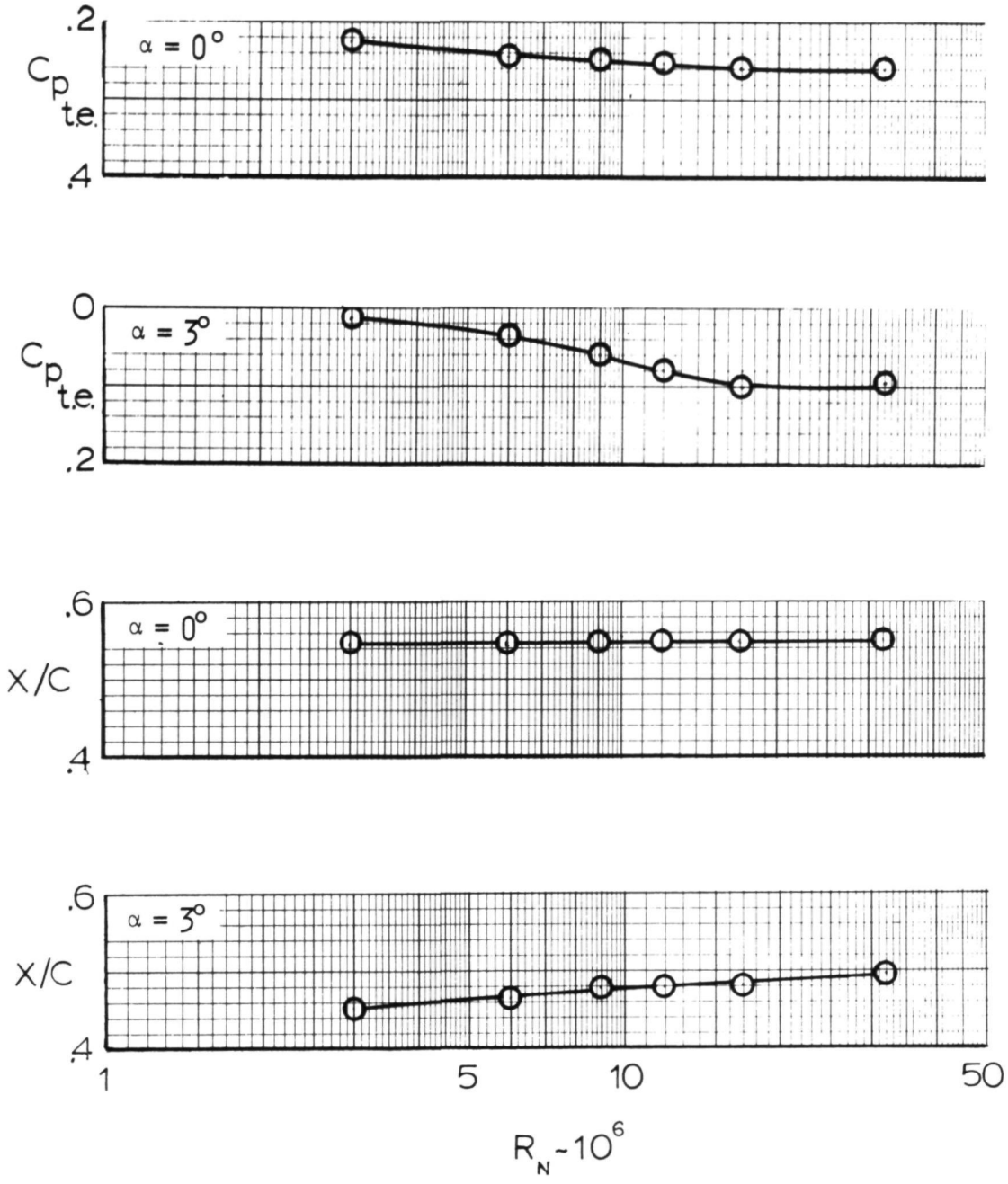

Figure 86. - Variation of airfoil trailing edge pressure and shock location with Reynolds number at a Mach number of 0.75.

APPENDIX

TABLE I. FORCE DATA

M	α	R_N	C_n	C_d	C_m
.6007	-1.0000	3.13	.0183	.0103	-.0289
.6019	.0000	3.01	.1183	.0100	-.0305
.6014	1.0000	3.00	.2265	.0102	-.0312
.6012	2.0000	3.01	.3358	.0104	-.0316
.6030	3.0000	2.96	.4408	.0105	-.0312
.6025	4.0000	2.96	.5528	.0114	-.0322
.6010	6.0000	2.98	.7567	.0131	-.0281
.5994	8.0000	2.99	.9375	.0178	.0001
.6829	-1.0000	2.94	.0228	.0103	-.0352
.6844	.0000	2.95	.1269	.0105	-.0328
.6834	1.0000	2.96	.2423	.0106	-.0348
.6843	2.0000	3.18	.3580	.0113	-.0352
.6861	3.0000	3.08	.4702	.0118	-.0346
.6849	4.0000	2.90	.5909	.0127	-.0343
.6831	5.0000	2.92	.7018	.0145	-.0318
.6798	6.0000	2.87	.8291	.0176	-.0310
.6961	-1.0000	2.98	.0189	.0100	-.0340
.6987	.0000	2.94	.1319	.0102	-.0345
.7007	1.0000	2.89	.2458	.0108	-.0352
.7019	2.0000	2.91	.3654	.0114	-.0367
.7046	3.0000	2.91	.4828	.0127	-.0377
.7058	4.0000	2.91	.6062	.0156	-.0414
.7020	5.0000	2.92	.7047	.0225	-.0413
.7014	6.0000	2.95	.7448	.0397	-.0398
.7250	-1.0000	3.06	.0198	.0104	-.0363
.7253	.0000	3.04	.1419	.0108	-.0386
.7280	1.0000	3.06	.2562	.0119	-.0393
.7275	2.0000	3.06	.3821	.0139	-.0431
.7249	3.0000	3.05	.4941	.0183	-.0459
.7257	4.0000	3.03	.5482	.0258	-.0478
.7604	-1.0000	3.04	.0281	.0137	-.0448
.7610	.0000	3.02	.1469	.0166	-.0494
.7601	1.0000	3.06	.2400	.0199	-.0507
.7584	2.0000	3.06	.3223	.0212	-.0487
.7562	3.0000	3.06	.3922	.0255	-.0444
.7846	-1.0000	3.08	.0070	.0195	-.0525
.7846	.0000	3.09	.0856	.0213	-.0501
.7836	1.0000	3.03	.1650	.0236	-.0483
.8040	-1.0000	3.11	-.0687	.0247	-.0439
.8069	.0000	3.00	.0064	.0261	-.0395
.8067	1.0000	3.01	.0210	.0084	-.0307

TABLE I. (Continued)

M	α	R_N	C_n	C_d	C_m
.6021	-1.0000	6.43	.0183	.0087	-.0298
.6024	- .5000	6.49	.0701	.0084	-.0303
.6029	.0000	6.10	.1271	.0083	-.0315
.6026	.5050	6.09	.1780	.0084	-.0314
.6028	1.0000	6.10	.2343	.0084	-.0324
.6029	1.5000	6.06	.2911	.0085	-.0332
.6042	2.0000	6.02	.3463	.0088	-.0335
.6053	2.5000	6.00	.3969	.0085	-.0343
.6044	3.0000	6.00	.4550	.0087	-.0346
.6035	3.5050	6.01	.5106	.0089	-.0348
.6058	4.0000	6.02	.5653	.0091	-.0350
.6017	5.0050	5.92	.6837	.0098	-.0349
.6006	6.0000	5.97	.7959	.0112	-.0313
.5997	8.0000	5.87	.9863	.0146	-.0013
.6843	-1.0000	6.29	.0214	.0087	-.0344
.6856	.0000	6.29	.1333	.0086	-.0347
.6843	1.0000	6.06	.2550	.0088	-.0371
.6857	2.0050	5.96	.3788	.0092	-.0388
.6862	3.0050	5.77	.4991	.0092	-.0395
.6849	4.0000	6.07	.6305	.0103	-.0402
.6834	5.0000	5.89	.7605	.0117	-.0395
.6817	6.0000	6.28	.9018	.0165	-.0387
.7016	-1.0000	6.17	.0203	.0085	-.0353
.7044	.0000	5.97	.1398	.0087	-.0371
.7039	1.0000	5.88	.2631	.0088	-.0392
.7063	2.0000	5.79	.3880	.0096	-.0405
.7040	3.0000	5.75	.5206	.0111	-.0435
.7010	4.0000	5.77	.6526	.0134	-.0458
.7022	5.0000	5.79	.7853	.0186	-.0478
.7010	6.0000	5.65	.8271	.0504	-.0627
.7207	-1.0000	6.02	.0213	.0088	-.0368
.7218	.0000	6.20	.1424	.0087	-.0384
.7222	1.0000	5.88	.2725	.0097	-.0418
.7212	2.0050	5.68	.4042	.0112	-.0448
.7195	3.0000	5.88	.5371	.0149	-.0479
.7218	4.0000	5.75	.6539	.0262	-.0585
.7548	-1.0000	6.16	.0313	.0123	-.0436
.7557	.0000	6.30	.1527	.0138	-.0483
.7515	1.0000	6.36	.2774	.0172	-.0524
.7523	2.0050	6.11	.3717	.0238	-.0554
.7527	3.0000	6.04	.4384	.0310	-.0518

TABLE I. (Continued)

M	α	R_N	C_n	C_d	C_m
.7829	-1.0000	5.94	.0222	.0186	-.0540
.7850	.0000	6.08	.1096	.0223	-.0554
.7871	1.0000	5.97	.1711	.0277	-.0507
.8056	-1.0000	5.77	-.0463	.0257	-.0501
.8071	.0000	6.05	.0156	.0288	-.0444
.8051	1.0000	6.03	.0956	.0317	-.0428
.6042	3.0000	5.81	.4625	.0074	-.0347
.6019	3.0000	2.98	.4717	.0058	-.0363
.6039	3.0000	8.73	.4644	.0086	-.0353
.6017	3.0000	11.73	.4630	.0082	-.0347
.6024	-1.0000	9.21	.0210	.0084	-.0307
.6019	.0000	9.59	.1266	.0087	-.0314
.6011	1.0000	9.19	.2334	.0084	-.0329
.6026	2.0000	9.27	.3455	.0082	-.0338
.6021	3.0050	9.20	.4596	.0087	-.0349
.6021	4.0000	9.15	.5711	.0090	-.0357
.5997	6.0000	9.11	.7969	.0104	-.0334
.5987	8.0000	9.06	.9933	.0145	-.0018
.6842	-1.0000	9.09	.0220	.0086	-.0345
.6857	.0000	9.31	.1388	.0085	-.0358
.6838	1.0000	9.19	.2597	.0087	-.0379
.6831	2.0000	9.16	.3803	.0092	-.0387
.6832	3.0000	9.16	.5094	.0094	-.0404
.6832	4.0000	9.00	.6367	.0101	-.0412
.6821	5.0000	9.23	.7673	.0127	-.0415
.6815	6.0000	9.12	.9095	.0184	-.0400
.7028	-1.0000	9.05	.0241	.0088	-.0358
.7038	.0000	9.40	.1434	.0082	-.0371
.7023	1.0000	9.01	.2656	.0087	-.0394
.7018	2.0000	9.18	.3944	.0096	-.0412
.7018	3.0000	9.20	.5256	.0109	-.0438
.7035	4.0000	9.15	.6596	.0150	-.0475
.7037	5.0050	9.04	.7723	.0237	-.0498
.7015	6.0000	9.02	.8323	.0385	-.0481
.7216	-1.0000	9.61	.0207	.0095	-.0381
.7247	.0000	9.44	.1457	.0094	-.0394
.7256	1.0000	9.32	.2705	.0106	-.0413
.7194	2.0000	9.55	.3940	.0117	-.0422
.7186	3.0050	9.24	.5253	.0150	-.0456
.7202	4.0050	9.20	.6399	.0249	-.0512
.7503	- .9950	9.42	.0255	.0111	-.0424
.7517	.0000	9.21	.1545	.0128	-.0452

TABLE I. (Continued)

M	α	R_N	C_n	C_d	C_m
.7514	1.0000	9.39	.2877	.0165	-.0530
.7490	2.0000	9.33	.4015	.0221	-.0565
.7499	3.0050	9.04	.4646	.0306	-.0549
.7790	-1.0000	9.12	.0177	.0175	-.0543
.7836	.0000	8.80	.1239	.0216	-.0594
.7825	.9950	8.81	.1939	.0266	-.0548
.8051	-1.0000	8.78	-.0625	.0253	-.0523
.8044	.0050	8.80	.0262	.0283	-.0489
.8049	1.0000	8.86	.1036	.0312	-.0452
.6035	- .9950	12.30	.0241	.0201	-.0297
.6053	.0000	11.93	.1278	.0082	-.0312
.6049	1.0000	11.83	.2372	.0082	-.0325
.6036	2.0000	11.90	.3490	.0082	-.0337
.6035	3.0050	11.93	.4642	.0087	-.0347
.6041	4.0000	11.79	.5742	.0089	-.0349
.6016	6.0050	11.71	.8061	.0106	-.0324
.6002	8.0000	11.62	1.0006	.0154	-.0005
.6825	-1.0000	11.73	.0263	.0085	-.0337
.6833	.0000	11.70	.1406	.0083	-.0350
.6831	1.0000	11.75	.2604	.0086	-.0369
.6820	2.0000	11.52	.3833	.0089	-.0383
.6820	3.0000	11.58	.5108	.0093	-.0400
.6827	4.0050	11.52	.6393	.0101	-.0405
.6811	5.0000	11.50	.7728	.0123	-.0403
.6789	6.0050	11.43	.9171	.0173	-.0381
.7000	-1.0000	11.39	.0267	.0085	-.0351
.7007	.0000	11.47	.1463	.0086	-.0370
.7008	1.0000	11.39	.2683	.0086	-.0388
.7003	2.0000	11.43	.3943	.0095	-.0406
.7018	2.9950	11.38	.5191	.0104	-.0423
.7018	4.0000	11.45	.6488	.0140	-.0442
.7003	5.0000	11.42	.7713	.0205	-.0459
.6987	6.0000	11.37	.8643	.0338	-.0447
.7225	-1.0000	11.50	.0256	.0089	-.0368
.7193	.0000	11.85	.1475	.0092	-.0383
.7203	1.0000	11.81	.2722	.0101	-.0410
.7206	2.0050	11.67	.4004	.0119	-.0441
.7193	3.0050	11.96	.5265	.0161	-.0473
.7226	4.0000	11.79	.6430	.0252	-.0518
.7526	-1.0000	11.70	.0271	.0112	-.0413
.7544	.0000	11.67	.1511	.0131	-.0455
.7529	1.0000	11.58	.2794	.0167	-.0509

TABLE I. (Continued)

M	α	R_N	C_n	C_d	C_m
.7510	2.000	11.60	.3962	.0225	-.0550
.7532	3.0000	11.62	.4571	.0325	-.0556
.7835	-1.0000	11.59	.0159	.0186	-.0549
.7858	.0000	11.59	.1169	.0233	-.0564
.7822	1.0000	11.59	.2019	.0275	-.0546
.6085	-1.0000	17.77	.0255	.0077	-.0298
.6086	.0000	17.67	.1244	.0075	-.0299
.6074	1.0050	17.54	.2356	.0075	-.0322
.6079	2.0000	17.35	.3406	.0074	-.0330
.6029	1.5000	18.35	.2888	.0077	-.0324
.6042	2.0050	17.75	.3369	.0074	-.0325
.6090	2.5000	17.63	.3880	.0077	-.0326
.6046	3.0000	17.42	.4463	.0078	-.0333
.6044	3.5000	17.31	.5014	.0079	-.0335
.6019	3.9950	17.08	.5614	.0081	-.0340
.6757	-1.0000	17.55	.0328	.0080	-.0348
.6817	.0000	17.62	.1515	.0078	-.0355
.6822	1.0000	17.56	.2604	.0078	-.0351
.6792	2.0050	17.41	.3877	.0084	-.0381
.6816	3.0000	17.41	.5050	.0086	-.0393
.6755	4.0000	17.24	.6365	.0093	-.0392
.6968	-1.0000	17.07	.0294	.0080	-.0346
.7003	.0000	17.23	.1456	.0080	-.0370
.7009	1.0000	17.30	.2745	.0084	-.0384
.7005	1.0000	17.26	.2772	.0079	-.0387
.7034	2.0000	17.36	.4011	.0088	-.0414
.7018	3.0000	17.38	.5240	.0098	-.0418
.7006	4.0050	16.92	.6608	.0129	-.0448
.7200	-1.0000	17.01	.0280	.0083	-.0355
.7229	.0000	17.06	.1494	.0089	-.0392
.7221	1.0000	17.01	.2776	.0101	-.0390
.7169	2.0000	17.55	.4061	.0108	-.0402
.7190	3.0000	17.07	.5447	.0157	-.0461
.7225	4.0000	17.20	.6640	.0258	-.0545
.7541	-1.0000	17.39	.0369	.0112	-.0426
.7525	.0000	17.46	.1632	.0126	-.0463
.7492	1.0000	17.30	.2948	.0155	-.0507
.7491	2.0000	17.22	.4173	.0215	-.0568
.7524	2.9950	17.19	.4766	.0297	-.0560
.7780	-1.0000	17.14	.0332	.0160	-.0542
.7803	.0000	17.09	.1484	.0206	-.0585
.7814	1.0000	17.11	.2244	.0268	-.0566

TABLE I. (Continued)

M	α	R_N	C_n	C_d	C_m
.6007	-1.0000	26.15	.0282	.0075	-.0304
.6007	.0000	25.67	.1325	.0072	-.0312
.6002	1.0000	25.29	.2383	.0074	-.0317
.5990	2.0000	25.11	.3537	.0077	-.0332
.5965	4.0000	25.57	.5824	.0080	-.0345
.6796	-1.0000	31.66	.0395	.0075	-.0342
.6837	.0000	31.37	.1540	.0073	-.0354
.6831	1.0000	30.06	.2691	.0072	-.0366
.6819	1.9950	30.21	.3956	.0078	-.0379
.6799	3.0000	30.80	.5180	.0085	-.0387
.6781	4.0000	30.54	.6389	.0090	-.0400
.5987	3.0000	24.82	.4653	.0078	-.0340
.6983	-1.0000	29.90	.0350	.0077	-.0353
.7025	.0000	32.48	.1501	.0075	-.0362
.7032	1.0050	31.94	.2775	.0076	-.0378
.7030	1.9950	31.37	.3952	.0081	-.0373
.7013	3.0050	31.14	.5275	.0094	-.0389
.7007	4.0050	32.90	.6483	.0116	-.0318
.7210	-1.0000	32.00	.0240	.0076	-.0332
.7203	.0050	31.06	.1458	.0080	-.0349
.7190	1.0000	30.57	.2828	.0085	-.0407
.7178	2.0000	32.14	.4127	.0100	-.0427
.7191	3.0050	32.10	.5474	.0125	-.0457
.7228	4.0000	31.91	.6732	.0234	-.0518
.7514	- .9950	31.63	.0297	.0098	-.0377
.7500	.0000	31.81	.1661	.0123	-.0445
.7486	1.0000	31.14	.2972	.0147	-.0493
.7494	2.0050	30.93	.4251	.0206	-.0555
.7515	3.0050	31.06	.4909	.0293	-.0518
.7788	-1.0000	32.17	.0398	.0163	-.0537
.7812	.0000	32.26	.1537	.0206	-.0580
.7826	1.0000	32.33	.2388	.0264	-.0582

TABLE II. POROSITY STUDY

M	α	R_{N_c}	C_N	C_d	C_m	Porosity
.5994	.000	6.51	.1123	.00824	-.0306	4.97
.5996	.000	6.54	.1196	.00828	-.0311	3.99
.5996	.000	6.58	.1236	.00850	-.0311	3.00
.5988	.000	6.40	.1327	.00849	-.0322	2.01
.5993	.000	6.53	.1436	.00869	-.0331	1.07
.5988	.000	6.61	.1598	.00884	-.0340	0.73
.5970	.000	6.42	.1187	.00838	-.0302	5.99
.7555	3.000	6.75	.4229	.02550	-.0518	6.01
.7503	3.000	6.57	.4528	.02735	-.0539	3.99
.7495	3.000	6.47	.4313	.03260	-.0527	2.01

TABLE III. TRANSITION STUDY

M	α	R_{N_c}	C_N	C_d	C_m	K_T/C
.6036	-1.000	6.84	.0134	.0090	-.0302	.00039
.6036	.000	6.97	.1155	.00864	-.0305	.00039
.6033	1.000	6.94	.2240	.00902	-.0319	.00039
.6056	3.000	6.64	.4458	.00920	-.0337	.00039
.6072	4.005	6.44	.5635	.00950	-.0350	.00039
.6041	6.000	6.77	.7861	.01134	-.0318	.00039
.6029	8.000	6.35	.9434	.01511	-.0050	.00039
.6014	-1.000	6.62	.0211	.00927	-.0293	.00046
.6017	.000	6.66	.1120	.00899	-.0291	.00046
.6026	1.000	6.77	.2084	.00909	-.0305	.00046
.6036	3.000	6.33	.3990	.00911	-.0315	.00046
.6029	4.000	6.48	.4950	.00979	-.0324	.00046
.6008	6.005	6.44	.683	.01095	-.0307	.00046
.6001	8.000	6.32	.881	.01320	-.0117	.00046
.6007	-1.000	6.79	.0196	.00969	-.0298	.00077
.6018	.000	6.93	.1124	.00963	-.0297	.00077
.6028	1.000	6.62	.2066	.00954	-.0298	.00077
.6056	3.000	6.55	.3986	.00993	-.0307	.00077
.6039	4.000	6.58	.4964	.01041	-.0303	.00077
.6029	.000	7.25	.1190	.00983	-.0297	.00129
.6043	1.000	6.96	.2109	.00966	-.0294	.00129
.6066	3.000	6.67	.4021	.01000	-.0300	.00129
.6051	4.000	6.87	.4991	.01082	-.0309	.00129
.6023	-1.000	7.27	.019	.00835	-.0305	Free
.6030	0.500	6.45	.069	.00709	-.0314	Free
.6035	0.000	6.28	.114	.00570	-.0310	Free
.6016	0.500	6.46	.160	.00688	-.0308	Free
.6012	1.000	6.48	.211	.00784	-.0322	Free
.6017	2.000	6.34	.310	.00782	-.0322	Free
.6036	3.000	6.23	.413	.00778	-.0331	Free
.6034	3.500	6.41	.463	.00810	-.0334	Free
.6038	4.000	6.25	.511	.00811	-.0341	Free

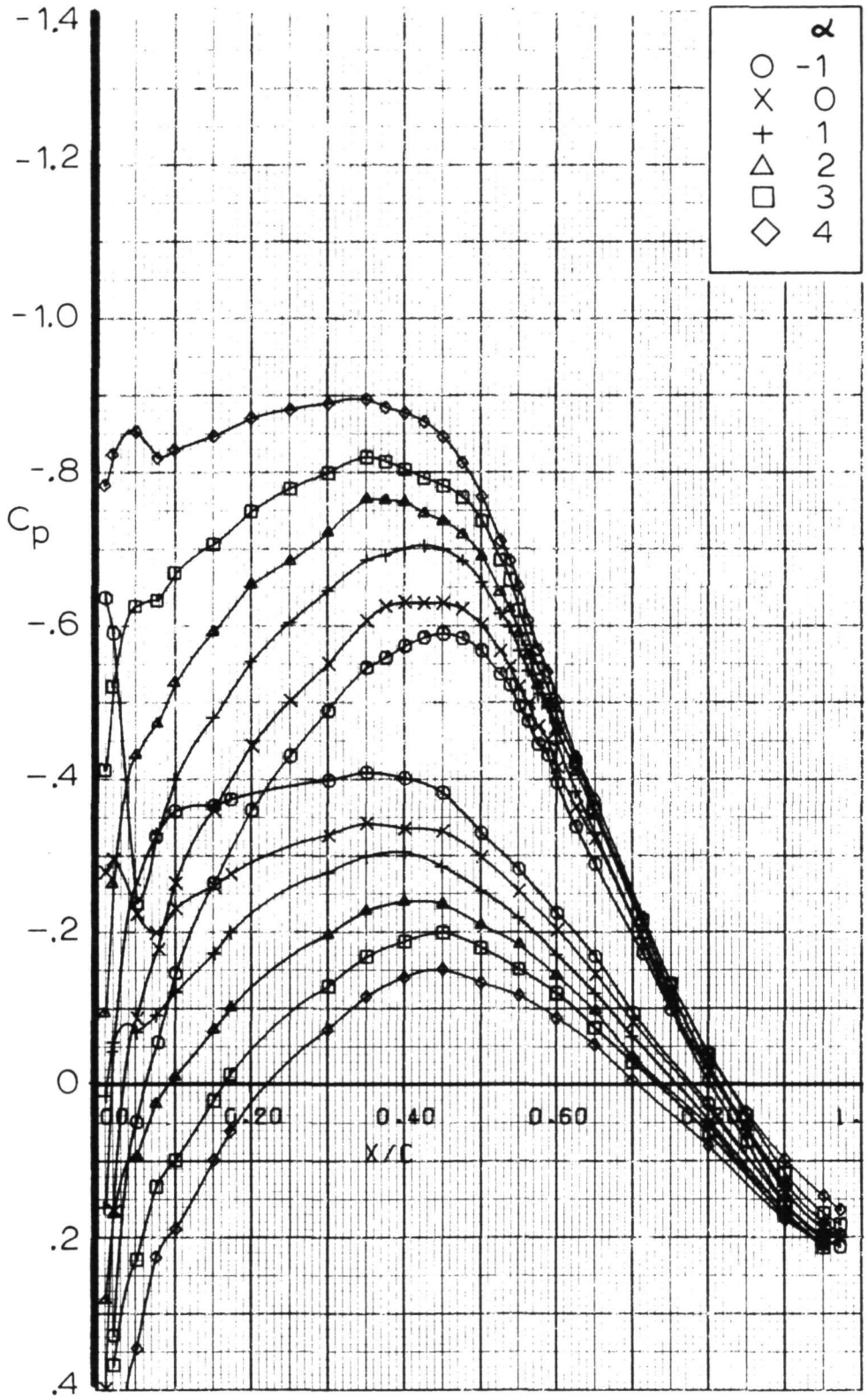

Figure 1.- Airfoil pressure distribution M = 0.6 R_N = 3 x 10^6.

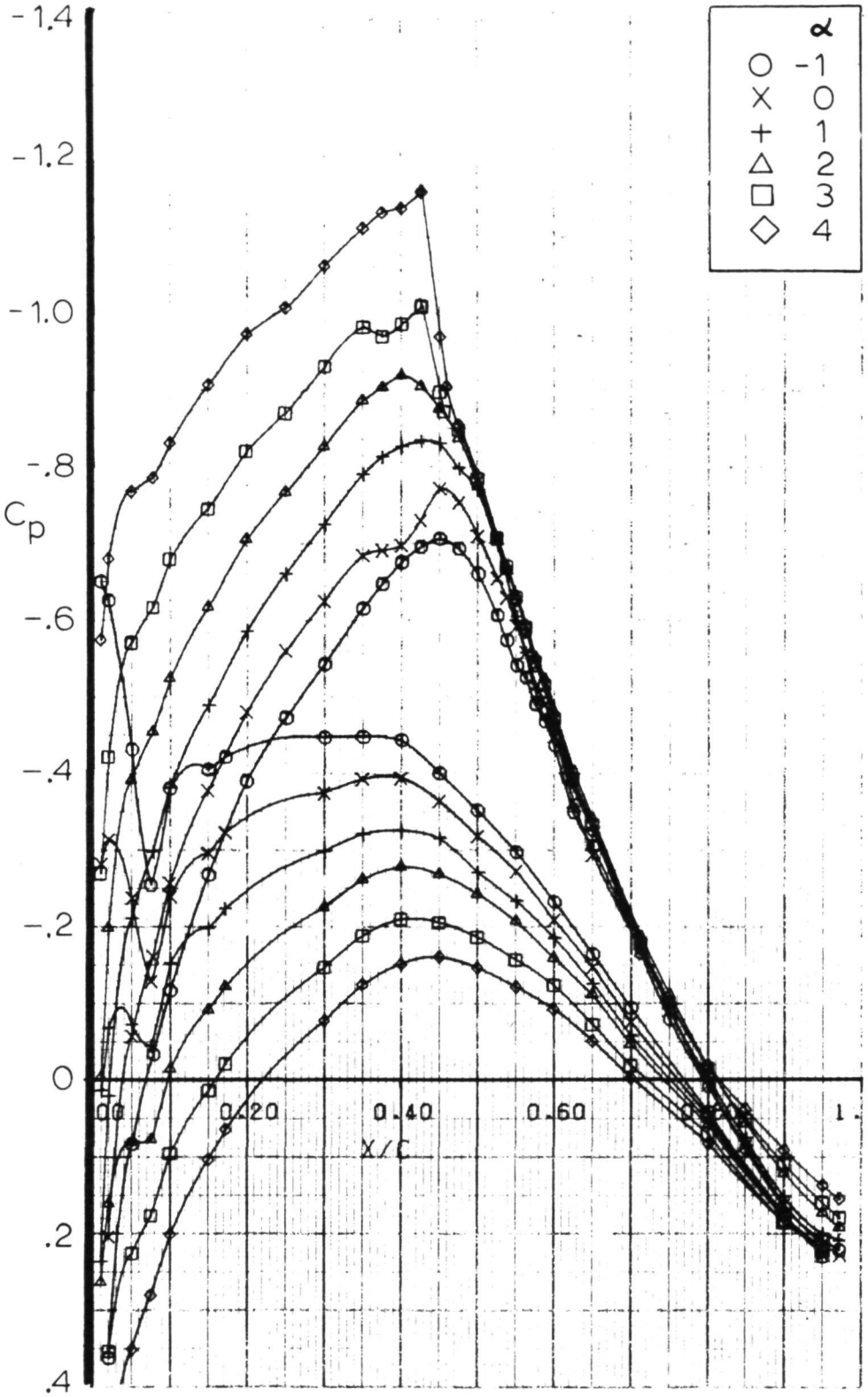

Figure 2 .- Airfoil pressure distribution M = 0.68 R_N = 3 x 10^6.

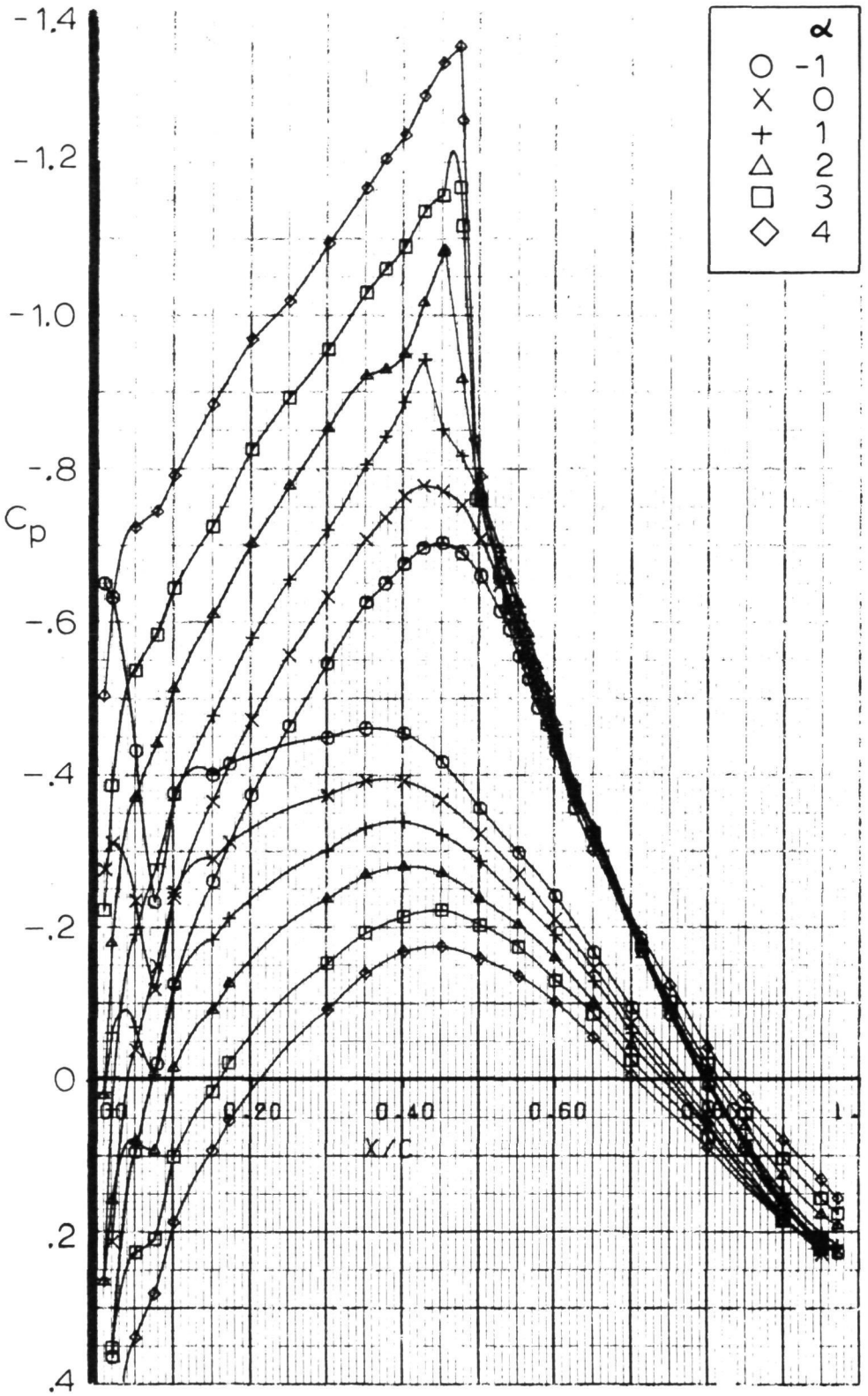

Figure 3.- Airfoil pressure distribution M = 0.70 R_N = 3 x 10^6.

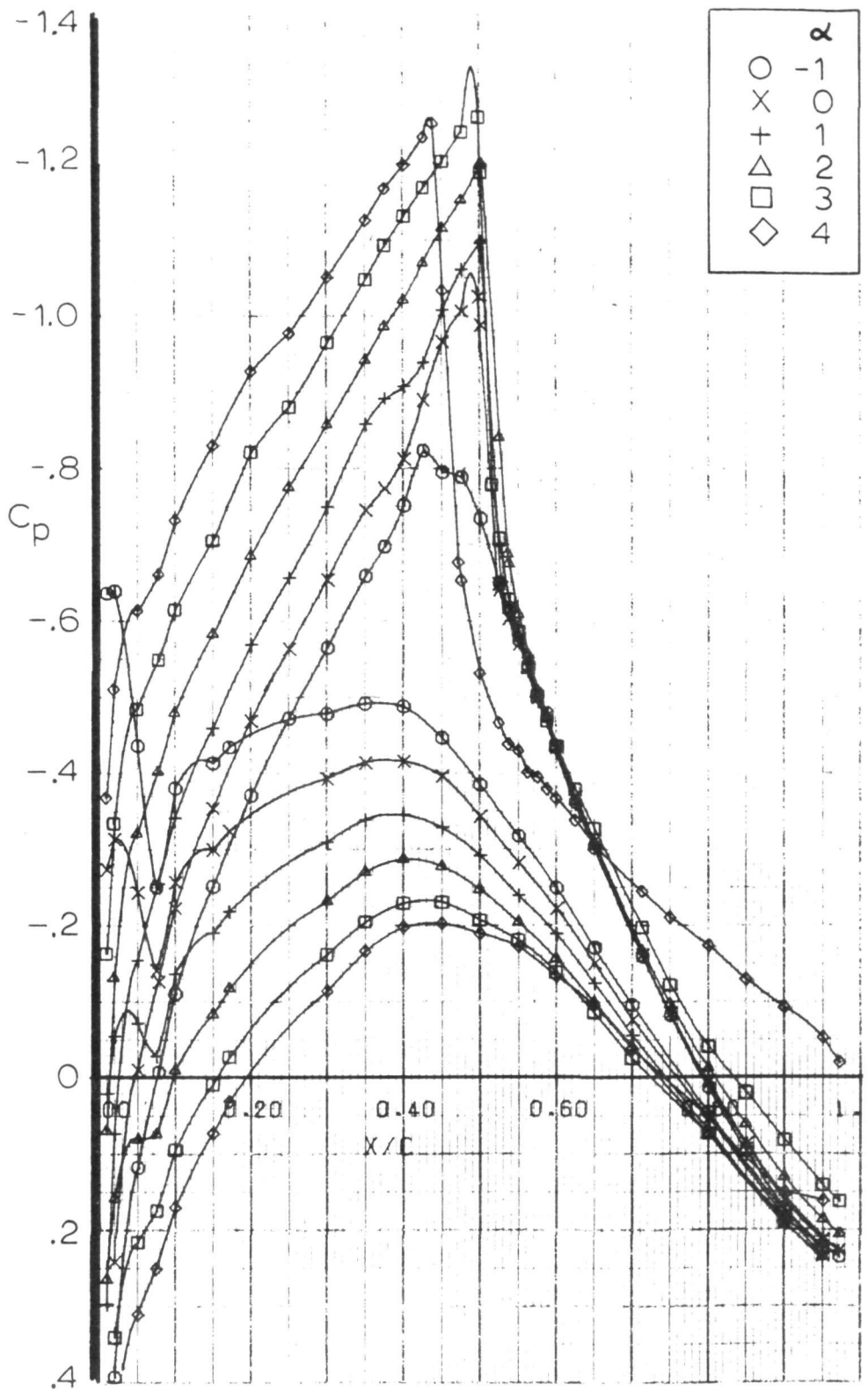

Figure 4.- Airfoil pressure distribution M = 0.72 R_N = 3 x 10^6.

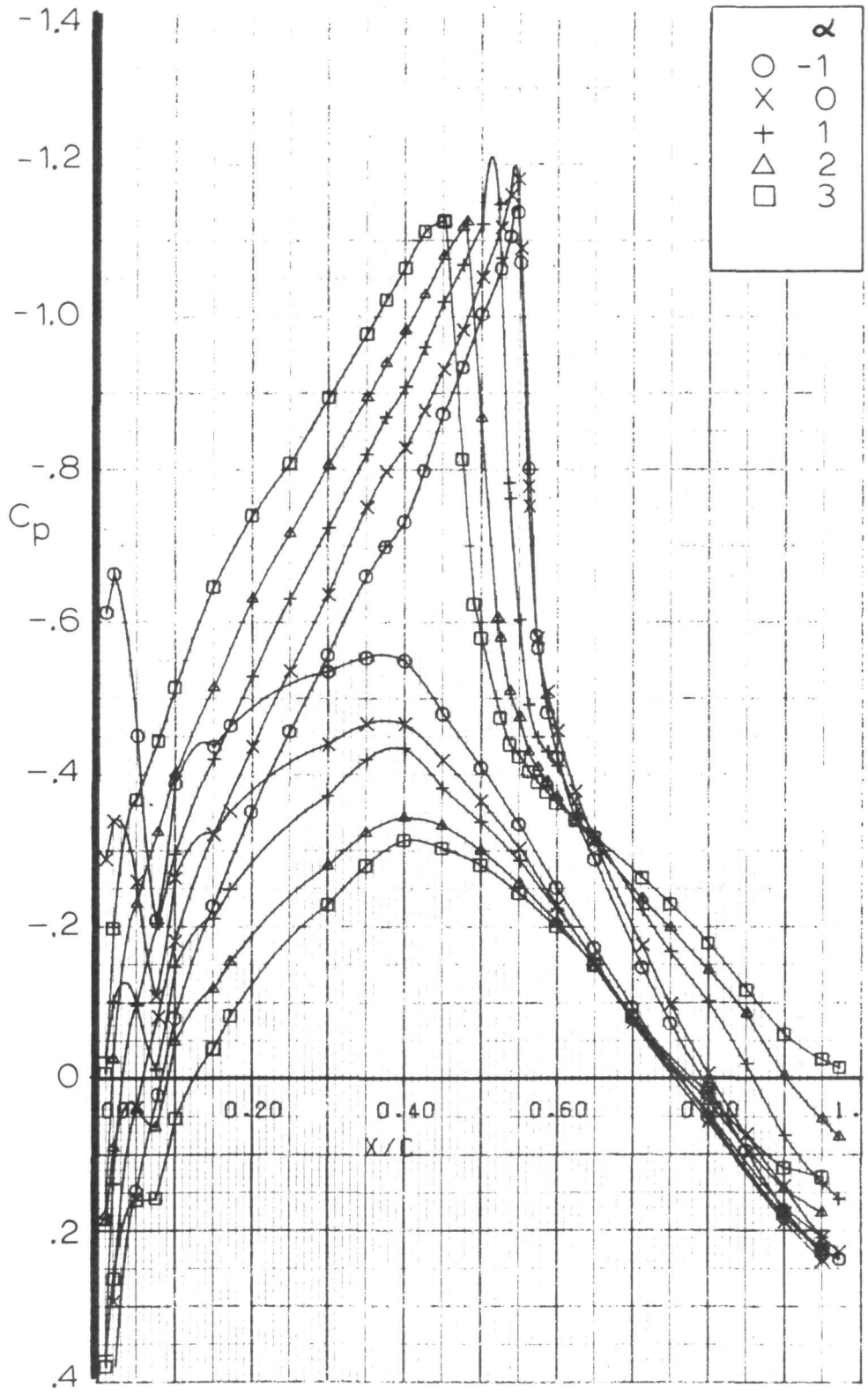

Figure 5 .- Airfoil pressure distribution M = 0.75 R_N = 3 x 10^6.

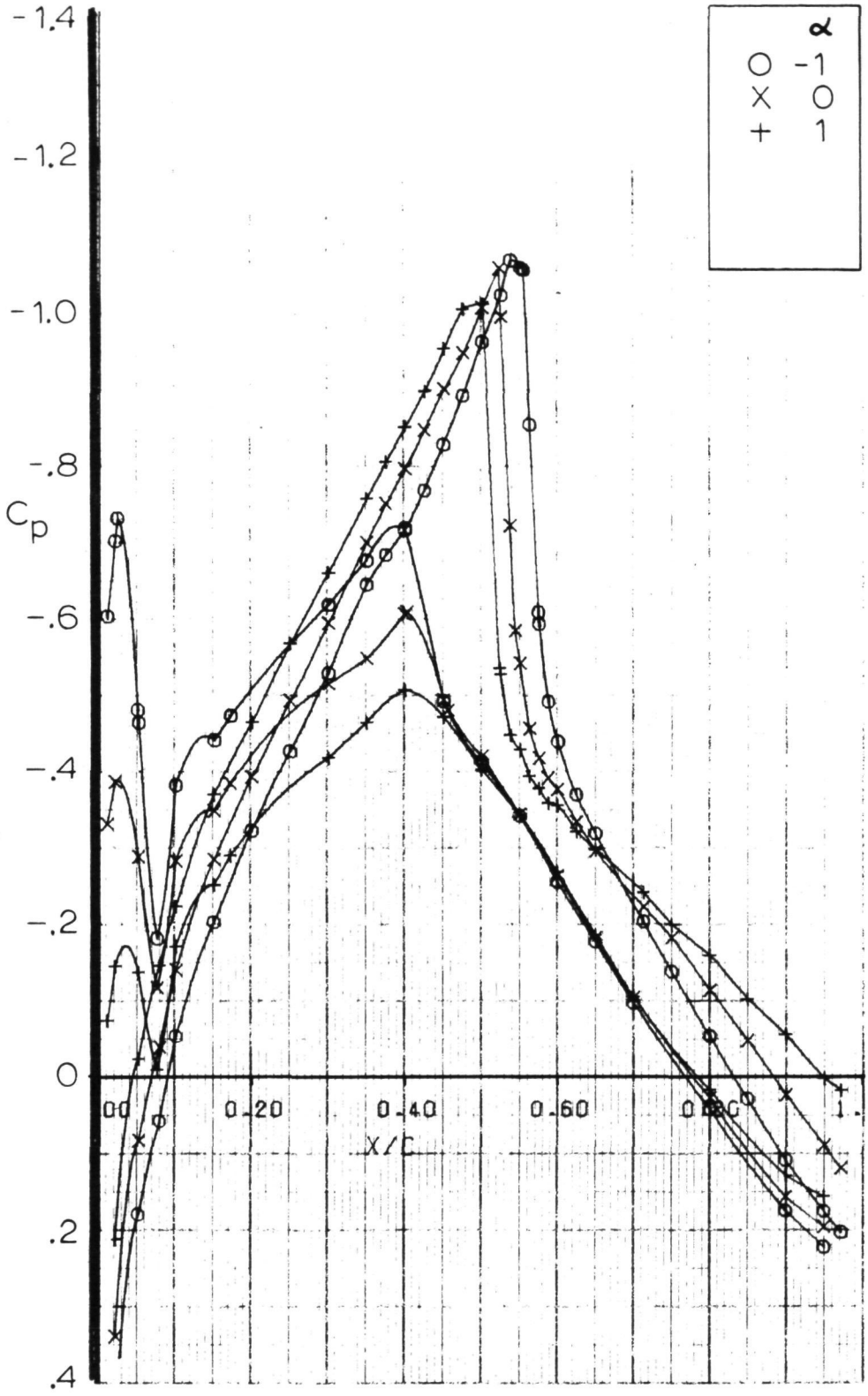

Figure 6 .- Airfoil pressure distribution M = 0.78 R_N = 3 x 10^6.

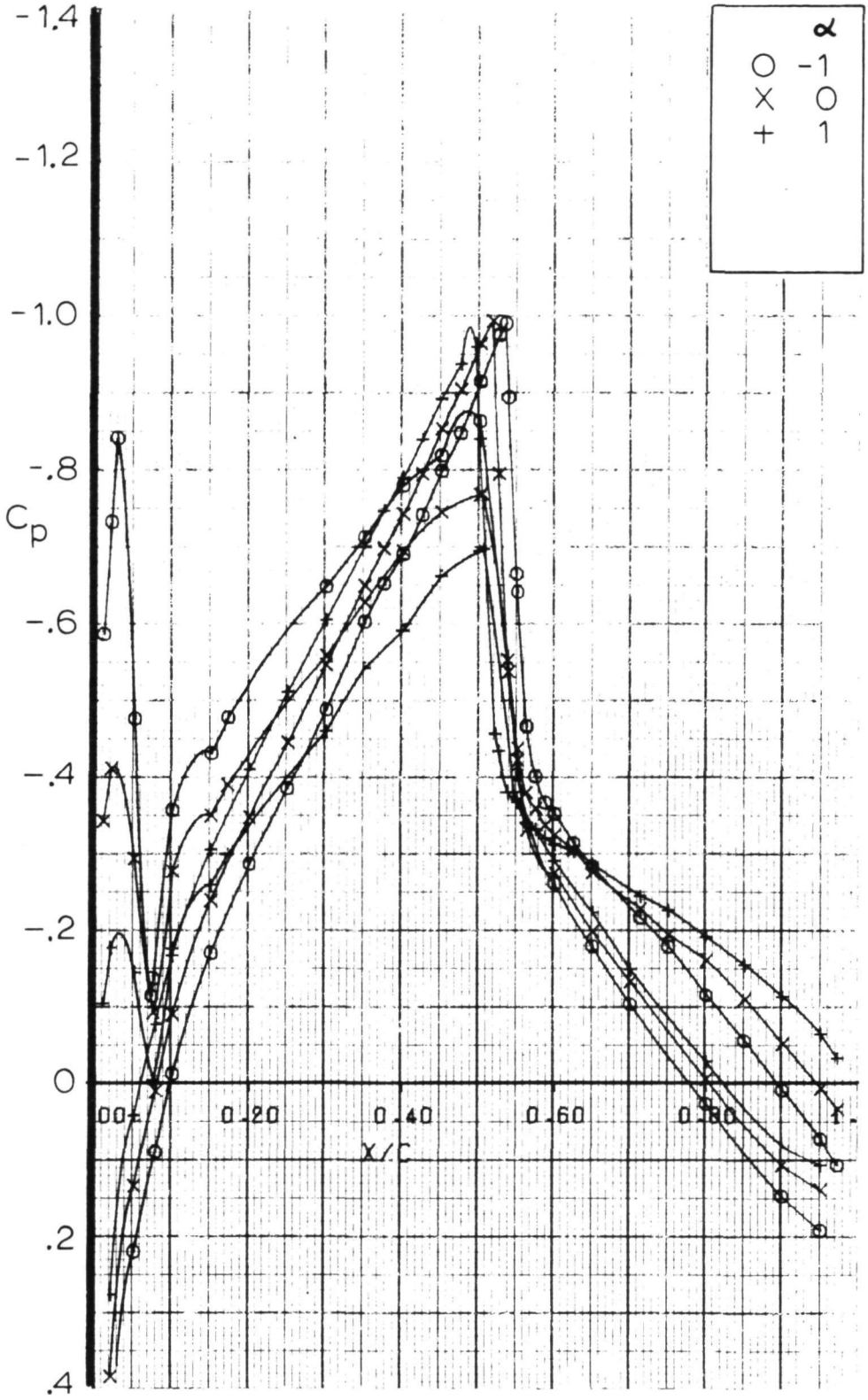

Figure 7.- Airfoil pressure distribution M = 0.80 R_N = 3 x 10^6.

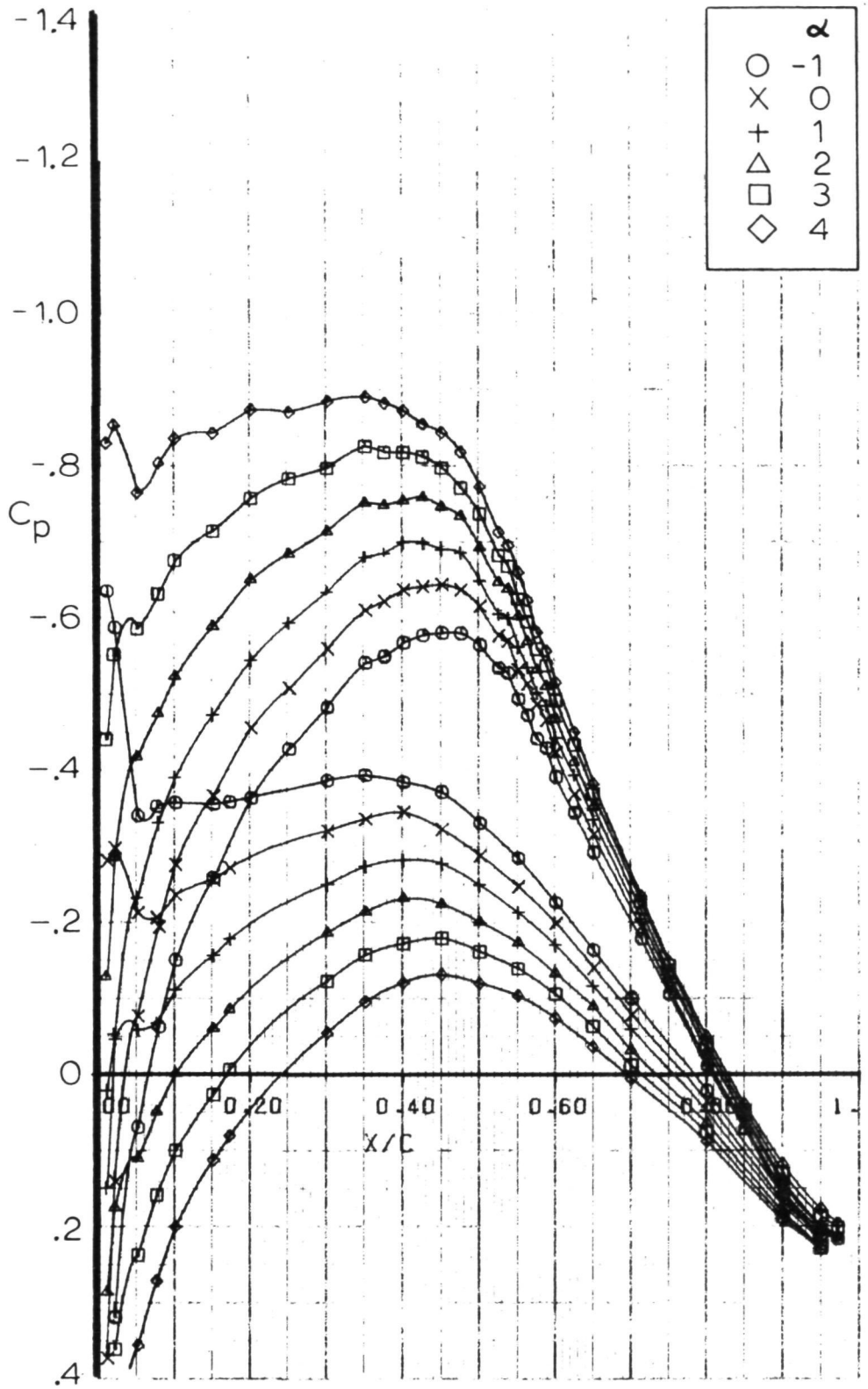

Figure 8.- Airfoil pressure distribution M = 0.6 R_N = 6 x 10^6.

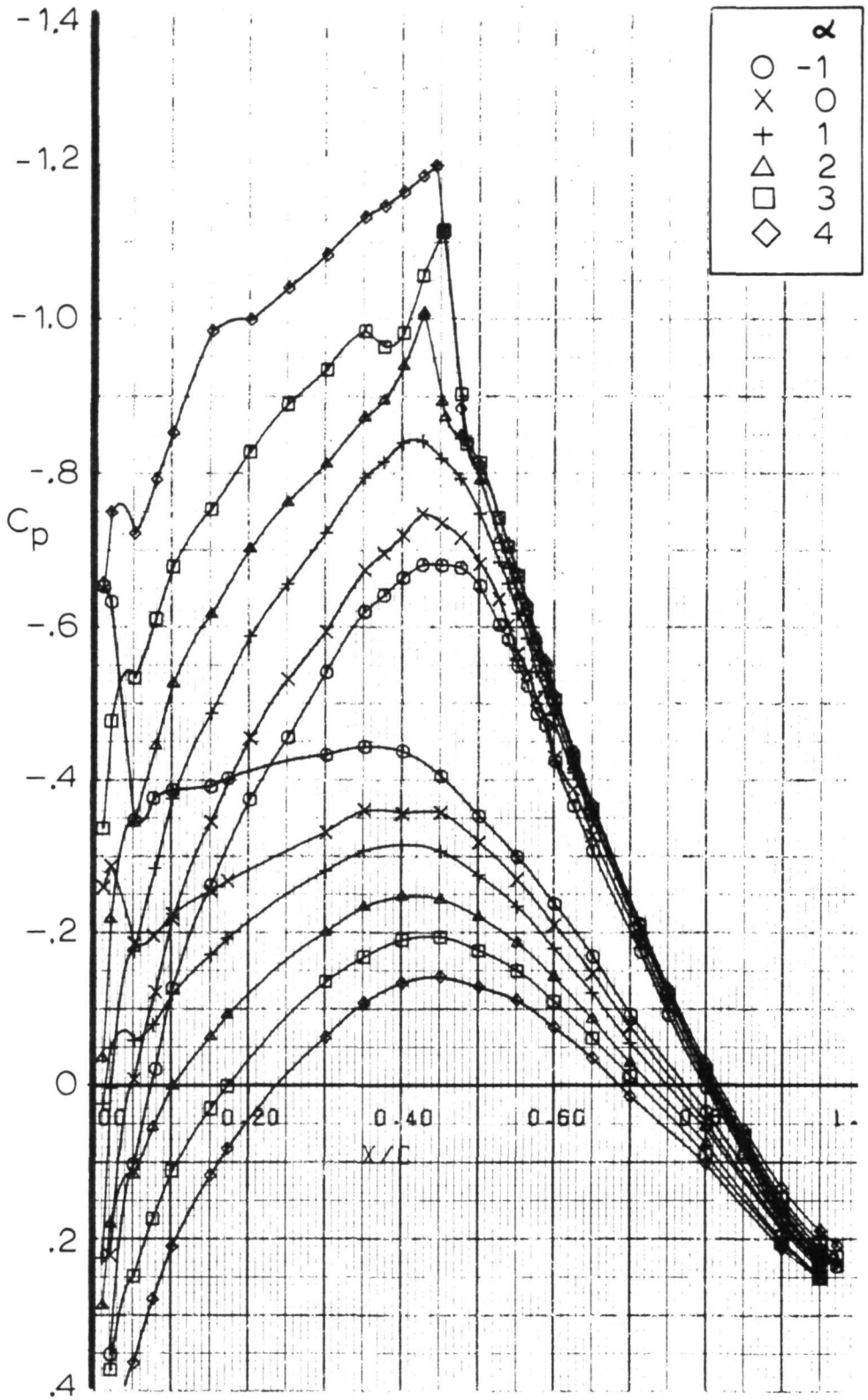

Figure 9.- Airfoil pressure distribution M = 0.68 R_N = 6 x 10^6.

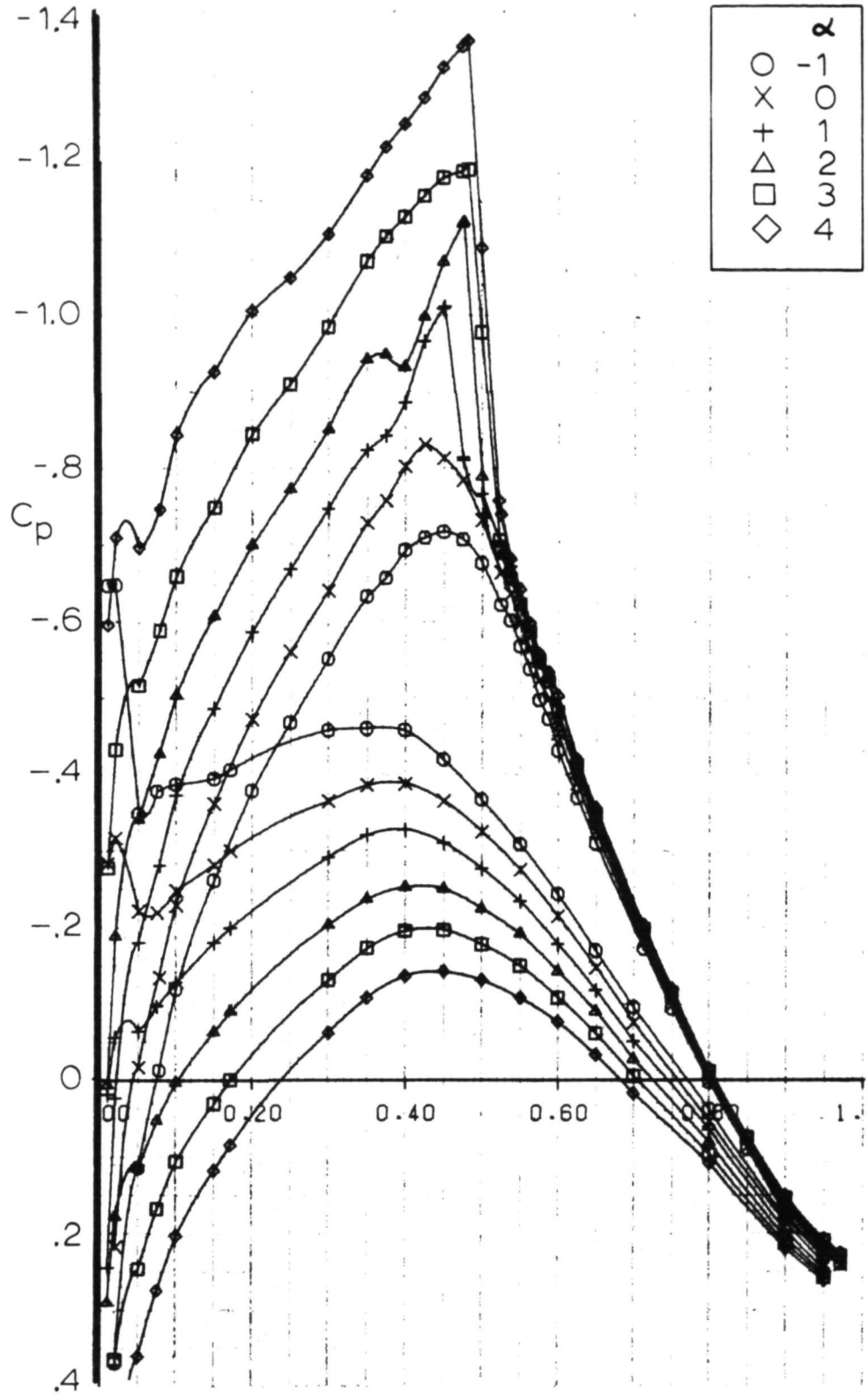

Figure 10.- Airfoil pressure distribution M = 0.70 R_N = 6 x 10^6.

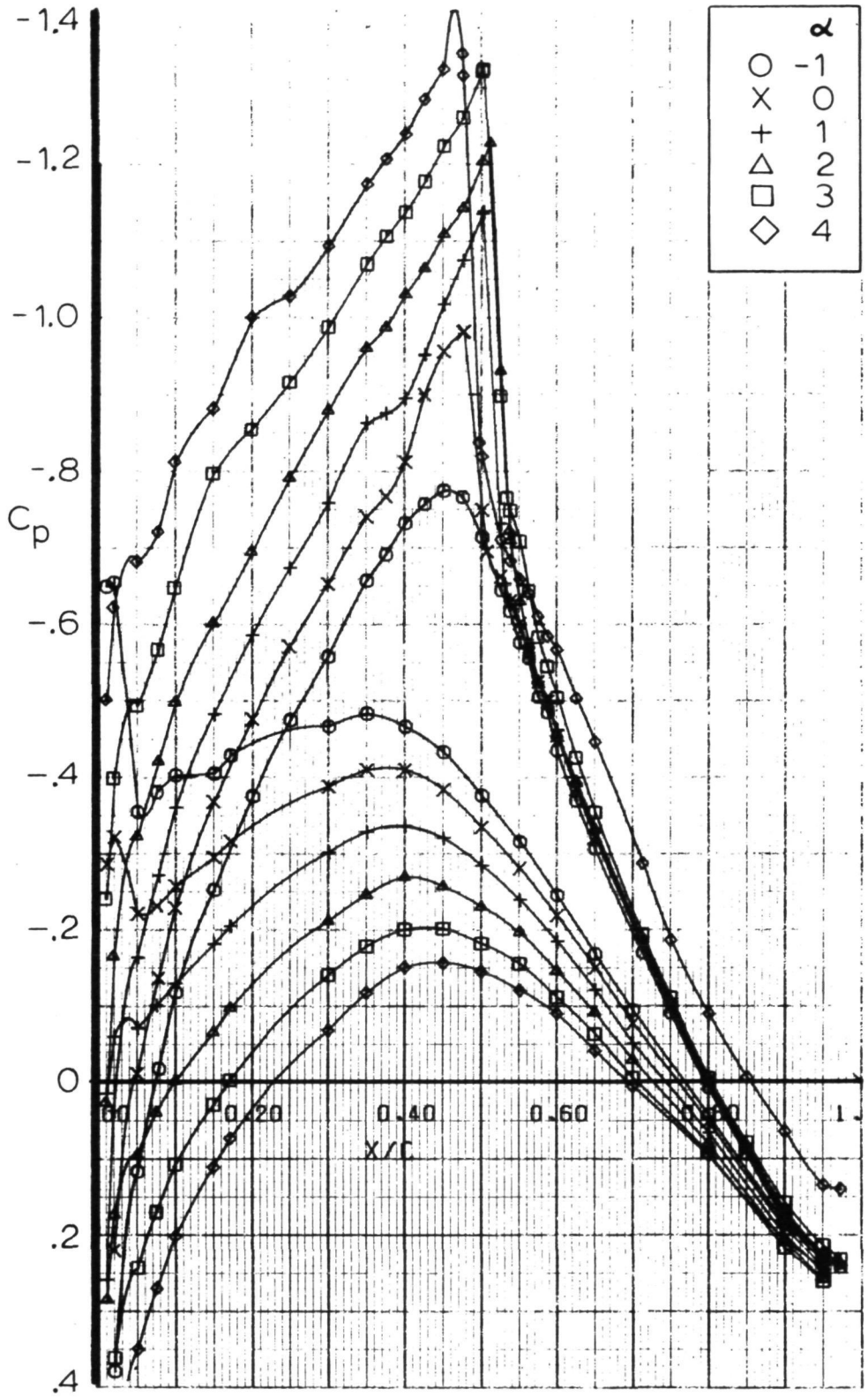

Figure 11.- Airfoil pressure distribution M = 0.72 R_N = 6 x 10^6.

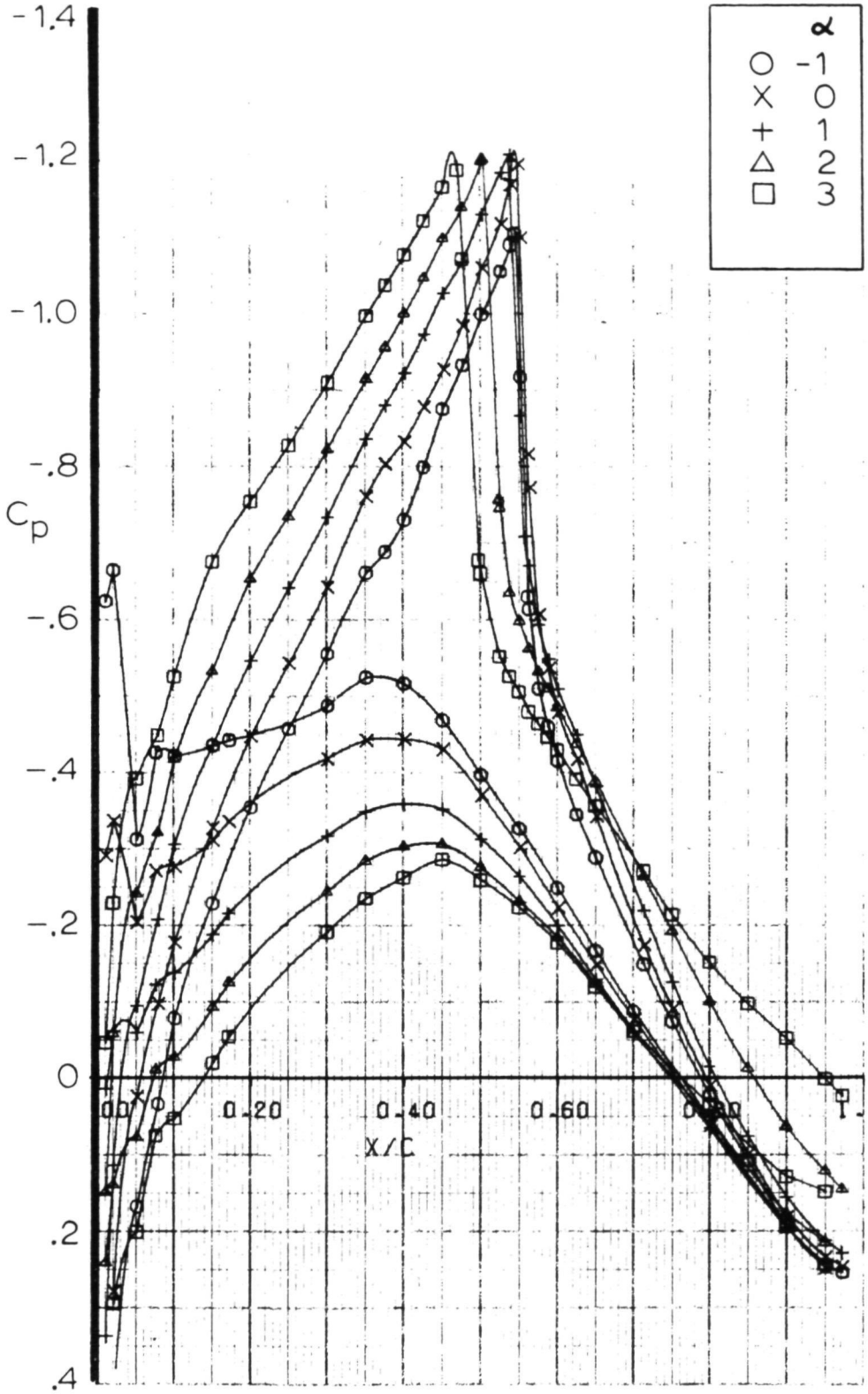

Figure 12.- Airfoil pressure distribution M = 0.75 R_N = 6 x 10^6.

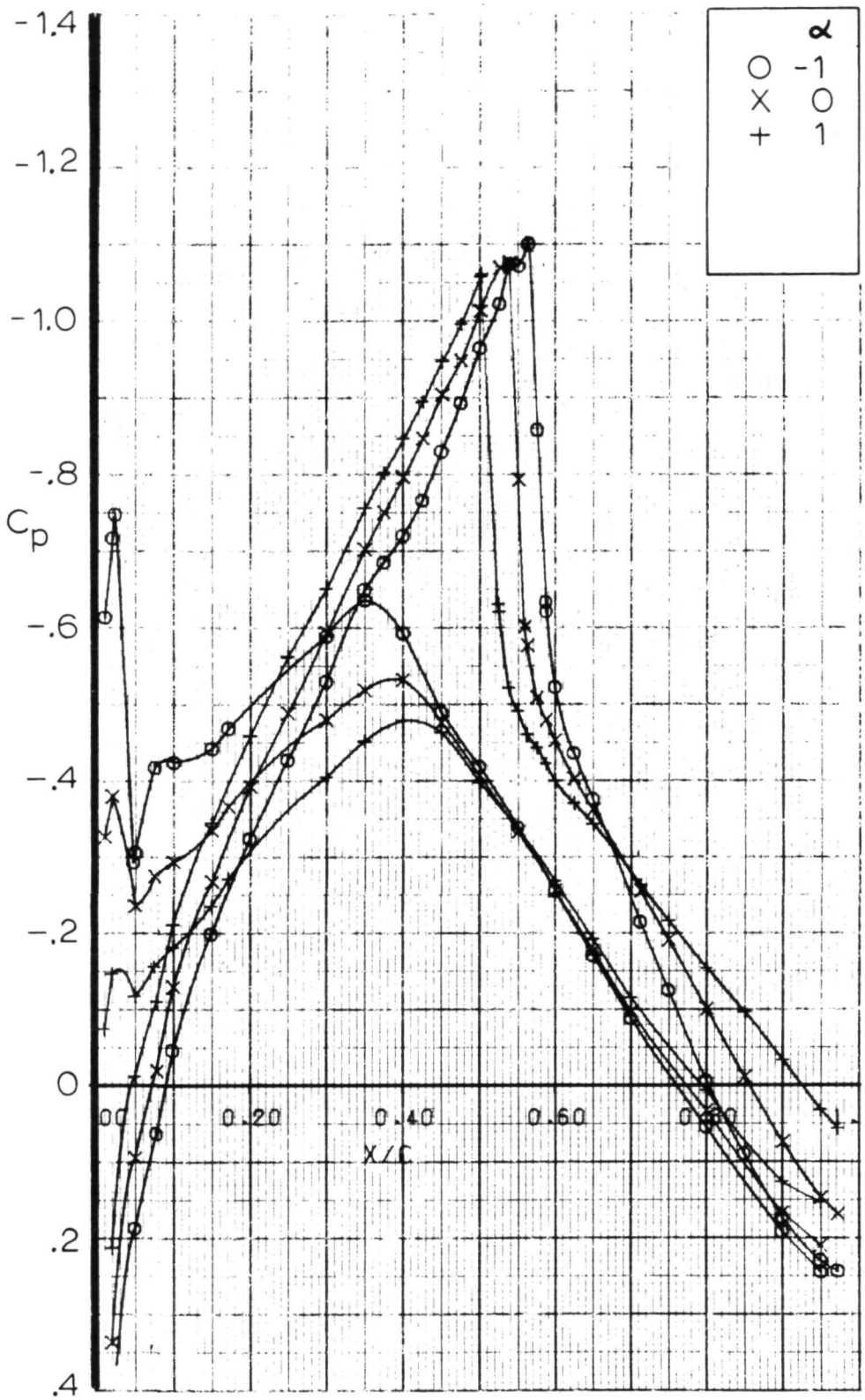

Figure 13.- Airfoil pressure distribution M = 0.78 R_N = 6 x 10^6.

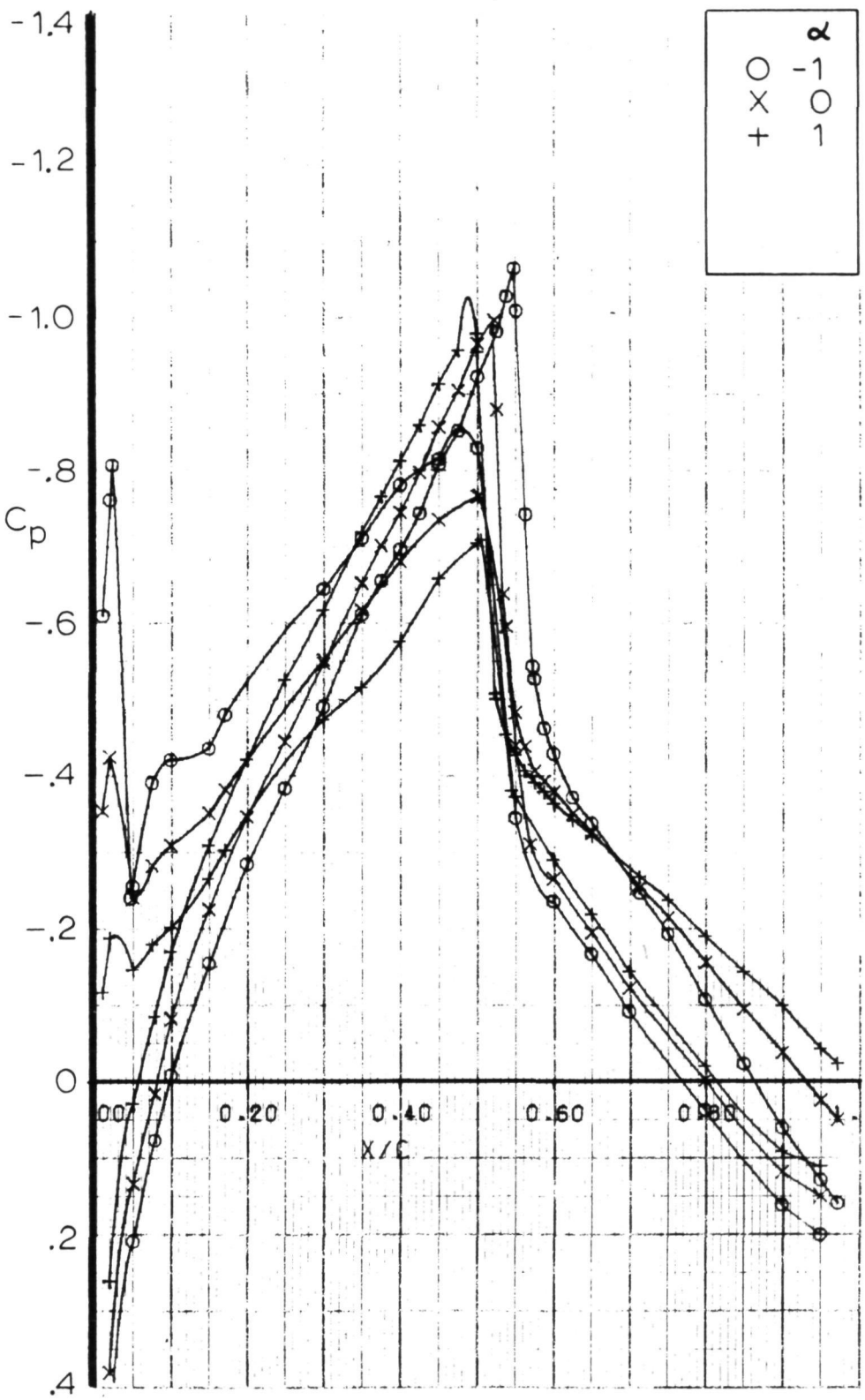

Figure 14.- Airfoil pressure distribution M = 0.80 R_N = 6 x 10^6.

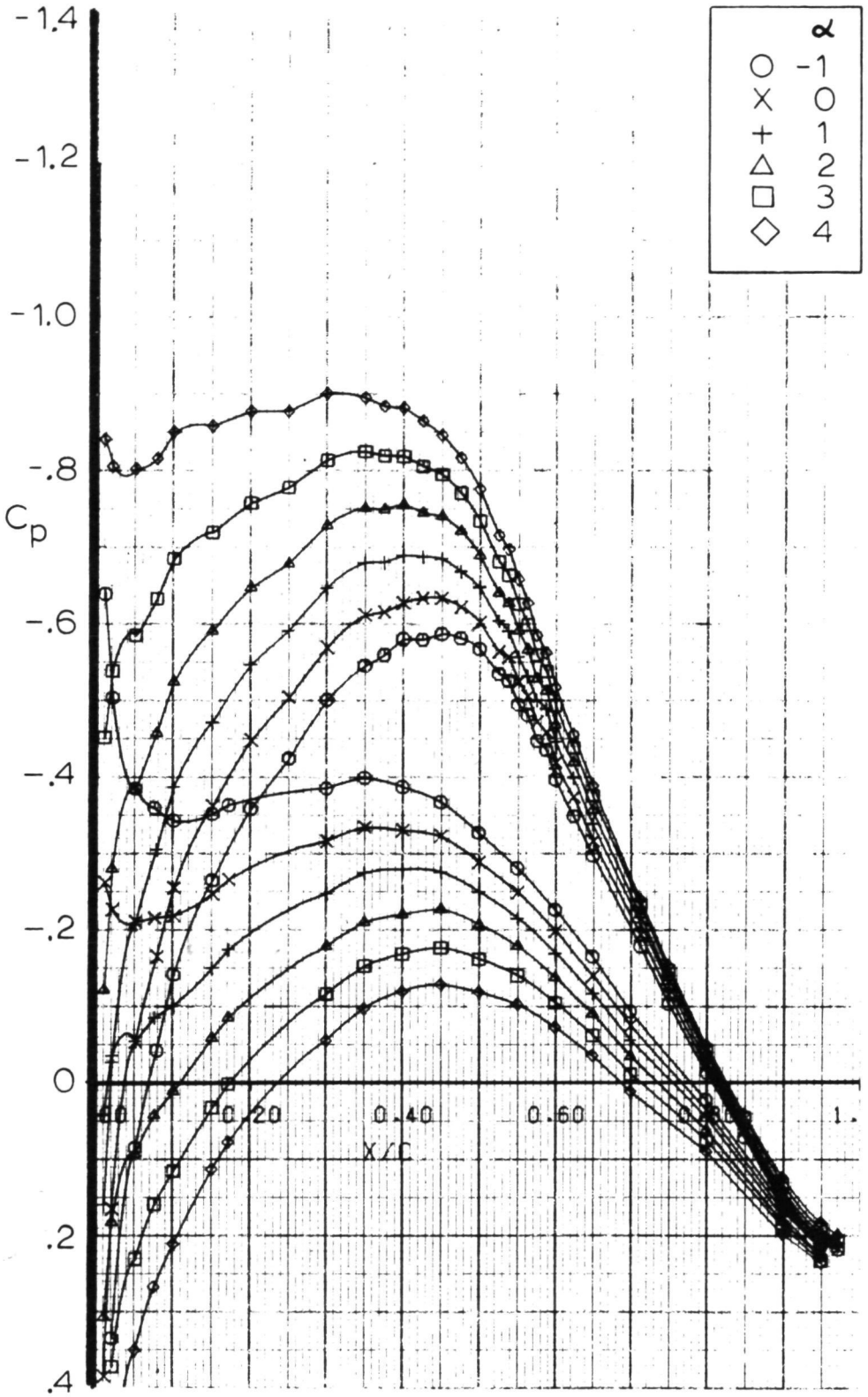

Figure 15.- Airfoil pressure distribution M = 0.6 R_N = 9 x 10^6.

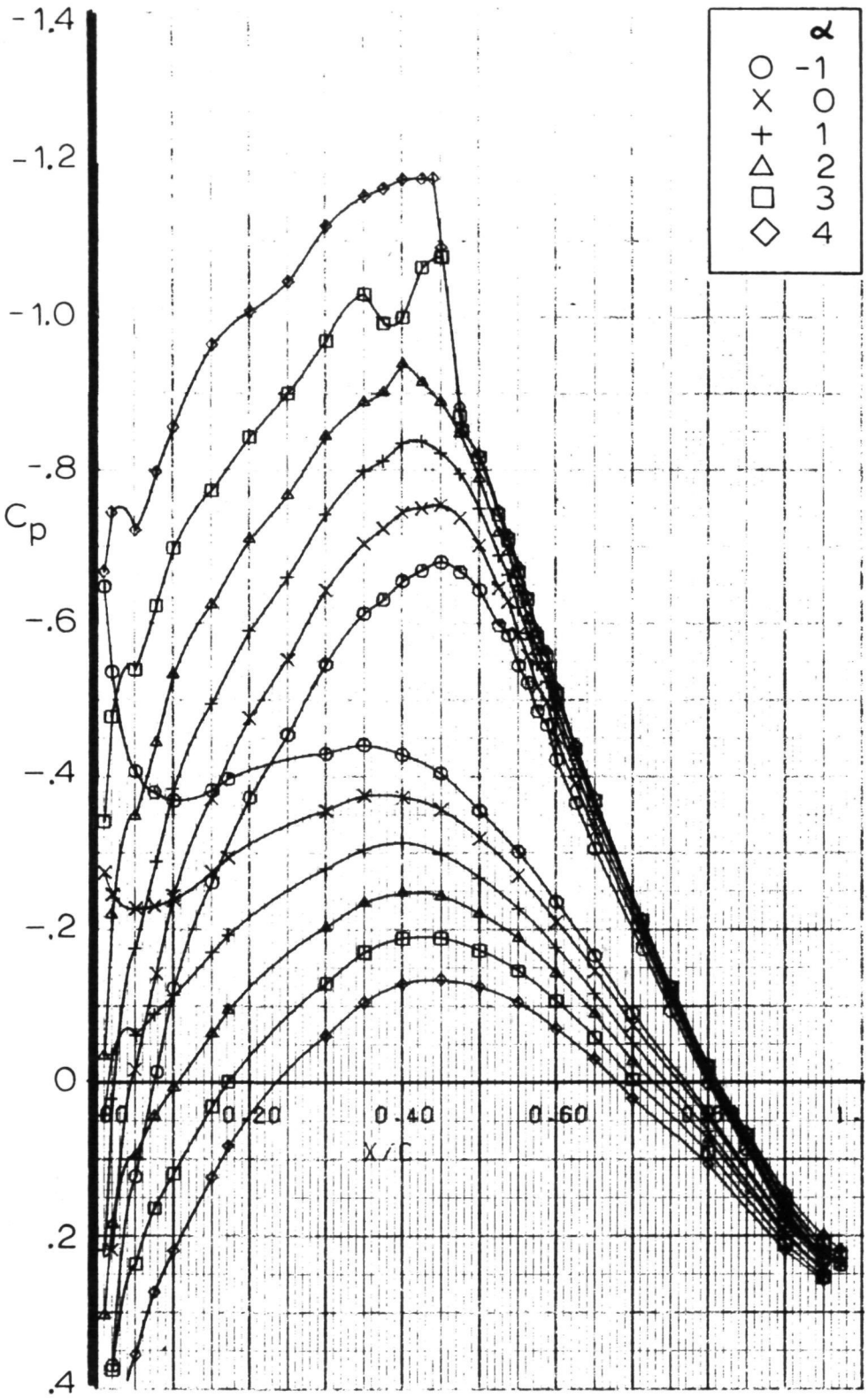

Figure 16 .- Airfoil pressure distribution M = 0.68 R_N = 9 x 10^6.

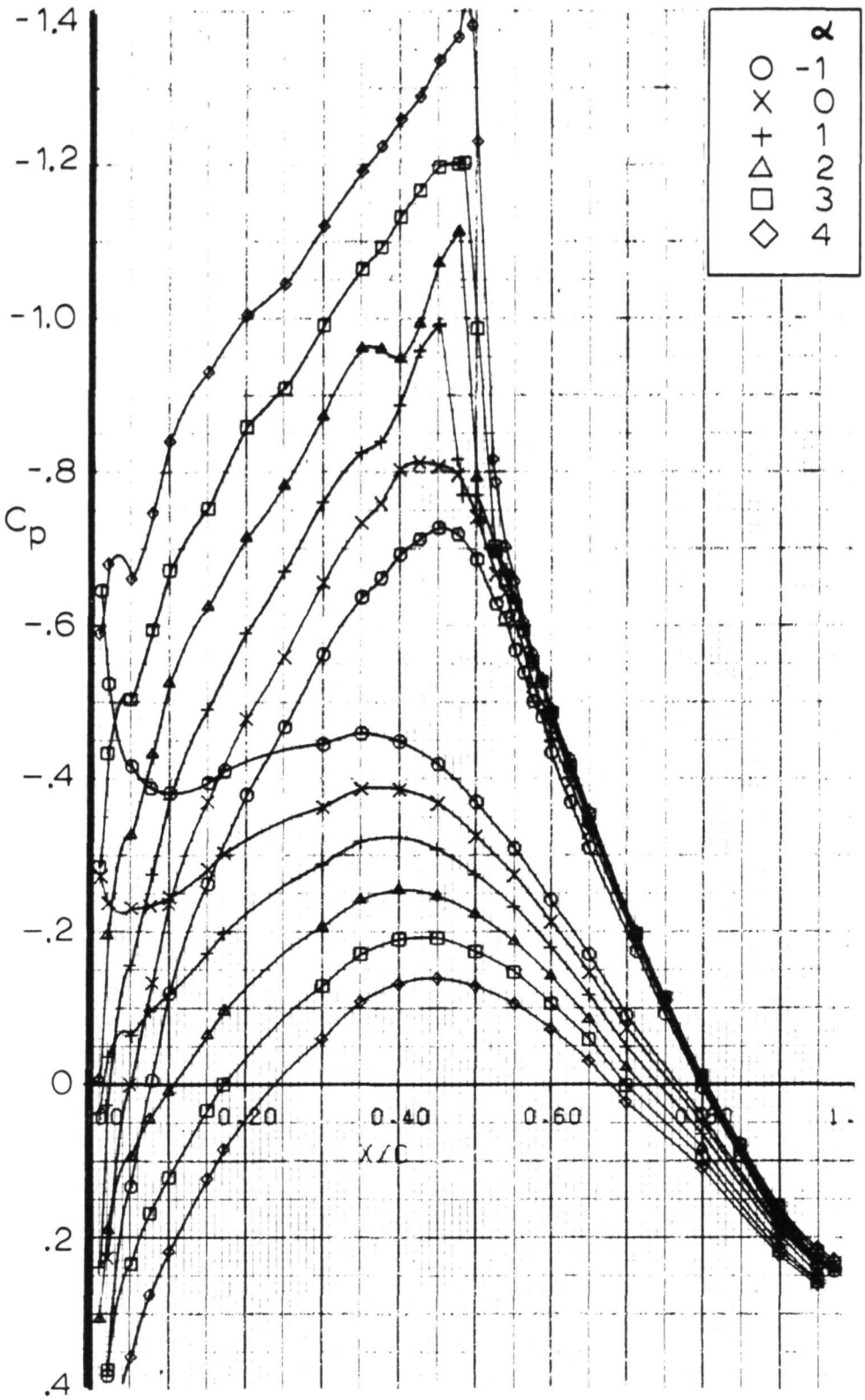

Figure 17.- Airfoil pressure distribution M = 0.70 R_N = 9 x 10^6.

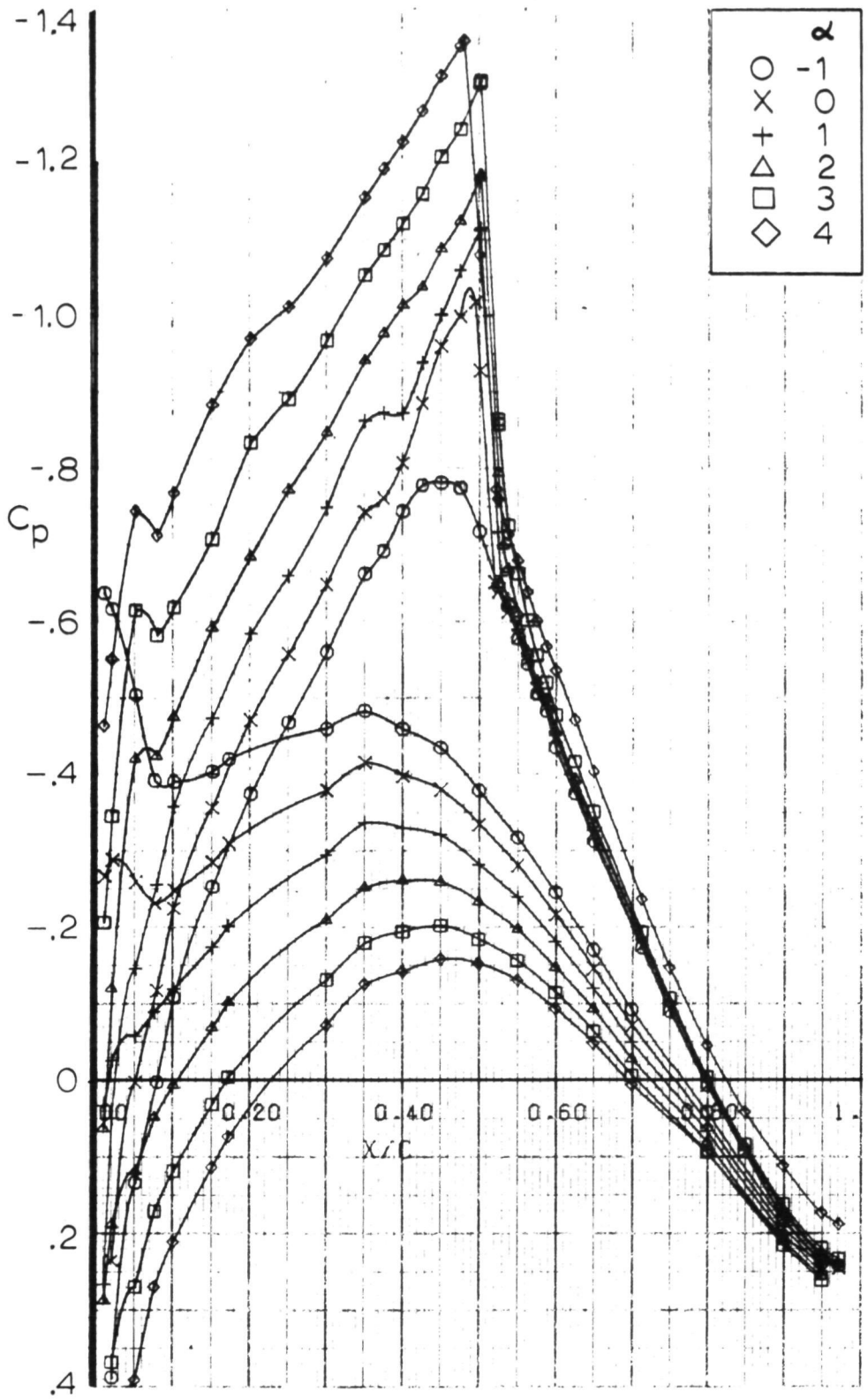

Figure 18.- Airfoil pressure distribution M = 0.72 R_N = 9 x 10^6.

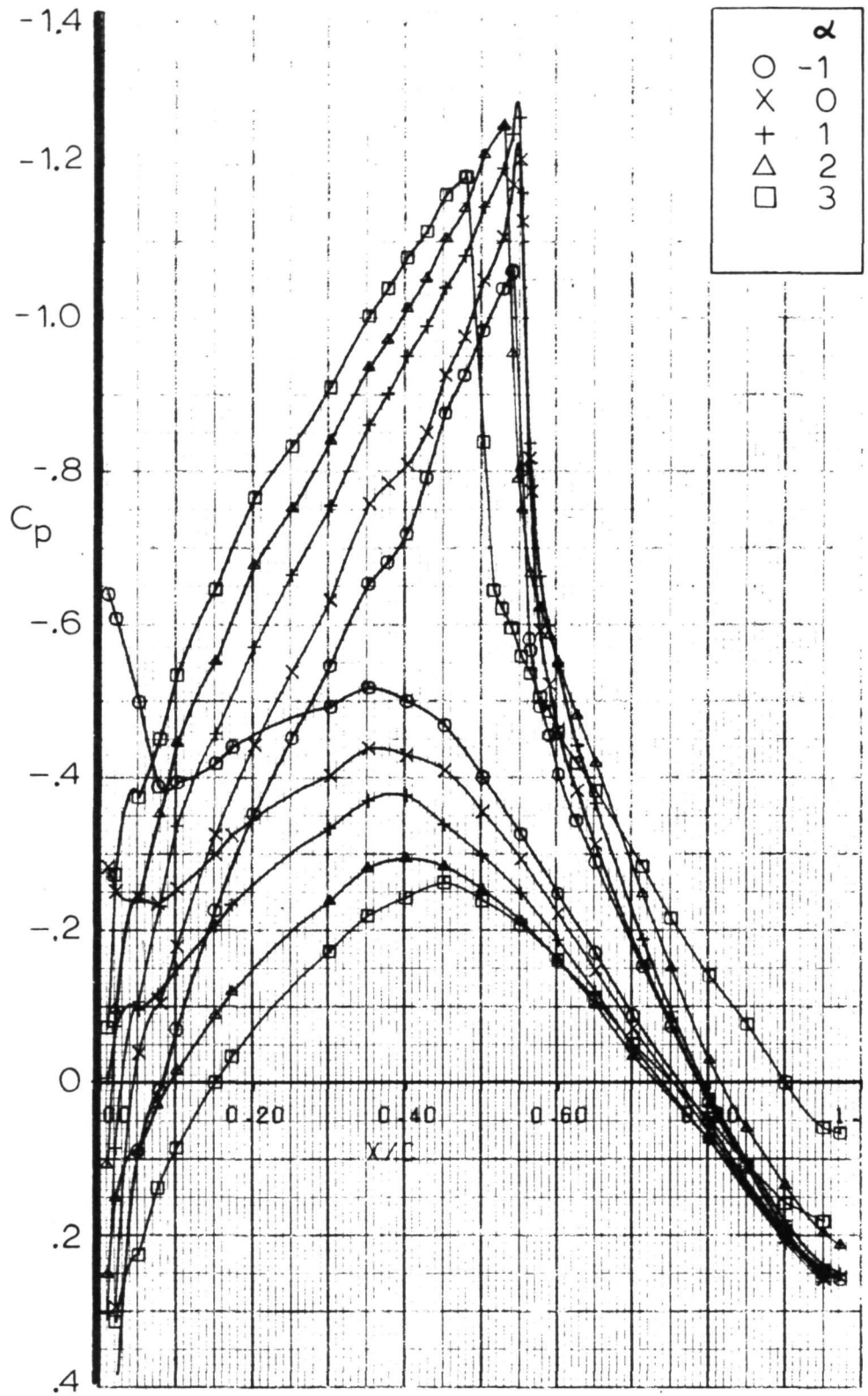

Figure 19.- Airfoil pressure distribution M = 0.75 R_N = 9 x 10^6.

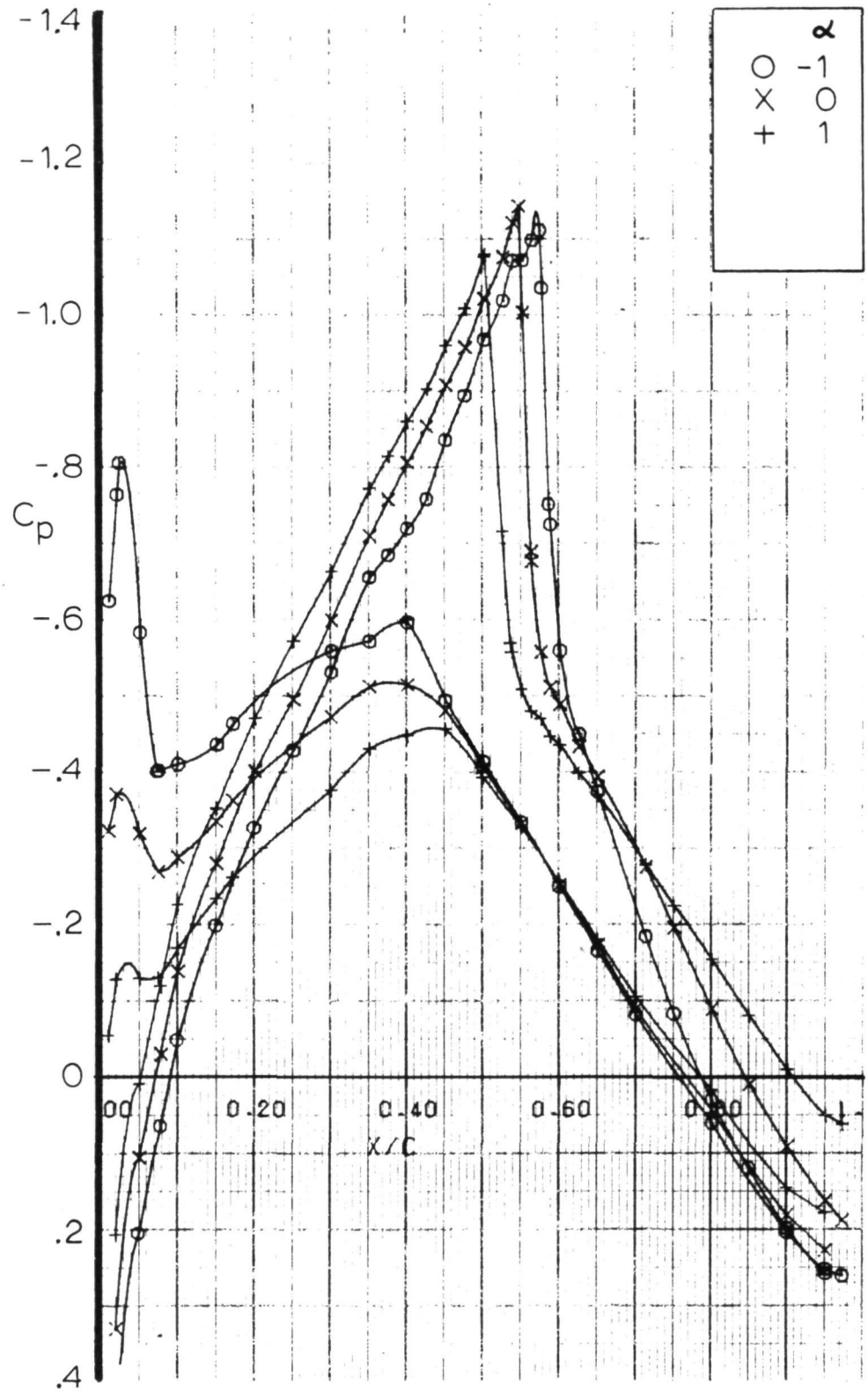

Figure 20.- Airfoil pressure distribution M = 0.78 R_N = 9 x 10^6.

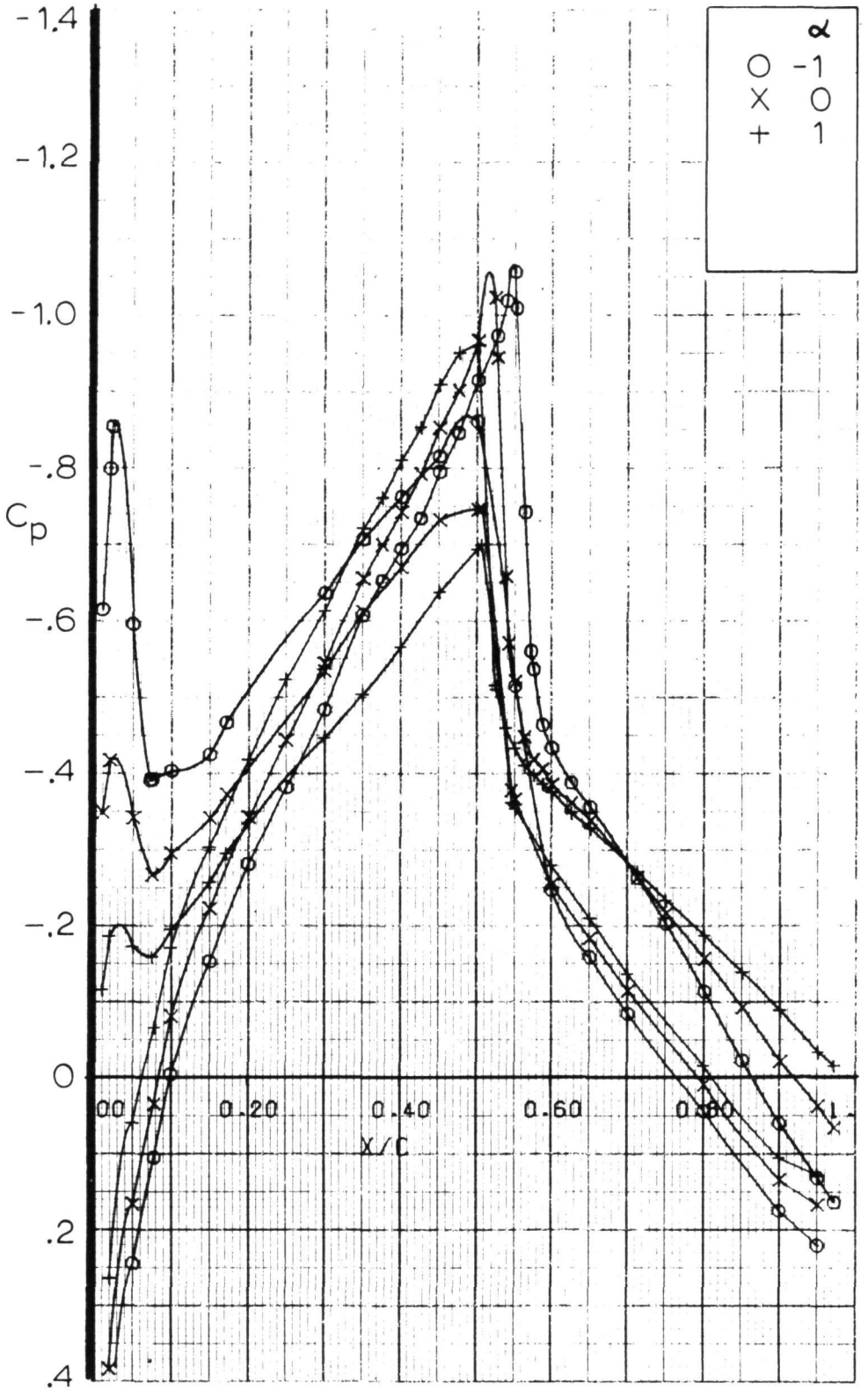

Figure 21.- Airfoil pressure distribution M = 0.80 R_N = 9 x 10^6.

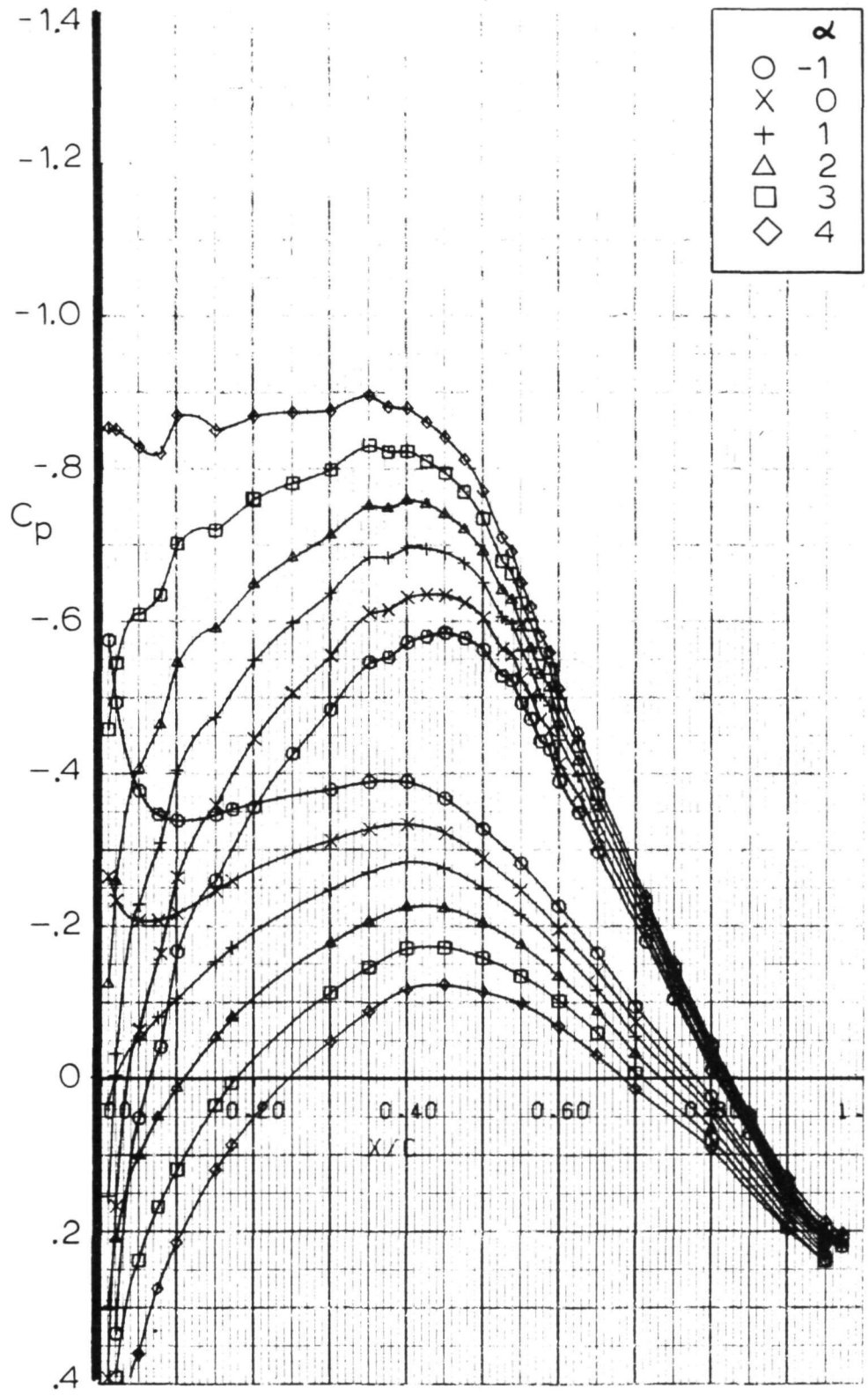

Figure 22.- Airfoil pressure distribution M = 0.6 R_N = 12 x 10^6.

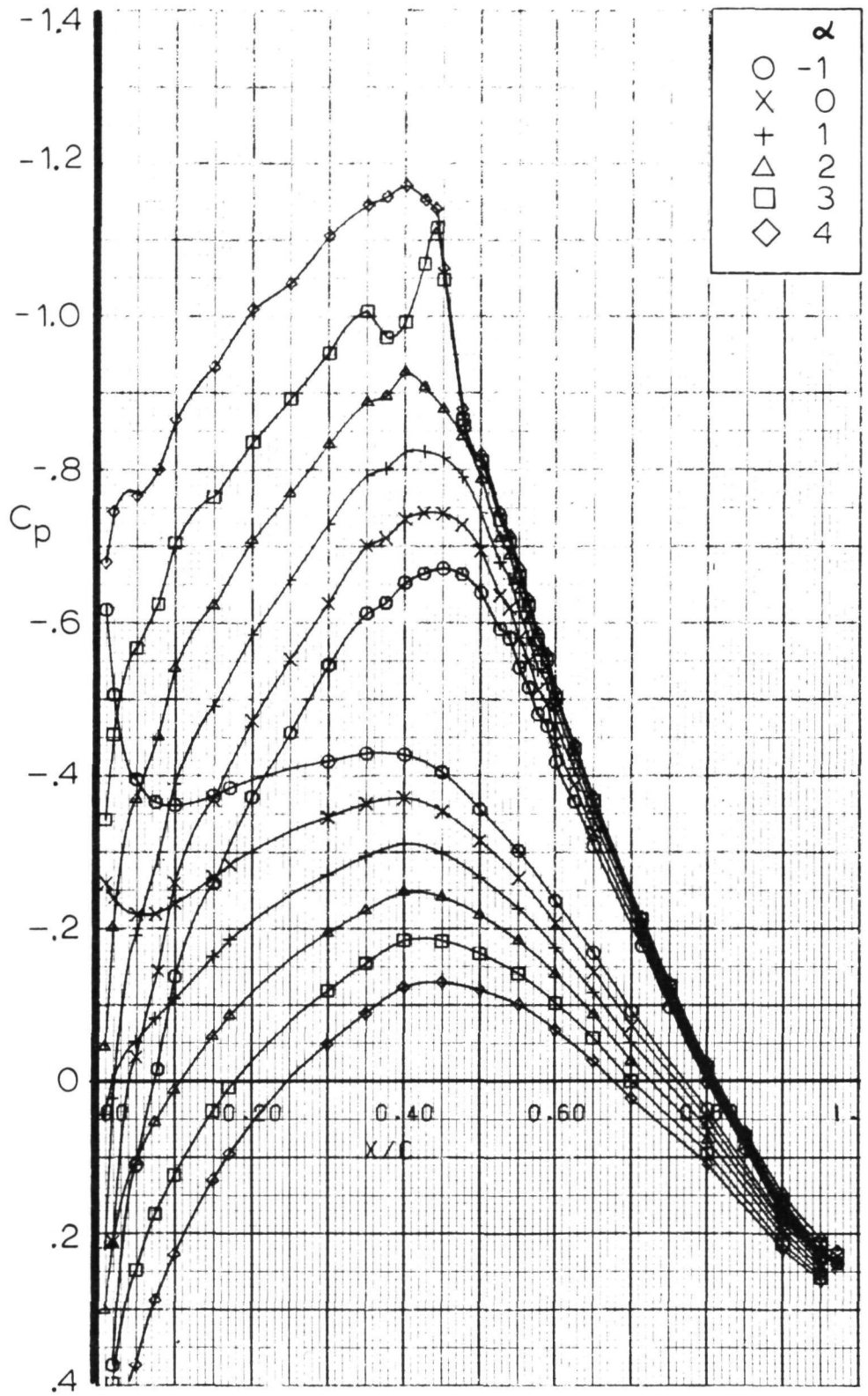

Figure 23.- Airfoil pressure distribution M = 0.68 R_N = 12 x 10^6.

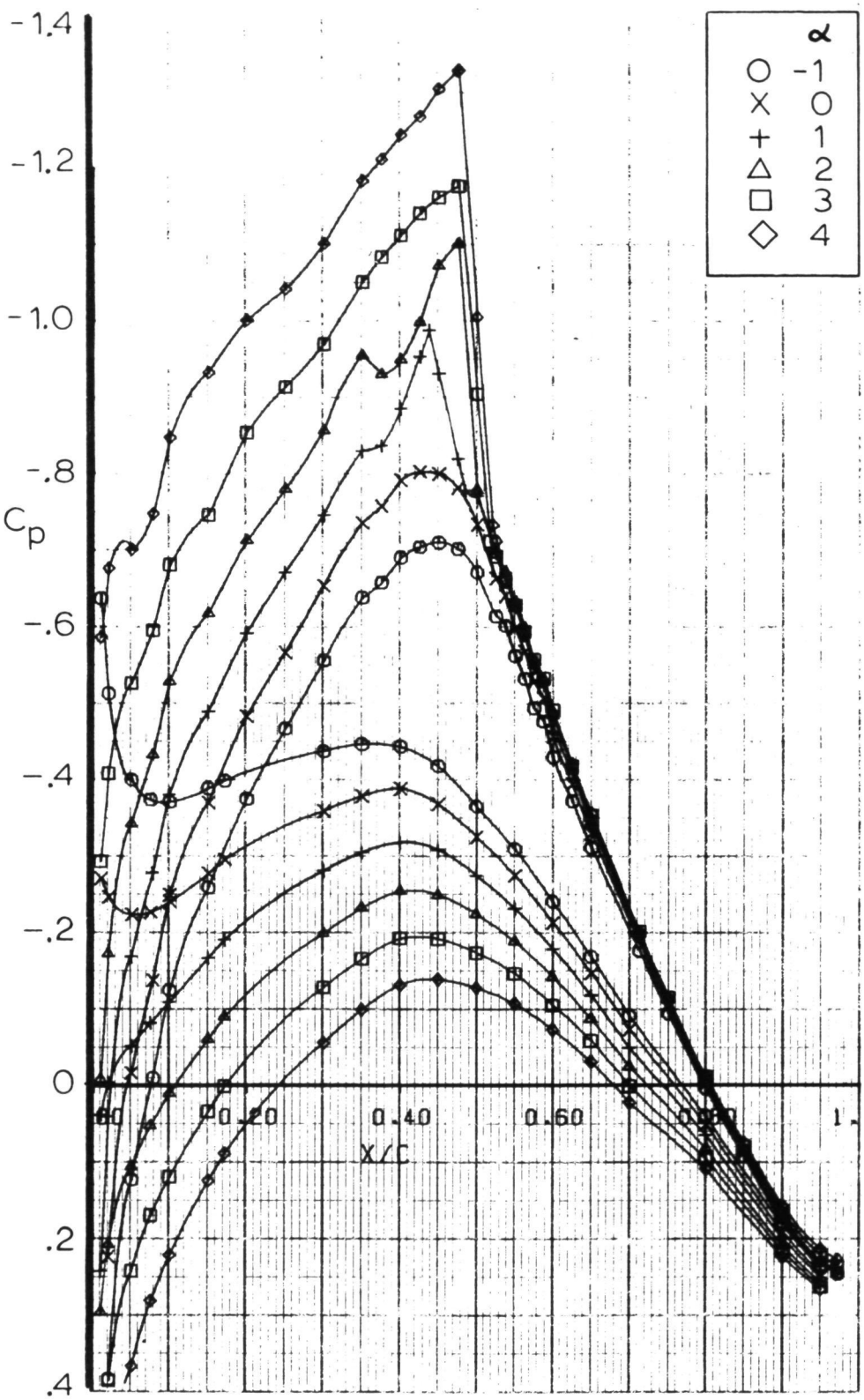

Figure 24.- Airfoil pressure distribution M = 0.70 R_N = 12 x 10^6.

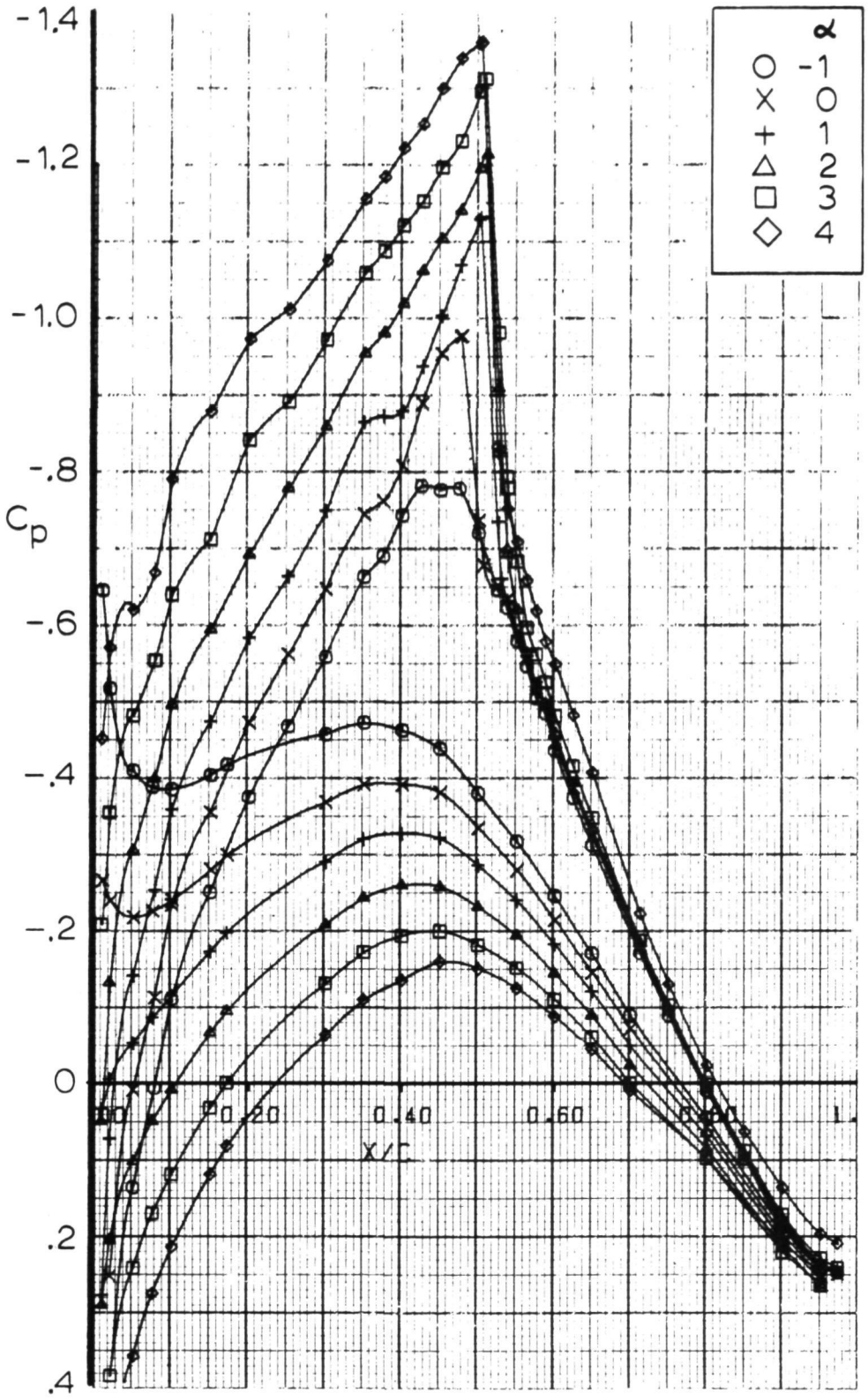

Figure 25.- Airfoil pressure distribution M = 0.72 R_N = 12 x 10^6.

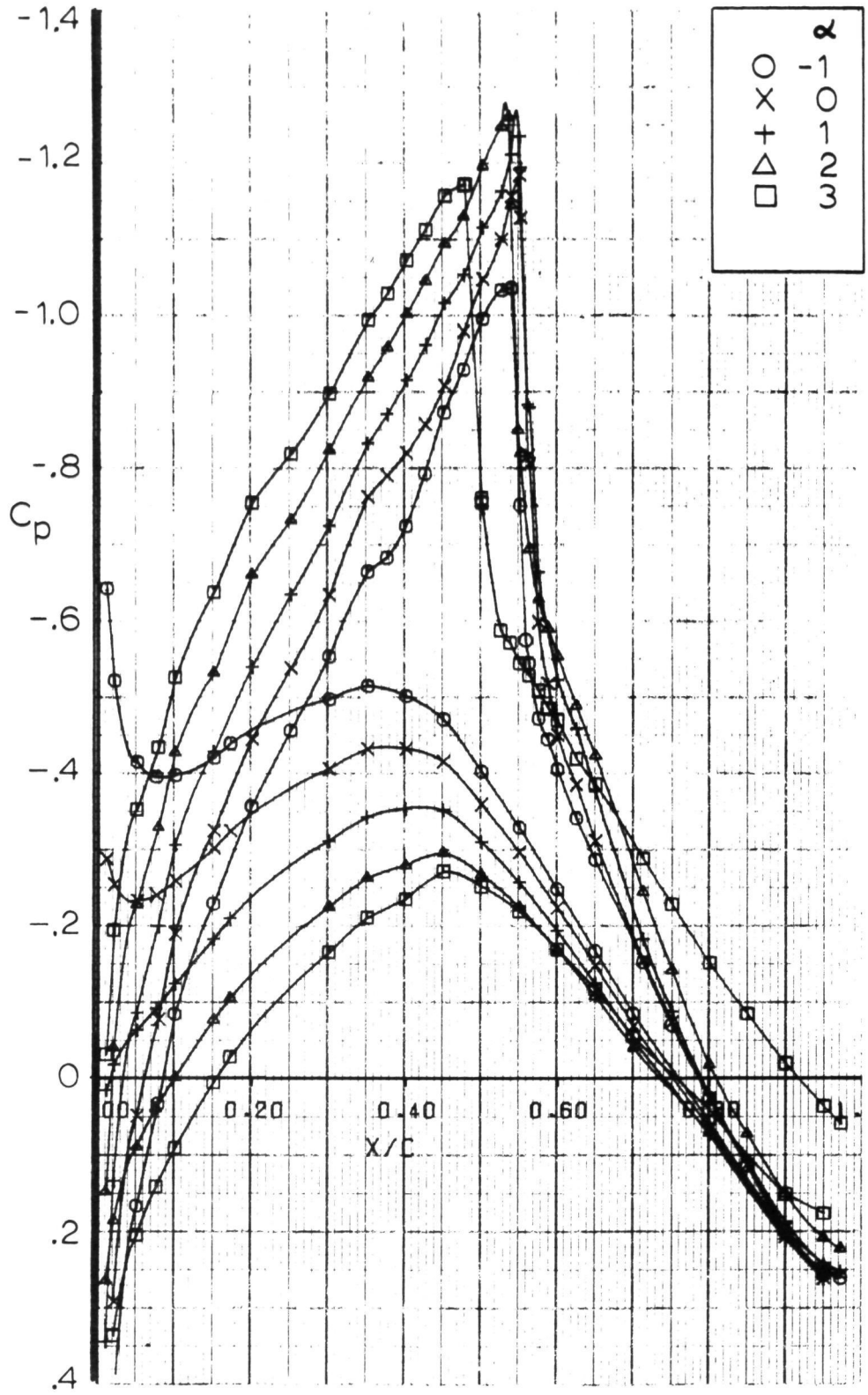

Figure 26.- Airfoil pressure distribution M = 0.75 R_N = 12 x 10^6.

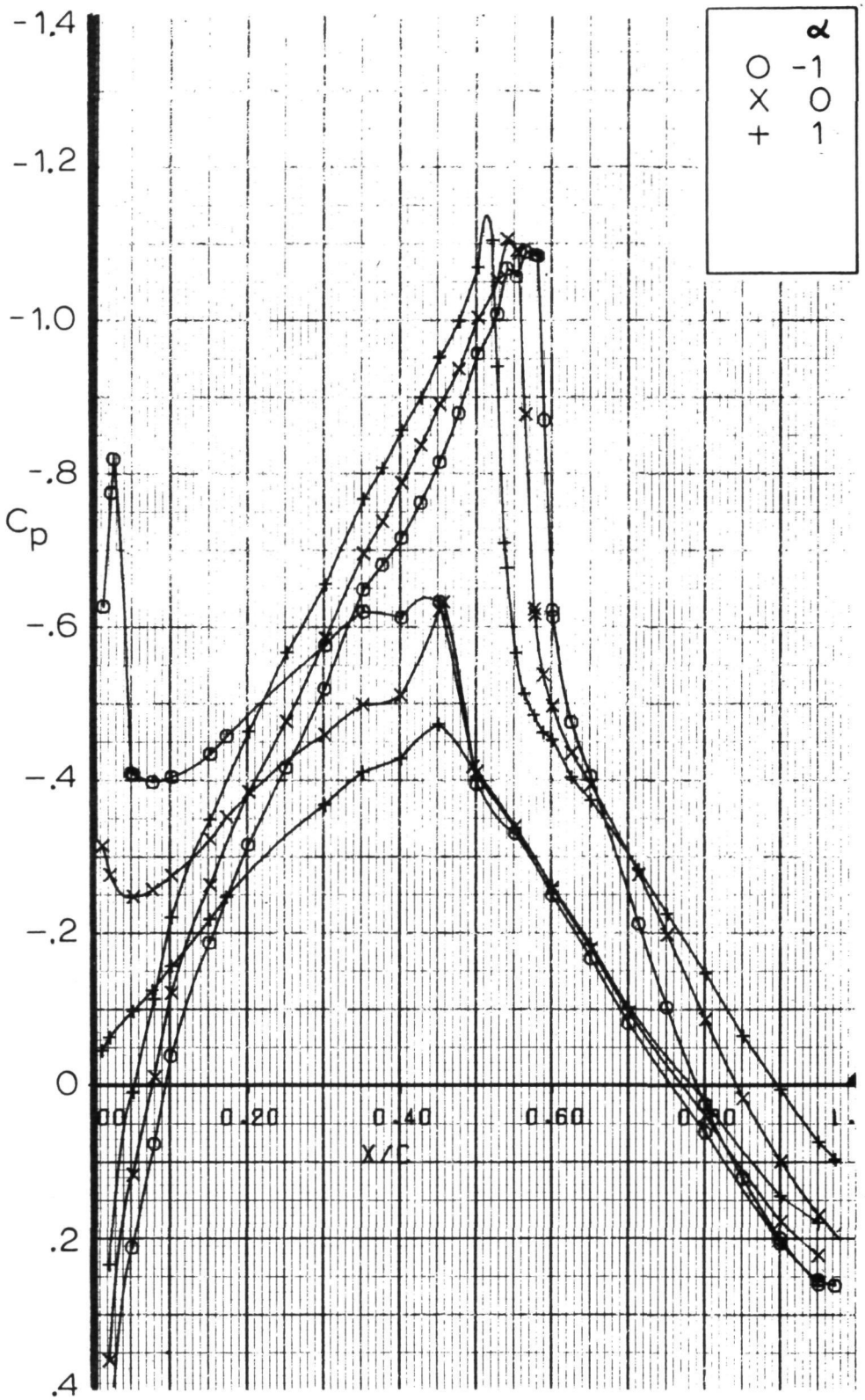

Figure 27.- Airfoil pressure distribution M = 0.78 R_N = 12 x 10^6.

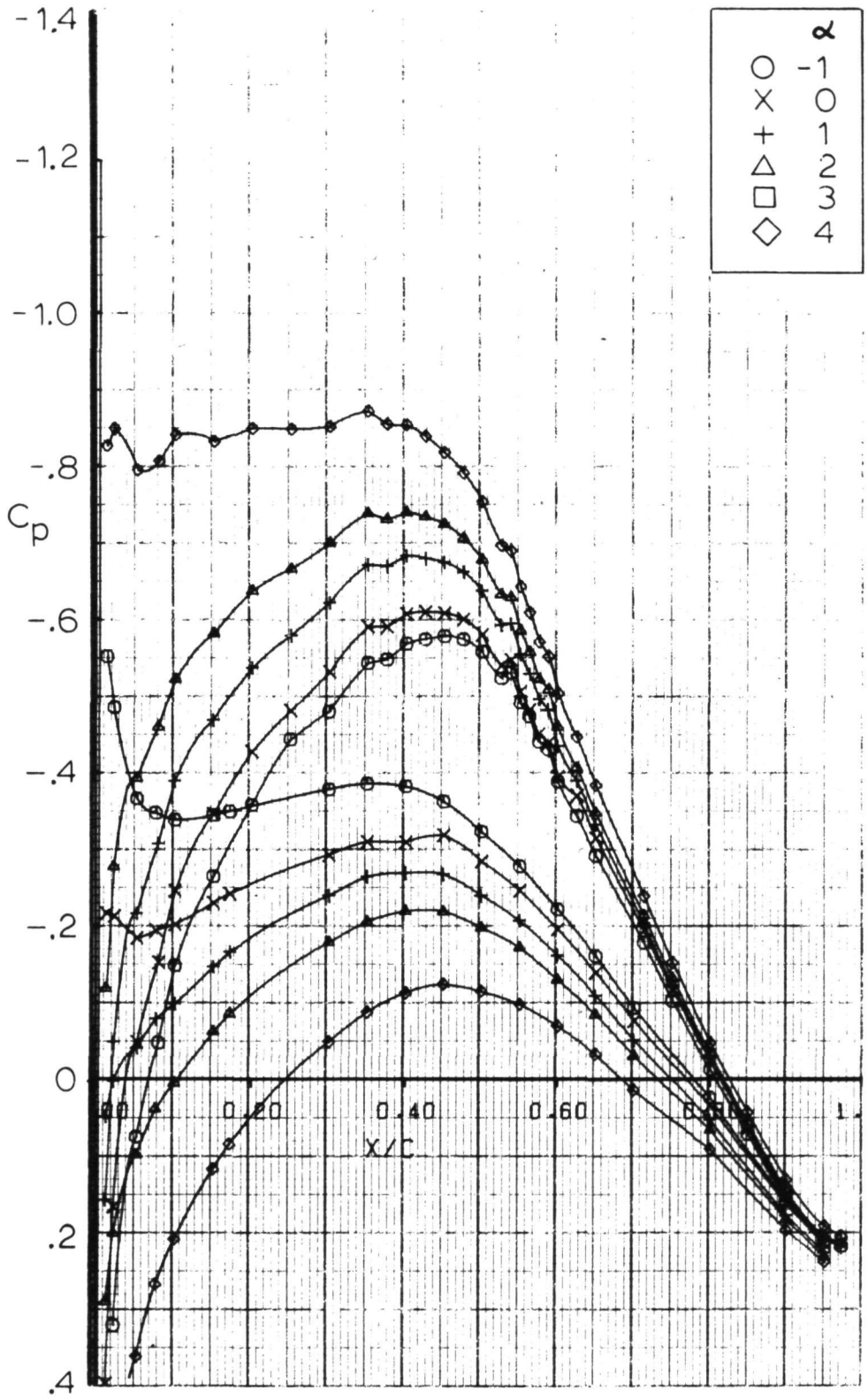

Figure 28.- Airfoil pressure distribution M = 0.6 R_N = 17 x 10^6.

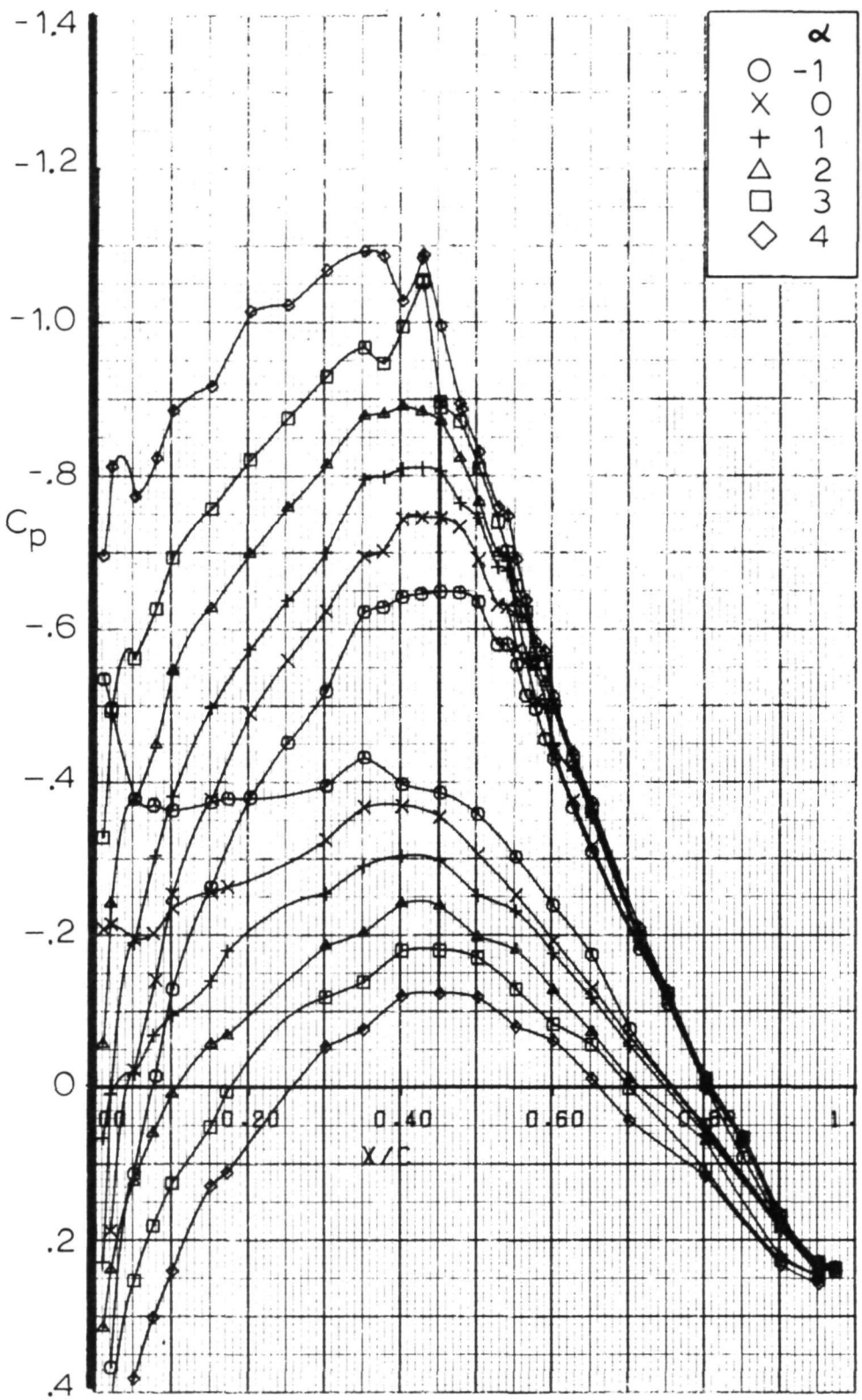

Figure 29.- Airfoil pressure distribution M = 0.68 R_N = 17 x 10^6.

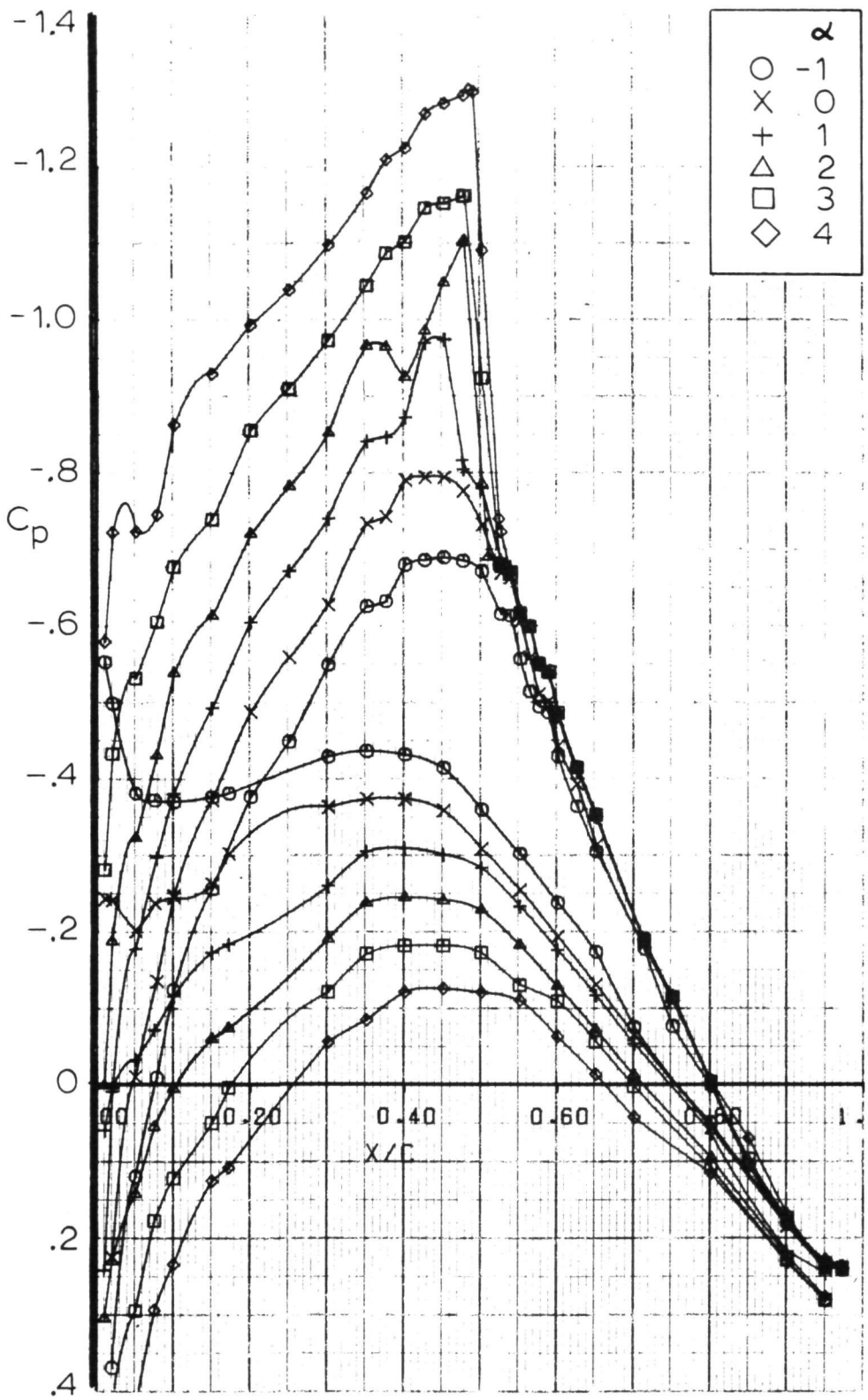

Figure 30.- Airfoil pressure distribution M = 0.70 R_N = 17 x 10^6.

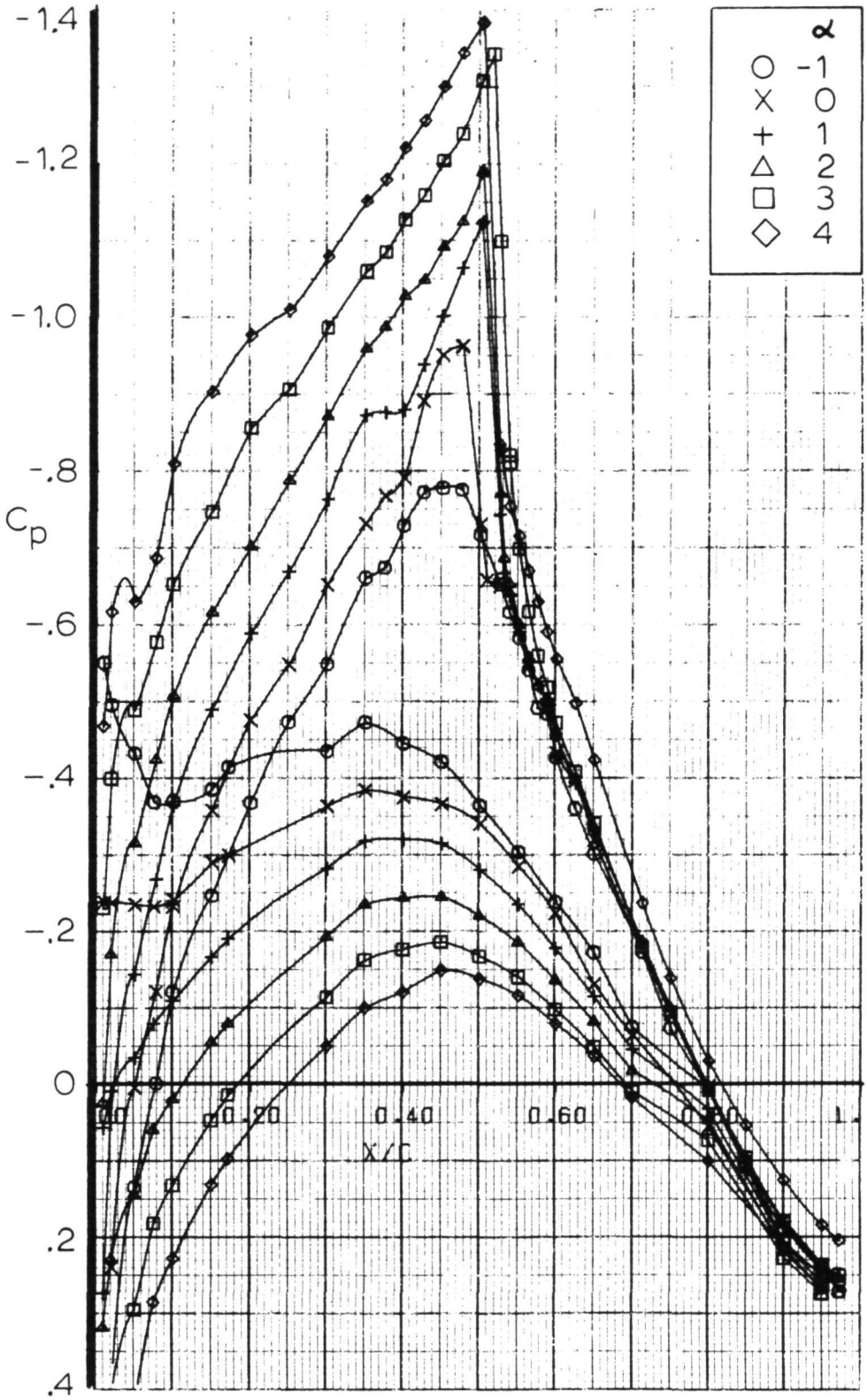

Figure 31.- Airfoil pressure distribution M = 0.72 R_N = 17 x 10^6.

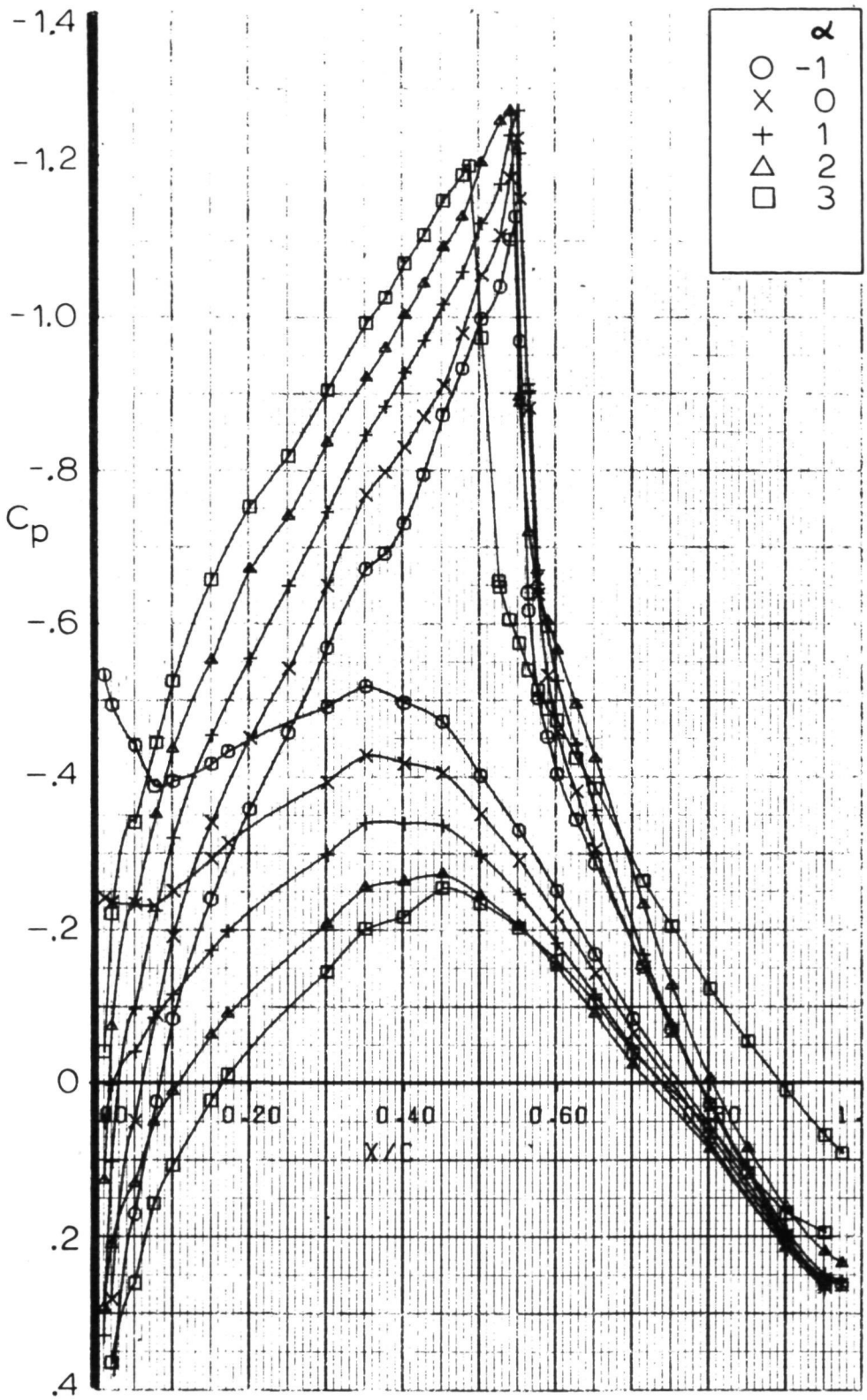

Figure 32.- Airfoil pressure distribution M = 0.75 R_N = 17 x 10^6.

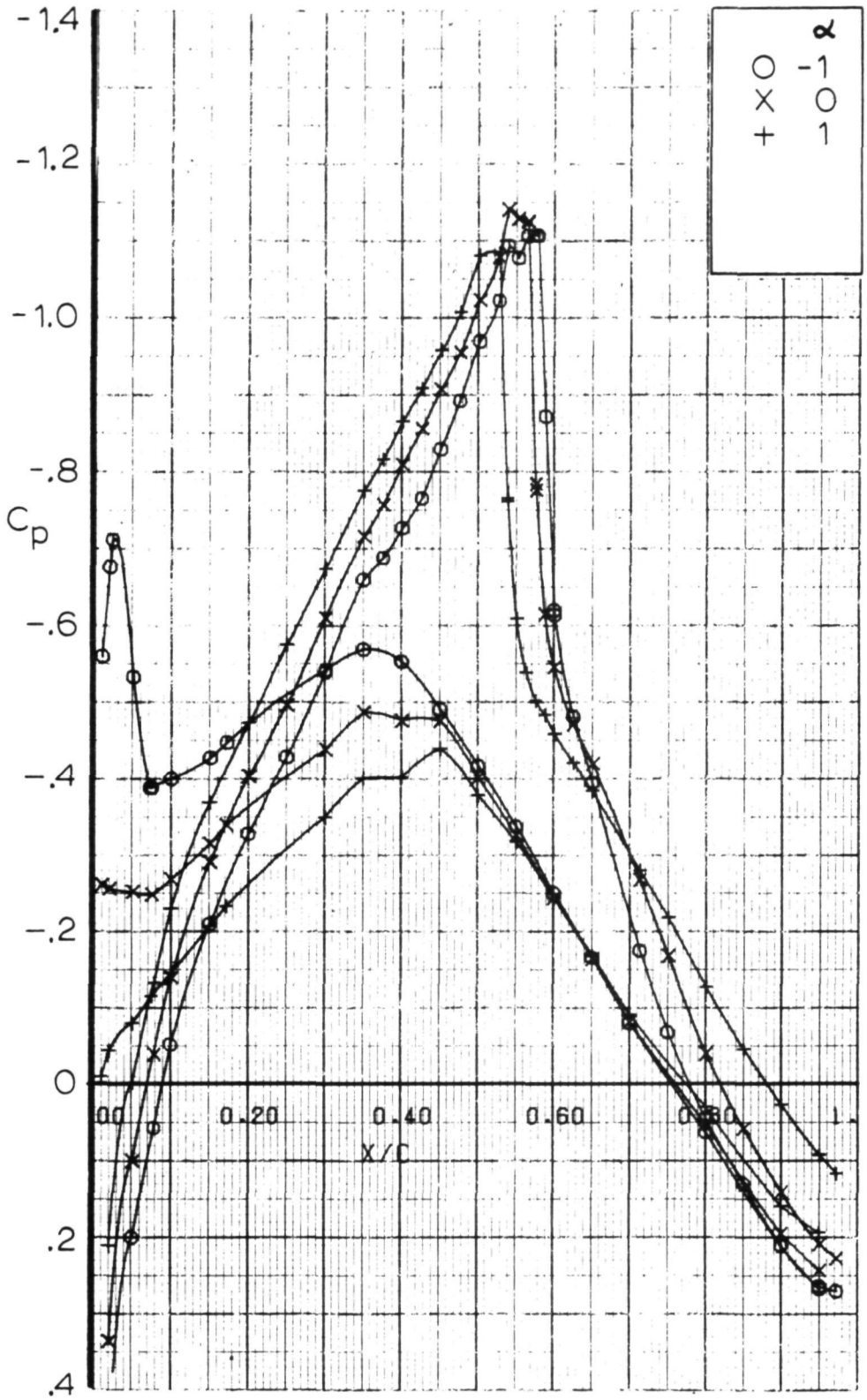

Figure 33.- Airfoil pressure distribution M = 0.78 R_N = 17 x 10^6.

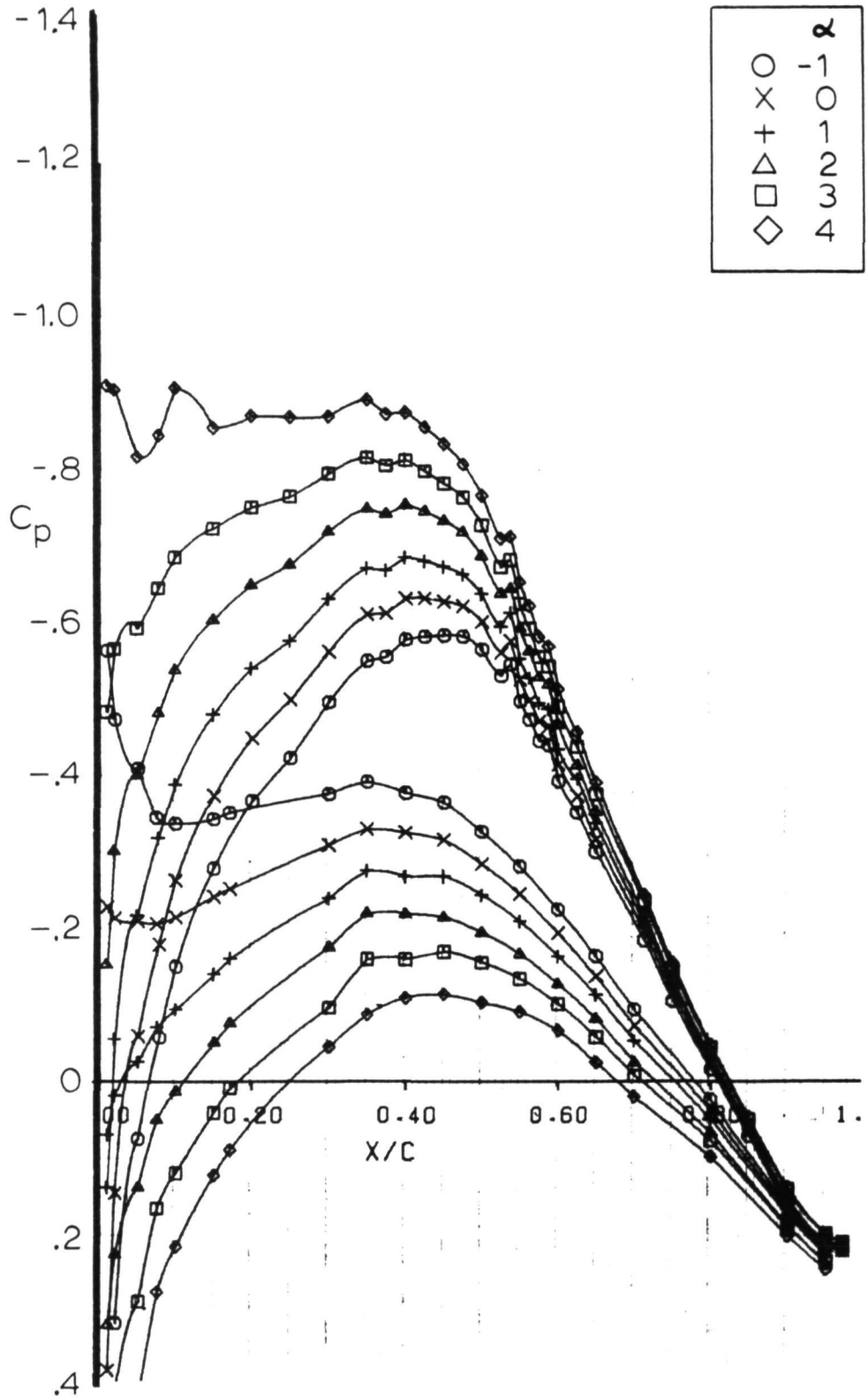

Figure 34.- Airfoil pressure distribution M = 0.6 R_N = 25 x 10^6.

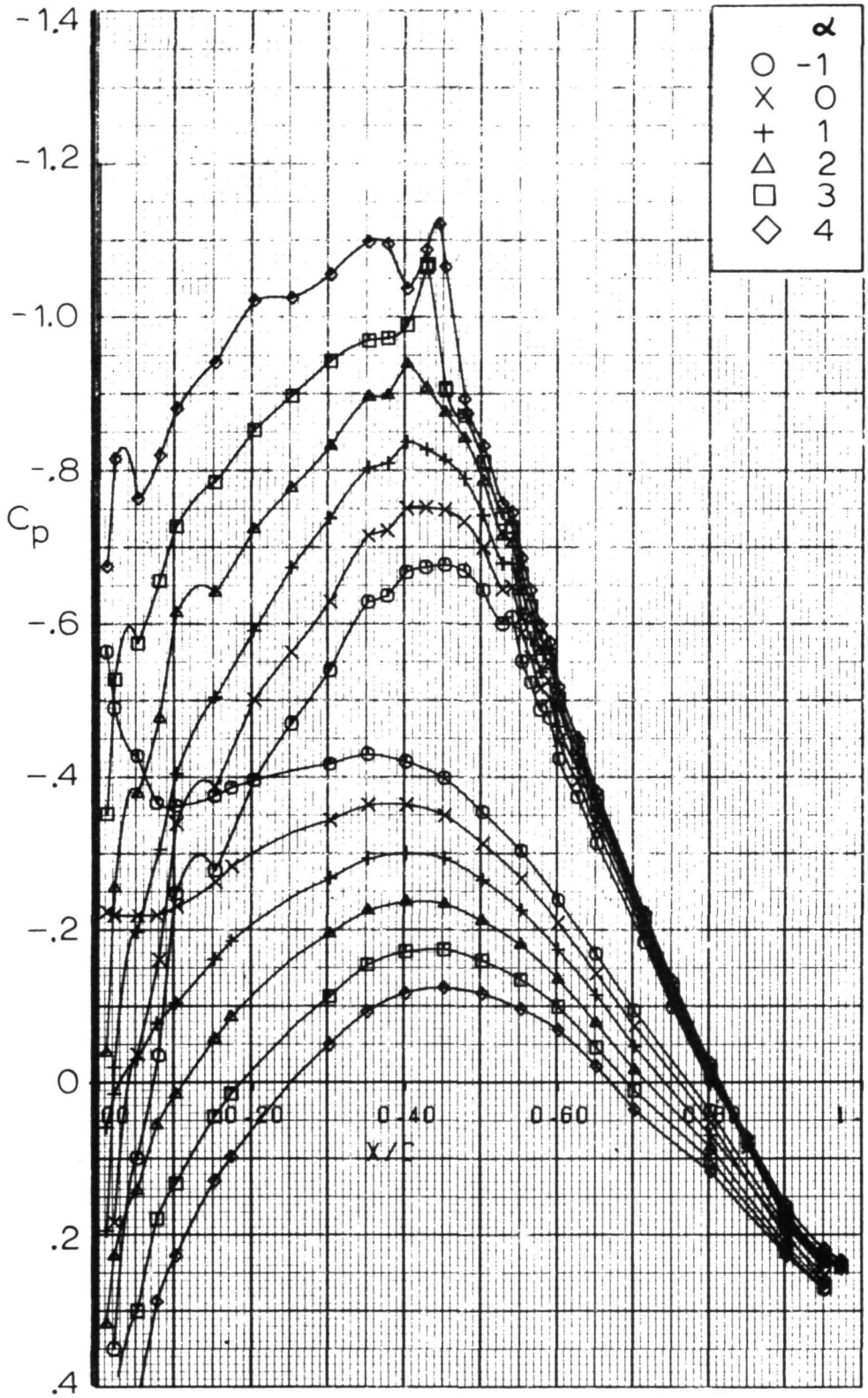

Figure 35.- Airfoil pressure distribution M = 0.68 R_N = 32 x 10^6.

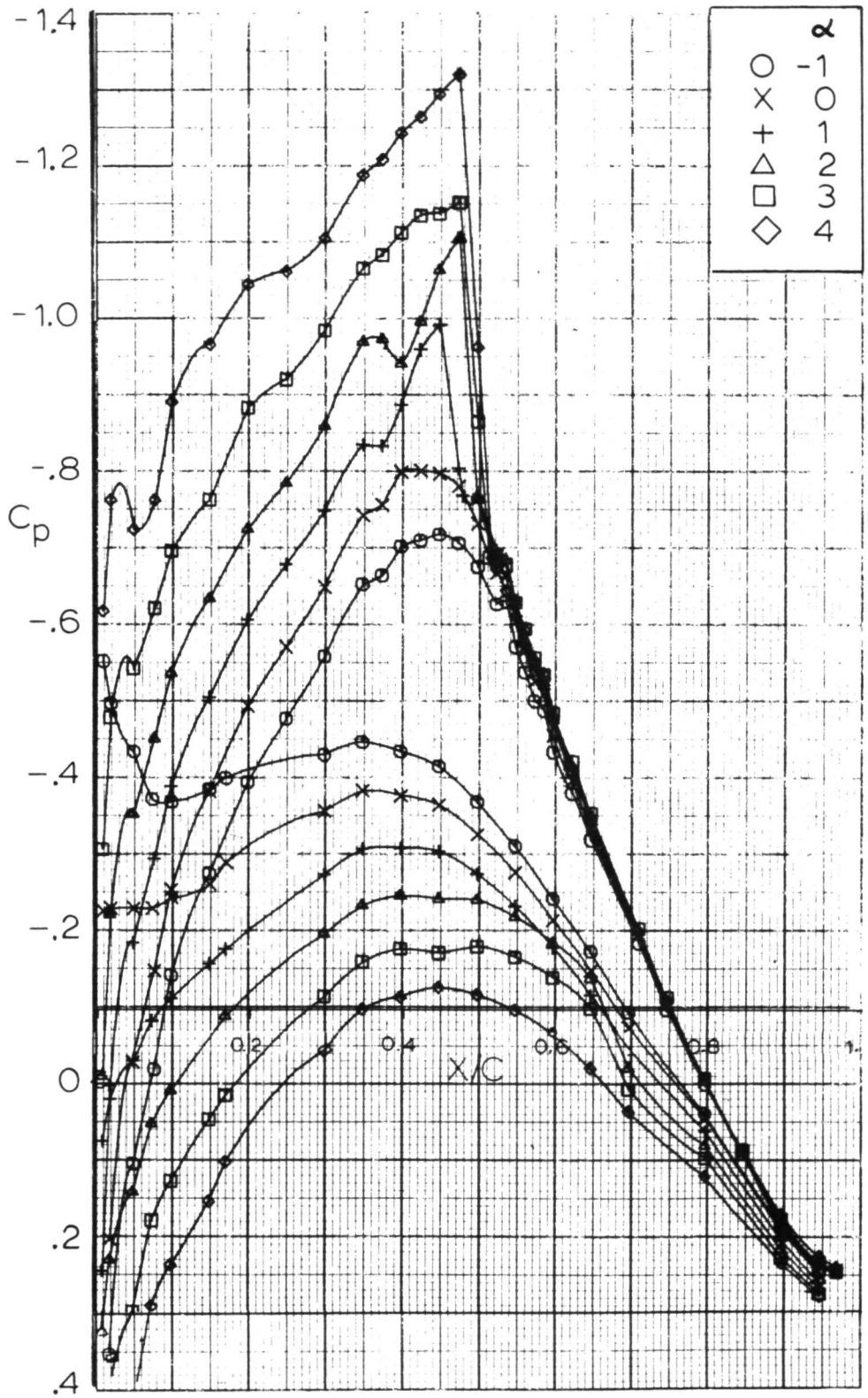

Figure 36 .- Airfoil pressure distribution M = 0.70 R_N = 32 x 10^6.

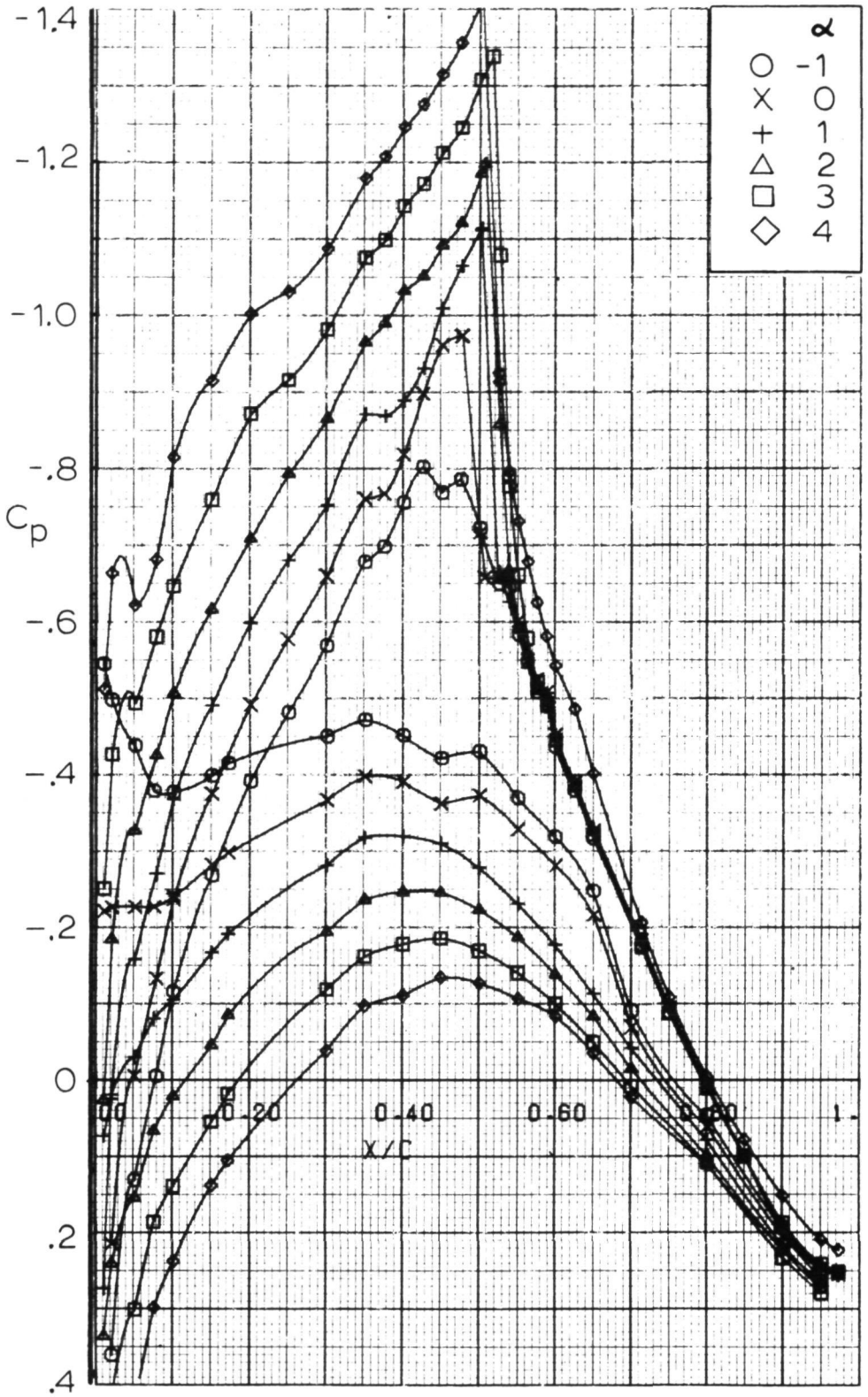

Figure 37.- Airfoil pressure distribution M = 0.72 R_N = 32 x 10^6.

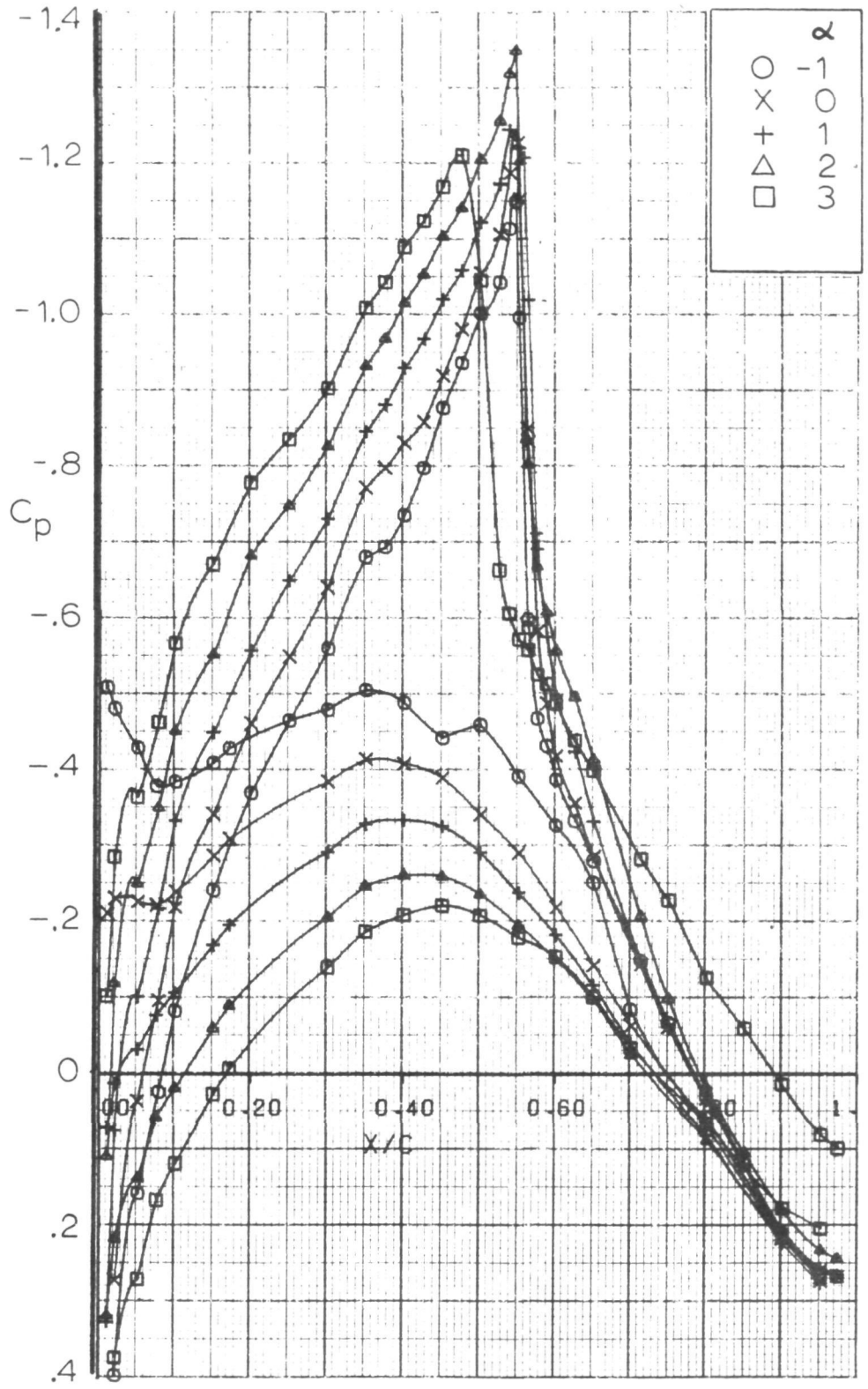

Figure 38.- Airfoil pressure distribution M = 0.75 R_N = 32 x 10^6.

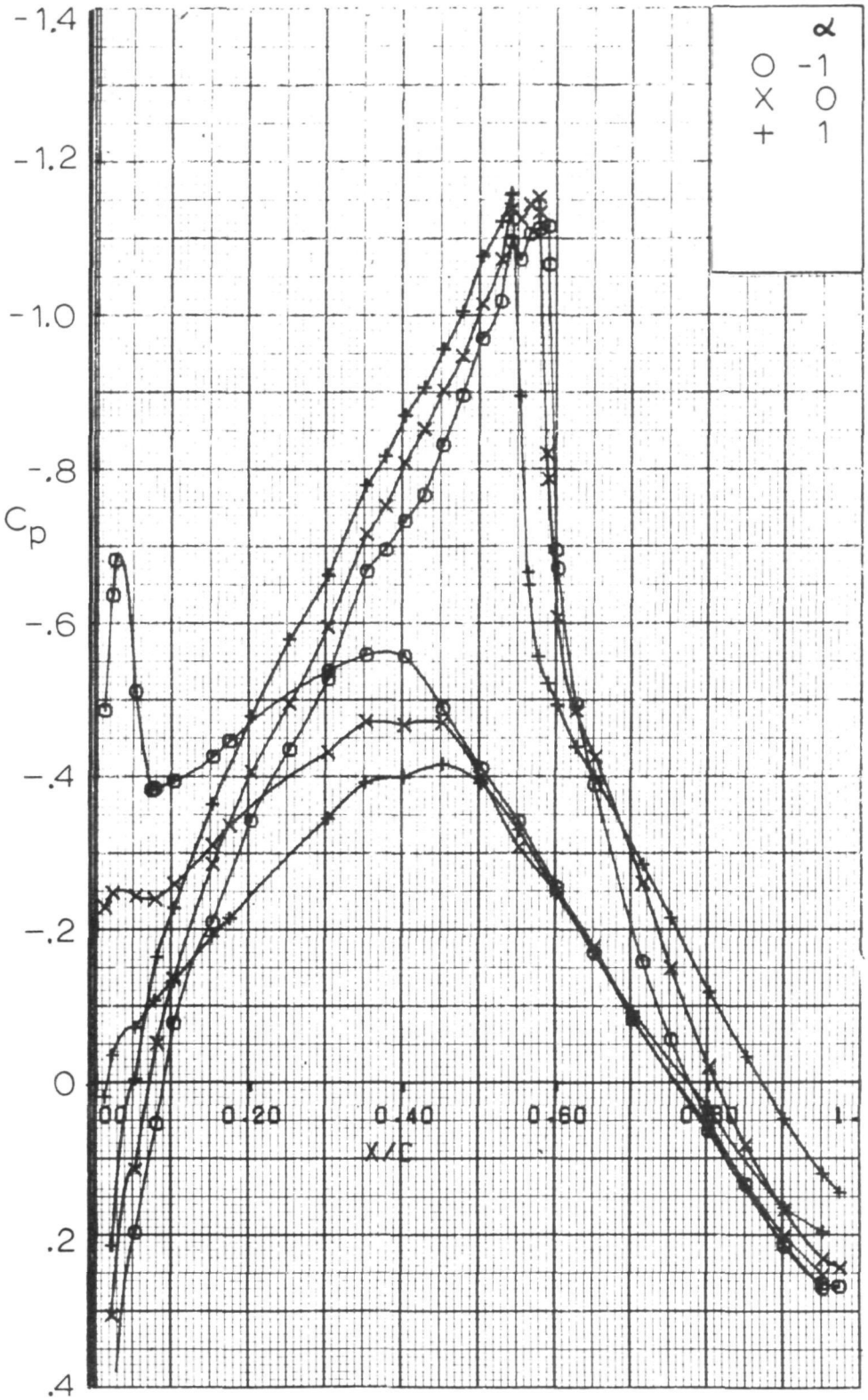

Figure 39.- Airfoil pressure distribution M = 0.78 R_N = 32 x 10^6.

☆ U.S. GOVERNMENT PRINTING OFFICE: 1975—635-049 70

NATIONAL AERONAUTICS AND SPACE ADMINISTRATION
WASHINGTON, D.C. 20546

OFFICIAL BUSINESS
PENALTY FOR PRIVATE USE $300

SPECIAL FOURTH-CLASS RATE
BOOK

POSTAGE AND FEES PAID
NATIONAL AERONAUTICS AND
SPACE ADMINISTRATION
451

U.S.MAIL

POSTMASTER: If Undeliverable (Section 158
Postal Manual) Do Not Retu

"The aeronautical and space activities of the United States shall be conducted so as to contribute . . . to the expansion of human knowledge of phenomena in the atmosphere and space. The Administration shall provide for the widest practicable and appropriate dissemination of information concerning its activities and the results thereof."

—NATIONAL AERONAUTICS AND SPACE ACT OF 1958

NASA SCIENTIFIC AND TECHNICAL PUBLICATIONS

TECHNICAL REPORTS: Scientific and technical information considered important, complete, and a lasting contribution to existing knowledge.

TECHNICAL NOTES: Information less broad in scope but nevertheless of importance as a contribution to existing knowledge.

TECHNICAL MEMORANDUMS: Information receiving limited distribution because of preliminary data, security classification, or other reasons. Also includes conference proceedings with either limited or unlimited distribution.

CONTRACTOR REPORTS: Scientific and technical information generated under a NASA contract or grant and considered an important contribution to existing knowledge.

TECHNICAL TRANSLATIONS: Information published in a foreign language considered to merit NASA distribution in English.

SPECIAL PUBLICATIONS: Information derived from or of value to NASA activities. Publications include final reports of major projects, monographs, data compilations, handbooks, sourcebooks, and special bibliographies.

TECHNOLOGY UTILIZATION PUBLICATIONS: Information on technology used by NASA that may be of particular interest in commercial and other non-aerospace applications. Publications include Tech Briefs, Technology Utilization Reports and Technology Surveys.

Details on the availability of these publications may be obtained from:

SCIENTIFIC AND TECHNICAL INFORMATION OFFICE

NATIONAL AERONAUTICS AND SPACE ADMINISTRATION

Washington, D.C. 20546